DEVELOPMENT OF BIOREDUCTIVE INHIBITORS OF CHECKPOINT KINASE 1 TO TARGET HYPOXIC TUMOURS

Cindy Körner

Trinity College

Supervisors: Dr Ester M. Hammond and Dr Stuart J. Conway

Trinity Term 2015

University of Oxford

ABSTRACT

Title: Development of bioreductive inhibitors of Checkpoint kinase 1 to target hypoxic tumours

Cindy Körner, Trinity College, Trinity Term 2015

Hypoxia (low physiological O_2 levels) is a characteristic of solid tumours. It not only alters the chemical microenvironment of a tumour but initiates a number of mechanisms which enable cells to cope and thrive under these conditions, resulting in therapy-resistant and aggressive tumours. The replication stress induced by severe hypoxia activates a DNA damage response which involves the kinases ATR and Chk1. Moreover, periods of hypoxia are often followed by reoxygenation, which induces DNA damage. Chk1 inhibitors have been used to potentiate chemotherapy with cytotoxic agents and have recently been proposed as single agents in tumours with high levels of replication stress. However, inhibition of Chk1 also affects normal DNA replication, cell cycle progression and DNA repair. The herein presented study chose known inhibitors of Chk1 and, with methods of synthetic organic chemistry, modified them into agents to selectively target hypoxic cells. Three different Chk1 inhibitors were selected and bioreductive analogues synthesised which were evaluated in chemical, biochemical and cellular assays. We found a convenient route to access a precursor of the bioreductive 2-nitroimidazole group and established a three-step protocol for the testing of bioreductive drugs. This protocol allows us to determine whether a bioreductive drug undergoes reduction and prodrug activation. In addition, bioreductive Chk1 inhibitors were shown to induce DNA damage and cellular toxicity in a hypoxia-selective fashion. While reduction of the prodrugs occurred in all three cases, fragmentation was always the rate-limiting step. We propose that the use of bioreductive Chk1 inhibitors is a promising strategy to target the most therapy-resistant tumour fraction while sparing normal tissue.

ACKNOWLEDGEMENTS

I am immensely grateful to my two supervisors Ester and Stuart for welcoming me in their research groups. Stuart has always been extremely motivating, even when things were challenging at times. I cannot even remember how many times I have heard an encouraging “I am sure you will crack it” from him. I consider myself very privileged that Ester took the chance of extending her research group with a chemist, who knew almost nothing about biology when she joined. She has given me the opportunity to grow scientifically, while always watching over me.

Both research groups have made my Oxford experience unforgettable with their help, support and friendships. From the Conway lab, I am especially grateful to Liam who became my main chemistry buddy and good friend. Working on this project would not have been even half as enjoyable without him. Everyone in G12 and G11 has contributed to making the chemistry lab an enjoyable place to work in. The members of the Hammond lab taught me everything I know about biology. I am extremely grateful for their patience and never-ending support. We spent so much time together in and out of the lab that they have become my Oxford family. Selva was the first to welcome me and from day one I could always count on him. Liam, Monica, GG and Kasia became wonderful friends with whom I share some unforgettable experiences, like running the London Marathon or getting grounded during a yoga class. Joana, Isabel and Zuzana have been an incredible source of knowledge and were always willing to offer a helping hand.

Many other people in the Gray Institute have become part of that Oxford family, particularly Dafni and Nikola. I have shared every major step during my time in Oxford with Nikola and after starting together we are now also finishing together.

I am especially indebted to Mike Stratford for opening the doors to his HPLC lab, teaching me how to use the machines and giving countless advice.

Mike was always there when needed, even *via* remote access if the system failed when everyone was home already.

I am grateful to the staff of the NMR and MS facility in the CRL, especially James Wickens. Thank you to Lisa Folkes, Remko Prevo and Graham Brown. I would also like to thank Niki Sibson, Sarah Norman, Katy Higgins and Larry Turner for their support.

Writing a thesis away from Oxford with a small baby has been a particular challenge. I cannot express how much Ester, Kasia, Monica, GG and Dafni have helped in motivating me and building me up when spirits were low. Ester, thank you so much for your incredible proof-reading skills!

I thank my mother, John and Antje for watching over baby Julian for many hours, but especially for their mental support during difficult times. Armando must be one of the happiest people that this work is finally written up. I am grateful for all the help and constant encouragement he has given me, for his patience and for being an awesome father. Julian, thank you for your smile.

TABLE OF CONTENTS

Abstract II
Acknowledgements III
Table of Contents V
List of Figures IX
List of Schemes XII
List of Tables XIII
Abbreviations XIV

Chapter 1
Introduction 18
1.1 Cancer and tumour hypoxia 18
1.2 The DNA damage response 25
1.2.1 DNA damage signalling 25
1.2.2 DNA Replication 28
1.2.3 Replication stress 30
1.2.4 ATR activation and ATR-mediated Chk1 activation 32
1.2.5 Function of Chk1 34
1.2.6 The DNA damage response in hypoxia 38
1.2.7 Hypoxia-induced ATR/Chk1 signalling 41
1.2.8 Reoxygenation 43
1.2.9 The importance of Chk1 in cell survival 44
1.3 Chk1 inhibition for the treatment of cancer 45
1.3.1 Checkpoint targeting in cancer therapy 45
1.3.2 Chk1 structure 49
1.3.3 Small-molecule inhibitors of Chk1 50
1.3.4 Chk1 inhibitors in clinical trials 55
1.4 Exploiting hypoxia for cancer therapy 58
1.4.1 Approaches to targeting hypoxic tumours 58
1.4.2 Classes of reductively activated prodrugs 64
1.5 Aim 68

Chapter 2

Development of a proof-of-concept bioreductive Chk1 inhibitor 71

2.1 Introduction 71

2.2 Rationale for hypoxia-selective Chk1 inhibition 72

2.3 Choice of inhibitor 74

2.4 Synthesis of prodrug 2 and the control compounds 1 and 12 78

2.5 Inhibitor 1 also targets AURKA 80

2.6 Mechanism of action 81

2.6.1 Chemical reduction of **2** 82

2.6.2 CYP450 reduction of **2** 86

2.7 Prodrug 2 is a hypoxia-selective Chk1/AURKA inhibitor 87

2.7.1 Prodrug **2** shows no inhibition of purified Chk1 or AURKA 87

2.7.2 Prodrug **2** acts selectively in hypoxia 89

2.7.3 Biological activity of **2** is not associated with the bioreductive group 93

2.8 Sensitivity to prodrug 2 can partly be predicted by basal levels of DNA damage 95

2.8 Discussion 99

Chapter 3

Synthesis and validation of a set of analogues based on a pyrazolopyridine Chk1 inhibitor 101

3.1 Introduction 101

3.1.1 Choice of Chk1 inhibitor 101

3.1.2 Synthesis outline 103

3.2 Chemical synthesis of 5-(chloromethyl)-2-nitroimidazole 38 105

3.2.1 Synthesis of the imidazole precursor 105

3.2.2 Conversion of imidazole **32** into 5-(cloromethyl)-2-nitroimidazole **38** 107

3.3 Chemical synthesis of the analogues 16-19 110

3.3.1 Synthesis of key intermediate **22** and Chk1 inhibitor **16** 110

3.3.2 Incorporation of the pyrazole substituents and synthesis of analogues **17-19** 112

3.4 *In vitro* testing of analogues 16-19 118

3.4.1 The Chk1 inhibitor **16** sensitises cancer cells to severe hypoxia 118

3.4.2 Initial validation of the analogues **16-19** 121

3.4.3 Investigation of the mechanism of activation of prodrug **18** 126

3.5 Discussion 132

Chapter 4

Development of a 2-nitroimidazole bioreductive prodrug based on a potent and selective Chk1-inhibitor 136

4.1 Introduction 136

4.2 *In vitro* testing of SAR020106 in hypoxia 137

4.3 Optimisation of synthesis and purification of 52 144

4.3.1 Synthesis of **52** 144

4.4 Validation of the bioreductive mechanism of action 152

4.4.1 The bioreductive prodrug **52** shows decreased Chk1 affinity and cytotoxicity 152

4.4.1 Inhibition of Chk1 by **52** requires reduction of the prodrug 154

4.4.2 Activation of **52** is not only CYP450-dependent 160

4.5 Biological evaluation of prodrug 52 162

4.5.1 The prodrug **52** is a hypoxia-selective Chk1 inhibitor 162

4.5.2 Treatment with **52** leads to an increased accumulation of DNA damage selectively in hypoxia 164

4.5.3 Clonogenic survival in response to **52** 166

4.5.4 Spheroid studies 168

4.6 Discussion 173

Chapter 5

Discussion 177

Chapter 6

Experimental 181

6.1 Materials 181

6.1.1 General laboratory materials and reagents 181

6.1.2 Drugs (commercially available and in-house) 183

6.1.3 Antibodies 185

6.2 Methods 187

6.2.1 Cell lines and tissue culture 187

6.2.2 Cryopreservation of cell lines 189

6.2.3 Drug treatments 189

6.2.4 Hypoxia treatment 190

6.2.5 γ-Irradiation 190

6.2.6 Analytical HPLC 190
6.3 Drug metabolism 191
6.3.1 Zinc reduction 191
6.3.2 Sodium dithionite reduction 192
6.3.3 CYP450 reductase assay 192
6.3.5 Metabolite analysis from cell lysates 193
6.4 Protein analysis 194
6.4.1 Protein sample preparation 194
6.4.2 SDS-PAGE (SDS-Polyacrylamide Gel Electophoresis) 194
6.4.3 Western Blotting 196
6.4.4. Immunofluorescence microscopy 197
6.5 Clonogenic survival 198
6.6 Spheroids 198
6.7 Analysis 200
6.8 General chemical experimental procedures 200
6.9 Synthetic Procedures 205
6.9.1 2-Nitroimidazole analogues 205
6.9.2 The pyrazolo-pyridine-based Chk1 inhibitor **16** and analogues **17-19** 210
6.9.3 Synthesis of the bioreductive Chk1 inhibitor **52** 230

Appendix A 232
Appendix B 243
Appendix C 244
References 245

LIST OF FIGURES

Figure 1.1. The hallmarks of cancer. 19
Figure 1.2. Schematic representation of the two main causes for tumour hypoxia and resulting physiological and biological consequences. 21
Figure 1.3. Schematic representation of the HIF-1α pathway. 23
Figure 1.4. Schematic representation of the DNA damage response. 27
Figure 1.5. DNA replication. 29
Figure 1.6. Activation of the ATR/Chk1 axis in response to replication stress. ... 33
Figure 1.7. Chk1 regulates cell cycle progression, replication and DNA repair… 37
Figure 1.8. Schematic representation of the DDR in severe hypoxia. 41
Figure 1.9. Selective targeting of p53 deficient cancer cells through inhibition of Chk1. 47
Figure 1.10. Chk1 kinase domains and ATP-binding site. 50
Figure 1.11. Targeting tumour hypoxia. 62
Figure 1.12. General mechanism for bioreductive prodrug activation. 64
Figure 1.13. Selected representatives of different classes of bioreductive prodrugs. 66
Figure 1.14. Schematic representation of the mechanism of action of a bioreductive Chk1 inhibitor. 69
Figure 2.1. Chk1 is phosphorylated and active in severe hypoxia and inhibition causes DNA damage. 73
Figure 2.2. Rationale for the design of a bioreductive prodrug based on the Chk1 inhibitor 1. 75
Figure 2.3. Structure of the bioreductive prodrug 2. 77
Figure 2.4. Representative image of 2 docked to Chk1 overlaying the X-ray crystal structure of inhibitor 1 bound to Chk1. 77
Figure 2.5. Clonogenic survival assay following AURKA inhibition in normoxia and severe hypoxia. 81
Figure 2.6. Chemical reduction of prodrug 2, HPLC traces. 84
Figure 2.7. Buffer treatment of an aliquot taken from the chemical reduction of 2. 85
Figure 2.8. CYP450 reduction of prodrug 2 and subsequent fragmentation. 86

Figure 2.9. IC_{50} values for compounds 1 and 2 against Chk1 and AURKA..... 88
Figure 2.10. Hypoxia-selective inhibition of H3 Ser10 phosphorylation through 2. 90
Figure 2.11. Hypoxia-selective induction of DNA damage by 2. 91
Figure 2.12. O_2 dependency of 2 toxicity. 93
Figure 2.13. Assessment of the cytotoxic effect of the 4-nitrobenzyl bioreductive group..... 95
Figure 2.14. Basal level of DNA damage in three lung cancer cell lines. 97
Figure 2.15. Colony survival assays in three lung cancer cell lines. 98
Figure 3.1. Design of a set of analogues based on Chk1 inhbitor 16. 102
Figure 3.2. Synthesis overview for Boc-protected analogues of 16-19, and potential steps for bioreductive group incorporation..... 104
Figure 3.3. Structure of the disubstituted compound 48..... 118
Figure 3.4. Compound 16 inhibits gemcitabine-induced Chk1 autophosphorylation on S296. 119
Figure 3.5. Clonogenic survival curves of H1299 and RKO cells treated with inhibitor 16 in severe hypoxia and normoxia. 120
Figure 3.6. IC_{50} determination for compounds 16-19 against purified Chk1..... 122
Figure 3.7. Effect of benzyl substituted analogue 19 on gemcitabine induced Chk1 activity and clonogenic survival. 124
Figure 3.8. Clonogenic survival curves of H1299 and RKO cells treated with bioreductive analogues 17 and 18. 125
Figure 3.9. Chemical reduction of 18 using zinc and NH_4Cl..... 127
Figure 3.10. Sodium dithionite reduction of prodrug 18. 129
Figure 3.11. Sodium dithionite reduction of prodrug 17. 130
Figure 3.12. Formation of metabolites from 18 in RKO cells. 131
Figure 4.1. Design of the bioreductive Chk1 inhibitor 52 based on SAR020106. 137
Figure 4.2. Optimisation of a 96-well clonogenic assay and dose-response curve for SAR020106 in HeLa cells. 138
Figure 4.3. Inhibition of Chk1 autophosphorylation by SAR020106 in RKO cells. 140
Figure 4.4. Chk1 is phosphorylated and active in response to severe hypoxia in FLO-1 cells and SAR020106 inhibits this activity. 141

Figure 4.5. Dose-response curve for SAR020106 in FLO-1 and OE21 cells. ... 142
Figure 4.6. SAR020106 treatment leads to DNA damage in OE21 cells in normoxia and severe hypoxia. ... 143
Figure 4.7. Initial test reactions for the formation of 52. ... 145
Figure 4.8. HMBC NMR spectrum of 52. ... 149
Figure 4.9. Selective hydrolysis of pyridinium species 53 and 54. ... 150
Figure 4.10. Purification of 52. ... 152
Figure 4.11. IC_{50} determination for 52 and SAR020106 against purified Chk1. 153
Figure 4.12. The bioreductive prodrug 52 has no effect on clonogenic survival in FLO-1 and OE21 cell at 21% O_2. ... 154
Figure 4.13. CYP450 reduces 52 to the hydroxylamine 55. ... 155
Figure 4.14. CYP450 reduction of 52 at different O_2 concentrations. ... 157
Figure 4.15. Metabolite analysis for 52 in FLO-1 and OE21 cells at various O_2 concentrations. ... 158
Figure 4.16. Comparison of 52 metabolism in a set of CYP450 mutant cell lines. ... 161
Figure 4.17. Prodrug 52 inhibits Chk1 selectively in severe hypoxia. ... 163
Figure 4.18. Treatment of FLO-1 cells with 52 results in increased accumulation of 53BP1 foci selectively in severe hypoxia. ... 165
Figure 4.19. Clonogenic survival assays comparing SAR020106 and 52 at two O_2 concentrations in three cell lines. ... 167
Figure 4.20. O_2-dependency of 52 metabolism and growth reduction in U87-MG spheroids. ... 171
Figure 4.21. Growth reduction in U87-MG spheroids following treatment with 52 and SAR020106. ... 172
Figure 5.1. How we test bioreductive prodrugs. ... 179
Figure B. HPLC traces of synthesis and purification of 52 for NMR analysis. ... 243
Figure C. Calibration curves for quantification of SAR020106, amine 56 and compound 52. ... 244

LIST OF SCHEMES

Scheme 1.1. Hypoxia-selective activation of the clinically advanced bioreductive prodrugs PR-104A and TH-302. 65
Scheme 2.1. Synthesis of prodrug precursor 7. 78
Scheme 2.2. Synthesis of amino linker 11. 79
Scheme 2.3. Final step in the synthesis of 2. 79
Scheme 2.4. Synthesis of control compounds 1 and 12. 80
Scheme 2.5. Proposed mechanism of prodrug 2 activation in hypoxia. 82
Scheme 2.6. Chemical reduction and activation of 2. 83
Scheme 3.1. Proposed synthesis of the 2-nitroimidazole precursor 32. 105
Scheme 3.2. Synthesis of the 2-nitroimidazole precursor 32. 106
Scheme 3.3. Conversion of the 2- and 5-substituents to give alcohol 35. 107
Scheme 3.4. Overview of optimised synthesis of 38. 110
Scheme 3.5. Synthesis overview of key intermediate 22. 111
Scheme 3.6. Synthetic alterations in the final steps towards Chk1 inhibitor 1. . 112
Scheme 3.7. Strategy A for the incorporation of the bioreductive group: Synthesis of different pyrazole building blocks. 113
Scheme 3.8. Proposed synthesis of 4-nitrobenzyl pyrazole building blocks. 113
Scheme 3.9. Strategy B for bioreductive group incorporation. 114
Scheme 3.10. Products obtained from an attempted one-step procedure to achieve chlorination and PMB-deprotection of 42. 115
Scheme 3.11. Synthesis of the analogues 17, 18 and 19 from key intermediate 22. 116
Scheme 4.1. Selective synthesis of either 52 or 53 for NMR analysis. 148

LIST OF TABLES

Table 1.1. Chk1 inhibitors in clinical trials 56
Table 3.1. Optimisation of conditions for the synthesis of bromo-2-nitroimidazole 37..... 108
Table 3.2. Optimisation of conditions for the synthesis of chloro-2-nitroimidazole 38..... 109
Table 3.3. Optimisation of pyrazole substituent incorporation..... 117
Table 4.1. Optimisation of synthesis of the regioisomers 52 and 53. 147
Table 6.1. Chemicals and reagents 181
Table 6.2. Drugs used in this study..... 184
Table 6.3. Primary antibodies used for western blotting (WB) or immunofluorescence (IF) 185
Table 6.4. Secondary antibodies used for western blotting (WB) or immunofluorescence (IF) 186
Table 6.5. HPLC conditions 191
Table 6.6. Reaction components and volumes for CYP450 reductase assay... 193
Table 6.7. Recipe for stacking gel..... 195
Table 6.8. Recipe for separating gel (7.5-15%)..... 195
Table 6.9. PerkinElmar Flexar, Dionex Acclaim® method 203

ABBREVIATIONS

2OG	2-Oxoglutarate
5FU	5-Fluorouracil
9-1-1	RAD9-HUS1-RAD1
53BP1	p53-Binding protein 1
AKT	Synonym for protein kinase B
AML	Acute myeloid leukaemia
AND-1	Acidic nucleoplasmic binding protein 1
APS	Ammonium persulfate
AURKA	Aurora kinase A
AT	Ataxia telangiectasia
ATM	Ataxia telangiectasia mutated
ATP	Adenosine triphosphate
ATR	Ataxia telangiectasia mutated and Rad3 related
ATRIP	ATR-interacting protein
Boc	tert-Butoxycarbonyl
Bp	Base pair
Br	Broad
BRCA2	Breast cancer 2, early onset
BSA	Bovine serumalbumin
CAIX	Carbonic anhydrase IX
CBP	CREB-binding protein
CDC	Cell division cycle
CDI	Carbonyldiimidazole
CDT1	Chromatin licensing and DNA replication factor 1
CDK	Cyclin-dependent kinase
Chk1	Checkpoint kinase 1
Chk2	Checkpoint kinase 2
CODD	*C*-Terminal O_2-dependent degradation domain
COSY	Homonuclear correlation spectroscopy
C-TAD	*C*-Terminal transactivation domain
CYP450	Cytochrome P450 oxidoreductase

d	Doublet
DAPI	4’,6-Diamidino-2-phenylindole
DDK	Dbf4/Drf1-dependent CDC7 kinase
DDR	DNA damage response
DMEM	Dulbecco’s modified Eagle’s medium
DMF	*N,N*-Dimethylformamide
DMSO	Dimethyl sulfoxide
DNA	Deoxyribonucleic acid
dNTP	Deoxyribose nucleoside triphosphate
DSB	Double stand break
ED_{50}	Median effective dose
EDTA	Ethylenediaminetetraacetic acid
EME1	Essential Meiotic Structure-Specific Endonuclease 1
Eq	Equivalent
ES	Electrospray
ESI	Electrospray ionisation
FA	Fanconi anemia
FA	Formic acid, methanoic acid
FBS	Foetal bovine serum
FI	Field ionisation
FIH	Factor inhibiting HIF
G6P	Glucose-6-phosphate
G6PDH	Glucose-6-phosphate dehydrogenase
GINS	Go-itchi-ni-san
Glut1	Glucose transporter 1
H2AX	Histone family H2A, member X
H3	Histone H3
H3K9me3	Histone 3 lysine 9 tri-methylation
HAP	Hypoxia-activated prodrug
HIF-1	Hypoxia-inducible factor-1
HMBC	Heteronuclear multiple bond correlation
HPLC	High performance liquid chromatography
HR	Homologous recombination
HRE	Hypoxia responsive element

HSQC	Heteronulear single quantum correlation
HU	Hydroxyurea
IC_{50}	Half maximal inhibitory concentration
IF	Immunofluorescence
IgG	Immunglobulin G
IR	Ionising radiation
MCM	Mini-chromosome maintenance
MRN	MRE11-RAD50-NBS1
mRNA	Messenger ribonucleic acid
MS	Mass spectrometer *or* mass spectrum
MUS81	MUS81 Structure-Specific Endonuclease Subunit
MYCN	MYC-neuroblastoma-related
NBS	*N*-Bromosuccinimide
NMP	*N*-Methyl-2-pyrolidone
NODD	*N*-Terminal O_2-dependent degradation domain
NSCLC	Non-small cell lung cancer
OCT	Optimal cutting temperature compound
ORC	Origin recognition complex
PARP	Poly (ADP-ribose) polymerase
PBS	Phosphate buffered saline
PCNA	Proliferating cell nuclear antigen
PDA	Photodiode array
PE	Petroleum ether
PFA	Paraformaldehyde
PHD	Prolyl hydroxylase domain
PP2A	Protein phosphatase 2A
PPB	Potassium phosphate buffer pH 7.4
ppm	Parts per million
preRC	Pre-replication complex
q	Quartet
RFC	Replication factor C
RNAi	Ribonucleic acid interference
RNR	Ribonucleotide reductase
ROS	Reactive oxygen species

RPA	Replication protein A
RT	Room temperature, refers to the ambient temperature
s	Singlett
SD	Standard deviation
SDS	Sodium dodecyl sulphate
SE	Standard error
siRNA	Small interfering ribonucleic acid
SSB	Single strand break
t	Triplet
TBAI	Tetrabutylammonium iodide
TBS	Tris-buffered saline
TCA	Trichloroacetic acid
TEMED	Tetramethylethylenediamine
TFA	Trifluoroacetic acid
THF	Tetrahydrofuran
TIM	Timeless homologue
TIPIN	Timeless-interacting protein
TLC	Thin layer chromatography
TLK1	Tousled-like kinase 1
TMS	Tetramethylsilane
TOF	Time of flight
TOPBP1	Topoisomerase binding protein 1
Tris-HCl	Tris(hydroxymethyl)aminomethane hydrochloride
UV	Ultraviolet
VCB	Von Hippel-Lindau elongin C/B complex
VHL	Von Hippel-Lindau protein
WB	Western blot
wt	Wild-type

CHAPTER 1

INTRODUCTION

1.1 Cancer and tumour hypoxia

Cancer is a group of diseases that can affect any part of the human body. It is characterised by uncontrolled cell proliferation and the ability to invade adjacent tissue and spread to other organs to form metastases. Cancer arises in a multistage process of iterative genetic alterations that drive the progression into malignant tumours. An article published by Hanahan and Weinberg in 2000 described six hallmarks of cancer which has more recently been expanded by two additional emerging hallmarks and two enabling characteristics (Figure 1.1) (Hanahan and Weinberg 2000; Hanahan and Weinberg 2011). The authors suggested that cancer cells acquire a distinct set of characteristics on their way to becoming malignant that is common to all types of cancer.

Normal cells have mechanisms by which they control cell proliferation to avoid the accumulation of errors. In this way healthy cells have several backup mechanisms to ensure the appropriate completion of every cell cycle and this may include cell death in extreme circumstances. Through mutation, cancer cells, on the other hand, acquire the ability to evade these growth controlling mechanisms, leading to uncontrolled proliferation. This in turn can drive further mutation and genomic instability.

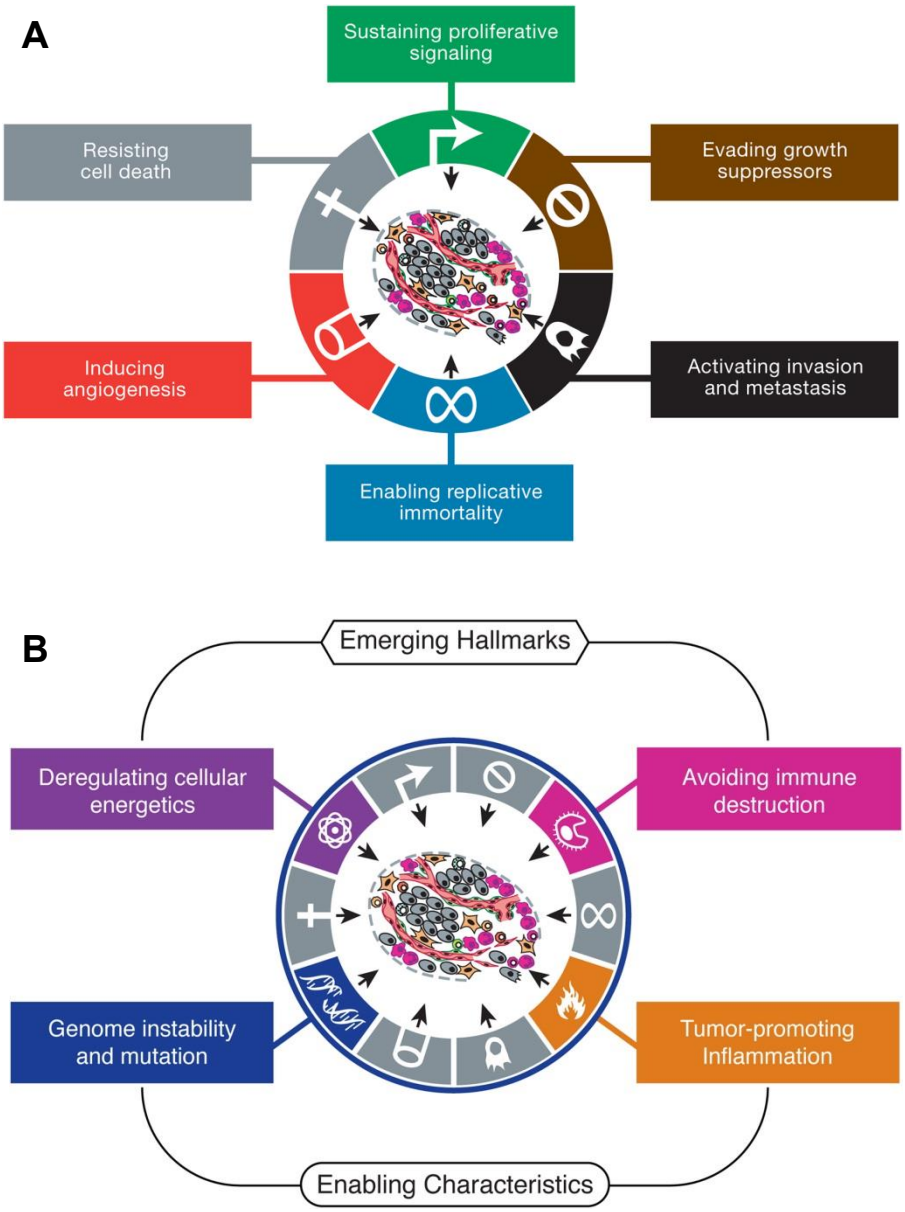

Figure 1.1. The hallmarks of cancer.
A) The originally described hallmarks of cancer and B) the expansion by two emerging hallmarks and two enabling characteristics. Reprinted with permission from Cell, vol 144, issue 5, 4 March 2011, Hanahan D., Weinberg R.A., Hallmarks of Cancer: The Next Generation, 646-674, Copyright (2011), with permission from Elsevier.

The metabolic demand of normal tissue is met by an adequate blood supply. A rapidly growing solid tumour on the other hand has a higher consumption of oxygen and nutrients and quickly outgrows the available blood supply (Vaupel and Harrison 2004). In an attempt to make up for the resulting shortage, the tumour initiates a process called angiogenesis in which it generates its own vasculature from the host vascular network (Bergers and Benjamin 2003).

The resulting vessel network however is primitive and highly aberrant with structural and functional abnormalities. Tumour vessels are often leaky and haemorrhagic due to missing endothelial lining. Together with a lack of lymphatic drainage this causes the accumulation of fluid in the interstitial space, high interstitial fluid pressure and the collapse of blood vessel. As a result, regions within the tumour arise that are characterised by very low O_2 levels (hypoxia) and energy deficiency (Vaupel and Harrison 2004). The cellular energy production in those areas shifts towards glycolysis which produces lactate as a by product and causes tumour acidosis (Figure 1.2, C) (Vaupel, Kallinowski, and Okunieff 1989).

Traditionally two mechanisms have been described that are responsible for the development of tumour hypoxia although this classification is an oversimplification and different subtypes exist to each mechanism (Bayer et al. 2011). Diffusion-limited hypoxia arises as a function of distance from a perfused blood vessel. The O_2 gradient causes the development of chronically hypoxic regions at 100-180 µm away from functional vessels (Figure 1.2) (Evans et al. 1997; Thomlinson and Gray 1955). In addition, the severe abnormalities in the tumour vasculature can cause transient changes in blood flow (perfusion-limited O_2 supply, Figure 1.2, A) leading to acute or cycling hypoxia (Dewhirst, Cao, and Moeller 2008; Brown 1979). This condition can last minutes to hours and is typically followed by reoxygenation upon reperfusion of microvessels (Figure 1.2, B).

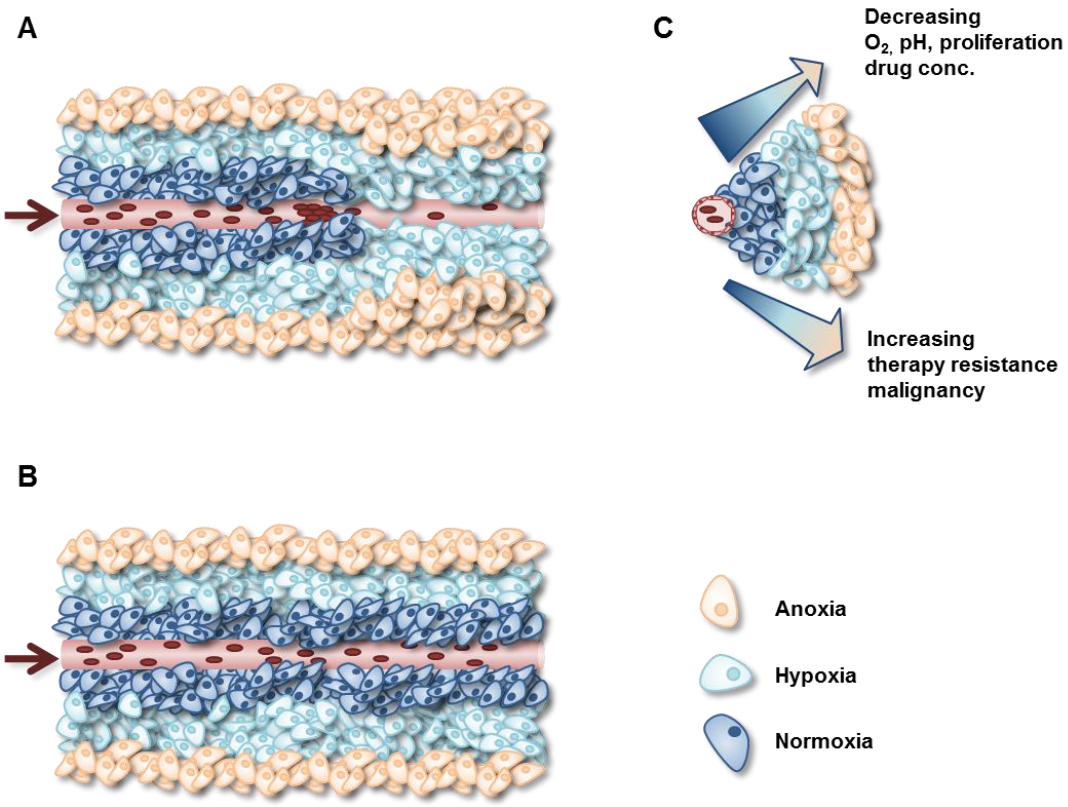

Figure 1.2. Schematic representation of the two main causes for tumour hypoxia and resulting physiological and biological consequences.
A) O_2 from a functional blood vessel is rapidly consumed by the tumour cells closest to the vessel, resulting in an O_2 gradient towards increasing distance from the vessel. Cells become increasingly hypoxic, reaching a state of anoxia at the outer rim (diffusion-limited hypoxia). The abnormalities in the tumour vasculature can cause temporary and partial closures of blood vessels (perfusion-limited hypoxia), in which case the oxygenation status of adjacent tumour cells shifts towards more severe hypoxia. B) Vessel closures are often temporary and cells become reoxygenated upon vessel reperfusion. C) The biological consequences of tumour hypoxia and acidosis result in greater therapy resistance and malignancy. Adapted from (Jordan and Sonveaux 2012; Siemann and Horsman 2015).

Hypoxia is characteristic to most solid tumours and can be found in a wide range of cancers. It typically ranges between 0.3% and 4.2% O_2 depending on the type of tissue but can reach complete anoxia (Vaupel and Mayer 2007; McKeown 2014). It is important to note that oxygenation status is tissue specific and varies even in normally oxygenated tissue. Therefore, what might be a physiologically normal oxygen level in one organ can be classified as hypoxic in a different organ and *vice versa*.

In response to hypoxia levels of the transcription factor Hypoxia-inducible factor-1 (HIF-1) rise, which mediates the cellular adaptation to the hostile hypoxic environment through the regulation of several biological processes (Vaupel and Harrison 2004). HIF-1 is a heterodimer consisting of an oxygen-regulated α-subunit (HIF-1α) and a constitutively expressed β-subunit (HIF-1β/ARNT) (Wang and Semenza 1995). In an O_2–dependent mechanism PHD proteins (prolyl-hydroxylase domain proteins, PHDs 1-3) carry out prolyl-4-hydroxylation of one of the O_2–dependent degradation domains (*N*-terminal NODD or *C*-terminal CODD) of HIF-1α (Bruick and McKnight 2001). This marks the protein for proteosomal degradation through the von Hippel-Lindau protein (VHL) elongin C/B complex (VCB) (Ivan et al. 2001; Jaakkola et al. 2001). In addition, the asparaginyl hydroxylase Factor Inhibiting HIF (FIH) hydroxylates Asn803 in the presence of O_2 (Lando et al. 2002; Hewitson et al. 2002). This residue is part of the *C*-terminal transactivation domain (C-TAD) of HIF-1α and hydroxylation prevents interaction with the p300 and CBP transcription coactivators (Schofield and Ratcliffe 2004) (Figure 1.3). The HIF hydroxylases are Fe(II)/2-oxoglutarate (2OG) -dependent oxygenases. Among them PHD2 has been recognised as the primary HIF prolyl hydroxylase which has been shown to react particularly slow with O_2, reflecting its role as an O_2 sensor (Berra et al. 2003; Takeda et al. 2008; Flashman et al. 2010). In the absence of O_2, HIF-1α accumulates and translocates to the nucleus where it forms a complex in conjunction with HIF-1β which then binds to the HRE (hypoxia responsive elements) enhancer regions in hypoxia-sensitive target genes (Figure 1.3). HIF-1 thus regulates the expression of an array of genes including those involved in glycolysis, angiogenesis and erythropoiesis (Vaupel and Harrison 2004).

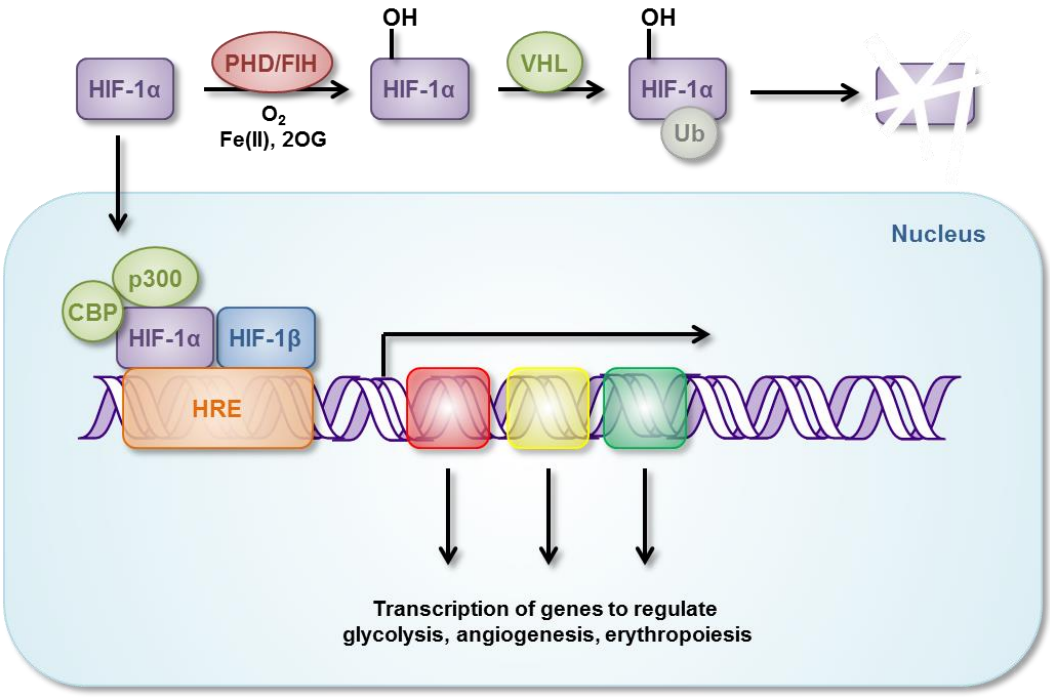

Figure 1.3. Schematic representation of the HIF-1α pathway.
In the presence of O_2, Fe(II) and 2OG HIF-1α is hydroxylated by PHDs which marks the protein for ubiquitination by the VHL tumour suppressor and subsequent proteosomal degradation. Under hypoxia, HIF-1α accumulates, translocates to the nucleus and forms a transcription factor in conjunction with HIF-1β. This HIF-1 complex binds to HREs in the promoters of genes involved in the cellular adaptation to hypoxia. Adapted from (Meijer et al. 2012).

Interestingly, HIF-1 has recently been shown to autoregulate its own α-subunit through an epigenetically regulated transactivation loop. A normally repressed HRE in the promoter of HIF-1α was shown to be demethylated and active in colon cancer cell lines and specimens (Koslowski et al. 2011). This transactivation could be disrupted by an inhibitor of protein-protein interaction between HIF-1α and HIF-1β (Asby et al. 2014). Loss of function of the VHL tumour suppressor and oncogene amplification in cancer cells can further activate HIF-1 and drive malignant progression (Kaelin 2008; Semenza 2013).

Hypoxia has been associated with resistance to all forms of conventional cancer therapy, malignant progression and poor patient prognosis (Harris 2002; Overgaard 2011; Hockel et al. 1996). Cellular sensitivity to ionising radiation (IR) depends on the tissue specific intrinsic radiosensitivity and extrinsic factors of the

tumour microenvironment. A poor oxygenation status of the irradiated tissue is one of the most important limiting factors in radiotherapy (Moeller, Richardson, and Dewhirst 2007; Thomlinson and Gray 1955). The importance of O_2 in radiotherapy has been attributed to two mechanisms. Firstly, O_2 can react with the free radicals that originate from water radiolysis, thus forming DNA-damaging reactive oxygen species (ROS). Secondly, O_2 can "fix" the radical-induced damage, a term which describes the formation of DNA peroxides which are less easily repaired than simple DNA strand breaks. Severely hypoxic cells (<0.1% O_2) are 2.5 to 3 times more radio resistant than their oxygenated counterparts, a phenomenon which has been termed the oxygen enhancement effect (Gray et al. 1953).

Resistance to chemotherapy stems from a range of mechanisms (Shannon et al. 2003). The poor vasculature of hypoxic tumours impairs drug delivery to those regions. In addition, tumour acidosis compromises the uptake of weakly basic drugs such as doxorubicin (Skovsgaard 1977). Most chemotherapeutics are antiproliferative agents and their action relies on the uncontrolled division of cancer cells. In hypoxia proliferation is inhibited which compromises the response to most chemotherapeutics. Severely hypoxic cells undergo p53-dependent apoptosis (Graeber et al. 1996; Hammond et al. 2002; Leszczynska et al. 2015). Cells with an impaired p53 pathway can thus escape cell death leading to the selection of cells with diminished apoptotic potential and increased resistance to anticancer therapy in severe hypoxia (Graeber et al. 1996; Kim et al. 1997).

1.2 The DNA damage response

1.2.1 DNA damage signalling

Cells are constantly subjected to various types of environmental and endogenous insults to their genetic material. Environmental sources of DNA damage include ultraviolet (UV) radiation from the sunlight, IR and chemical toxins. While these types of DNA damaging agents can be avoided, spontaneous DNA damage is the result of normal cell metabolism and has been estimated to generate up to 10^5 lesions per cell and day (Hoeijmakers 2009). From these different types of threats a multitude of lesions can arise which bring upon a change in the physicochemical structure of the DNA and pose a threat to genomic integrity. DNA lesions can block vital processes such as DNA replication and transcription or cause genomic aberrations if proliferation resumes with unresolved damage (Jackson and Bartek 2009; Harper and Elledge 2007; Ciccia and Elledge 2010). In order to deal with any threat to the genome, cells have evolved a complex and highly conserved signalling network known as the DNA damage response (DDR) (Figure 1.4). The DDR can be regarded as the DNA damage surveillance programme which detects an insult, mediates its presence and responds to it with cell cycle arrest and DNA repair or cell death (Ciccia and Elledge 2010; Harper and Elledge 2007). Defects within the DDR can result in enhanced mutation rates and cancer predisposition as evident in human DNA repair syndromes such as AT (ataxia telangiectasia), a genetic disorder which arises due to mutations in the *ATM* (ataxia telangiectasia mutated) gene (Jackson and Bartek 2009; Shiloh and Kastan 2001; Savitsky et al. 1995).

Traditionally, the DDR has been divided into two major branches based on the apical kinase central to the signalling cascade (Figure 1.4). The ATM/Chk2

(checkpoint kinase 2) pathway is activated following the detection of DSBs (double strand breaks) by the MRN (MRE11-RAD50-NBS1) complex while the ATR/Chk1 (ataxia telangiectasia mutated and Rad3 related/checkpoint kinase 1) pathway is activated by RPA-coated (replication protein A) SSBs (single strand breaks). Both pathways converge on the CDKs (cyclin-dependent kinases), which, in complex with cyclin proteins, are regulators of cell cycle progression. By preventing CDK activation, cells can arrest at checkpoints within the cell cycle (G_1/S, S, G_2/M). This arrest allows sufficient time for repair to take place before proliferation resumes. Reflecting the great diversity of lesions that can occur, cells have evolved a repertoire of repair pathways to neutralise them (Helleday et al. 2008; Sancar et al. 2004).

A key player within the DDR is the tumour suppressor p53. Upon genotoxic stress, p53 becomes stabilised and acts as a transcription factor which transactivates a number of genes involved in cell cycle arrest and apoptosis or senescence. In response to DNA damage, p53 sustains a G_1/S cell cycle arrest by stimulating the expression of $p21^{Waf1/Cip1}$, which is an inhibitor of CDKs and was one of the first p53 targets to be identified (Brugarolas et al. 1995; Deng et al. 1995). In addition, p53 can stimulate the expression of 14-3-3 proteins which bind to CDK-cyclin complexes to sequester them away from their substrates (Chan et al. 1999; Laronga et al. 2000). It is important to note that, in addition to initiating G_1/S cell cycle arrest, the p53-p21 axis is crucial to keep the checkpoint active (Bartek and Lukas 2001). Importantly, the majority of cancers harbour defects within the p53 pathway (Petitjean et al. 2007) and have an impaired G_1/S checkpoint, rendering these cells dependent on the remaining functional checkpoints. Through the regulation of a range of different pro-apoptotic

mediators p53 can contribute to the activation of programmed cell death (Vousden and Lu 2002).

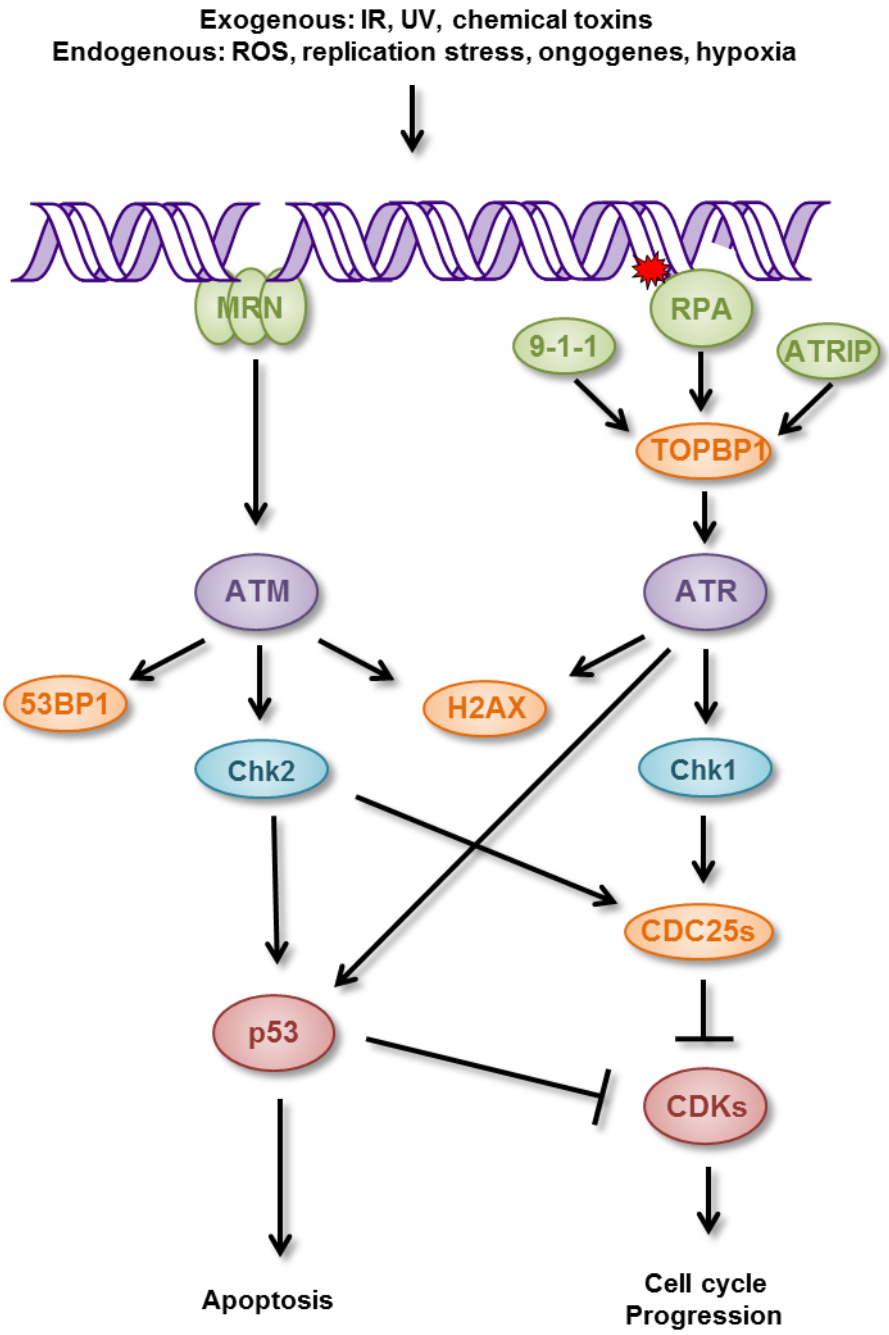

Figure 1.4. Schematic representation of the DNA damage response.
The DDR can be divided into two major branches. DSBs are sensed by the MRN complex which activates the ATM/Chk2-mediated signalling cascade. Following SSBs and replication stress, RPA binds to ssDNA to recruit ATRIP and 9-1-1 which, together with TOPBP1, initiate the ATR/Chk1 response. There is crosstalk between the two pathways and they both converge on the downstream effectors p53 and CDC25s, to induce apoptosis or cell cycle arrest. Adapted from (Sulli, Di Micco, and d'Adda di Fagagna 2012).

1.2.2 DNA Replication

One of the main triggers of the DDR is aberrant structures occurring during the course of DNA replication. These lead to stalling or slowing down of the replication fork which initiates an ATR/Chk1-mediated DDR commonly referred to as the replicative stress response (Hills and Diffley 2014; Zeman and Cimprich 2014; González Besteiro and Gottifredi 2015).

DNA replication is tightly regulated and involves the initiation, elongation and termination of the replication process (Figure 1.5) (Masai et al. 2010). Binding of the ORC (origin recognition complex) to DNA marks replication origins. Prior to the S phase of the cell cycle origins are licensed, the pre-RC (pre-replication complex) is formed at sites of ORC binding through recruitment of CDC6 (cell division cycle 6), CDT1 (chromatin licensing and DNA replication factor 1) and the MCM2-7 (mini-chromosome maintenance 2-7) complex. Multiple origins initiate the replication process, with each single active origin initiating a pair of replication forks. The number of licensed origins has been shown to exceed the number of replication origins. Activation of these dormant origins is an important mechanism to allow completion of global replication during replication stress and prevent genomic instability (Woodward et al. 2006; Ge, Jackson, and Blow 2007; Kawabata et al. 2011).

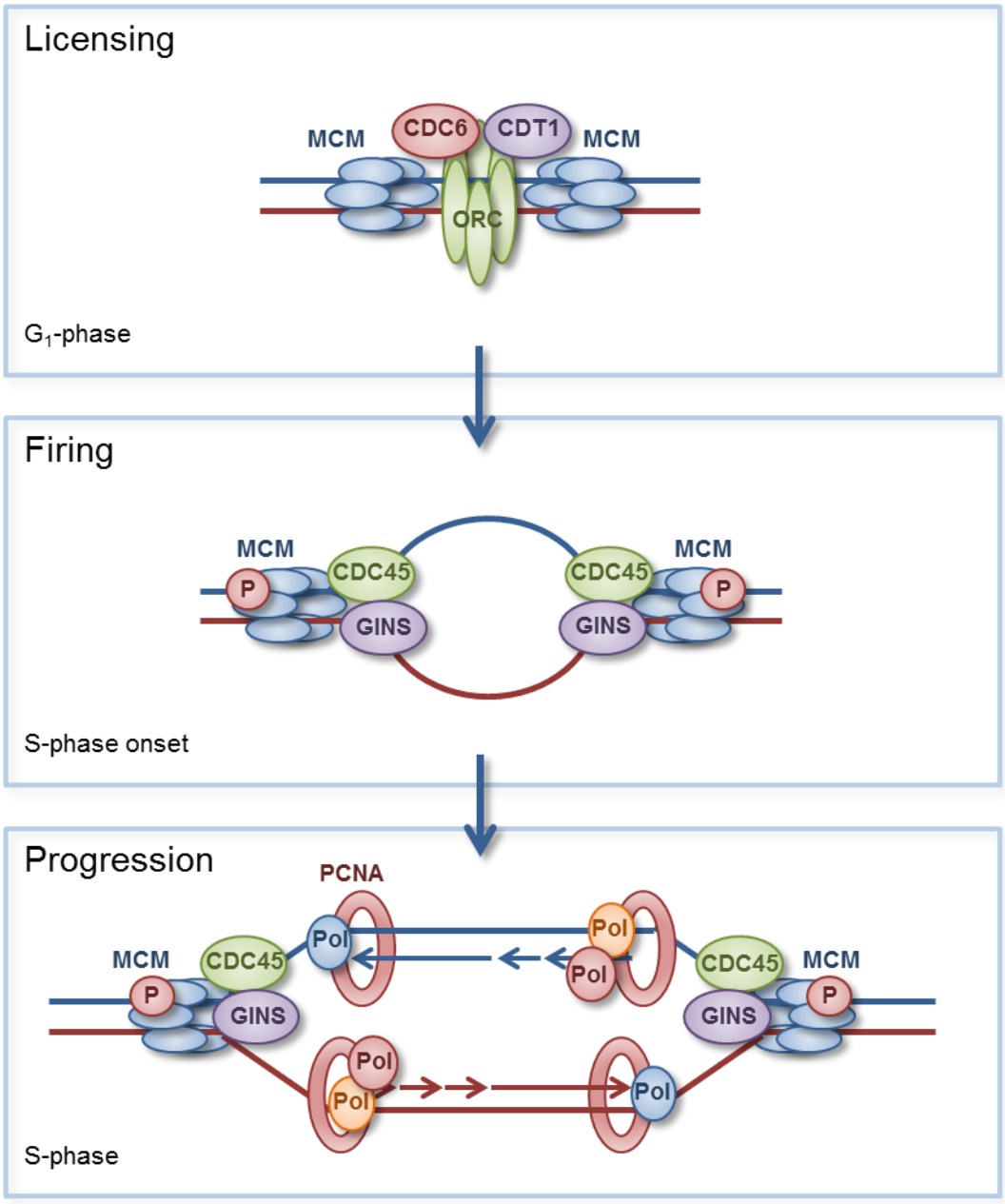

Figure 1.5. DNA replication.
Origins are licensed in the G_1 phase of the cell cycle through recruitment of the MCM2-7 helicase to sites of ORC, CDC6 and CDT1 binding and formation of the preRC. At the onset of S phase the preRC becomes phosphorylated which initiates formation of the replisome by loading of CDC45 and GINS and initiation of replication (origin firing). The MCM2-7 and CDC45 replicative helicases unwind the DNA, the PCNA sliding clamp tethers a set of DNA polymerases to the replication for which carry out DNA synthesis. Adapted from (Jones and Petermann 2012).

The pre-RC becomes phosphorylated by CDK2-Cyclin E complex and DDK (Dbf4/Drf1-dependent CDC7 kinase) in early S phase (Krude et al. 1997; Lei et al. 1997) which promotes treslin-dependent loading of CDC45 (cell division cycle 45) and GINS (go-itchi-ni-san) complex, initiating the actual process of DNA

synthesis (Takayama et al. 2003; Ilves et al. 2010; Guo et al. 2015). The replication machinery is called the replisome. Within this multi-component protein complex, the replicative MCM helicase unwinds the DNA while PCNA (sliding clamp proliferating cell nuclear antigen) tethers a set of DNA polymerases to the chromosome which carry out the DNA synthesis (Stukenberg, Studwell-Vaughan, and O'Donnell 1991). In this way, the replication forks move bi-directionally away from the origin during the elongation process. Each replication fork consists of a leading strand, where elongation is continuous, and a lagging strand where synthesis is stepwise and followed by ligation of Okazaki fragments. Replication is terminated, when forks from adjacent origins converge (Branzei and Foiani 2010).

1.2.3 Replication stress

Replication is a high risk process which requires the cell to coordinate the availability of replication factors and nucleotides with origin firing and fork progression speed (Anglana et al. 2003; Conti et al. 2007). Replication stress arises if this balance is disturbed and the cellular response is a checkpoint activation mediated by ATR and Chk1, reducing the rate of DNA replication through decreased origin firing and slowing or stalling of the replication process (Seiler et al. 2007; Masai et al. 2010).

There are many sources of replication stress, including a shortage of essential replication factors, fork barriers such as DNA lesions or transcription complexes and oncogene overexpression (Zeman and Cimprich 2014; González Besteiro and Gottifredi 2015).

DNA synthesis requires the availability of nucleotide building blocks. If these are limiting, fork progression can slow down. Experiments in budding yeast have shown that the ATR and Chk1 homologs Mec1 (mitosis entry checkpoint protein 1) and Rad53, respectively, were required for fork stabilisation following treatment with HU (hydroxyurea), an inhibitor of RNR (ribonucleotide reductase) which is the enzyme that provides the DNA building blocks (Cobb et al. 2003; Lopes et al. 2001). Replication stress arising from depletion of the dNTP (deoxyribose nucleoside triphosphate) pools was shown to ultimately cause genetic instability and cellular transformation (Bester et al. 2011). The firing of too many origins caused by elevated CDK activity can deplete the dNTP pools leading to fork slowing and replication stress (Beck et al. 2012). Various reports have shown that overexpression of oncogenes also causes replication stress. Activation of *RAS* (rat sarcoma) resulted in hyper-proliferation and DNA hyper-replication and the activation of the DDR, ultimately inducing senescence (Di Micco et al. 2006). Cyclin E overexpression was shown to accelerate S phase entry and cause origin hyper-activation resulting in the activation of the DDR and induction of senescence in U2OS cells (Bartkova et al. 2005; Bartkova et al. 2006). Bester and coworkers demonstrated that cyclin E overexpression led to deregulated cell proliferation due to accelerated S phase entry despite insufficient dNTP pools (Bester et al. 2011). Premature origin firing and increased origin density as a result of *MYC*-overexpression was recently attributed to a direct function of MYC upstream of CDC45 and GINS (Srinivasan et al. 2013).

If replication stress persists, replication forks that have been stalled for prolonged periods of time can lose their ability to restart and generate fork-associated DSBs through activity of the MUS81-Eme1 (MUS81 Structure-Specific

Endonuclease Subunit – Essential Meiotic Structure-Specific Endonuclease 1) endonuclease complex (Hanada et al. 2007). Under these circumstances only new origin firing can achieve completion of global replication (Petermann et al. 2010).

Despite the different origins of replication stress, the resulting cellular response is the activation of the ATR/Chk1 pathway through distinct DNA structures formed at sites of replication stress.

1.2.4 ATR activation and ATR-mediated Chk1 activation

A slowly progressing or stalled replication fork can give rise to regions of ssDNA if the enzymatic activities of the DNA polymerase and the replicative helicase uncouple, resulting in extensive unwinding of the DNA into long stretches of ssDNA (Pacek and Walter 2004; Byun et al. 2005). Similarly, processing of DNA lesions also generates ssDNA through exonuclease resection of the damaged structures (Aylon, Liefshitz, and Kupiec 2004; Ira et al. 2004).

Activation of the ATR/Chk1 pathway (Figure 1.6) requires ssDNA as well as primer-template junctions which are found following DNA damage and at stalled forks (MacDougall et al. 2007). The exposed stretches of ssDNA are bound by RPA. A specific interaction between RPA and ATRIP (ATR-interacting protein) then recruits ATR to sites of replication stress, thus forming an ATR-ATRIP complex (Zou and Elledge 2003). Independent of ATR-ATRIP, the 9-1-1 (RAD9-HUS1-RAD1) checkpoint clamp is loaded onto primer-template junctions by Rad17-RFC (RAD17-Replication factor C complex) (Majka et al. 2006; Zou, Cortez, and Elledge 2002). Consequently, the ATR activator TOPBP1 (Topoisomerase Binding Protein 1) is recruited to sites of 9-1-1 binding where it

interacts with both, 9-1-1 and ATR-ATRIP, to activate ATR (Lee, Kumagai, and Dunphy 2007; Mordes et al. 2008).

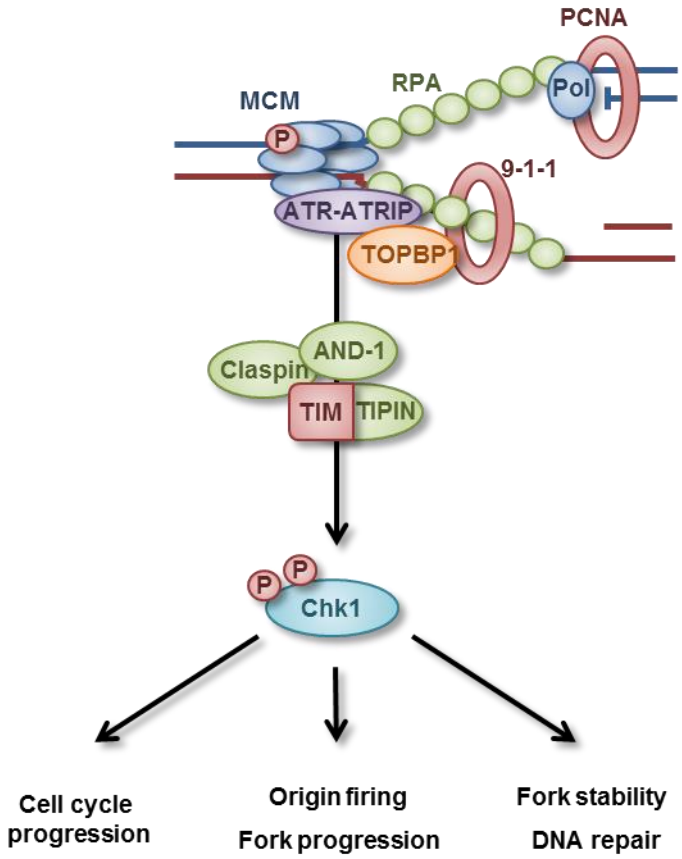

Figure 1.6. Activation of the ATR/Chk1 axis in response to replication stress.
Stalled replication forks give rise to regions of ssDNA. These become coated by RPA which binds ATRIP and loads the 9-1-1 clamp. 9-1-1 attracts TOPBP1 and ATRIP recruits ATR to the fork which then becomes activated by TOPBP1. Subsequent ATR-mediated Chk1 phosphorylation requires Claspin, TIM-TIPIN and AND-1. Once activated, Chk1 can initiate various downstream responses. Adapted from (Jones and Petermann 2012).

Once activated, ATR phosphorylates Chk1 on S317 and S345 in a process requiring several other proteins including TOPBP1, Claspin, the TIM-TIPIN (TIMELESS homologue – TIMELESS-interacting protein) heterodimeric complex and AND-1 (acidic nucleoplasmic binding protein 1) (Chou and Elledge 2006; Errico, Costanzo, and Hunt 2007; Kemp et al. 2010; Kumagai and Dunphy 2000; S. Liu et al. 2006; Hao et al. 2015). ATR-dependent phosphorylation of Chk1 at sites of DNA damage induces the release of Chk1 from chromatin into

the nucleoplasm where it undergoes autophosphorylation on serine 296 (Kasahara et al. 2010; Smits, Reaper, and Jackson 2006).

1.2.5 Function of Chk1

Chk1 is a serine/threonine protein kinase that was initially identified in fission yeast where it was found essential for DNA damage-induced cell cycle arrest (Walworth, Davey, and Beach 1993). Phosphorylated and active Chk1 serves different functions of which the best characterised are the Chk1-mediated checkpoint responses. Chk1 regulates the G_1/S and intra S phase checkpoints as well as mitotic entry (G_2/M checkpoint).

The CDC25 dual-specificity phosphatases (CDC25A, -B and -C) activate CDK-Cyclin complexes and thereby promote cell cycle progression (Boutros, Dozier, and Ducommun 2006). CDC25s regulate S phase entry and progression through CDK2-Cyclin E and CDK2-Cyclin A, respectively (Sørensen et al. 2003) while CDK1-Cyclin B promotes G_2/M progression (De Souza, Ellem, and Gabrielli 2000).

Chk1 has been shown to negatively regulate all three isoforms of the CDC25s. Chk1-dependent phosphorylation either marks CDC25s for proteosomal degradation or creates a binding site for 14-3-3 proteins (Busino et al. 2003; Jin et al. 2003). Binding of 14-3-3 enables sequestration of the phosphatases to the cytoplasm and away from their substrates (Hermeking and Benzinger 2006; Boutros, Dozier, and Ducommun 2006) or blocks interaction between CDC25 and CDK-Cyclin complexes (Chen, Ryan, and Piwnica-Worms 2003). Following UV irradiation, Chk1 autophosphorylation on S296 was required for Chk1-dependent degradation of CDC25A to block premature entry into mitosis (Kasahara et al. 2010).

Interestingly, inhibition of CDK-Cyclin complexes through Chk1 activity is further reinforced by the WEE1 kinase. WEE1 is activated by Chk1 and phosphorylates CDK-Cyclin complexes on Tyr15 which negatively regulates the activity of the complex (Parker and Piwnica-Worms 1992). Thus, the Chk1-mediated DDR provides a double-lock mechanism to block cell cycle progression through the CDC25s and WEE1.

Importantly, Chk1 has been proven to also have basal activity in the absence of damage. A representation of the role of Chk1 in normal cell cycle progression can be seen in Figure 1.7, A. Chk1-dependent degradation of CDC25A regulates S phase entry and progression not only under stressed but also unperturbed conditions (Sørensen et al. 2003; Sørensen et al. 2004). Normal G_2/M transition was shown to be controlled through centrosome-associated Chk1. Chk1 localises to the centrosome during interphase to prevent premature CDK1 activation through phosphorylation of CDC25B, but was not found at the centrosome during mitosis when CDK1 activation was required (Krämer et al. 2004; Schmitt et al. 2006). Normal mitotic entry was also suggested to be transcriptionally regulated by Chk1 (Shimada et al. 2008). Chk1 was shown to phosphorylate histone H3 on Tyr11, thereby enabling acetylation at the promoters of *CDK1* and *CYCLIN B1* and triggering transcription of these genes (Shimada et al. 2008). Interestingly, under unperturbed conditions around 20% of total Chk1 is chromatin bound but upon DNA damage, the entire Chk1 pool is released into the nucleoplasm, suggesting that transcriptional regulation of G_2/M progression through Chk1 selectively occurs in the absence of damage (Smits, Reaper, and Jackson 2006). The dissociation of Chk1 from chromatin is

dependent on ATR-mediated phosphorylation on S317 and S345 and required for checkpoint activation (Smits, Reaper, and Jackson 2006).

In addition to controlling cell cycle progression, different aspects of DNA replication are regulated through Chk1 such as origin firing, replication fork progression and stability (Figure 1.7, B). Following treatment with the topoisomerase inhibitor camptothecin, a Chk1-dependent reduction in the initiation of DNA replication was observed (Seiler et al. 2007). In agreement with this, inhibition of Chk1 results in increased origin firing (Syljuåsen et al. 2005; Maya-Mendoza et al. 2007). Recently evidence has emerged that checkpoint-activated Chk1 blocks the initiation of new replication clusters while preferentially promoting late origin firing within already active clusters through an as of yet unknown mechanism (Ge and Blow 2010; Platel et al. 2015). Chk1 can block the initiation of replication by negatively regulating treslin-mediated loading of CDC45 onto chromatin and disabling the association of CDC45 and the preRC at origins of replication (Liu et al. 2006; Guo et al. 2015). Inhibition or depletion of Chk1 in camptothecin- or UV-treated cells resulted in decreased fork progression (Seiler et al. 2007; Speroni et al. 2012) and this might be linked to increased origin firing under those conditions (Petermann, Woodcock, and Helleday 2010). Petermann and coworkers recovered replication fork progression in Chk1-depleted cells by simultaneously inhibiting/depleting CDC7 to inhibit origin firing (Petermann, Woodcock, and Helleday 2010).

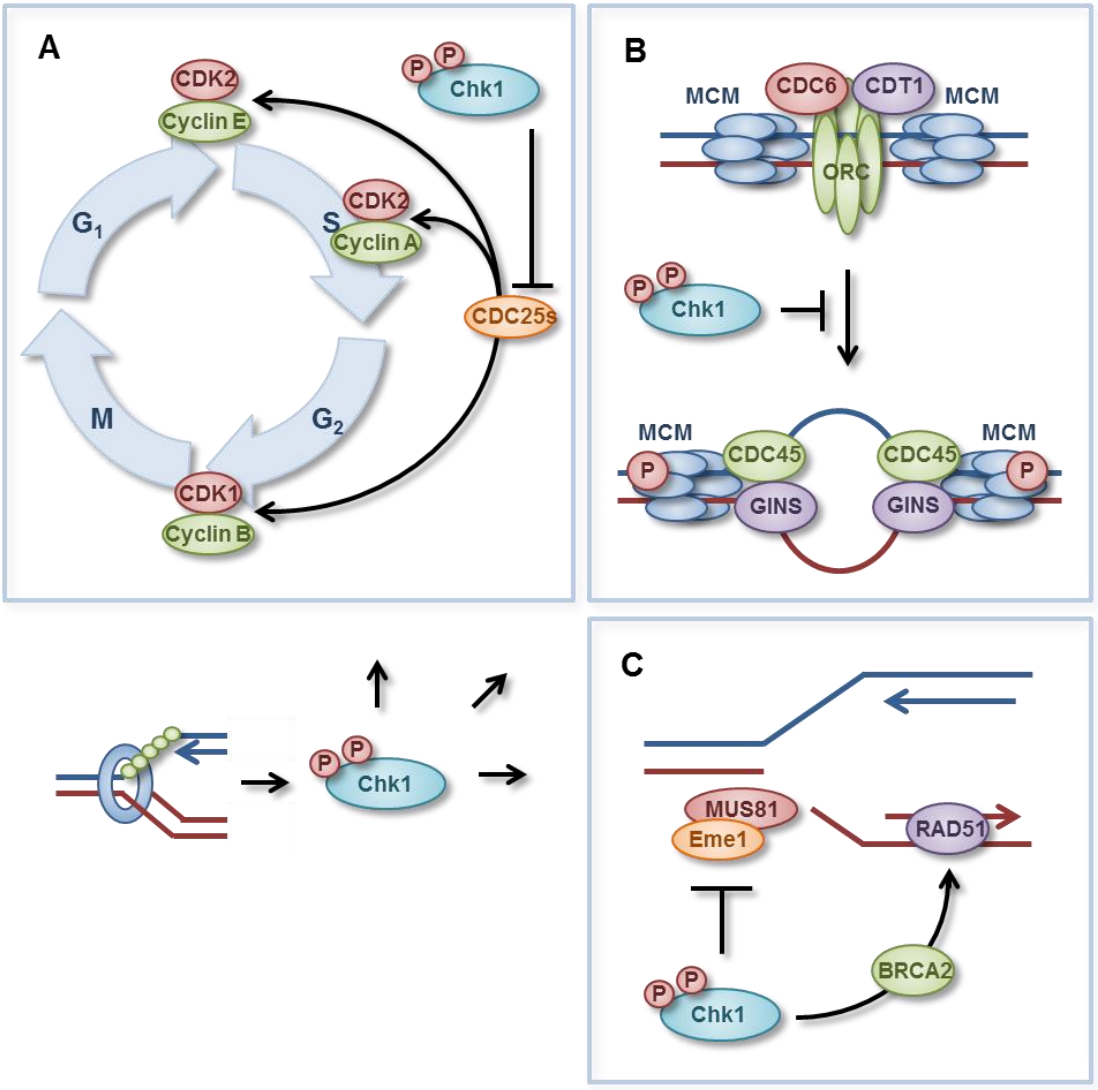

Figure 1.7. Chk1 regulates cell cycle progression, replication and DNA repair.
A) Chk1 negatively regulates the CDC25 dual-specificity phosphatases which are activators of CDK/Cyclin complexes. Chk1 thereby blocks cell cycle progression. B) Active Chk1 blocks origin firing by preventing the association of CDC45 with the preRC. C) Chk1 prevents the formation of DSBs at stalled forks by protecting them from the MUS81-Eme1 endonuclease. In addition, Chk1 promotes HR repair by phosphorylating BRCA2 which recruits RAD51 to sites of damage. Adapted from (Boutros, Lobjois, and Ducommun 2007; Jones and Petermann 2012).

As mentioned earlier, stalled replication forks can eventually collapse and generate fork-associated DSBs through activity of the MUS81-Eme1 endonuclease complex (Hanada et al. 2007). Chk1 promotes DNA repair through HR (homologous recombination) following fork collapse by phosphorylating BRCA2 (breast cancer 2, early onset) and RAD51 to promote BRCA2-mediated loading of RAD51 onto DNA (Figure 1.7, C) (Sørensen et al. 2005; Bahassi et al.

2008). Inhibition or depletion of Chk1 by siRNA (small interfering ribonucleic acid) could prevent and also reverse RAD51 foci formation (Sørensen et al. 2005; Montano et al. 2013; Engelke et al. 2013). Interestingly, in addition to promoting the repair of collapsed forks, Chk1 seems to protect stalled forks from MUS81-Eme1 to avoid DSB-formation in the first place. Chk1 deficient cells showed higher levels of DNA damage and this was dependent on MUS81-Eme1 (Forment et al. 2011).

1.2.6 The DNA damage response in hypoxia

It has been well documented that severe levels of hypoxia (<0.1% O_2) activate a DNA damage response in the absence of detectable damage, as assessed by comet assay and the absence of 53BP1 (p53-binding protein 1) foci (Schematic representation of the hypoxic DDR in Figure 1.8) (Bencokova et al. 2009; Hammond et al. 2002; Hammond, Dorie, and Giaccia 2003; Olcina et al. 2013). Despite the lack of DNA strand breaks in severe hypoxia, H2AX is robustly phosphorylated on serine 139 (also known as γH2AX) in a pan-nuclear fashion (Bencokova et al. 2009). In response to DNA damaging agents, γH2AX forms discrete foci but the contrary has been shown in response to replication stress with an ATR-dependent, pan-nuclear signal (Toledo et al. 2011; Syljuåsen et al. 2005), suggesting that the γH2AX signal in severe hypoxia originates from replication stress (Hammond et al. 2002).

The replicative stress response initiated by severe hypoxia has been linked to a decreased level in dNTP pools (Pires, Bencokova, Milani, et al. 2010). Maintenance of adequate dNTP levels requires activity of RNR which is the only known enzyme responsible for the *de novo* synthesis of the DNA building blocks

through reduction of ribonucleotides to deoxyribonucleotides (Nordlund and Reichard 2006). Eukaryotic RNR is an O_2-dependent enzyme which requires O_2 in order for its smaller R2 subunit to remain in its catalytically active form and therefore RNR activity is likely to be compromised in hypoxia (Nordlund and Reichard 2006; Eklund et al. 2001). As described earlier, depletion of the dNTP pool has been shown to give rise to replication stress (Bester et al. 2011; Poli et al. 2012; Beck et al. 2012). Under severe hypoxia, origin firing is decreased, fork progression slowed down and the number of stalled replication forks increased (Pires, Bencokova, McGurk, et al. 2010). The critical structure that initiates recruitment of replication stress proteins, including ATR, are RPA-coated stretches of ssDNA. The formation of RPA foci at regions of ssDNA was seen in hypoxia and this is believed to initiate the hypoxia-induced DDR (Pires, Bencokova, Milani, et al. 2010).

Interestingly, activation of ATM also occurs in severe hypoxia (Bencokova et al. 2009). This observation is in contrast to the well-established role of ATM as a sensor and responder to DSBs (Jackson and Bartek 2009) since the hypoxia-induced activation of ATM occurs in the absence of detectable damage and independently of the MRN complex (Bencokova et al. 2009). A recent report shows that ATM activation in severe hypoxia requires a specific chromatin context. Hypoxia induces histone H3 lysine 9 tri-methylation (H3K9me3), a modification associated with condensed chromatin and replication stress in this background leads to the activation of ATM (Olcina et al. 2013). ATM inhibition in severe hypoxia resulted in decreased replication rates demonstrating a role for ATM in facilitating replication during replication stress. More recently, chromatin condensation has been shown to be an integral part of the DDR and the

activation of ATM as well as ATR in a condensed chromatin context was demonstrated in the absence of damage (Burgess et al. 2014).

The hypoxic DDR also involves the tumour suppressor p53. P53 is activated in response to severe hypoxia through ATR-dependent phosphorylation (Hammond et al. 2002) and also the ATM/Chk2 axis (Gibson, Bindra, and Glazer 2005). P53 was shown to be essential for hypoxia-induced apoptosis (Graeber et al. 1996). Loss of the *P53* gene or mutations within the p53 pathway reduces hypoxia-induced cell death and severe hypoxia thus selects for cells with diminished apoptotic potential (Graeber et al. 1996). A recent study showed that in response to severe hypoxia p53 induces a select group of genes, some of which induce apoptosis by inhibition of the pro-survival protein AKT (synonym for protein kinase B). The loss of pro-apoptotic genes induced by p53 in severe hypoxia was shown to correlate with poor clinical outcome in patients with various cancer types (Leszczynska et al. 2015; Yun and Glazer 2015).

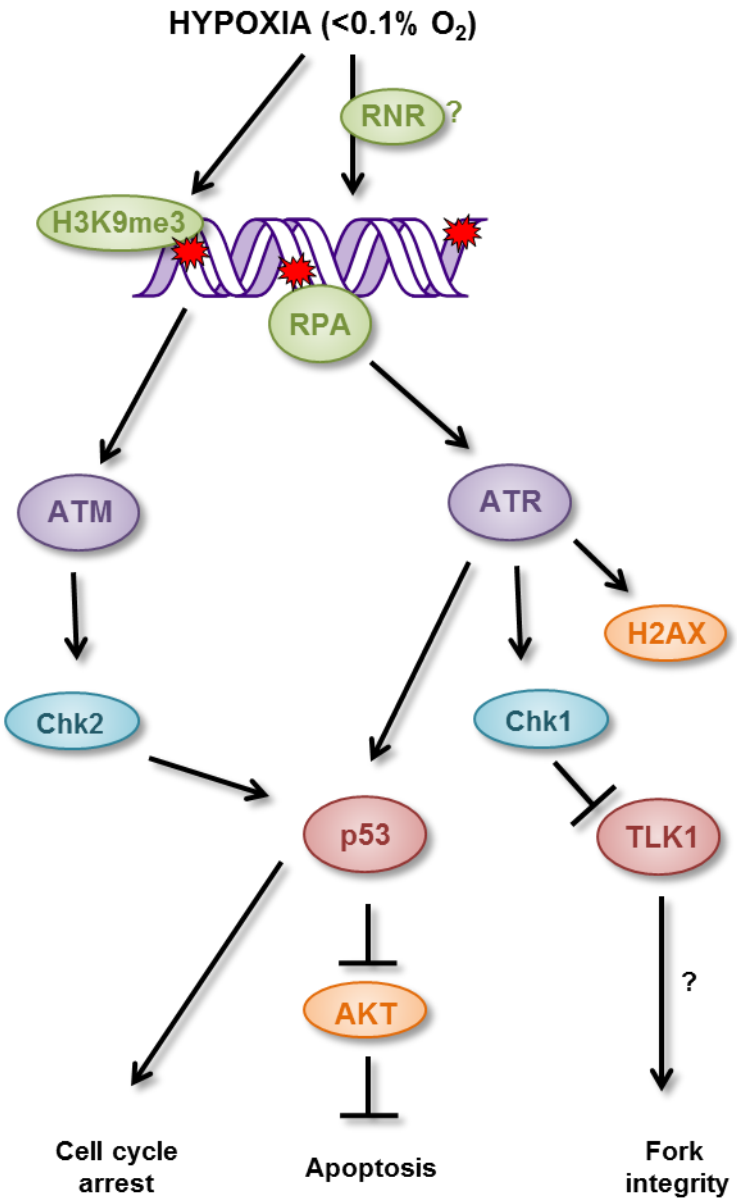

Figure 1.8. Schematic representation of the DDR in severe hypoxia.
Severe hypoxia initiates a DDR, probably stemming from decreased RNR activity and depletion of the dNTP pool. The hypoxia-induced DDR involves both, the ATR and ATM kinases. ATR is activated in response to RPA-coated ssDNA while ATM activation additionally requires the histone modification H3K9me3. Both kinases phosphorylate downstream targets leading to cell cycle arrest, p53-dependent apoptosis through inhibition of the pro-survival protein AKT and potentially stabilisation of replication forks.

1.2.7 Hypoxia-induced ATR/Chk1 signalling

In acute severe hypoxia, Chk1 is phosphorylated at the ATR-targeted sites S317 and S345 and inhibition or depletion of ATR or Chk1 resulted in the

accumulation of DNA damage (Hammond et al. 2002; Hammond, Dorie, and Giaccia 2004). Moreover, Chk1 autophosphorylation on S296 and Chk1-mediated phosphorylation of TLK1 (tousled-like kinase 1) indicate that Chk1 is active in severe hypoxia (Pires, Bencokova, McGurk, et al. 2010; Cazares-Körner et al. 2013). TLK1 is an S phase active kinase which is inactivated through Chk1-dependent phosphorylation following genotoxic stress and was recently found to promote histone supply during DNA replication (Groth et al. 2003; Krause et al. 2003; Silljé et al. 1999; Klimovskaia et al. 2014).

The exact role of Chk1 during severe hypoxia however is unclear. Although everything seems to point towards a role for Chk1 during the hypoxia-induced replicative stress response, inhibition of Chk1 during severe hypoxia did not affect the number of ongoing replication forks and an overall decrease of fork progression speed upon Chk1 inhibition was not exacerbated by severe hypoxia (Pires, Bencokova, Milani, et al. 2010). It is likely that initiation of new origins of replication is inhibited even in the absence of Chk1 due to a shortage of dNTPs in severe hypoxia, but complex rescue-experiments are required to test this hypothesis.

Interestingly, Chk1 signalling during severe hypoxia is a transient response and phosphorylation of serines 317, 345 and 296 and of TLK1 decrease during prolonged hypoxic exposure (Pires, Bencokova, Milani, et al. 2010; Cazares-Körner et al. 2013). This suggests that the hypoxia-induced DDR is not sustained under chronic severe hypoxia (>12 h) and this hypothesis is supported by the observation that under those conditions the number of RPA foci decreased (Pires, Bencokova, Milani, et al. 2010; Pires, Bencokova, McGurk, et al. 2010).

1.2.8 Reoxygenation

The tumour microenvironment is dynamic and periods of hypoxia are often followed by reoxygenation due to changes in perfusion of microvessels (Dewhirst, Cao, and Moeller 2008). Reoxygenation induces significant amounts of DNA damage and this is most likely due to the generation of ROS since free radical scavengers could prevent this damage (Hammond, Dorie, and Giaccia 2003). In response to reoxygenation-induced oxidative damage hypoxia-induced ATM-Chk2 signalling is maintained resulting in p53 phosphorylation and a Chk2-mediated G_2 arrest. Upon loss of Chk2, this response was abrogated and cells underwent apoptosis (Freiberg, Hammond, et al. 2006; Freiberg, Krieg, et al. 2006).

Following acute periods of severe hypoxia (<12 h), replication restart can occur after reoxygenation however cells with a functional p53 pathway undergo apoptosis. After prolonged exposure to severe hypoxia (>12 h), disassembly of the replisome prevents the resumption of replication even after reoxygenation (Pires, Bencokova, Milani, et al. 2010). Thus, reoxygenation following hypoxia-induced arrest either leads to checkpoint activation and continued proliferation or loss of replication ability and cell death. The fate of the cell depends on the duration of the hypoxic stress as well as the specific genetic background. Importantly, cells exposed to severe hypoxia for prolonged time periods do not contribute to tumour growth since they are unable to proliferate even if reoxygenation occurred. It has however been shown that DNA repair mechanisms can become compromised in hypoxic conditions that still allow replication or replication restart. Propagation of such cells can contribute to genetic instability and malignant progression since replication restart takes place

in the presence of ROS-induced damage, with impaired DNA repair capabilities and often in a *P53* mutant background (Luoto, Kumareswaran, and Bristow 2013).

If acutely severely hypoxic cells are reoxygenated in the presence of a Chk1 inhibitor, the numbers of newly fired replication origins increase, pointing towards a role for Chk1 in delaying origin firing after reoxygenation-induced damage (Pires, Bencokova, Milani, et al. 2010). Loss of Chk1 through siRNA knockdown sensitised HCT116 cells to acute severe hypoxia followed by reoxygenation and resulted in reduced clonogenic survival (Hammond, Dorie, and Giaccia 2004). Similarly, various Chk1 inhibitors have been used to demonstrate increased cell killing and accumulation of DNA damage if Chk1 is lost during severe hypoxia/reoxygenation (Pires, Bencokova, McGurk, et al. 2010; Hasvold et al. 2013; Cazares-Körner et al. 2013). It is therefore likely that Chk1 delays origin firing following reoxygenation in order to allow repair of ROS-induced damage to take place before replication is resumed.

1.2.9 The importance of Chk1 in cell survival

Early research showed that the deletion of Chk1 results in a G_2/M checkpoint defect in mouse blastocysts and in embryonic lethality through apoptosis (Liu et al. 2000; Takai et al. 2000). Similar results were obtained in mouse breast tissue where depletion of Chk1 triggered apoptosis (Lam et al. 2004). Through site-specific mutagenesis it has been established that different Chk1 phosphorylation sites regulate the essential and DNA damage functions of Chk1, suggesting that those two functions are uncoupled (Wilsker et al. 2008; Niida et al. 2007). While targeted mutation of S317 in Chk1 abrogated the G_2/M

checkpoint and affected DNA replication, this mutation did not impact cell viability. On the other hand, mutation of S345 failed to create a viable cell line and this was attributed to phosphorylation of Chk1 on S345 during unperturbed mitosis (Wilsker et al. 2008).

Partial deletion of Chk1 was associated with increased genomic instability. Chk1 heterozygosity caused high levels of CDC25A and resulted in tumorigenic haploinsufficient phenotypes displaying inappropriate G_2/M and G_1/S cell cycle transitions and the accumulation of DNA damage in S-phase (Lam et al. 2004). Moreover, heterozygous mutations in *Chk1* have been found in different cancers (Menoyo et al. 2001; Bertoni et al. 1999). A more recent study showed that although Chk1 heterozygosity caused abnormalities in mouse mammary glands, only simultaneous deletion of one allele of p53 resulted in tumour formation. On the other hand, Chk1 deficiency in p53 null mice inhibited tumourigenesis, suggesting the relationship between Chk1 and p53 to be complex (Fishler et al. 2010).

These studies demonstrate that caution is warranted when inhibiting Chk1 in cancer therapy due to its pivotal role in normal cell proliferation and genome integrity. Inhibition of Chk1 can drive tumour development in favourable genetic backgrounds.

1.3 Chk1 inhibition for the treatment of cancer

1.3.1 Checkpoint targeting in cancer therapy

A general strategy in cancer therapy is cell death through the induction of excessive DNA damage by radio- or chemotherapy. Toxicities towards normal,

especially highly proliferating cells (such as the hair follicles or the epithelia in the gastrointestinal tract) limit the doses of any such therapeutic regime. The therapeutic window is the dose range of an agent that can cause a therapeutic effect while staying within a tolerable toxicity range. Widening of this window has been suggested through the exploitation of differences between healthy and cancerous cells. As described earlier, cells can activate a complex DDR in response to DNA damage. An integral part of the DDR is the activation of cell cycle checkpoints which cause cell cycle arrest while also mediating the recruitment of DNA repair factors to enable the timely repair of any damage before proliferation can resume. If the extent of damage is beyond the cell's repair capacity, programmed cell death is initiated to prevent genetic aberrations.

Cancer cells often harbour defects in their checkpoint machinery. Deletions in the *P53* gene or other defects in the ATM-Chk2-p53 pathway are the most common mutations in cancer (Petitjean et al. 2007; Hollstein et al. 1991). They lead to G_1/S checkpoint deficiency and a greater reliance on the remaining functional processes (*i.e.* the Chk1-controlled S and G_2/M checkpoints) later throughout the cell cycle in order to avoid mitotic entry in the presence of damage. Targeting of these checkpoints through inhibition of Chk1 is therefore an attractive strategy to chemo-sensitise p53-defective cancers to standard DNA damaging agents (Figure 1.9) (Chen et al. 2012; Garrett and Collins 2011).

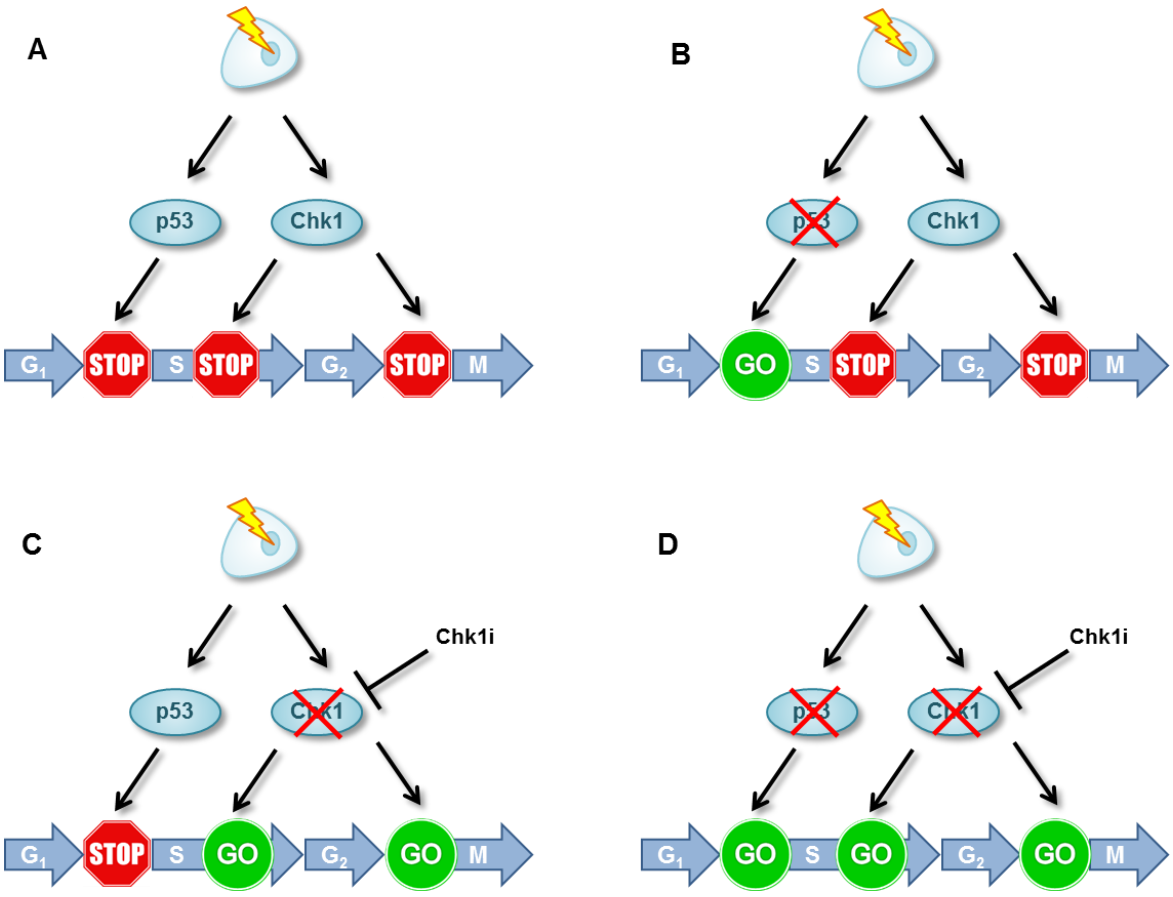

Figure 1.9. Selective targeting of p53 deficient cancer cells through inhibition of Chk1.
A) In response to DNA damage (yellow symbol) untransformed cells have checkpoints in place to stop cell cycle progression before entering mitosis. B) Cancer are commonly G_1/S checkpoint deficient due to mutation in the *TP53* gene or the p53 pathway. They rely on the Chk1-regulated S and G_2/M checkpoints. C) Inhibition of Chk1 in normal cells is compatible with viability since DNA repair takes place during the G_1/S checkpoint. D) Inhibition of Chk1 in p53-deficient cancer cells results in cell death due to premature mitosis. Adapted from (Chen et al. 2012; Ma, Janetka, and Piwnica-Worms 2011).

More recently, evidence has emerged that Chk1 inhibitors demonstrate single agent activity in tumours with specific genetic backgrounds such as DNA repair defects, a constitutive activation of the DDR or oncogene-induced replication stress. Such a relationship is commonly termed as synthetic lethality and presents an elegant strategy for selectively targeting malignancies over normal cells (Shaheen et al. 2011; Brough et al. 2011).

The FA (Fanconi Anemia) pathway is responsible for the repair of DNA crosslinks and defects in this pathway have been linked to chromosomal instability and cancer predisposition (Wang 2007). Cells deficient in the FA

pathway are sensitive to Chk1 inhibition or silencing by siRNA and in turn silencing of FA genes resulted in Chk1 hyper-activation (Chen et al. 2009). Cells derived from patients with complex karyotype acute myeloid leukaemia (AML) were sensitive to Chk1 inhibition by the kinase inhibitor UCN-01 and Chk1 siRNA and this was linked to the constitutive activation of the DDR in these cells (Cavelier et al. 2009). Inhibition of Chk1 with a potent small molecule inhibitor was also cytotoxic in a range of melanoma cell lines with high levels of endogenous DNA damage (Brooks et al. 2013)

Sensitivity to inhibition of the ATR/Chk1 pathway has further been linked to oncogene-induced replication stress. *In vivo*, the development of MYC-driven lymphomas and pancreatic tumours with high levels of replication stress could be completely prevented in a particular mouse model of the ATR-Seckel syndrome in which ATR is significantly downregulated (Murga et al. 2011). In line with this, MYC-driven lymphomas were effectively targeted through inhibition of Chk1 in several studies (Murga et al. 2011; Ferrao et al. 2012; Bryant, Scriven, and Massey 2014). Chk1 was shown to be phosphorylated at S345 and S296 in different neuroblastomas and higher Chk1 mRNA levels were found in MYCN- (MYC-neuroblastoma-related) amplified tumours. In addition, the sensitivity of neuroblastoma cell lines to Chk1 inhibition correlated with MYCN protein levels (Cole et al. 2011). Likewise, MYC was proposed to directly upregulate Chk1 mRNA and protein levels and Chk1 shown to be essential for the survival of MYC-overexpressing cells (Höglund et al. 2011). In line with these findings, gene amplification of Chk1 rendered cells more tolerant towards oncogene-induced replication stress (López-Contreras et al. 2012). A recent study suggests that Chk1 inhibition mediates single agent activity by reactivating the protein

phosphatase 2A (PP2A) tumour suppressor which inhibits MYC activity through dephosphorylation (Khanna et al. 2013).

1.3.2 Chk1 structure

Chk1 is an evolutionarily highly conserved serine/threonine protein kinase (Sanchez et al. 1997). This class of kinases binds substrate proteins and transfers the terminal phosphate group from ATP to the hydroxyl of a serine or threonine on the substrate protein. The human genome encodes hundreds of protein kinases, all of which share a highly conserved catalytic domain. The 88-residue, β-sheet-rich *N*-terminal lobe and the 210-residue, mainly helical *C*-terminal lobe of the kinase are connected by the hinge region (residues 84-89) (Figure 1.10, A) (Chen et al. 2000; Zhao et al. 2002). The ATP-binding site is located at the interface of the two lobes where ATP binds with the adenine ring forming polar interactions with the hinge region of the kinase (Figure 1.10, B). A hydrophilic channel which extends into the substrate binding site binds the ribose and the triphosphate group of ATP. The substrate protein binding region is mainly located within the *C*-terminal lobe. The activation lobe generally regulates the activity of a kinase through conformational changes in response to posttranslational modifications, such as phosphorylation. It contains the highly conserved DFG and APE (three-letter amino acid abbreviations) motifs at the start and end of the lobe which, together with the flexible glycine-rich loop (residues 16-23) are crucial for the function of the kinase in coordinating the magnesium ions to the phosphates of ATP (Johnson et al. 1998).

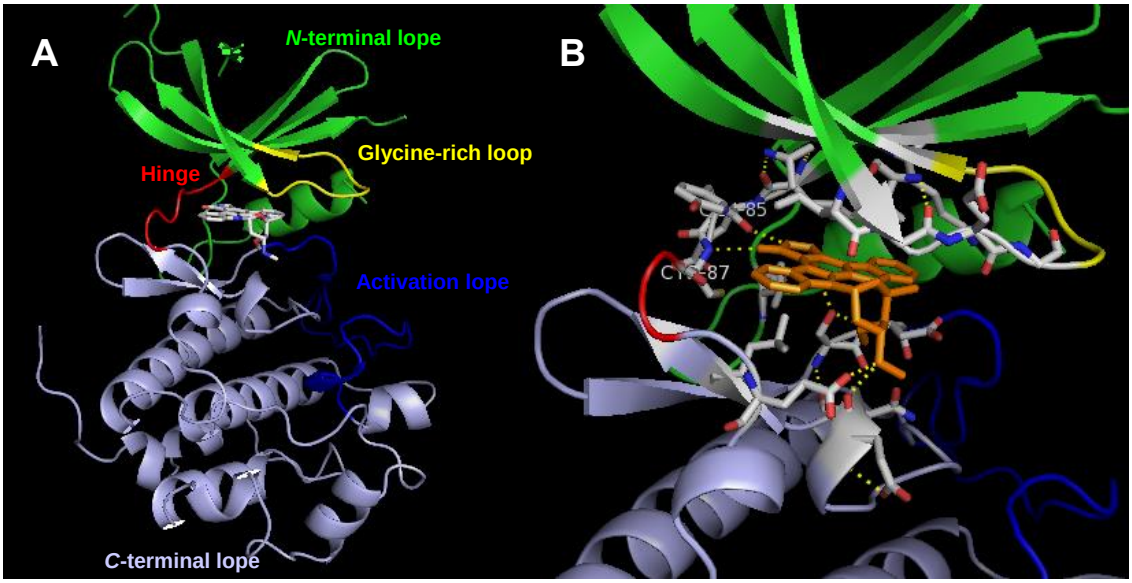

Figure 1.10. Chk1 kinase domains and ATP-binding site.
Chk1 kinase is shown in complex with the ligand UCN-01 (PDB 1nvq) since to date there is no crystal structure available with the natural substrate ATP (Zhao et al. 2002). A) The main domains of Chk1 are depicted, with the catalytically important glycine-rich loop and hinge-region surrounding the ligand binding-site. The flexible activation lope is part of the *C*-terminal domain. The *N*-terminal lope consists mainly of β-structures while the *C*-terminal lope is heavy in α-helices. B) Shown are the residues that make up the ATP-binding site (Sanchez et al. 1997) and polar interactions with the ligand UCN-01. The residues Cys87 and Glu85 within the hinge region are highlighted as they are important residues for the binding of most ATP-competitive Chk1 inhibitors.

1.3.3 Small-molecule inhibitors of Chk1

Over the last decade enormous progress had been made in understanding the underlying biology and suitable contexts for Chk1 inhibition. At the same time the development of selective inhibitors has advanced rapidly. Many research groups have published inhibitors of Chk1, some of which have progressed through preclinical studies and entered clinical trials.

Although there have been some publications reporting allosteric Chk1 inhibitors (Converso et al. 2009; Vanderpool et al. 2009), by far the vast majority to date are ATP-competitive inhibitors that bind to the Chk1 hinge region. Most small molecule inhibitors of Chk1 have been published with crystal structures

which typically show binding to the hinge region through the formation of hydrogen bonds with one or more of the three residues Glu85, Tyr86 and Cys87 (Matthews, Jones, and Collins 2013).

UCN-01 (7-hydroxystaurosporine) was originally isolated as a selective protein kinase C inhibitor (Takahashi et al. 1987) but also inhibits Chk1, Chk2 and CDK1 amongst other targets. Early studies showed that UCN-01 abrogated the IR-induced G_2/M checkpoint in HeLa cells by preventing 14-3-3 binding and phosphorylation of CDC25C (Graves et al. 2000). Similarly, Chk1 depletion or inhibition by UCN-01 prevented G_2/M arrest following doxorubicin treatment and induced apoptosis (Luo et al. 2001). In U2OS cells UCN-01 reduced the degradation of CDC25A after IR, resulting in increased CDK2/Cyclin E and CDK2/Cyclin A activity and unscheduled S phase entry and progression (Sørensen et al. 2003). UCN-01 further enhanced the antiproliferative effect of cisplatin in A549 and H596 lung cancer cells and potentiated camptothecin-induced DNA damage in HCT116 colon cancer cells (Mack et al. 2003; Furuta et al. 2006).

Since the discovery of UNC-01 a range of more selective and potent Chk1 inhibitors have been developed. The dual Chk1/Chk2 inhibitor AZD7762 evolved from a thiophene carboxamide hit in a high throughput screen (Janetka et al. 2008). Further lead optimisation, improved selectivity for Chk1, *in vitro* potency, cellular activity and oral bioavailability (Oza et al. 2012). AZD7762 enhanced the activity of different DNA damaging agents in cancer cell lines and xenograft models and abrogated the G_2/M checkpoint *in vivo* (Zabludoff et al. 2008). Treatment with AZD7762 chemosensitised to gemcitabine through increased origin firing, destabilisation of stalled forks and premature mitotic entry (McNeely

et al. 2010). Studies in isogenic cell lines demonstrated that p53-status determined the sensitivity to AZD7762 in combination with gemcitabine (Zabludoff et al. 2008). In addition, AZD7762 radiosensitised a range of p53-mutant cancer cell lines, while showing less effect on p53-wt cells, including normal fibroblasts (Mitchell et al. 2010). AZD7762 potentiated the response of pancreatic cancer xenograft models to fractionated radiation and showed a radiosensitising effect in lung cancer brain metastases (Morgan et al. 2010; Yang et al. 2011).

Preclinical data for the selective small molecule Chk1 inhibitor LY2603618 has recently been disclosed and shows the characteristic phenotypic responses of Chk1 inhibition (Calvo et al. 2014; King et al. 2014). Doxorubicin-induced G_2/M arrest in HeLa cells was abrogated by LY2603618 leading to premature mitosis. Potentiation of gemcitabine toxicity was observed in p53-mutant HT29 cells while p53 wt HCT116 cells were not further sensitised (King et al. 2014). Combination therapy with the antimetabolite pemetrexed was evaluated in two NSCLC (non-small cell lung cancer) cell lines and corresponding animal models. While treatment with LY2603618 alone did not affect cell proliferation, combination with pemetrexed resulted in a failure to progress through S phase. Significant reduction in tumour growth was observed in mouse models with the combination treatment and LY2603618 subsequently entered clinical trials (Calvo et al. 2014).

The Chk1 inhibitor PF-00477736 shows 100-fold selectivity for Chk1 over Chk2 and abrogated the camptothecin-induced G_2/M arrest in different cancer cell lines (Blasina et al. 2008). In HT29 cells PF-00477736 potentiated the cytotoxic effect of gemcitabine through abrogation of the gemcitabine-induced S-phase arrest and increased cell death by apoptosis. Similarly, *in vivo* toxicity of

gemcitabine was enhanced by PF-00477736 as evidenced by increased γH2AX levels and apoptosis (Blasina et al. 2008).

MK-8776 (previously SCH900776) is a selective Chk1 inhibitor that potentiated the effect of the antimetabolites HU and gemcitabine when tested in a range of cancer cell lines (Montano et al. 2012; Guzi et al. 2011). Similarly, sensitisation to the antimetabolite cytarabine was observed in cells derived from AML clinical specimens at concentrations that did not affect normal myeloid progenitors (Schenk et al. 2012). Surprisingly, p53 status did not determine sensitivity to treatment with HU or cytarabine in combination with MK-8776 (Montano et al. 2012; Schenk et al. 2012). Studies in pancreatic cancer cell lines and xenografts demonstrated a selective sensitisation of HR repair proficient cells to MK-8776 in combination with gemcitabine-based chemoradiation. In these cell lines the formation of RAD51 foci was prevented upon treatment with MK-8776 (Engelke et al. 2013). At collapsed replication forks Chk1 promotes BRCA2-mediated loading of RAD51 onto DNA to initiate DSB repair through HR (Sørensen et al. 2005; Bahassi et al. 2008). One report demonstrated that following gemcitabine treatment, MDA-MB-231 breast cancer cells were not initially dependent on Chk1 to stabilise stalled replication forks but inhibition of Chk1 with MK-8776 18 h after the addition of gemcitabine resulted in collapsed forks and cell death (Montano et al. 2013). The 18 h time frame correlated with the time required for RAD51 loading, suggesting that the observed toxicity was due to inhibition of Chk1-induced HR repair. This report might have important consequences for the design of clinical trials in combination with gemcitabine as it suggests that delayed administration of the Chk1 inhibitor might result in the greatest response (Montano et al. 2013).

Preclinical data for the dual Chk1/Chk2 inhibitor LY2606368 has recently been published and demonstrated single agent activity (King et al. 2015). LY2606368 caused cell death by replication catastrophe through a combination of unscheduled replication, DNA damage accumulation in S-phase and checkpoint abrogation. The induction of DNA damage required CDC25A and CDK2 indicating that LY2606368 caused increased initiation of replication. This resulted in the depletion of the RPA pool, a failure to protect ssDNA and the formation of DSBs. The inability to arrest cells prior to mitosis caused massive chromosome breakage and cell death through replication catastrophe. DNA damage and tumour growth inhibition in xenograft studies further demonstrated the single-agent activity of LY2606368 (King et al. 2015).

The potent and highly selective Chk1 inhibitor SAR020106 evolved from a morpholino-purine hit of a fragment-based screen through several optimisation steps (Matthews et al. 2009; Reader et al. 2011; Matthews et al. 2010). SAR020106 radiosensitised p53-mutant cells and enhanced the toxicity of gemcitabine and irinotecan in SW620 colon cancer cells and tumour bearing nude mice (Borst et al. 2013; Walton et al. 2010). Hybridisation of SAR020106 with one of the evolutionarily preceding lead compounds resulted in the orally bioavailable inhibitor CCT244747 which demonstrated efficacy as a single agent in MYCN-driven neuroblastoma and in combination with several anticancer agents in preclinical studies (Lainchbury et al. 2012; Walton et al. 2012).

1.3.4 Chk1 inhibitors in clinical trials

The majority of clinical studies have evaluated the use of Chk1 inhibitors in combination with chemotherapeutic agents. An overview of Chk1 inhibitors that have entered clinical trials can be seen in Table 1.1.

Several phase I and II clinical trials have been conducted with UCN-01 in combination therapy with different chemotherapeutics and as single agent. However, UCN-01 displayed a range of off-target effects combined with an exceptionally long half-life and low systemic clearance in cancer patients. Free drug levels were low due to its high affinity to human α-acid glycoprotein and exceeding of the binding affinity resulted in serious side effects. This prevented further development of UCN-01 (Fuse et al. 1998; Fuse et al. 2005).

Three phase I clinical trials with AZD7762 alone or in combination with gemcitabine or irinotecan commonly caused haematological and cardiac dose-limiting toxicities and the AZD7762 development programme has consequently been discontinued (Ho et al. 2011; Seto et al. 2013; Sausville et al. 2014). However, a total and durable response was seen in one patient with an invasive small-cell cancer following combination therapy with AZD7762 and irinotecan for five months (Ho et al. 2011). Whole-genome sequencing of the tumour revealed that a mutation in the Mre11 complex gene *RAD50* prevented normal ATM signalling which was synthetically lethal with Chk1 inhibition on an irinotecan treatment regime (Al-Ahmadie et al. 2014). Thus, although clinical development of AZD7762 has been discontinued, this outlier response demonstrates that a patient cohort with mutations in the Mre11 complex could benefit greatly from this combination therapy.

Table 1.1. Chk1 inhibitors in clinical trials

Compound	Selectivity	Clinical trials (combinations)
UCN-01 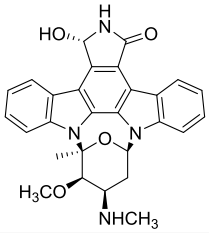	Chk1 IC_{50} 0.011 μM Chk2 IC_{50} 1.04 μM Chk1 IC_{50} 0.011 μM	Various Ph i-II (mono, cisplatin, carboplatin, topotecan, irino, fluorouracil, cytarabine) in pts with different types of cancers, mainly AST. Haematotoxicity and hypotension Discontinued
AZD7762 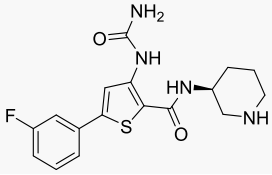	Chk1 IC_{50} 5 nM Chk2 IC_{50} <10 nM CDK1 IC_{50} >5 nM	3 x Ph I (mono, gem, irino) in western & Japanese pts with AST. Cardiac & haematological toxicities. Discontinued
LY2603618 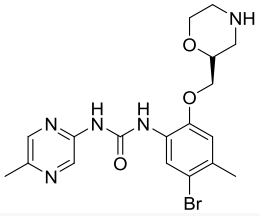	Chk1 IC_{50} 0.007 μM Chk2 IC_{50} 12 μM CDK1 IC_{50} >20 μM CDK2 IC_{50} >20 μM	Various Ph I-II (gem, pemetrexed, cisplatin) in pts with AST and NSCLC. Haematotoxicity
PF-00477736 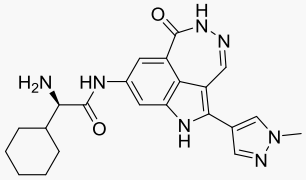		1x Ph I (gem) in pts with AST. Haematological toxicities. Discontinued
MK-8776 (SCH900776) 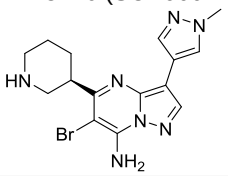	Chk1 IC_{50} 0.003 μM Chk2 IC_{50} 1.5 μM CDK2 IC_{50} 0.16 μM	3 x Ph I (gem, cytarabine, HU) in pts with AST, lymphoma, leukaemia. Good response with cytarabine in AML. Low toxicity. HU-study withdrawn 1 x Ph II (cytarabine) in AML. Ongoing
GDC-0475 Structure undisclosed		1 x Ph I (mono/gem) in pts with RST or lymphoma. Completed, results awaiting
GDC-0575 Structure undisclosed		1 x Ph I (mono/gem) in pts with RST or lymphoma. Recruiting
LY2606368 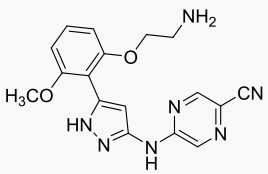	Chk1 IC_{50} <1 nM Chk2 IC_{50} 8 nM	3 x Ph I (mono) in pts with AST or breats/ovarian cancer. 58% disease control as mono in mSCC. Haematotoxicity 1 x Ph II (different chemotherapeutics) in AST. Recruiting

AST (advanced solid tumours), gem (gemcitabine), irino (irinotecan), mono (monotherapy), mSCC (metastatic squamous cell carcinoma), Ph (Phase), pts (patients), RST (refractory solid tumours).

The first selective Chk1 inhibitor to enter clinical trials was LY2603618. Different phase I and II have been conducted with LY2603618 in combination with gemcitabine, cisplatin or pemetrexed in various cancer types showing tolerable haematological toxicities and some clinical responses (Weiss et al. 2013; Doi et al. 2015).

One phase I dose escalation study has been conducted with PF-00477736 in combination with gemcitabine. Patients commonly suffered from severe haematotoxicity (Brega et al. 2010) and the development of PF-00477736 has been discontinued.

MK-8776 underwent three phase I clinical trials in combination with the antimetabolites gemcitabine, HU or cytarabine. While the study with HU has been withdrawn, results have recently been disclosed on the other two trials. In patients with advanced solid tumours MK-8776 was very well tolerated as monotherapy. Combination with gemcitabine caused some adverse effects, mainly haematotoxicity, but resulted in two partial responses and stable disease in 13 out of 30 patients (Daud et al. 2015). Complete tumour remission was seen in 8 out of 24 patients who received sequential cytarabine/MK-8776 treatment for refractory acute leukaemia. MK-8776 was well tolerated and did not exacerbate toxicities commonly observed from cytarabine treatment (Karp et al. 2012). Subsequently a currently active phase II trial was initiated where the cytarabine/MK-8776 combination is studied in relapsed AML.

LY2606368 is currently undergoing four phase I clinical trials. Three of which are evaluating the drug as a single agent and in the fourth study patients with advanced or metastatic cancer are treated with LY2606368 in combination with different chemotherapeutics. LY2606368 showed single-agent activity in

patients with metastatic squamous cell carcinoma of the anus and a 58% disease control rate (one complete response, three partial responses and 11 patients with stable disease). High incidence of haematotoxicity was observed, but this was transient and manageable (Bendell et al. 2015). In contrast to previously described Chk1 inhibitors which had to be administered intravenously, GDC-0425 and GDC-0575 are the first orally bioavailable Chk1 inhibitors that have entered phase I clinical trials. Neither medicinal chemistry nor preclinical data has been published on these compounds as of yet. Both inhibitors are evaluated in phase I clinical trials as monotherapy and in combination with gemcitabine in patients with refractory solid tumours or lymphoma. While the study with GDC-0575 is currently actively recruiting patients, the trial with GDC-0425 is now completed but results have not been disclosed yet.

1.4 Exploiting hypoxia for cancer therapy

1.4.1 Approaches to targeting hypoxic tumours

The tumour microenvironment strongly influences the outcome of anticancer therapy. One major characteristic of the tumour microenvironment is hypoxia which arises as the tumour outgrows its own blood supply. Cells that thrive under oxygen deprivation have adapted to those conditions through mechanisms that suppress DNA repair, promote the expression of oncogenes, escape cell death and drive genomic instability and malignant progression (Luoto, Kumareswaran, and Bristow 2013; Vaupel and Mayer 2007; Harris 2002; Glazer et al. 2013; Graeber et al. 1996). Hypoxia impacts all forms of anticancer therapy and correlates with poor patient prognosis (Hockel et al. 1996; Vaupel and Mayer

2007). However, at the same time it also provides an opportunity for the selective targeting of tumours over normal tissue since hypoxia does not occur under physiological conditions in healthy organs and is a characteristic feature of solid tumours. The interest in exploiting the differences between hypoxic and normal tissues has prompted the development of various therapeutic strategies (Figure 1.11).

HIF-1 is the master regulator of O_2 homeostasis and mediates the cellular adaptation to hypoxia, thus playing an important role in tumour cell survival (Harris 2002). High expression levels of HIF-1 have been associated with poor prognosis in a variety of malignancies, including oropharyngeal, cervical, breast and oesophageal cancer, and HIF-1 is an attractive target for anti-cancer therapy (Aebersold et al. 2001; Burri et al. 2003; Bos et al. 2003; Matsuyama et al. 2005; Hockel et al. 1996). Due to the challenges in the direct inhibition of a transcription factor like HIF-1, reported inhibitors of HIF-1 are often indirectly associated with HIF-1, targeting upstream activators of HIF-1 or downstream effectors (Melillo 2007). HIF-1 is involved in a broad spectrum of signalling pathways and some reported nonselective strategies to target HIF-1 include inhibitors of topoisomerase I (Rapisarda et al. 2004), the chaperone HSP60 (Isaacs et al. 2002), mammalian target of rapamycin (Majumder et al. 2004) and histone deacetylase (Kong et al. 2006). Direct targeting of HIF-1 has been achieved by reduction of the transcriptional induction of HIF-1α through the use of the camptothecin analogue SN-38 (Jeong et al. 2014). As a direct inhibitor of HIF-1 heterodimerisation, Miranda and coworkers have reported a cyclic peptide inhibitor which presents the first example of a direct inhibitor of HIF-1α to HIF-1β binding (Miranda et al. 2013). It is important to note that HIF-1 activity is also

influenced by factors other than hypoxia and therefore it is not a strictly hypoxia-specific target (Semenza 2003; Giaccia, Siim, and Johnson 2003).

Targeting the DDR is an emerging and promising strategy to treat hypoxic tumour cells. Different approaches can be taken to exploit the changes in DNA damage signalling under hypoxia (Figure 1.11) (Olcina, Lecane, and Hammond 2010; Scanlon and Glazer 2015; Hammond et al. 2014).

Firstly, the activation of the DDR in response to severe hypoxia has been shown to involve a number of potentially drugable targets, including Chk1, Chk2, ATM, ATR and members of the FA pathway. The inhibition or depletion of ATR or Chk1 during severe hypoxia results in the accumulation of DNA damage (Hammond et al. 2002; Hammond, Dorie, and Giaccia 2004). In addition, Chk2 is phosphorylated in an ATM-dependent manner and active during severe hypoxia (Freiberg, Hammond, et al. 2006; Gibson, Bindra, and Glazer 2005; Gibson, Bindra, and Glazer 2009). ATM has recently been shown to be required for DNA replication during hypoxia-induced replication stress and ATM inhibition resulted in the accumulation of DNA damage (Olcina et al. 2013). The FA pathway is activated in response to hypoxia in an ATR-dependent manner and required to avoid DNA damage accumulation and hypoxia-induced apoptosis (Scanlon and Glazer 2014). Reoxygenation following transient severe hypoxia leads to ROS-induced DNA damage and the activation of the ATM-Chk2 axis in a classical manner (Hammond, Dorie, and Giaccia 2003; Bencokova et al. 2009; Freiberg, Krieg, et al. 2006). Reoxygenation initiates replication restart, which is regulated by ATM as well as ATR/Chk1 (Pires, Bencokova, Milani, et al. 2010; Olcina et al. 2013). Inhibition or depletion of Chk1, Chk2, ATR or ATM sensitises cells to severe hypoxia/reoxygenation, highlighting them as potential therapeutic targets

also in combination with radiation (Hammond, Dorie, and Giaccia 2004; Freiberg, Hammond, et al. 2006; Freiberg, Krieg, et al. 2006; Pires et al. 2012).

Secondly, more prolonged exposure to hypoxia induces transcriptional repression of different DNA repair pathways, including HR, FA and MMR (mismatch repair) (Scanlon and Glazer 2015; Luoto, Kumareswaran, and Bristow 2013). Synthetically lethal interactions in a context of reduced DNA repair can be identified and exploited, a concept which has been termed context synthetic lethality or conditional synthetic lethality (Chan et al. 2010; Chan and Giaccia 2011). Most notably, the repression of the HR protein RAD51 under hypoxia was shown to be synthetically lethal with inhibition of PARP1 (poly(ADP-ribose) polymerase 1) in clonogenic survival assays and *in vivo* tumour models (Bindra et al. 2004; Chan et al. 2008; Chan et al. 2010).

Thirdly, the hypoxia-mediated selection for cells with impaired apoptotic potential can be reversed by pharmacological reactivation of p53 or induction of apoptosis through the inhibition of the pro-survival protein AKT (Graeber et al. 1996; Kim et al. 1997; Leszczynska et al. 2015).

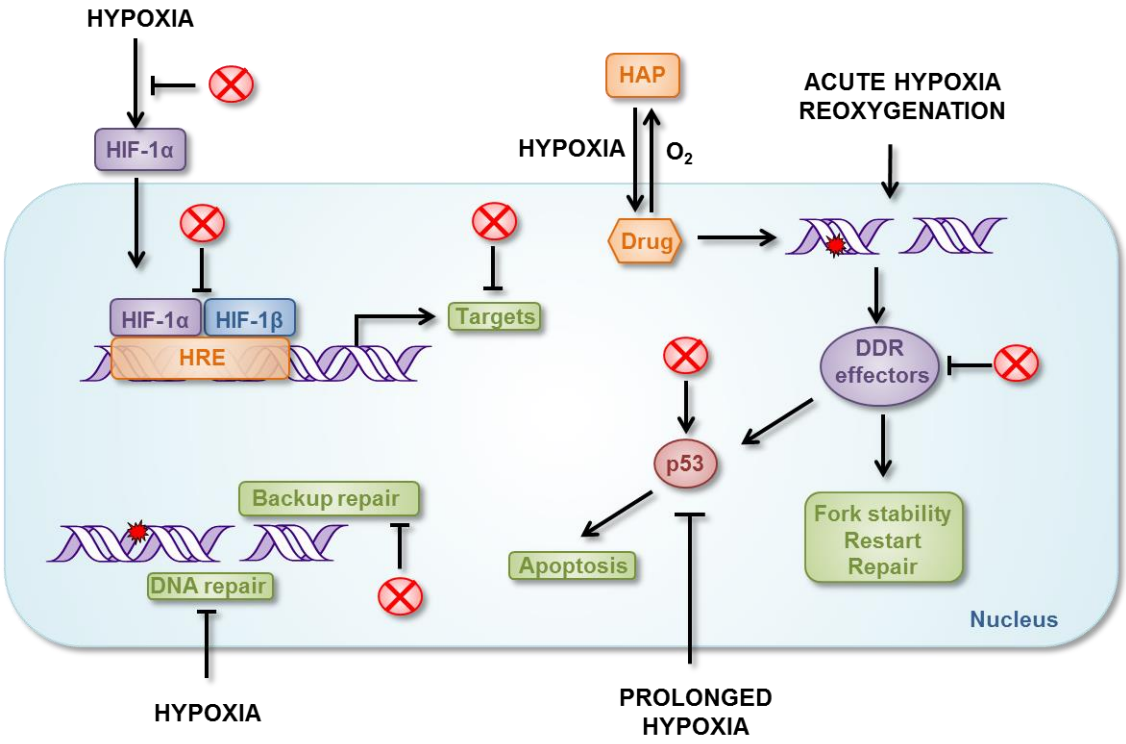

Figure 1.11. Targeting tumour hypoxia.
Different approaches for hypoxia-selective tumour cell targeting are illustrated. Hypoxia stabilises HIF-1α, which in conjunction with HIF-1β, trans activates genes that promote tumour cell survival. Various stages in the HIF-1 pathway have been targeted (shown as red crosses). Hypoxia-induced repression of DNA repair renders cells reliant on backup mechanisms whose inhibition results in context synthetic lethality. Acute severe hypoxia and reoxygenation activate the DDR. Inhibition of DDR effector kinases sensitises cells to these conditions and potentiates DNA damage from cancer therapy. Activation of p53 in response to acute severe hypoxia promotes p53-dependent apoptosis which results in the selection for cells with defects in p53 signalling and diminished apoptotic potential. Small molecule activators of p53 can restore the hypoxia-induced apoptosis. The use of bioreductive drugs can directly exploit the differences between the chemical microenvironment of normally oxygenated and hypoxic cells. The presence of O_2 prevents the activation of a bioreductive drug through rapid back-oxidation into the prodrug. Adapted from (Wilson and Hay 2011).

Bioreductive drugs are non-toxic prodrugs of a biologically active agent, which become selectively activated under hypoxic conditions (Denny 2000; Chen and Hu 2009; Wilson and Hay 2011; Guise et al. 2014). Historically, the development of the first bioreductive drugs originated from attempts to overcome hypoxia-induced radiation resistance and thus, early bioreductive drugs were primarily radiosensitisers (Brown 1984; Overgaard 1994). The activation of these drugs under conditions of low O_2 levels follows a general mechanism (Figure 1.12). In order to achieve hypoxia-selective prodrug activation, the bioreductive

drug must be a substrate for cellular one-electron reductases, of which the most extensively studied, is CYP450 (cytochrome P450 oxidoreductase). One-electron reduction converts the prodrug into a radical anion, which is rapidly reoxidised in the presence of O_2. This cycling renders the one-electron reduction of the prodrug futile and guarantees high levels of prodrug and only very low levels of prodrug-radical at any given time. In the absence of O_2, on the other hand, the prodrug radical can accumulate and either act as a cytotoxin itself or undergo further molecular changes into a biologically active agent. This can occur through direct fragmentation of the prodrug radical or following further stepwise one-electron reduction. The specific mechanism of activation depends of the class of bioreductive drug and different classes will be described in the following paragraph. A competing mechanism for this hypoxia-selective stepwise one-electron reduction is the bypassing of the O_2-sensitive prodrug radical by direct enzymatic two-electron reduction. It is therefore important that bioreductive drugs are substrates for one-electron reductases and not competing two-electron reductases, since O_2-independent prodrug activation can contribute to normal tissue toxicity (Knox et al. 1988; Celli et al. 2006; Guise et al. 2010).

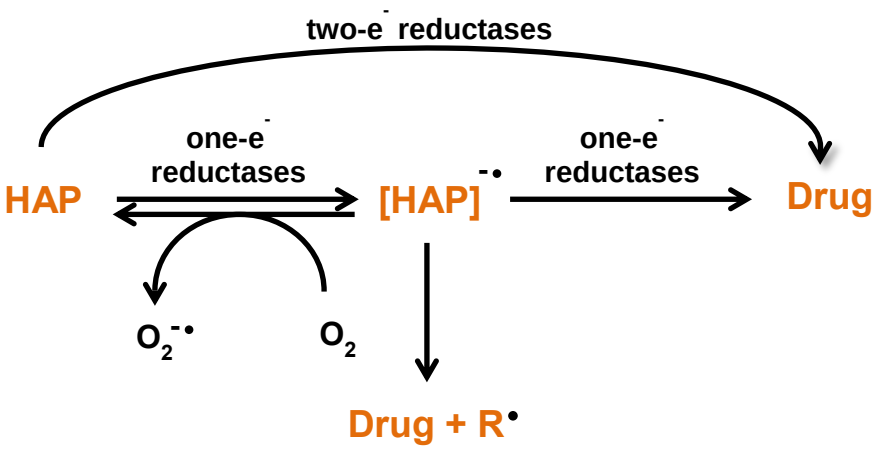

Figure 1.12. General mechanism for bioreductive prodrug activation.
The bioreductive prodrug (HAP for hypoxia-activated prodrug) is reduced to the corresponding prodrug radical anion by cellular one-electron (e^-) reductases such as CYP450. In oxygenated cells, O_2 can accept the unpaired electron and rapid back-oxidation to the original prodrug takes place, rendering one-electron reduction ineffective. In the absence of O_2, the prodrug radical can fragment into a biologically active agent and a residual radical or further reduction can take place to generate an active compound (generally 4- or 6-electrons overall). In some cases, two-electron reductases can circumvent the hypoxia-selective reduction of the prodrug and result in prodrug activation even in oxygenated tissue. Adapted from (Wilson and Hay 2011).

1.4.2 Classes of reductively activated prodrugs

Four different classes of bioreductive prodrugs, nitro(hetero)aromatics, quinones, *N*-oxides and transition metal complexes, have been described as trigger units for bioreduction (Chen and Hu 2009). Nitro(hetero)aromatic compounds, such as misonidazole and nimorazole, were originally designed as O_2-mimicking radiosensitisers (Wardman 2007) and derivatives have been developed into hypoxic imaging agents for immunohistochemistry or PET (positron emission tomography) (Hammond et al. 2014). Nitro(hetero)aromatic groups have been used as bioreductive switches embedded within the structure of bioreductive drugs or as trigger units that initiate fragmentation of a prodrug to release a biologically active molecule. The clinically advanced examples

PR-104A and TH-302 and their mechanism of activation are shown in Scheme 1.1.

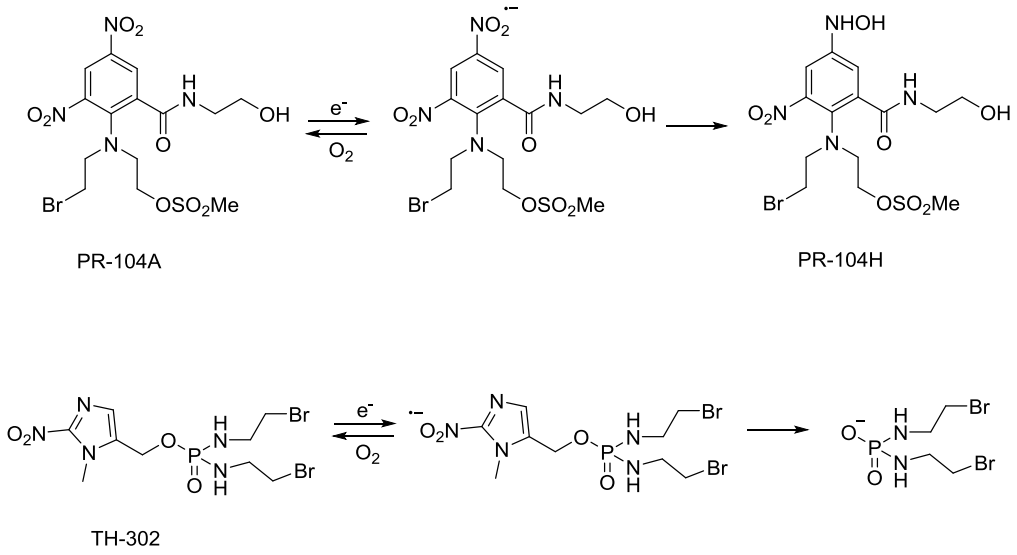

Scheme 1.1. Hypoxia-selective activation of the clinically advanced bioreductive prodrugs PR-104A and TH-302.
Examples of two nitroaryl-triggered bioreductive drugs. In case of the nitrobenzamide mustard PR-104 the nitroaromatic group acts as an electronic switch to increase electron density upon reduction to the hydroxylamine PR-104H and generate an activated nitrogen mustard. Conversely, the 1-methyl-2-nitroimidazole group in TH-302 ejects an active cytotoxin upon hypoxia-selective reduction.

PR-104, the phosphate ester of PR104A, has undergone various phase I and II clinical trials in patients with solid tumours. Upon bioreduction in hypoxia, PR-104A forms an activated DNA-crosslinking agent which has been shown to kill cancer cells (Singleton et al. 2009). Different reductases have been shown to mediate bioreduction of PR-104A, including CYP450 and the O_2-independent aldo-keto reductase 1C3 (Guise et al. 2012; Guise et al. 2007; Guise et al. 2010). The most clinically advanced nitroaromatic bioreductive prodrug to date is TH-302. Hypoxia-selective fragmentation of TH-302 releases a DNA-crosslinking nitrogen mustard with up to 550-fold *in vitro* selectivity towards hypoxic over oxygenated cells (Duan et al. 2008; Meng et al. 2012). Following similarly promising *in vivo* studies in mono and combination therapy (Liu et al. 2012; Sun

et al. 2012), TH-302 entered clinical trials and is currently undergoing a number of phase II and III trials.

The observation that the quinone mitomycin C was preferentially activated into cytotoxic metabolites under hypoxia, prompted the development of improved and more hypoxia selective quinones (Kennedy, Rockwell, and Sartorelli 1980; Phillips, Hendriks, and Peters 2013). One intensively studied representative of this class of bioreductive prodrugs is E09 (Figure 1.13). E09 is activated under hypoxia by CYP450 but is also a substrate for the two-electron reductase NQO1 (DT-diaphorase) which results in loss of hypoxia-selectivity in cells expressing NQO1 (Saunders et al. 2000; Danson et al. 2004). Nevertheless, excellent hypoxia selectivity was observed in cells lacking NQO1 and E09 is currently in phase III trials for the treatment of bladder cancer (Plumb and Workman 1994).

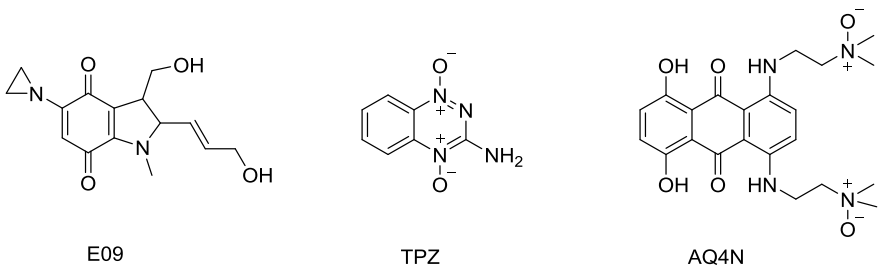

Figure 1.13. Selected representatives of different classes of bioreductive prodrugs.
Shown are the quinone E09, the aromatic *N*-oxide TPZ and the aliphatic *N*-oxide AQ4N.

Aromatic and aliphatic *N*-oxides as hypoxia-selective prodrugs include TPZ (tirapazamine) and AQ4N (Figure 1.13). TPZ has been intensively studied in clinical trials and advanced into phase III studies. Studies in the 80s and 90s revealed excellent hypoxia selectivity for TPZ and improved efficacy of radiotherapy and cisplatin (Zeman et al. 1986; Brown and Lemmon 1991; Siim et al. 1997). The drug progressed into clinical trials with promising results in phase I

and II trials (Treat et al. 1998; Marcu and Olver 2006). However, combination treatment with TPZ *versus* the respective treatment alone, revealed no therapeutic benefit in the TPZ-treated patients in phase III clinical trials (Williamson 2005; Rischin et al. 2010). Importantly, hypoxia was not measured in these studies and the lack of therapeutic benefit is likely based on the failure to choose the appropriate patient population. Selecting the right candidate patient population for a therapeutic regime is as important as finessing the anticancer agents themselves and it is therefore crucial to accurately identify and measure hypoxia through tissue-based biomarkers or imaging techniques such as PET (Hammond et al. 2014).

Notably, a common feature of most bioreductive prodrugs that have been reported to date is the induction of DNA damage, mostly through DNA crosslinking or alkylation, resulting is some residual normal tissue toxicity. Another disadvantage of these agents is that they have a limited diffusion distance and cannot diffuse away from the hypoxic into surrounding oxygenated regions of a tumour. Targeted agents that do not act through a covalent binding mechanism could, on the other hand, kill a greater cell population through the bystander effect (diffusion into surrounding tissue) (Wilson and Hay 2011). A few examples of targeted bioreductive drugs have been reported, where nitroaromatic groups where used to convert a biologically active agent into a hypoxia-selective agent. These include inhibitors of lysyl oxidase and O^6-alkylguanine-DNA alkyltransferase (Granchi et al. 2009; Zhu et al. 2011). Future efforts in the bioreductive field will likely go into the development of more such targeted agents, in an effort to combat hypoxia-mediated therapy resistance without compromising patient safety.

1.5 Aim

The hypoxic fraction of a solid tumour contains the most therapy resistant tumour subpopulation, with regards to all forms of cancer therapy, including surgery (Hockel et al. 1996; Harris 2002; Overgaard 2011). It is therefore important to find novel ways to target hypoxic cancer cells while minimising toxicity to healthy organs. Exploiting the differences between hypoxic tumours and normal cells is an elegant way of improving the therapeutic index (increased killing of tumour cells relative to normal tissue). Various strategies have been reported, including drugs that are synthetically lethal with mutations commonly found in hypoxic cancers and the use of hypoxia-activated anticancer agents (Bristow and Hill 2008; Wilson and Hay 2011).

Severe hypoxia induces a replicative stress response which involves the ATR/Chk1 axis (Hammond et al. 2002; Hammond, Dorie, and Giaccia 2004). In addition, Chk1 inhibitors have recently emerged as single agents in tumours with high levels of oncogene-induced replication stress (Murga et al. 2011; Ferrao et al. 2012; Bryant, Rawlinson, and Massey 2014). Moreover, inhibition of Chk1 during severe hypoxia/reoxygenation was shown to result in increased origin firing and reduced clonogenic survival, highlighting a potential for targeting hypoxic tumours through the inhibition of Chk1 (Pires, Bencokova, Milani, et al. 2010; Pires, Bencokova, McGurk, et al. 2010; Cazares-Körner et al. 2013). It is important to keep in mind that Chk1 plays a pivotal role during normal DNA replication and cell cycle progression and inhibition of Chk1 leads to the accumulation of DNA damage, genomic instability and tumourigenesis in favourable genetic backgrounds (Syljuåsen et al. 2005; Lam et al. 2004).

To exploit the intrinsic sensitivity of hypoxic cells to Chk1 inhibition while minimising normal tissue toxicity, we proposed to develop Chk1 inhibitors that are exclusively active in the chemical environment of a hypoxic tumour. These agents are designed in such a way that their activation requires the stepwise enzymatic reduction of a bioreductive nitro(hetero)aromatic trigger unit (Figure 1.14). We will choose known inhibitors of Chk1 from the literature which possess a functional moiety that can be substituted with a nitro(hetero)aromatic trigger unit and modify them into bioreductive prodrugs.

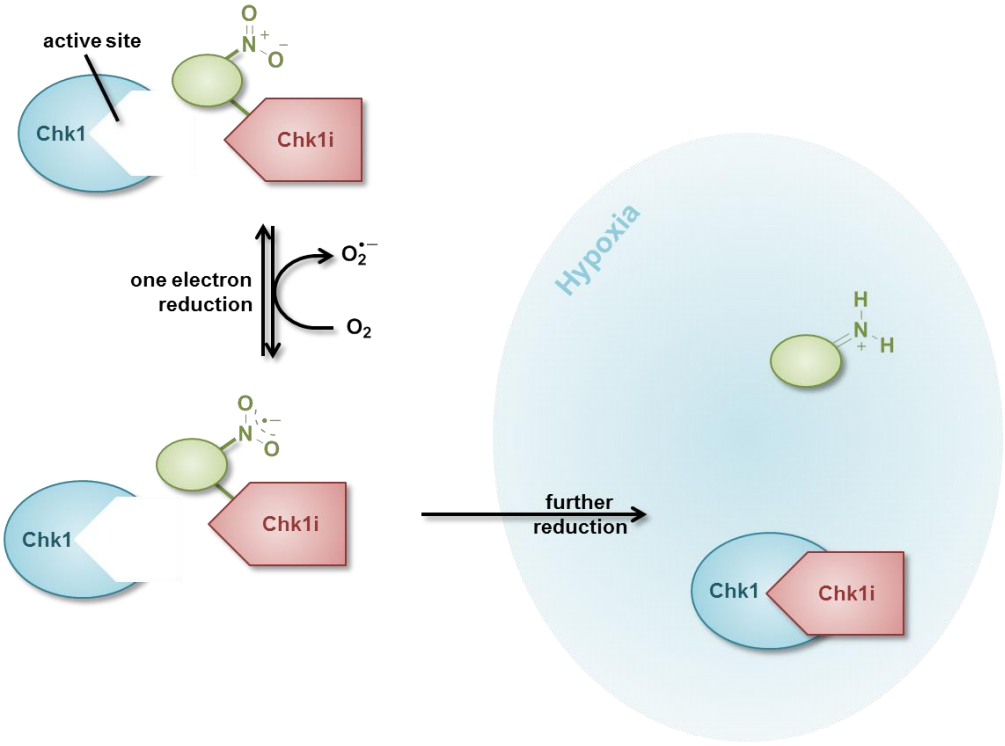

Figure 1.14. Schematic representation of the mechanism of action of a bioreductive Chk1 inhibitor.
The Chk1 inhibitor (Chk1i) is masked with a bioreductive nitro-aromatic trigger unit (marked in green) which acts as a barrier to inhibitor-kinase interaction. One-electron reductases reduce the nitro group to a radical anion which undergoes rapid back-oxidation in the presence of O_2. In hypoxia, further reduction takes place, resulting in fragmentation of the prodrug and release of the Chk1 inhibitor.

While initially focussing of synthesising an easily accessible proof-of-concept compound, we intend to synthesise more drug-like molecules once our concept has proven applicable. In addition to performing organic synthesis, this

project will require us to establish a way of testing whether our bioreductive prodrugs undergo a hypoxia-selective mechanism of activation. We will set up different assays to investigate the mechanism of prodrug activation. Cell-based experiments will be performed in order to test whether exposure to our bioreductive prodrugs will result in the same phenotypic responses (cell death, DNA damge, Chk1 inhibition) as the treatment with a Chk1 inhibitor but in a hypoxia-selective fashion.

The majority of previously reported bioreductive prodrugs were DNA alkylators or other non-specifically toxic agents. This strategy, on the other hand, is proposed to enable the selective activation of a targeted agent within the most therapy resistant tumour fraction.

CHAPTER 2

DEVELOPMENT OF A PROOF-OF-CONCEPT BIOREDUCTIVE CHK1 INHIBITOR

The results presented in this chapter are published (Cazares-Körner et al. 2013). Figures and schemes have been reprinted or adapted with permission from ACS chemical biology, 8,7, Cazares-Körner C., Pires I.M., Swallow, I.D., Grayer, S.C., O'Connor L.J., Olcina, M.M., Christlieb, M., Conway, S.J. and Hammond, E.M., CH-01 is a hypoxia-activated prodrug that sensitizes cells to hypoxia/reoxygenation through inhibition of Chk1 and Aurora A, 1451-1459. Copyright 2013 American Chemical Society.

2.1 Introduction

Inhibition of Chk1 has been widely studied in combination with DNA damaging agents and as a single therapy in tumours with high levels of oncogene-induced replication stress (Murga et al. 2011; Ferrao et al. 2012; Bryant, Scriven, and Massey 2014; Cole et al. 2011). Due to its pivotal role in normal replication, cell cycle progression and DNA repair, however, inhibition of Chk1 causes DNA damage and genomic instability in normal tissue, and can thus contribute to malignant progression (Syljuåsen et al. 2005; Lam et al. 2004).

We have exploited two features of hypoxic cells in order to target hypoxic cancer cells over normal tissue. Severe hypoxia induces a replicative stress response which involves ATR and Chk1, and loss or inhibition of Chk1 has been shown to sensitise cells to hypoxia/reoxygenation (Pires, Bencokova, Milani, et

al. 2010). In addition, the differences between the hypoxic tumour microenvironment and normal tissue provide the opportunity to design agents that are selectively targeted towards regions of low physiological O_2 levels. With regard to these characteristics, we have synthesised and tested a bioreductive Chk1 inhibitor which becomes activated selectively in hypoxia.

2.2 Rationale for hypoxia-selective Chk1 inhibition

Chk1 has previously been shown to be involved in the hypoxia-induced DDR (see 1.2.7) (Pires, Bencokova, Milani, et al. 2010; Pires, Bencokova, McGurk, et al. 2010). In order to confirm a role for Chk1 in severe hypoxia, we used western blotting and demonstrated that Chk1 is phosphorylated and active in severe hypoxia (Figure 2.1, A). Phosphorylation of the ATR-targeted sites Ser317 and Ser345 is accompanied by increased phosphorylation of the Chk1 target TLK1 (Ser695) (Pires, Bencokova, McGurk, et al. 2010) and the Chk1 autophosphorylation site (Ser296). The total levels of Chk1 protein decrease during prolonged exposure to severe hypoxia as has been reported (Pires, Bencokova, Milani, et al. 2010).

Increased DNA damage and a potential for tumourigenesis have been demonstrated upon inhibition or deletion of Chk1 (Syljuåsen et al. 2005; Fishler et al. 2010). In order to highlight this issue, we subjected primary human lung fibroblasts to Chk1 inhibition and measured DNA damage accumulation at different time points. In the absence of additional stress and under normoxic conditions, WI38 cells were treated with the Chk1 inhibitor Gö6976 (Kohn, Yoo, and Eastman 2003) and the number of 53BP1 foci measured as a marker of DNA damage (Figure 2.1, B).

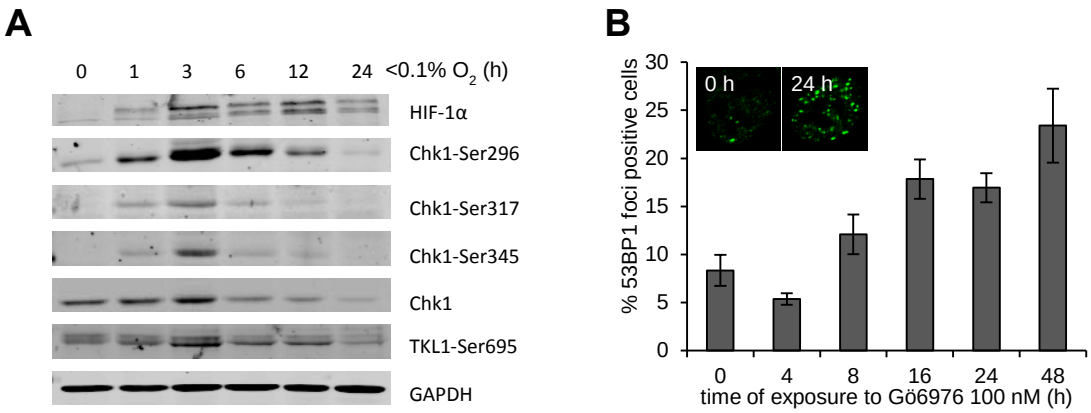

Figure 2.1. Chk1 is phosphorylated and active in severe hypoxia and inhibition causes DNA damage.
A) RKO cells were exposed to hypoxia (<0.1% O_2) for the time indicated and western blotting carried out. Hif-1α is shown as a hypoxia marker and GAPDH is shown as a loading control. B) WI38 cells were treated with 100 nm Gö6976 for the times indicated and cell with >6 nuclear 53BP1 foci counted. The inset shows an example. Error bars represent the standard error between technical replicates for the represented experiment (n=3).

A basal level of damage (8% of cells) was detected in WI38 cells which increased upon increasing exposure time to Gö6976 (23% of cells at 48 h), highlighting that inhibition of Chk1 leads to the accumulation of damage in untransformed cells. The inhibition of Chk1 has been well documented as an anti-cancer strategy but also bears the potential to trigger tumourigenesis due to the role of Chk1 in maintaining genome integrity.

In this regard and especially given the activation of Chk1 following severe hypoxia/reoxygenation, we proposed that a bioreductive Chk1 inhibitor could circumvent the issues arising from Chk1 inhibition in normal tissue. We decided to synthesise a Chk1 inhibitor prodrug where the inhibitor is masked by a hypoxia activated group, reduction of which leads to the release of the active inhibitor selectively under hypoxic conditions.

2.3 Choice of inhibitor

In addition to the non-specific staurosporine derivative UCN-01 (Busby et al. 2000; Yu et al. 2002) and the clinically advanced Chk1/2 inhibitor AZD7762 (Zabludoff et al. 2008) a review of the literature on Chk1 inhibitors at the time revealed a wide patent literature (Janetka and Ashwell 2009) along with the second generation ATP-competitive inhibitor PF477736 (Blasina et al. 2008; Zhang et al. 2009), which showed increased selectivity for Chk1 over other kinases. We further came across various reports of new drug-like scaffolds of ATP-competitive Chk1 inhibitors (including (G. T. Wang et al. 2005; Lin et al. 2006; Brnardic et al. 2007; Foloppe et al. 2005)).

We examined the published synthetic routes of different inhibitors for their versatility to incorporate a bioreductive group into the molecule while also focussing on ease and efficacy of synthesis. Limiting our focus to inhibitors which were published with a crystal structure in order to rationalise prodrug design, we chose the furanopyrimidine inhibitor **1** published by Foloppe and coworkers (Foloppe et al. 2005) as the basis for a bioreductive prodrug (Figure 2.2). Importantly, the study reported the inhibitor together with a synthetic route and an SAR study around this scaffold which revealed that substitution of the inhibitor hydroxyl group resulted in reduced binding affinity.

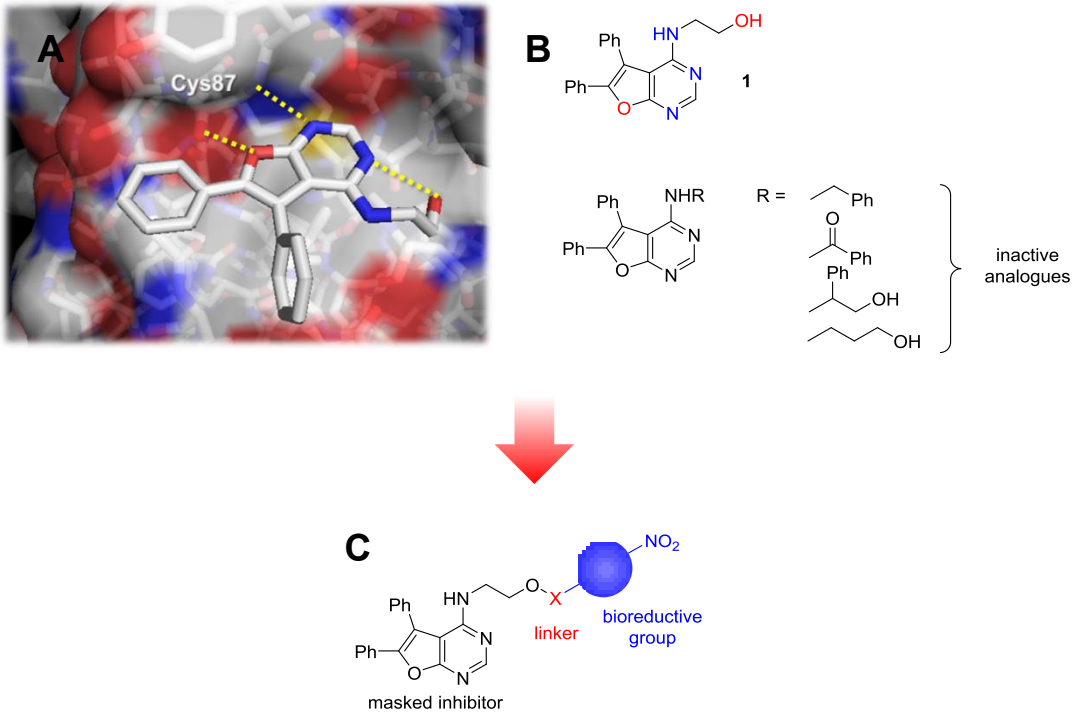

Figure 2.2. Rationale for the design of a bioreductive prodrug based on the Chk1 inhibitor 1.
A) Crystal structure of **1** in the ATP-binding site of Chk1 (PDB 2brb). Interactions are shown as dashed yellow lines. Note the staggered conformation of the hydroxyl side chain due to an intramolecular hydrogen bond. B) Structure of **1** and presentation of inactive analogues with different side chain substituents. C) Proposed concept of a bioreductive prodrug based in inhibitor **1**.

Reduction in affinity upon hydroxyl substitution was thought to be the result of a disrupted intramolecular hydrogen bond between the hydroxyl and the heterocyclic core in the substituted analogues (Figure 2.2, A). In addition, due to the orientation of the hydroxyl side chain pointing into the active site, bulky substituents were not tolerated (Figure 2.2, B). Given these SAR data which were supported by an x-ray crystal structure of inhibitor **1** in the ATP-binding site of Chk1 (Figure 2.2, A), we chose to synthesise a bioreductive analogue of **1** (Figure 2.2, C) which we predicted would show no Chk1 affinity until activation *via* reduction and fragmentation had taken place.

We proposed a prodrug where the inhibitor is masked by a bioreductive group *via* the hydroxyl group of the inhibitor (Figure 2.2, C). Taking into account

that we intended to synthesise a proof-of-concept prodrug, we wanted to keep the synthesis straightforward and short. The published synthesis of **1** consisted of five standard reactions which we expected to be robust and facile to carry out (Foloppe et al. 2005). We chose to substitute **1** with a nitro aromatic bioreductive group for two main reasons:

i. Nitro aromatics have been reported as trigger units which upon reduction initiate fragmentation of the prodrug to release an active agent (*e.g.* a cytotoxin) (Wilson and Hay 2011; Guise et al. 2014).
ii. Reduction of the nitroaromatic moity is known to proceed *via* a one-electron mechanism with a reversible first step, *i.e.* formation of the initial nitro radical by one-electron reduction is reversible in the presence of oxygen. Nitro reduction is therefore hypoxia selective (Wilson and Hay 2011).

Among the family of reported nitroaromatic bioreductive groups are various nitrobenzyls (with and without germinal substitution) and nitroimidazoles. Of these especially 2-nitroimidazoles have been shown to have improved bioreductive and tissue penetration properties (Meng et al. 2012), the synthetic precursor to such a prodrug was not readily available without extending the synthetic chemistry efforts. For reasons of synthetic ease we therefore chose the 4-nitrobenzyl bioreductive group and proposed the bioreductive Chk1 inhibitor **2** (Figure 2.3).

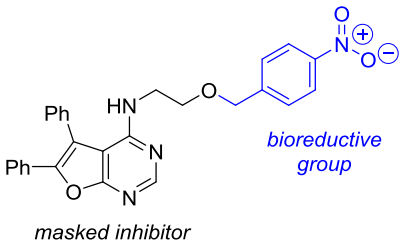

Bioreductive prodrug 2

Figure 2.3. Structure of the bioreductive prodrug 2.
Highlighted are the two parts of the molecule, the masked Chk1 inhibitor in black and the bioreductive 4-nitrobenzyl moiety in blue.

Based on the study by Foloppe and coworkers (Foloppe et al. 2005) we predicted **2** to be inactive against Chk1 and this assumption was backed up by docking studies (Figure 2.4).

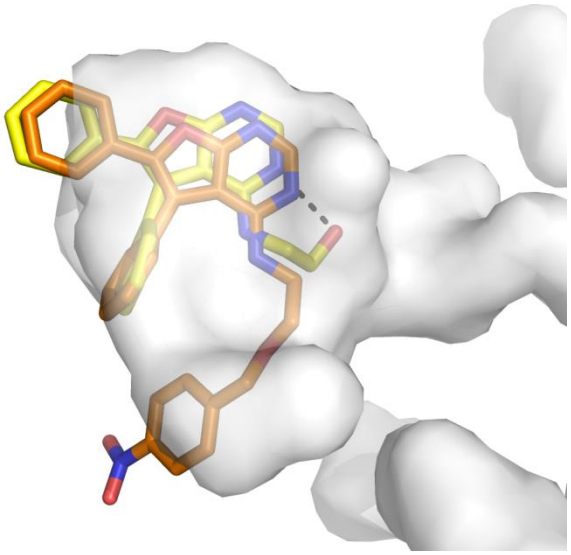

Figure 2.4. Representative image of 2 docked to Chk1 overlaying the X-ray crystal structure of inhibitor 1 bound to Chk1.
Shown in yellow carbons is the inhibitor **1** in the binding site of the original crystal structure (PDB 2brb). Depicted in black is an intramolecular interaction. Docking of the 4-nitrobenzyl prodrug **2** (carbon = orange) revealed a less favourable binding mode than that of inhibitor **1**. Docking was carried out by Samuel C. Grayer using AutoDock Vina.

Docking was based on the published crystal structure of **1** bound to Chk1 (PDB 2brb). This structure had revealed a polar intramolecular interaction between the hydroxyl group and the heterocyclic core of the inhibitor. Docking of the bioreductive prodrug **2** into this receptor showed that **2** could not adopt the

staggered conformation necessary for this intramolecular interaction. In addition, the size of the bioreductive group forced the side chain out of the active site. Overall, this binding mode was energetically less favoured than binding of the active inhibitor **1**, suggesting a reduced affinity of prodrug **2**.

2.4 Synthesis of prodrug 2 and the control compounds 1 and 12

Inhibitor **1** was synthesised following conditions similar to those employed by Foloppe and coworkers (Scheme 2.1) (Foloppe et al. 2005; Cazares-Körner et al. 2013). Optimisation of the formation of furan **4** from benzoin **3** and malononitrile was achieved by heating under reflux in dioxane in the dark and under an inert atmosphere (argon) instead of stirring at RT in DMF as had been originally reported. Synthesis of the prodrug precursor **7** was carried out in three further steps. Treatment of **4** with acetic formic anhydride furnished formamide **5**, which cyclised upon heating to give bicycle **6** in 51% yield over two steps. Reaction of **6** with $POCl_3$ gave chloride **7** in good yield (81%).

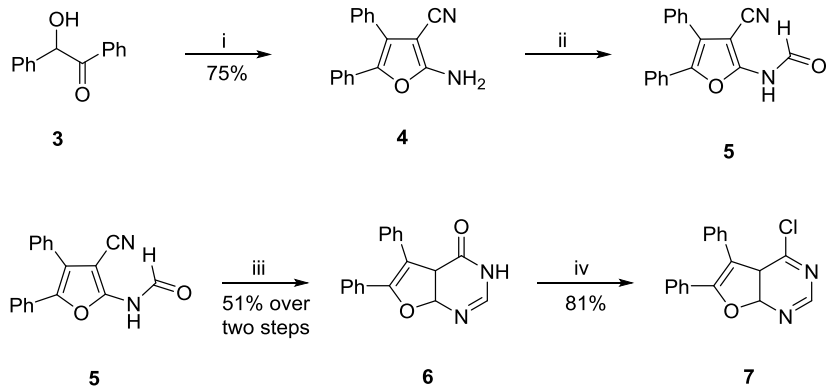

Scheme 2.1. Synthesis of prodrug precursor 7.
Reagents and conditions: i) Malononitrile, Et_2NH, dioxane, reflux, 16 h; ii) Acetic formic anhydride, 85 °C, 6 h; iii) neat, 220 °C, 30 min; iv) $POCl_3$, 55 °C, 2 h. Synthesis was carried out by I. Diane Swallow.

Hypoxia-sensitive amino linker **11**, the second building block of the proposed bioreductive prodrug **2**, was synthesised from commercially available phthalimide **8** and benzyl bromide **9** in two steps (Scheme 2.2).

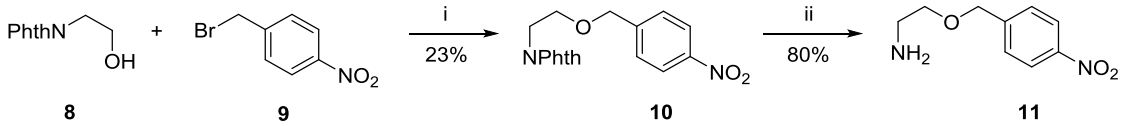

Scheme 2.2. Synthesis of amino linker 11.
Reagents and conditions: i) NaH, TBAI, THF, RT, 24 h; ii) hydrazine monohydrate, EtOH, RT, 3 d. Synthesis was carried out by I. Diane Swallow.

With both building blocks at hand, the bioreductive prodrug **2** was obtained in 91% yield by facile electrophilic aromatic substitution of amine **11** with chloride **7** (Scheme 2.3).

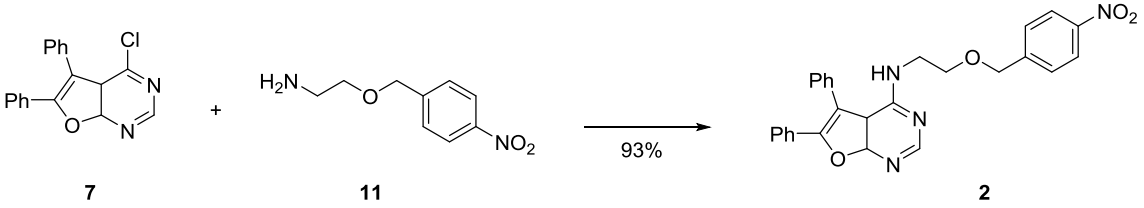

Scheme 2.3. Final step in the synthesis of 2.
Reagents and conditions: Et_3N, DMF, 80 °C, 6 h. Synthesis was carried out by I. Diane Swallow.

In addition to **2**, we further synthesised the two control compounds **1** and **12** as reference compounds for bioreductive and cytotoxicity assays with **2** (Scheme 2.4). The active inhibitor **1** was considered vital for various aspects of the project, ranging from technical tasks such as optimising HPLC conditions to assessing the bioreductive prodrug release in hypoxia. Nitro benzylether **12** was synthesised in order to investigate effects of the bioreductive group itself in cellular assays.

Inhibitor **1** was obtained by employing conditions used in the original publication (Foloppe et al. 2005). Refluxing of chloride **7** with ethanolamine in ethanol afforded **1** in excellent yields (Scheme 2.4, a).

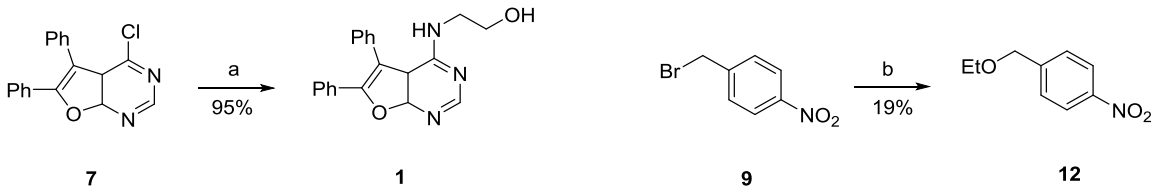

7 1 9 12

Scheme 2.4. Synthesis of control compounds 1 and 12.
Reagents and conditions: a) ethanolamine, EtOH, reflux, 6 h (Synthesis by I. Diane Swallow); b) NaH, EtOH, THF, 0 °C to RT, 2 h.

The bioreductive control compound **12** was obtained by Williamson ether synthesis using 4-nitrobenzyl bromide **9** and ethanol (Scheme 2.4, b). Despite poor yields (19%), sufficient amounts of **12** were obtained for testing and further optimisation of the reaction was not undertaken.

2.5 Inhibitor 1 also targets AURKA

During the course of this work, Chk1 inhibitor **1** was shown to also inhibit Aurora kinase A (AURKA) with a reported IC_{50} value of 306 nM (Coumar, Chu, et al. 2010; Coumar, Tsai, et al. 2010). AURKA plays an important role at the onset of mitosis (reviewed in (Nikonova et al. 2013; Malumbres and Pérez de Castro 2014) by regulating centrosome maturation (Hannak et al. 2001; Hirota et al. 2003) and bipolar spindle assembly (Tsai et al. 2003). Overexpression of AURKA in a variety of tumours has been linked to transcriptional induction through HIF-1α (Klein, Flügel, and Kietzmann 2008). In glioblastoma, AURKA expression has been shown to be induced by hypoxia and its inhibition resulted in decreased cell survival (Lehman et al. 2012). Recent studies in hepatocelluar carcinoma suggest that there might be a link between AURKA and HIF-1α promoting malignant phenotypes (Cui et al. 2013). Although inhibitors of AURKA are undergoing clinic

development (Malumbres and Castro 2014), these agents have not been tested in hypoxia.

Given our lack of knowledge about AURKA function in hypoxia we asked whether its inhibition by a small molecule inhibitor had an effect on cell survival in severe hypoxia. In particular, we intended to ensure that AURKA inhibition did not result in protection of severely hypoxic cells. RKO colorectal cancer cells were incubated with the known and selective AURKA inhibitor MLN8237 (Görgün et al. 2010; Manfredi et al. 2011; Sells et al. 2015) in severe hypoxia and normoxia. Both, normoxic and severely hypoxic cells were equally sensitive to inhibition of AURKA by MLN8237 as shown by a colony survival assay (Figure 2.5, A).

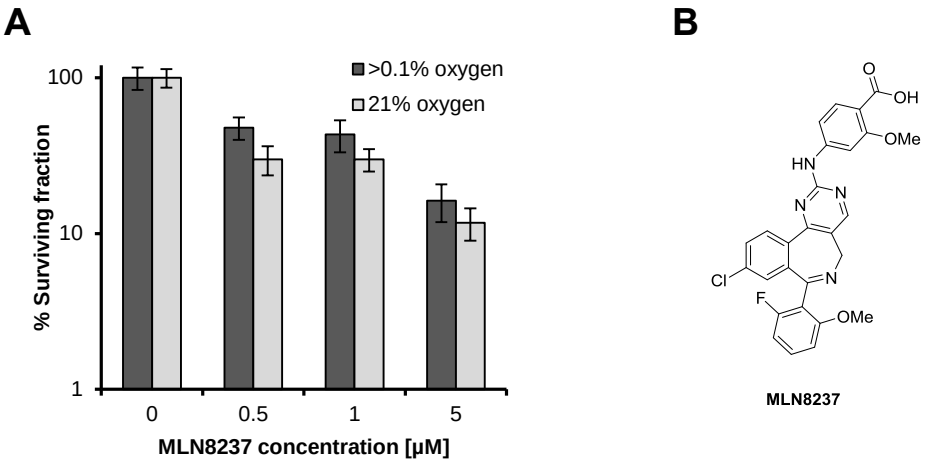

Figure 2.5. Clonogenic survival assay following AURKA inhibition in normoxia and severe hypoxia.
A) RKO cells were treated with the AURKA inhibitor MLN8237 at oxygen and drug doses as indicated for 16 h and clonogenic survival assessed. Error bars represent the standard error between technical replicates for the represented experiment (n=3). B) Chemical structure of the AURKA inhibitor MLN8237.

2.6 Mechanism of action

Based on previous reports, we proposed that prodrug **2** would undergo hypoxia-selective activation according to the mechanism outlined in Scheme 2.5.

The stepwise one-electron reduction of the nitro group can be carried out by a variety of reductases, such as CYP450.

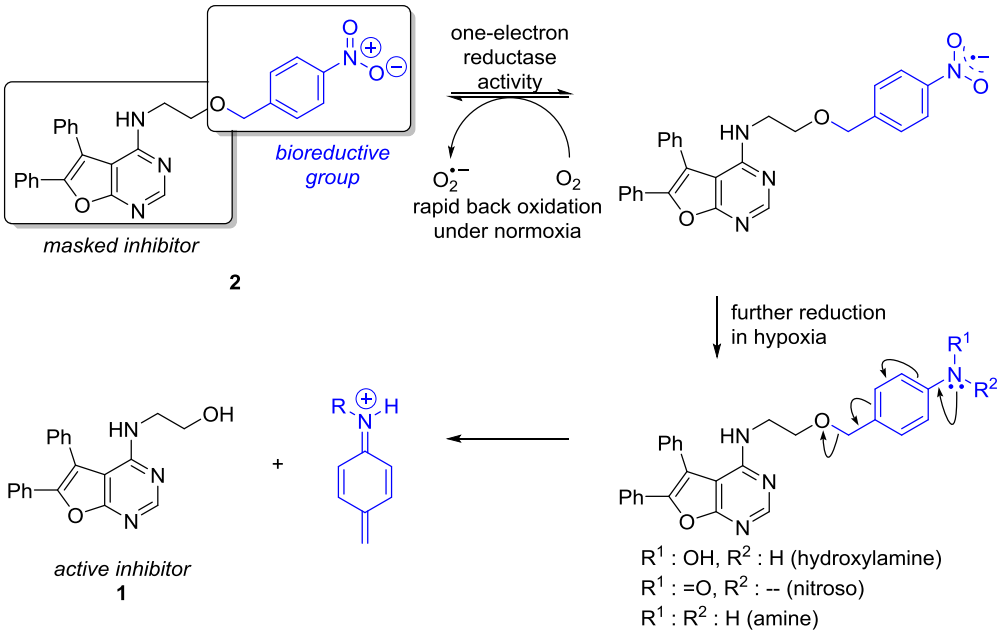

Scheme 2.5. Proposed mechanism of prodrug 2 activation in hypoxia.
One-electron reduction of the bioreductive group is reversible in normoxia, In hypoxia further reduction of the nitro group can take place and the thus generated electron donating substituent initiated fragmentation of the prodrug.

To evaluate whether **2** underwent the mechanism of activation as predicted, we carried out two experiments in progressively more biologically relevant conditions, a chemical followed by an enzymatic reduction of **2**.

2.6.1 Chemical reduction of **2**

We employed a method reported by Shigenaga and coworkers for the chemical reduction of **2** (Shigenaga et al. 2012). They demonstrated the activation of a peptide by reduction of an unnatural amino acid containing a 4-nitrobenzyl group to the corresponding 4-aminobenzyl using zinc and aqueous ammonium chloride. This reduction was followed by ejection of the peptide in sodium phosphate buffer. Using similar conditions in DMF we demonstrated the

formation of amine **14**, as was expected, and also nitroso **13** (as confirmed by mass spectrometry) from **2** after one hour, which released inhibitor **1** in aqueous conditions (Scheme 2.6).

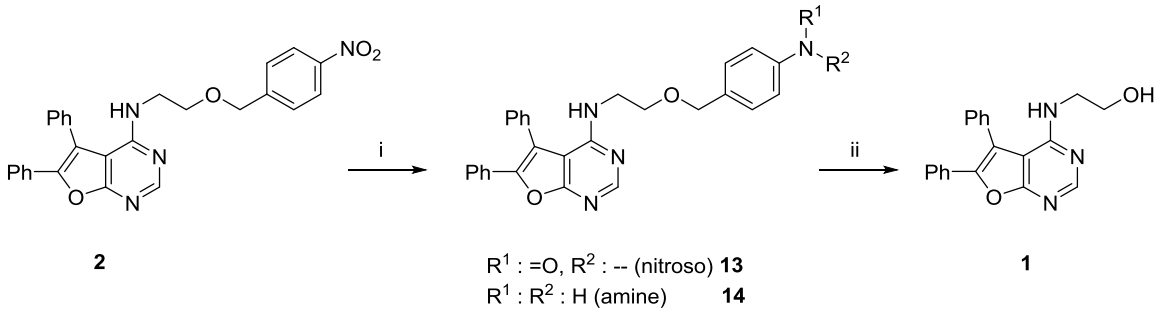

Scheme 2.6. Chemical reduction and activation of 2.
Reagents and conditions: i) Zn, NH_4Cl, DMF, 16 h, rt; ii) PPB, pH 7.4, 37 °C. Reduction carried out by Liam J. O'Connor.

Reduction of **2** was monitored by HPLC (Figure 2.6, A). After a reaction time of one hour the majority of prodrug **2** (82% total peak area) was reduced to mainly nitroso **13** (67% total peak area) and some amine **14** (15% total peak area). The reduced species **13** and **14** did not fragment to release the active inhibitor **1** under the reduction conditions, as demonstrated by an HPLC trace of the reaction mixture after one hour to which inhibitor **1** had been added as an internal reference (Figure 2.6, B).

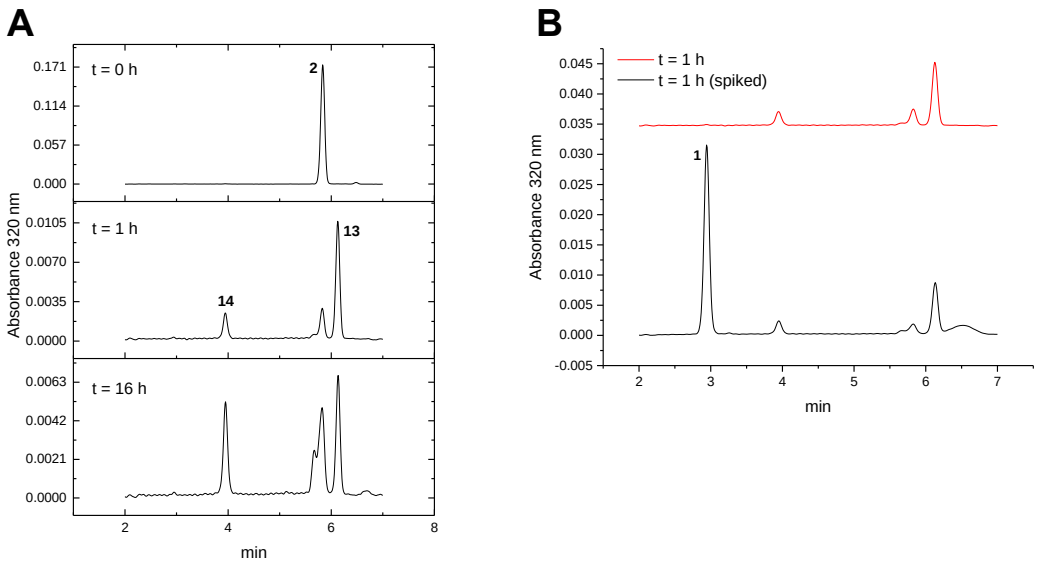

Figure 2.6. Chemical reduction of prodrug 2, HPLC traces.
A) Reduction of **2** using zinc and 10% ammonium chloride in DMF was monitored by HPLC at 0, 1, and 16 h. Characterisation of the new peaks by mass spectrometry identified them as the corresponding amine **14** and nitroso **13**. B) The active inhibitor **1** was used as an internal control in order to confirm that fragmentation of the reduced prodrug did not occur (Data provided by Liam J. O'Connor).

Reduction of a nitrobenzyl group by zinc and ammonium chloride to the corresponding nitroso had been reported before in the synthesis of nitroso benzoic acid derivatives (Pfister et al. 2008). We were, nevertheless, surprised to detect nitroso and amine but not the intermediate hydroxylamine, since the stepwise six electron reduction of a nitro group to an amine proceeds *via* the nitroso (two electrons) and the hydroxylamine (four electrons) (Tocher 1997).

To determine whether amine **14** and/or nitroso **13** fragmented under the conditions reported by Shigenaga and coworkers (Shigenaga et al. 2012), an aliquot of the reduction reaction mixture was taken after one hour, injected into PPB (pH 7.4) and incubated at 37 °C. Immediately upon injection into PPB (potassium phosphate buffer, pH 7.4), the formation of a precipitate could be observed, due to poor solubility of **2** and its reduced species in aqueous solution. Nevertheless, HPLC analysis confirmed some solubility of the three compounds

in PPB and supernatant as well as precipitate of the PPB reaction were monitored to assess progress of the reaction (Figure 2.7, A and B).

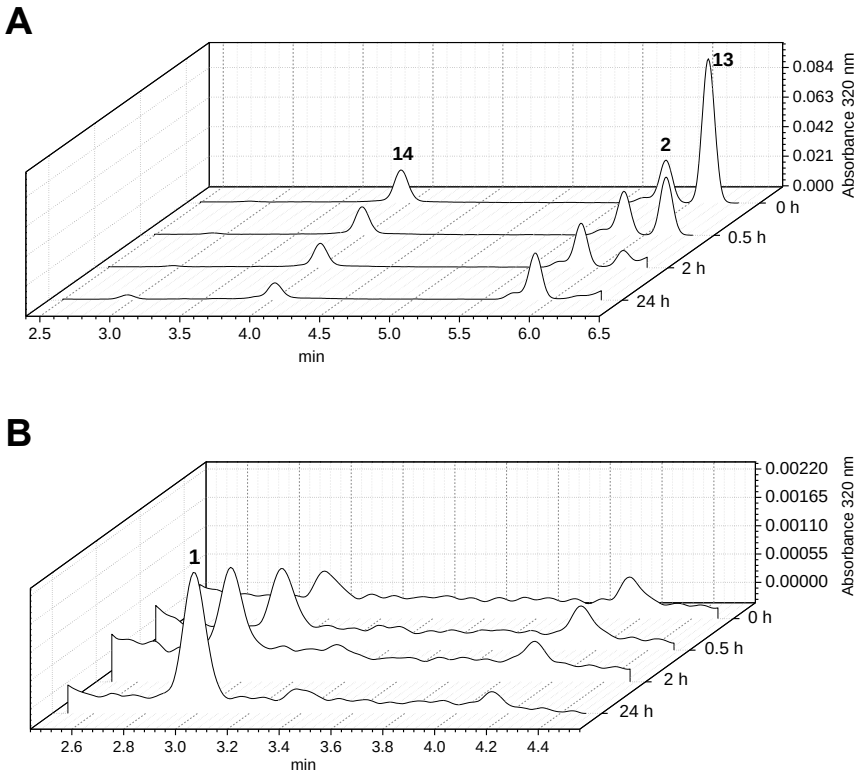

Figure 2.7. Buffer treatment of an aliquot taken from the chemical reduction of 2.
The t = 1 h aliquot from the zinc reduction of **2** was injected into PPB (pH 7.4), incubated at 37 °C and monitored. The A) formed precipitate (dissolved in acetonitrile) and B) supernatant were analysed by HPLC. In the precipitate, loss of nitroso **13** and amine **14** was observed while the formation of active inhibitor **1** could be seen in the supernatant (Data provided by Liam J. O'Connor).

Analysis of the precipitate after dissolving in acetonitrile revealed loss of nitroso and amine over time and simultaneous analysis of the respective supernatant demonstrated formation of the active inhibitor.

This experiment shows that amine **14** and nitroso **13** fragmented in aqueous solution to eject inhibitor **1** and, most importantly, demonstrates the potential for **2** to undergo activation in a reductive environment.

2.6.2 CYP450 reduction of **2**

To test whether **2** could also be reduced and activated under milder and biologically more relevant conditions, we next subjected the prodrug to enzymatic reduction by bactosomal CYP450 reductases in severe hypoxia. This experiment was considered highly relevant in resembling the reductive metabolism of **2** in cells under severe hypoxia, since nitro aromatic prodrugs had been reported to be substrates of CYP450 (Wilson and Hay 2011). Prodrug **2** was subjected to CYP450 under hypoxic conditions (<0.1% O_2) and the reduction monitored over time (Figure 2.8). Albeit slow and over the course of several hours, we observed reduction of **2** to the corresponding amine **14**, which accumulated over 24 h, followed by release of active inhibitor **1**.

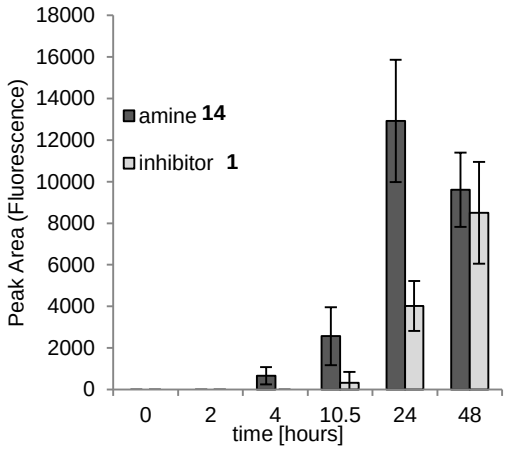

Figure 2.8. CYP450 reduction of prodrug 2 and subsequent fragmentation.
Exposure of **2** to CYP450 reductase in hypoxia (<0.1% O_2) results in reduction to amine **14** and generation of inhibitor **1**. A combination of photodiode array spectrophotometer, mass spectrometer and fluorescence spectrophotometer (λ_{ex} 320 nm, λ_{em} 380 nm) was used to detect and characterise the metabolites. Error bars represent the standard error between technical replicates for the represented experiment (n=3).

Interestingly, the previously observed nitroso **13** was not detected in this assay demonstrating that CYP450 reduced **2** fully to the corresponding amine. Due to the poor solubility of **2** in aqueous solutions and the resulting low concentration of prodrug and metabolites, we employed a sensitive fluorescence

spectrophotometer for the detection and quantification of metabolites arising from **2**.

In the chemical reduction of **2** using zinc and ammonium chloride we had seen rapid reduction of the parent compound to the corresponding nitroso and amine with an 82% conversion of **2** after one hour (assessed by peak area). Reduction using CYP450 on the other hand was much slower and the reduced species (amine **14**) peaked only after 24 h. This difference is unlikely to originate from a generally slower reduction by CYP450 but is probably due to the poor solubility of **2** in aqueous solution resulting in only small concentrations of **2** available for CYP450 reduction at any given time.

2.7 Prodrug 2 is a hypoxia-selective Chk1/AURKA inhibitor

*2.7.1 Prodrug **2** shows no inhibition of purified Chk1 or AURKA*

We hypothesized that substitution of the Chk1 inhibitor **1** to the prodrug **2** resulted in an overall significantly reduced binding affinity to the ATP binding site of Chk1. In order to test this hypothesis, a radioactive (^{33}P-ATP) filter-binding assay was carried out to determine IC_{50} values of the active inhibitor **1** and **2** against purified Chk1 and also AURKA. This assay confirmed our predictions on Chk1 inactivity of the prodrug **2** and also demonstrated no AURKA affinity (Figure 2.9). Active inhibitor **1** showed inhibition of Chk1 with a mean IC_{50} value of 1.75 µM (Figure 2.9, A) and had a mean IC_{50} value of 0.81 µM against AURKA (Figure 2.9, B).

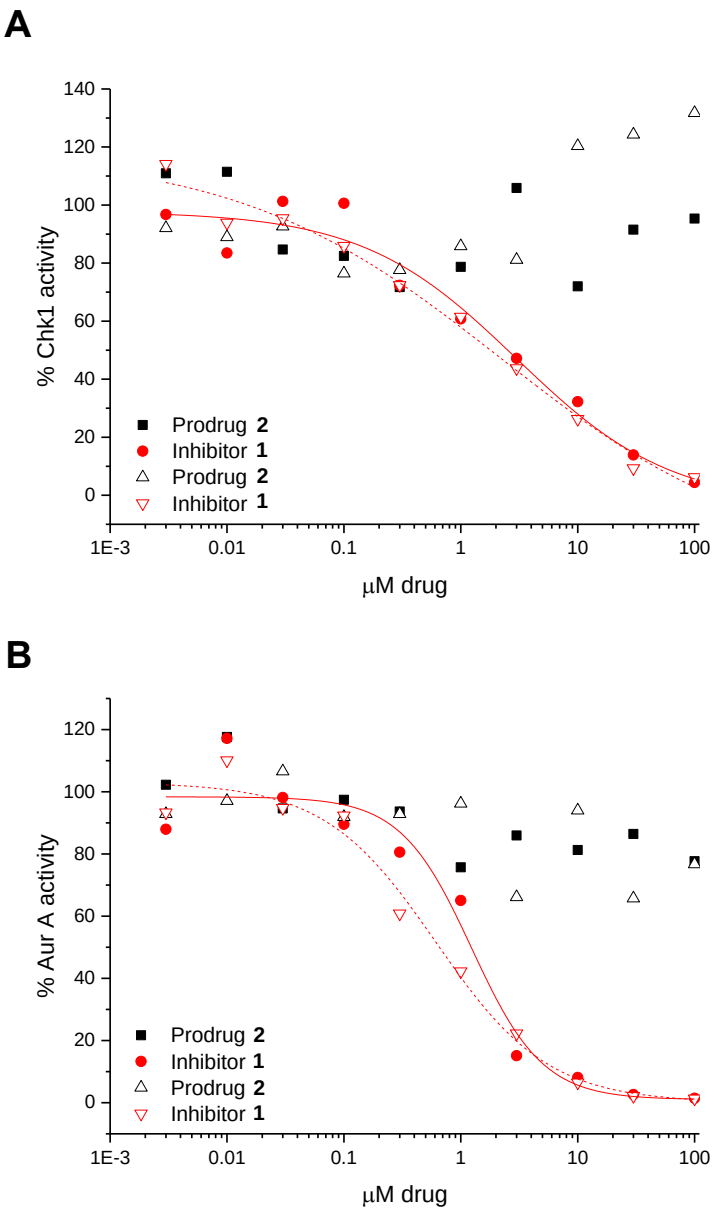

Figure 2.9. IC_{50} values for compounds 1 and 2 against Chk1 and AURKA.
A) Prodrug **2** shows no inhibition of Chk1 while an IC_{50} value of 1.75 μM was obtained with inhibitor **1**. B) Prodrug **2** shows no inhibition of Aurora kinase A while an IC_{50} value of 0.81 μM was obtained with inhibitor **1**. Mean IC_{50} values were obtained from duplicates using a radioactive (^{33}P-ATP) filter-binding assay. This analysis was carried out by The International Centre for Kinase Profiling, University of Dundee. Curves were fitted in OriginPro using a logistic model (y = A_2+(A_1-A_2)/(1+x/x_0)^p).

With these IC_{50} data, we were confident that **2** was inactive against Chk1 and AURKA at concentrations relevant for *in vitro* testing (up to 100 μM) and thus was a true prodrug of Chk1 and AURKA.

*2.7.2 Prodrug **2** acts selectively in hypoxia*

We had demonstrated that **2** was a true prodrug that showed no affinity to its targets Chk1 and AURKA. Further, with the knowledge that **2** underwent reduction and activation when exposed to CYP450 reductase in severe hypoxia, we next asked whether **2** could act as a kinase inhibitor in human cancer cells in a hypoxia-dependent fashion.

To answer this question we carried out western blotting in RKO cells for phosphorylation of histone H3 at serine 10 (pH3 Ser10), a target of AURKA/B (Crosio et al. 2002) and used the selective AURKA inhibitor MLN8237 (Görgün et al. 2010; Manfredi et al. 2011; Sells et al. 2015) as a reference compound for AURKA inhibition. Treatment of RKO cells with MLN8237 in normoxia revealed a clear decrease in pH3 Ser10, demonstrating that AURKA inhibition can result in reduced pH3 Ser10 (Figure 2.10). As expected, phosphorylation levels in the **2-**treated cells were similar to the DMSO treated controls, showing clearly that no activation of the prodrug had taken place in normoxia. In hypoxia (<0.1% O_2) pH3 Ser10 expression was decreased in the DMSO treated control cells, but even more so after treatment with **2**. After reoxygenation, we observed a marked decrease in pH3 Ser10 levels when cells had been treated with **2** while the signal in the control cells had returned to its basal levels.

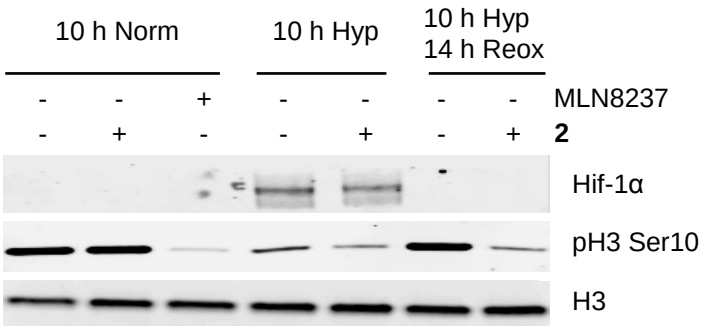

Figure 2.10. Hypoxia-selective inhibition of H3 Ser10 phosphorylation through 2.
RKO cells were exposed to hypoxia (<0.1% O_2), normoxia or hypoxia/reoxygenation as indicated in the presence of DMSO, 25 µM **2** or 500 nM MLN8237. The levels of pH3 Ser10 are shown as an indicator of AURKA activity. Hif-1α is shown as a hypoxia marker and H3 is shown as a loading control.

These data suggest that activation of prodrug **2** takes place in RKO cells selectively in severe hypoxia and that this hypoxic activation resulted in the generation of an inhibitor of AURKA.

It is noteworthy that pH3 Ser10 levels were reduced after 10 h of severe hypoxia and returned to basal levels after 14 h of reoxygenation. Phosphorylation of H3 at Ser10 is considered crucial during G_2/M transition by initiating chromosome condensation at the onset of mitosis (Van Hooser et al. 1998; Wei et al. 1998; Wei et al. 1999) and pH3 Ser10 is therefore considered a marker of mitosis. The decreased pH3 Ser10 levels indicate an arrest in G_2 phase in severe hypoxia which has been reported previously (Freiberg, Hammond, et al. 2006). Interestingly, that report demonstrated that in particular in response to reoxygenation after severe hypoxia, cells arrested in G_2. Thus a further decrease in pH3 Ser10 would be expected following reoxygenation.

It is well known that inhibition of Chk1 causes increased initiation of DNA replication and impaired DNA repair, both of which are associated with DNA damage accumulation (Syljuåsen et al. 2005; Sørensen and Syljuåsen 2012). In this context we asked if **2** induced DNA damage in cells in a hypoxia-selective

manner and carried out western blotting and immunofluorescence microscopy for the DNA damage markers γH2AX and 53BP1, respectively. For western blotting, RKO cells were treated with **2** or DMSO and normoxia or hypoxia (<0.1% O_2). In normoxia no change in γH2AX levels upon treatment with **2** was observed, indicating that **2** did not induce DNA damage in normoxia (Figure 2.11, A). Exposure to severe hypoxia alone induces replication stress and lead to a robust induction of γH2AX as had been reported before (Bencokova et al. 2009; Hammond et al. 2002). This signal was increased in the cells treated with **2** (Figure 2.12, A).

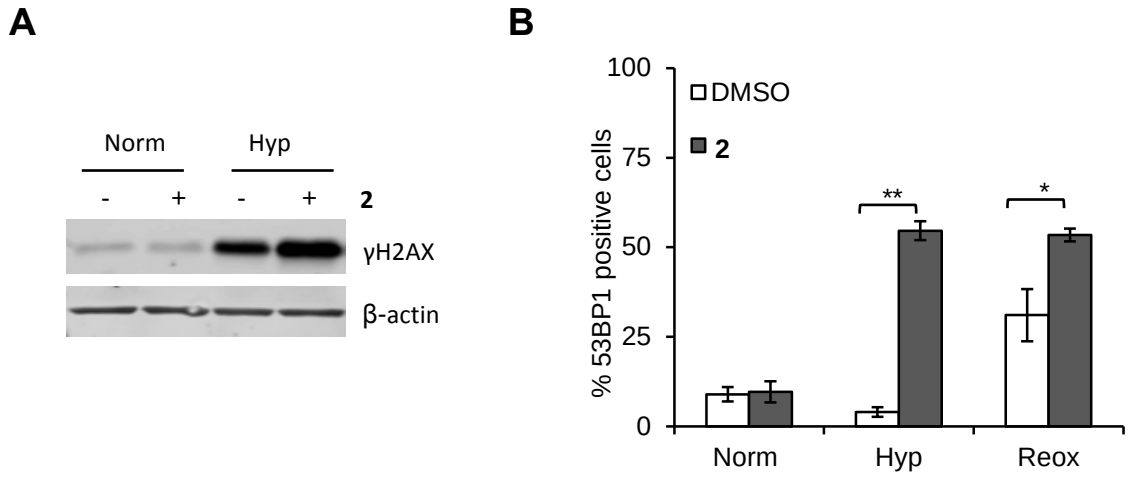

Figure 2.11. Hypoxia-selective induction of DNA damage by 2.
A) RKO cells were exposed to hypoxia (<0.1% O_2) or normoxia for 6 h in the presence of DMSO or 25 μM **2**, as indicated. The levels of γH2AX are shown as a marker of DNA damage. Actin is shown as a loading control. B) RKO cells were exposed to normoxia, hypoxia (<0.1% O_2, 6 h) or hypoxia followed by 18 h reoxygenation in the presence of DMSO or 25 μM **2**, as indicated. Shown is the percentage of cells with >6 53BP1 foci. * indicates $p<0.05$. ** indicates $p<0.0001$. Error bars represent the standard error between technical replicates for the represented experiment (n=3).

As an alternative way to access the induction of DNA damage by **2** we measured the formation of 53BP1 foci. RKO cells were exposed to normoxia, severe hypoxia or severe hypoxia followed by reoxygenation in the presence of DMSO or **2**. Consistent with the results from the western blot in Figure 2.11, A, **2** did not induce increased DNA damage in normoxia (Figure 2.11, B). In contrast

to γH2AX, which is a marker of DNA damage and also replication stress, 53BP1 foci formation is a clear indicator for DSBs. The number of 53BP1 foci did not increase in severe hypoxia but following reoxygenation-induced damage as has been reported before (Bencokova et al. 2009; Hammond et al. 2002). Importantly, treatment with **2** resulted in a significant increase in DNA damage in a hypoxia-dependent fashion. Moreover, reoxygenation-induced damage was exacerbated in the presence of **2**. Taken together, these results clearly demonstrate that **2** selectively induces DNA damage following exposure to severe hypoxia.

Inhibition of both, Chk1 and AURKA, has been investigated as a therapeutic strategy with selective inhibitors undergoing clinical trials (reviewed in (Ma, Janetka, and Piwnica-Worms 2011; McNeely, Beckmann, and Bence Lin 2014; Dar et al. 2010; Malumbres and Castro 2014; Katsha et al. 2015)). We carried out a clonogenic survival assay in a range of O_2 concentrations in order to answer two questions:

i. Does treatment with **2** lead to hypoxia-selective cell killing?

ii. If i. applies, what is the cut-off O_2 concentration at which we see a cytotoxic effect with **2**?

RKO cells were treated with **2**, exposed to O_2 concentrations ranging from 20% to <0.1% O_2 and a colony survival assay carried out for each individual O_2 concentration (Figure 2.12).

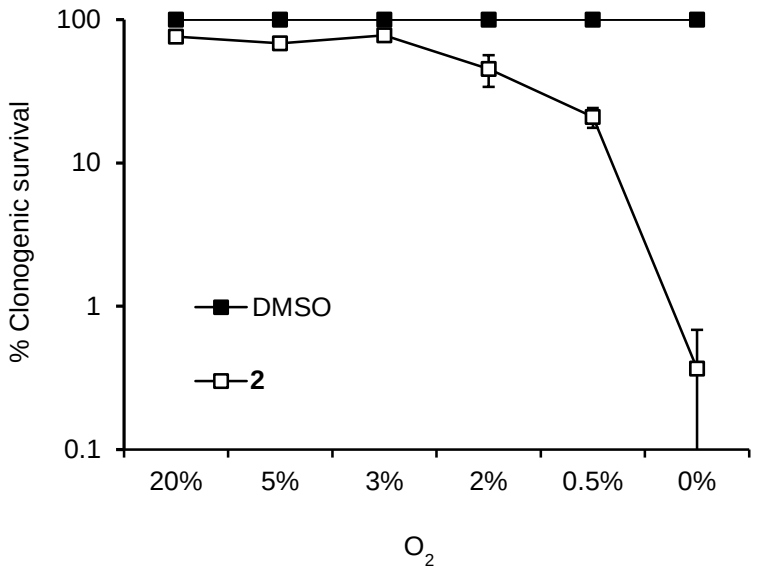

Figure 2.12. O_2 dependency of 2 toxicity.
RKO cells were exposed to the indicated O_2 concentrations in the presence of DMSO or 25 μM **2** and clonogenic survival assays carried out. Error bars represent the standard error between three technical replicates for the represented experiment (n=3). Data obtained by Isabel M. Pires.

We observed a correlation between O_2 concentration and loss in clonogenic survival. In comparison to the DMSO treated control cells a significant loss in viability could only be seen at O_2 concentrations of 2% and below. This result was encouraging as it suggests that activation of **2** occurs in a range of O_2 concentrations below the oxygenation level of normal tissue.

*2.7.3 Biological activity of **2** is not associated with the bioreductive group*

Given the mechanism of activation for the prodrug **2**, the observed biological effects, especially the induction of DNA damage and the loss of viability in an O_2-dependent manner, might at least partially be due to the liberation of the bioreductive group. The metabolite arising from the 4-nitrobenzyl group could act as a cytotoxin in itself, as has been observed with other bioreductive groups (Jaffar et al. 1998; Tanabe et al. 2005). To investigate this possibility we assessed the toxicity of ethyl ether **12** (Figure 2.13, A) in comparison with the

prodrug **2** in RKO cells. Given **12** underwent the same mechanism of activation as prodrug **2**. Exposure of **12** to severe hypoxia was expected to result in the release of compound **15** and ethanol (Figure 2.14, A). Importantly, **15** also results from hypoxia metabolism of prodrug **2** and since the amounts of ethanol produced by the reductive metabolism of **12** were low enough to be tolerated by the cells, any cytotoxicity observed with ethyl ether **12** in hypoxia could be addressed to metabolite **15**.

We treated RKO cells with hypoxia (>0.1% O_2) or normoxia for 24 h in the presence of DMSO, 25 µM active inhibitor **1**, 25 µM prodrug **2** or 25 µM ethyl ether **12** and carried out a clonogenic survival assay (Figure 2.14, B). In normoxia, treatment with inhibitor **1** resulted in a reduction of clonogenic survival and the sensitivity of RKO cells to **1** was increased after severe hypoxia/reoxygenation, as expected. Confirming previous results on the hypoxia-selective mechanism of action of prodrug **2**, treatment with **2** had no effect on clonogenic survival in normoxia but lead to a significant decrease of viability after hypoxia/reoxygenation. Importantly, treatment with ethyl ether **12** did not affect clonogenic survival in normoxia or severe hypoxia, suggesting that the metabolite from the bioreductive group itself did not enhance cytotoxicity. We can thus conclude that the reduction in viability following exposure to **2** solely originates from the release of inhibitor **1**.

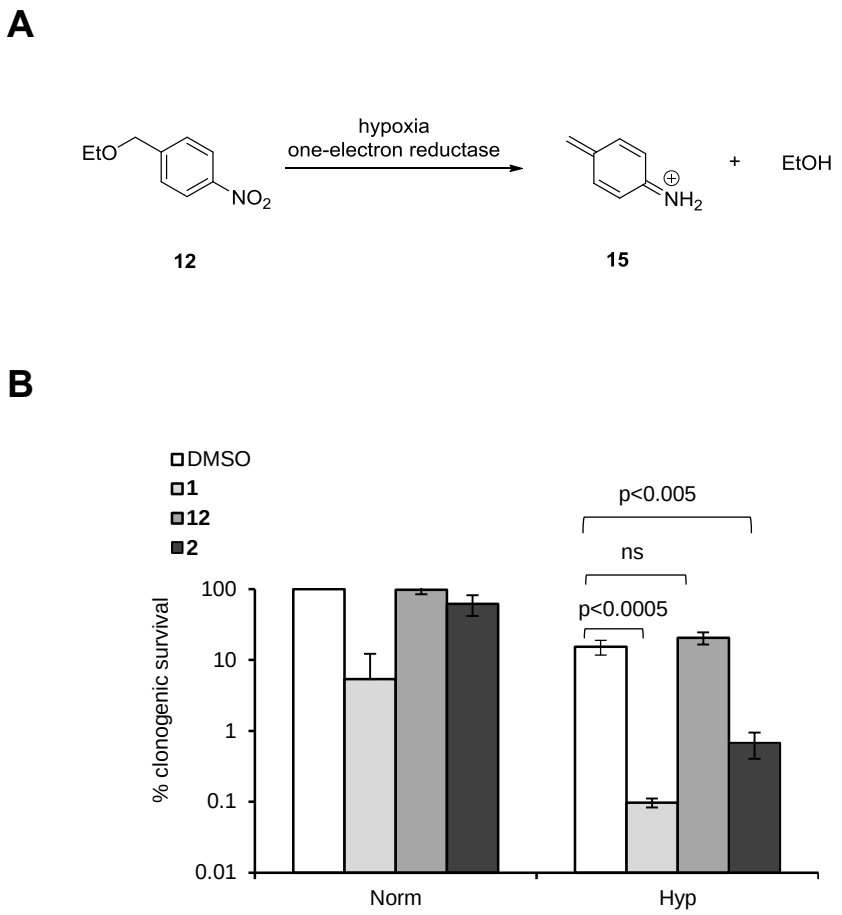

Figure 2.13. Assessment of the cytotoxic effect of the 4-nitrobenzyl bioreductive group. A) Proposed mechanism of activation for the ethyl ether **12**, resulting in the generation of **15** and pharmacologically irrelevantly small amounts of ethanol. B) Clonogenic survival assays were carried out in either hypoxia (<0.1% O_2) or normoxia (24 h treatment) using RKO cells in the presence of DMSO or 25 μM of either active inhibitor **1**, prodrug **2** or ethyl ether **12**. Error bars represent the standard error between three technical replicates for the represented experiment (n=3).

2.8 Sensitivity to prodrug 2 can partly be predicted by basal levels of DNA damage

It has been shown that tumours with high levels of oncogene-induced replication stress could be targeted though inhibition of the ATR-Chk1 pathway. For example, a number of studies have demonstrated that cells with elevated levels of the MYC or Ras oncogenes showed increased sensitivity to inhibition of ATR or Chk1 (Cole et al. 2011; Gilad et al. 2010; Murga et al. 2011; Höglund et

al. 2011; W.-J. Wang et al. 2013). Interestingly, the use of Chk1 inhibitors as single agents has also been proposed in MYC-driven tumours (Ferrao et al. 2012; Khanna et al. 2013).

Based on these reports, we proposed that sensitivity to **2** could be predicted by assessing the basal levels of DNA damage in a cell line. We chose three lung cancer cell lines in which we tested whether clonogenic survival following treatment with **2** correlated with basal levels of DNA damage. A recent review has highlighted the potential for targeting lung cancer through the inhibition of checkpoint kinases (Syljuåsen et al. 2015). Among other reasons, the high level of oncogenic stress in most lung cancers was mentioned as a feature contributing to checkpoint sensitivity.

The three cell lines A549, H1299 and H1975 were stained for the DNA damage markers 53BP1 and γH2AX (Figure 2.14, A). Cells were scored as positive or negative for the respective marker, depending on the number of foci counted per cell (Figure 2.14, B)

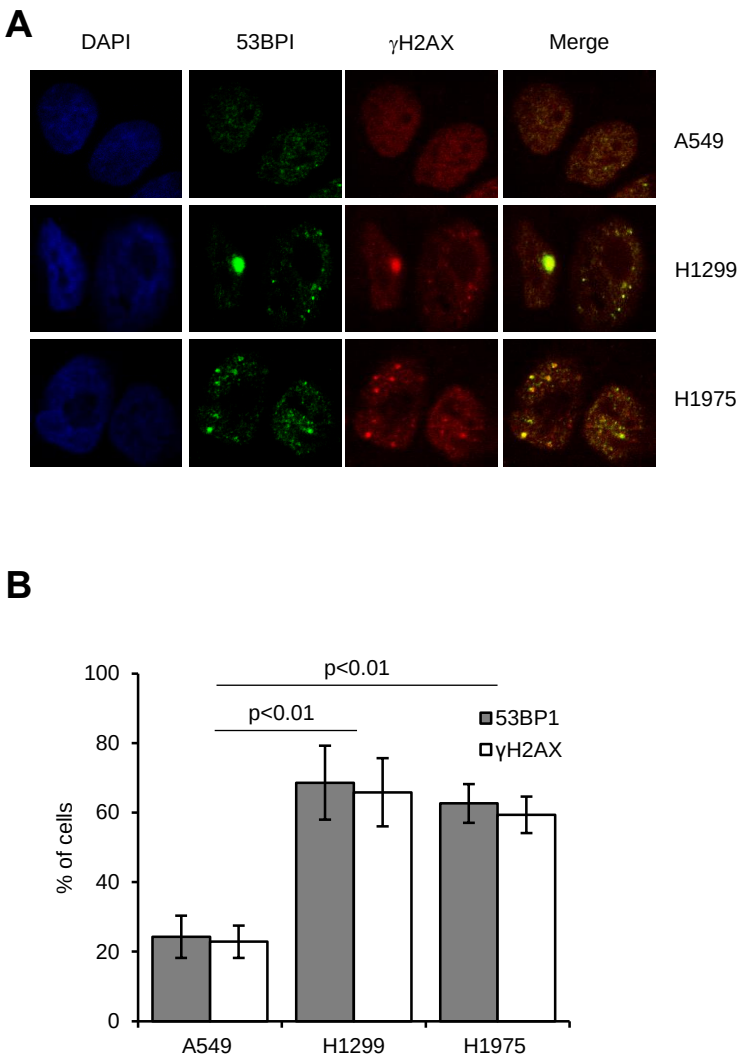

Figure 2.14. Basal level of DNA damage in three lung cancer cell lines.
A) A549, H1299 and H1975 cells were stained for 53BP1 (green) and γH2AX (red) as markers of endogenous DNA damage. Representative images are shown. B) Percentage of the number of cells stained positive for the shown marker (53BP1 (grey), γH2AX (white)). Error bars represent the standard error between three technical replicates for the represented experiment (n=3).

A significant number of cells positive for both markers was found in all three cell lines. Importantly, the number of cells scored positive correlated very well between the two markers. While the A549 cell line showed the lowest level of endogenous damage (24% (53BP1) and 22% (γH2AX)) a high proportion of cells in the H1299 (69% (53BP1) and 66% (γH2AX) and H1975 (63% (53BP1) and 59% (γH2AX) cell lines stained positive. These results suggest that the A549 cell

line should be less sensitive to **2** treatment in severe hypoxia than the other two cell lines.

In order to test this hypothesis we carried out a clonogenic survival assay where the three cell lines were exposed to **2** for 24 h in severe hypoxia or normoxia (Figure 2.15). Most sensitive to **2** in severe hypoxia was the H1975 cell line with a 63% reduction in survival upon treatment with **2**. The other two cell lines showed comparable sensitivities.

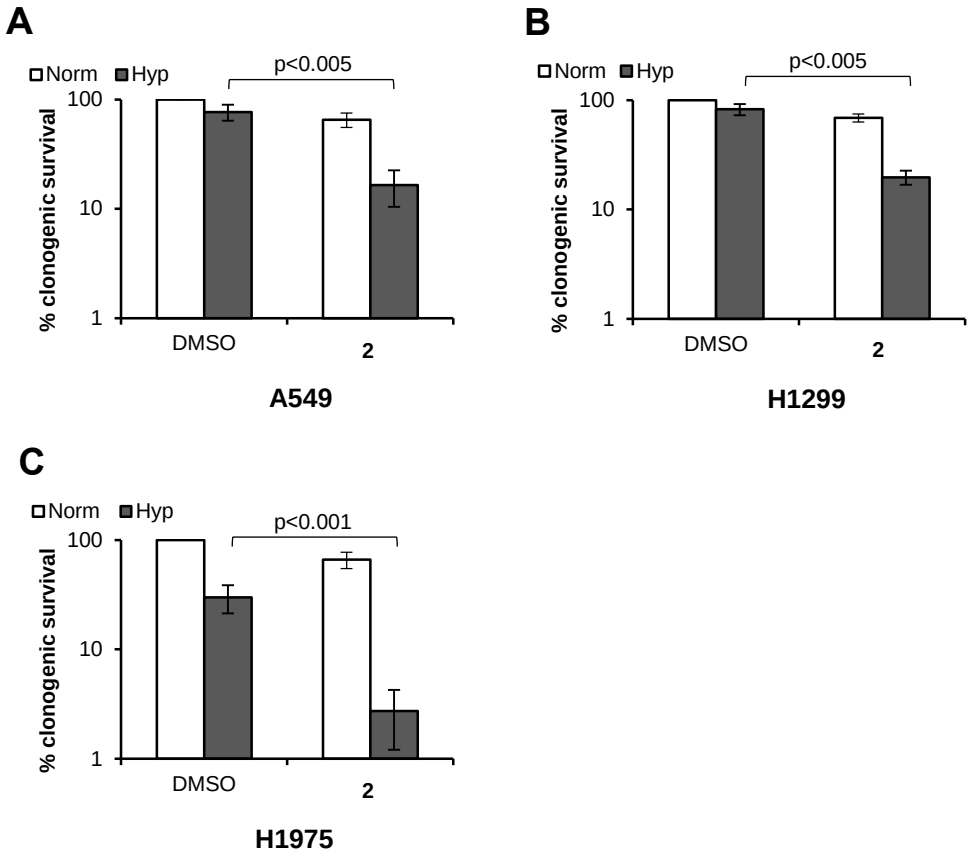

Figure 2.15. Colony survival assays in three lung cancer cell lines.
The three lung cancer cell lines A) A549, B) H1299 and C) H1975 were exposed to 25 μM **2** or DMSO and hypoxia (<0.1% O_2) or normoxia for 24 h. Colony survival assays were carried out. Error bars represent the standard error between three technical replicates for the represented experiment (n=3) (Data obtained by Monica M. Olcina).

This data shows once again that sensitivity to **2** is potentiated in severe hypoxia. Although the results in these three cell lines suggest that some correlation may exist between the endogenous level of DNA damage in a cell line

and its sensitivity to **2**, a larger panel of cell lines would have to be used in order to draw a valid conclusion.

The sensitivity of a cell line to **2** will undoubtedly depend on activation of **2** in hypoxia combined with the cell line specific endogenous sensitivity to the inhibition of Chk1 and AURKA. Reduction and activation of **2** in a cell line depends on the level of endogenous reductases to which **2** is a substrate. We have shown that this includes CYP450 but other one-electron reductases are likely to act as activating enzymes as well (Wilson and Hay 2011).

2.8 Discussion

We have confirmed a role for Chk1 in the hypoxia-induced DDR in showing that Chk1 is phosphorylated and active in response to severe hypoxia. Inhibition of Chk1 resulted in the accumulation of DNA damage in WI38 normal lung fibroblasts, which supports the concerns raised regarding inhibition of Chk1 in normal tissue. In order to exploit the sensitivity of severely hypoxic cells to inhibition of Chk1 and avoid normal tissue toxicity, we have designed and synthesised a bioreductive 4-nitrobenzyl analogue **2**, based on the published Chk1/AURKA inhibitor **1**. Prodrug design was rationalised by a published SAR study around **1** and by docking studies. The prodrug was shown to have significantly reduced binding affinity to Chk1 in comparison with **1** and underwent reduction and activation in a reducing environment. Poor solubility of **2** is likely the cause for slow reduction by CYP450. Once reduced, fragmentation of the prodrug was also slow and occurred over several hours. Importantly, we demonstrated that compound **2** is a hypoxia-selective inhibitor of AURKA and induces DNA damage only following exposure to hypoxia. Reduction in

clonogenic survival was shown to be O_2-dependent and treatment with **2** caused significant cell kill only at O_2 concentrations below 3%. Using the bioreductive control compound **12**, we showed that the hypoxia-selective cytotoxicity observed with **2** was not due to the metabolite from the bioreductive group, suggesting that cytotoxicity was solely due to the release of Chk1 inhibitor **1**. Finally, experiments in three lung cancer cell lines suggest that the sensitivity of a cell line to **2** might correlate with the endogenous levels of DNA damage in that cell line.

CHAPTER 3

SYNTHESIS AND VALIDATION OF A SET OF ANALOGUES BASED ON A PYRAZOLOPYRIDINE CHK1 INHIBITOR

3.1 Introduction

3.1.1 Choice of Chk1 inhibitor

With prodrug **2** we developed a proof-of-concept bioreductive Chk1 inhibitor. Our next aim was to to apply this concept to the development of a compound with superior pharmacokinetic and bioreductive properties. Our goal was to identify a potent and selective Chk1 inhibitor, and we were looking for a compound that had already undergone extensive *in vitro* testing and shown good pharmacokinetic properties. Furthermore, the Chk1 inhibitor of choice required a suitable functionality for bioreductive group attachment, that was also available for alkylation and possessed a good leaving group ability, to ensure rapid reductively-triggered prodrug fragmentation. Only functionalities that play a role in the binding of the inhibitor to Chk1 were considered in order to reduce the affinity of the bioreductive prodrug. We focused on inhibitors with a published synthetic route, versatile enough to allow bioreductive group incorporation without having to make major alterations to the synthesis.

Our inhibitor of choice was pyrazolopyridine **16**, an ATP-competitive inhibitor that had emerged from a fragment-based screen (Matthews et al. 2009). The authors had employed X-ray crystallography to reveal three interactions formed between **16** and the ATP-binding site of Chk1 (Figure 3.1, A). The

pyrazolopyridine core was shown to occupy the ATP pocket, with the heterocycle binding to the protein backbone through Glu85 and Cys87. The morpholine substituent extended into the ribose-binding pocket, forming a salt bridge between its primary amine and the carboxylate of Glu91. Compound **16** presented a primary amine and a heterocyclic amine as potential sites for substitution with a bioreductive group. Although an interaction between the primary amine and the protein backbone was evident from the crystal structure (Figure 3.1, A), the amine pointed into a solvent-exposed region and we reasoned that substitution on that position could be tolerated and not lower the binding affinity significantly. Therefore and because of a very tight interaction between the heterocyclic core of the inhibitor and the kinase hinge region, we decided to substitute the heterocycle with a bioreductive group. We proposed that substitution of pyrazole N1 with a bioreductive group would result in a prodrug with significantly reduced binding affinity and intended to synthesise a comprehensive set of four analogues (Figure 3.1, B).

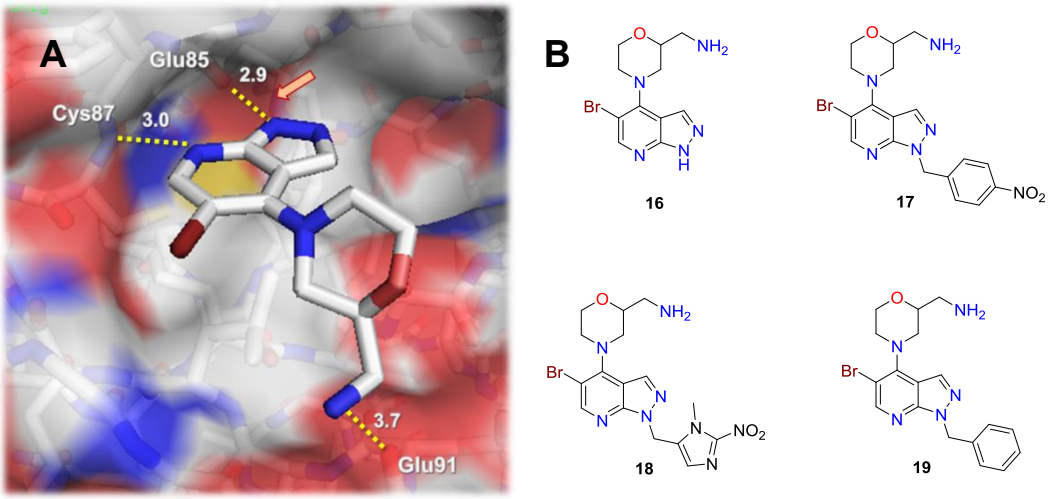

Figure 3.1. Design of a set of analogues based on Chk1 inhbitor 16.
A) X-Ray crystal structure of **16** in the ATP-binding site of Chk1 (PDB 2wmw). Interactions are shown as dashed yellow lines with their length given in Å. An arrow indicates the chosen site of substitution. B) The proposed set of analogues derived from inhibitor **16**, comprising the two bioreductive prodrugs **17** and **18** and the benzyl analogue **19**.

We planned to synthesise inhibitor **16** as a positive control for *in vitro* toxicity and cell survival assays and also as a reference compound for HPLC work when elucidating the mode of action of the bioreductive analogues **17** and **18**. Through minimal modification of the published synthetic route towards **16**, we expected to obtain the two hypoxia-activated analogues **17** and **18**. With the 4-nitrobenzyl analogue **17** we were building on the success of **2** (also a 4-nitrobenzyl-triggered prodrug) and expected **17** to have similar bioreductive properties to **2**. An improved version was proposed to be the 2-nitroimidazole **18**, with better bioreductive and tissue-penetration properties. In addition, we intended to synthesise benzyl-substituted **19** which, due to the lack of a hypoxia-sensitive trigger unit was proposed to be inactive and a negative control compound.

3.1.2 Synthesis outline

In order to synthesise the proposed compounds **17-19**, we planned to follow a published route for the synthesis of the inhibitor core (Matthews et al. 2009; Misra, Rawlins, et al. 2003; Misra, Xiao, et al. 2003). In addition, the building block for the 2-nitroimidazole bioreductive group had to be synthesised and we intended to follow a previously published synthetic route (Cavalleri, Ballotta, and Lancini 1972).

Inspection of the published synthetic route towards **17** revealed three steps that could enable the incorporation of a bioreductive group (Figure 3.2). Instead of using 4-anisaldehyde to form the PMB-protected pyrazole **21**, we reasoned that the use of a nitro-aromatic aldehyde corresponding to the desired

bioreductive group would avoid the overall use of a protecting group and shorten the synthesis (Figure 3.2, A).

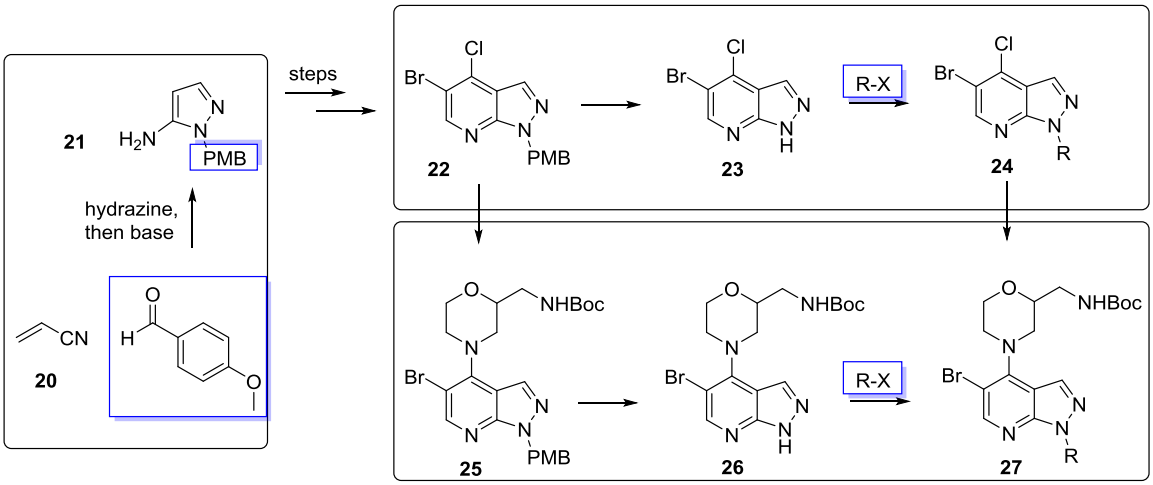

Figure 3.2. Synthesis overview for Boc-protected analogues of 16-19, and potential steps for bioreductive group incorporation.
Highlighted in blue are the three opportunities for incorporation of the bioreductive group R. A) At the stage of pyrazole formation. Instead of the shown 4-anisaldehyde we proposed that the corresponding aldehyde of the bioreductive group could be used for pyrazole formation. B) After bicyclic core formation. Replacement of the PMB group by the bioreductive group, followed by incorporation of the morpholine ring to give bioreductive building block **27**. C) As final synthetic step prior to Boc-deprotection.

Alternatively, the pyrazolopyridine core structure **22** could be formed as published (Misra, Xiao, et al. 2003; Misra, Rawlins, et al. 2003). PMB-deprotection followed by attachment of the bioreductive group was proposed to give **24** and, after nucleophilic aromatic substitution and Boc-deprotection, afford the analogues **17-19** (Figure 3.2, B). Reversal of these two steps would allow for attachment of the bioreductive group in the last step, prior to deprotection (Figure 3.2, C). Our primary focus was on the less step-intensive strategy A, but in case that failed, discrimination between alternatives B and C was to depend on the overall yield and cost of either strategy.

3.2 Chemical synthesis of 5-(chloromethyl)-2-nitroimidazole 38

3.2.1 Synthesis of the imidazole precursor

Although 5-(chloromethyl)-2-nitroimidazole **38** and the corresponding alcohol **35,** are commercially available, we decided to synthesise **38** *via* a previously published route (Scheme 3.1) (Cavalleri, Ballotta, and Lancini 1972; Asato and Berkelhammer 1972) due to the relatively high expenses of **38,** and the potentially large quantities required for the synthesis of a bioreductive drug. In particular, if that drug was going to be evaluated in animal models a quick, robust and inexpensive synthetic route was required.

Based on the previously published report we initially intended to synthesise **31** to then obtain the imidazole precursor **32** in a reaction with cyanamide at pH 4.5 in aqueous HCl or in 10% *v/v* acetic acid (Cavalleri, Ballotta, and Lancini 1972; Asato and Berkelhammer 1972) (Scheme 3.1). From here, a series of standard functional group manipulations would yield the building block **38**.

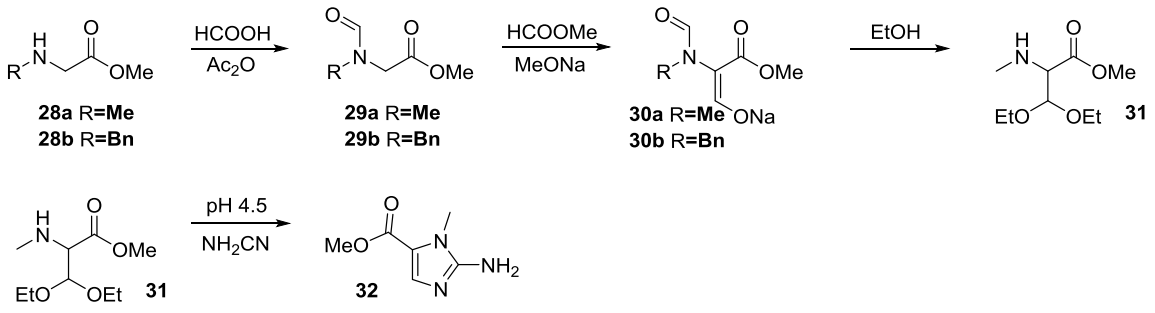

Scheme 3.1. Proposed synthesis of the 2-nitroimidazole precursor 32.
We proposed formation of enolate **30a** in two steps, following a published procedure for the benzylated analogue **30b** (Schmidt and Geiger 1963; Soede-Huijbregts et al. 2001). De-formylation and pyrazole formation as published was expected to give **32** (Cavalleri, Ballotta, and Lancini 1972).

To obtain the sodium enolate **30a**, we followed a procedure that reported the *N*-benzylated analogue **30b** from the corresponding benzylated methylester

28b, using formic acid and acetic anhydride followed by methyl formate and sodium methoxide in toluene (Schmidt and Geiger 1963; Soede-Huijbregts et al. 2001). Although we could isolate formate **29a** following this procedure, subsequent formation and isolation of sodium enolate **30a** was not successful in our hands. Further attempts to obtain acetal **31** directly from *N*-formate **29a** without isolating enolate **30a** were also unsuccessful, and consequently we decided to attempt a one-pot sequence of reactions towards **32** without isolation of intermediates. Matteucci and coworkers have previously published a synthesis of imidazole **32** from sarcosine methylester **28a** in three steps (Matteucci et al. 2007). They formed enolate **30a** by reaction of sarcosine methylester **28a** in ethylformate with an excess sodium hydride, **30a** was used without further purification for deformylation with HCl in ethanol. Heterocycle formation was subsequently achieved with cyanamide by heating under reflux in an aqueous, acetate-buffered system. Following this procedure, formation of imidazole **32** was achieved from sarcosine methylester **28a** in 38% yield over three steps (Scheme 3.2).

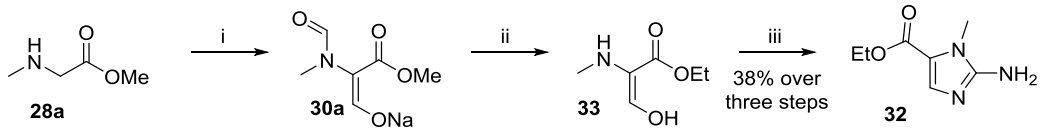

Scheme 3.2. Synthesis of the 2-nitroimidazole precursor 32.
Published conditions were modified and imidazole **32** obtained in three steps with 38% overall yield (Matteucci et al. 2007). Conditions: i) EtCHO, NaH, THF, 0 °C to RT, 18 h; ii) conc. HCl in EtOH, reflux, 1h; iii) NH_2CN, $NaOAc \cdot 3\ H_2O$, 10% *v/v* AcOH, 100 °C, 18 h.

The reported conditions for the synthesis of ester **32** were modified, and instead of carrying out the formylation neat in ethylformate, we found that a suspension in THF was an easier to handle reaction system, where reactants were better suspended and heat generation could be managed. Furthermore, we isolated pure amine **32** as a precipitate from the crude reaction by adjusting the

reaction mixture to pH 8-9, instead of extracting the product with ethyl acetate, as reported (Matteucci et al. 2007). The sequence could be scaled up to 5 g of starting material **28a** without compromising the yield.

3.2.2 Conversion of imidazole **32** *into 5-(cloromethyl)-2-nitroimidazole* **38**

With a convenient synthesis of imidazole **32** in hand, we focussed on the conversion of its 2- and 5-substituents to obtain imidazole **38**. Nitration of **32** to imidazole **34** was attempted using sodium nitrite in 7% *v/v* sulfuric acid as had been reported, but no reaction took place in our hands as judged by mass spectrometry and NMR analysis (Asato and Berkelhammer 1972). When the reaction was carried out in 50% *v/v* aqueous AcOH with an excess of sodium nitrite, yields of 60-68% were obtained and increasing the acid concentration to 67% *v/v* aqueous AcOH resulted in 72% yield (Matteucci et al. 2007) (Scheme 3.3).

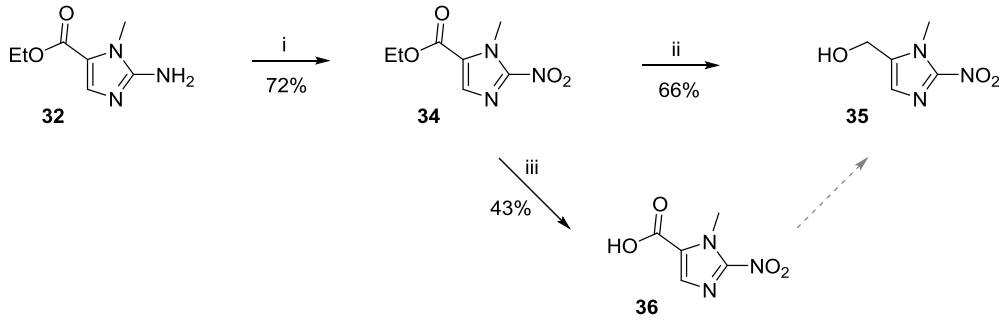

Scheme 3.3. Conversion of the 2- and 5-substituents to give alcohol 35.
2-Amino imidazole **32** was converted into the corresponding 2-nitro imidazole **34** (optimisation carried out by Liam J. O'Connor) followed by reduction to alcohol **35**. A previously reported two-step sequence *via* the carboxylic acid **36** was abandoned due to low yields in the ester hydrolysis (43%), reduction of acid **36** was not carried out (dashed arrow) (Hay, Wilson, and Denny 2000). Conditions: i) $NaNO_2$, 67% *v/v* AcOH, RT, 2 h; ii) $NaBH_4$, THF/MeOH, 0 °C, 2 h; iii) 1 M aq. NaOH, 18 h, RT.

Reduction of the ester **34** to alcohol **35** in two-steps *via* the corresponding carboxylic acid **36** had been reported as a high-yielding sequence (Hay, Wilson,

and Denny 2000). However, since we managed to isolate acid **36** in only 43% yield, we decided to abandon this strategy and reduction to the alcohol **35** was carried out directly with $NaBH_4$ in 66% yield.

In order to convert the hydroxyl group of imidazole **35** into a good leaving group, we intended to synthesise bromide **37**, and the standard halogenation conditions outlined in Table 3.1 (entries 1-5) were investigated. The Appel reaction did not show any indication of **37** formation (entry 1), and halogenation with thionyl bromide in the presence of catalytic DMF only gave traces of **37** (entry 2). Changing the solvent from THF to $CHCl_3$ and CH_2Cl_2 in a method employing PPh_3 improved yields only slightly, and the highest yield we obtained was a poor 29% (entry 5).

Table 3.1. Optimisation of conditions for the synthesis of bromo-2-nitroimidazole 37.

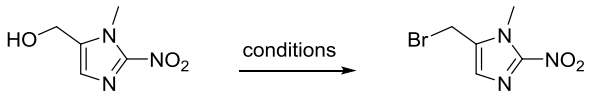

35 **37**

Entry	Conditions	Yield [%]
1	Br_2, PPh_3. acetonitrile, 0 °C to RT	-
2	$(COBr)_2$, cat. DMF, CH_2Cl_2. 0 °C to RT	traces
3	PBr_3, THF, 0 °C to RT	traces
4	PBr_3. $CHCl_3$. 0 °C to RT	16
5	PBr_3, CH_2Cl_2. -10 °C to RT	29

Due to the low yields observed under all these conditions, we decided to synthesise the corresponding chloride **38** instead. Formation of **38** was optimised by investigating similar conditions to those explored for formation of bromide **37**, and highest yields were obtained using thionyl chloride and pyridine in CH_2Cl_2 (Table 3.2, entry 3).

Table 3.2. Optimisation of conditions for the synthesis of chloro-2-nitroimidazole 38.

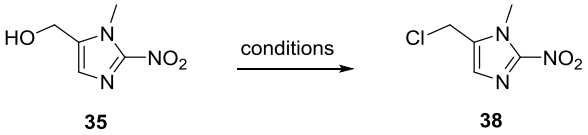

35 **38**

Entry	Conditions	Yield [%]
1	$(COCl)_2$, cat. DMF, CH_2Cl_2. 0 °C to RT	nd
2	PCl_3, CH_2Cl_2, 0 °C to RT	29
3	$SOCl_2$, pyridine, CH_2Cl_2. 0 °C to RT	66

Overall we found convenient conditions to obtain the bioreductive building block **38** from inexpensive sarcosine methylester **28a** in six steps, with an overall yield of 12% (Scheme 3.4). The imidazole formation could be scaled up to 5 g sarcosine methylester starting material, larger scales compromised the yield. Nitroimidazole **38** was crystalline and could be stored at -20 °C for four months without decomposition as judged by HPLC.

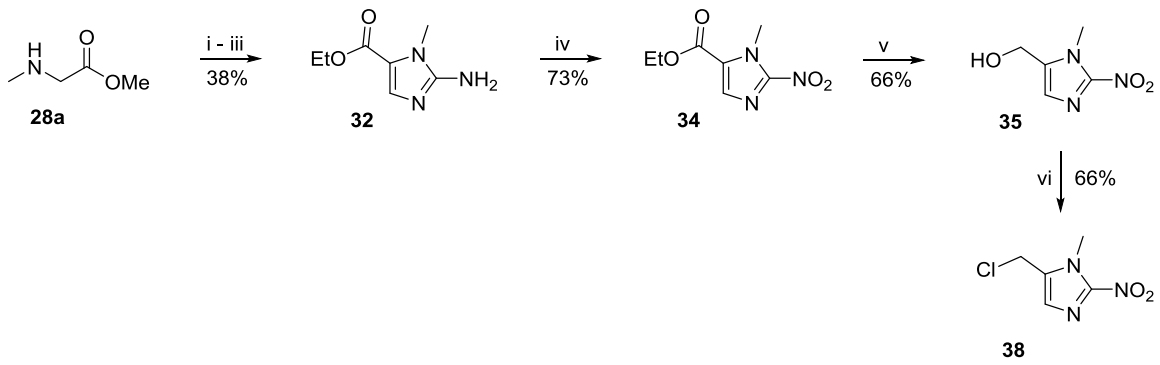

Scheme 3.4. Overview of optimised synthesis of 38.
Conditions: i) EtCHO, NaH, THF, 0 °C to RT, 18 h; ii) conc. HCl in EtOH, reflux, 1h; iii) NH_2CN, NaOAc·3 H_2O, 10% *v/v* AcOH, 100 °C, 18 h; iv) $NaNO_2$, 67% *v/v* AcOH, RT, 2 h; v) $NaBH_4$, THF\MeOH, 0 °C, 2 h; vi) $SOCl_2$, pyridine, CH_2Cl_2, 0 °C to RT, 5 h.

3.3 Chemical synthesis of the analogues 16-19

*3.3.1 Synthesis of key intermediate **22** and Chk1 inhibitor **16***

A previously published route was followed in the synthesis of **22** (Matthews et al. 2009; Misra, Rawlins, et al. 2003; Misra, Xiao, et al. 2003). Acrylonitrile **20** was reacted with hydrazine in a Michael type addition, followed by imine formation using 4-anisaldehyde (Scheme 3.5). Upon heating imine **39** under reflux with sodium hydroxide in ^{i}PrOH, and then adjusting to pH 4-5, PMB-protected pyrazole **21** was obtained, and could be used without further purification as had been reported (Misra, Rawlins, et al. 2003). Amine **21** was condensed with diethylethoxymethylenemalonate, which was then subjected to pyrolysis in diphenyl ether, to give the bicyclic core system **40**. Starting from acrylonitrile **20** no purification of any intermediates throughout the first four steps was necessary, and the inhibitor core **40** was obtained in 31% overall yield (Scheme 3.5).

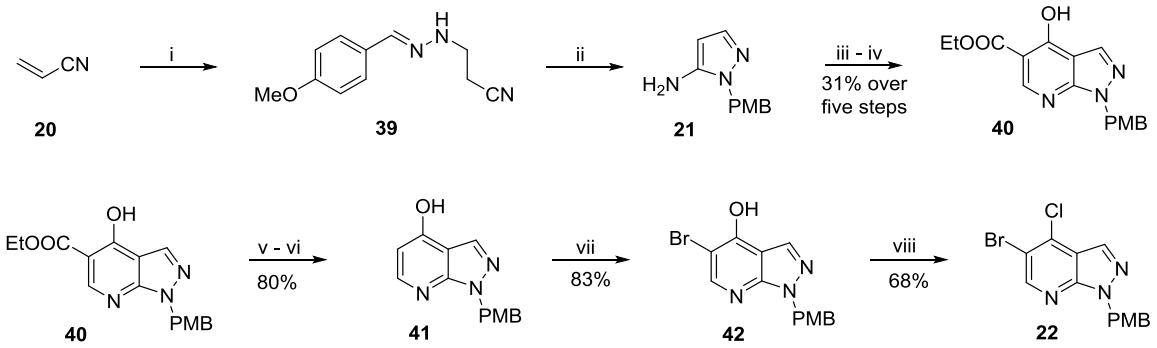

Scheme 3.5. Synthesis overview of key intermediate 22.
A previously published route was followed in the synthesis of **22** from acrylonitrile **20**, with synthetic alterations in the last two steps: Instead of bromine as published, NBS was used for formation of bromide **42**. Subsequent chlorination was carried out at milder conditions than originally published (Matthews et al. 2009; Misra, Xiao, et al. 2003; Misra, Rawlins, et al. 2003). Conditions: i) NH_2NH_2, THF, RT, 2 h. Then 4-anisaldehyde, 0 °C to RT, 6 h; ii) NaOH, ^{i}PrOH, reflux, 6 h; iii) diethylethoxymethylenemalonate 120 °C, 3 h; iv) Ph_2O, 240 °C, 24 h; v) 15% *v/v* aq. NaOH, EtOH, 90 °C, 6 h; vi) Ph_2O, 240 °C, 18 h; vii) NBS, AcOH, 60 °C, 2 h; viii) $POCl_3$, $C_2H_4Cl_2$, 75 °C, 2 h.

Ester hydrolysis and decarboxylation gave phenol **41** in 80% yield. Ortho-selective electrophilic aromatic substitution was carried out with NBS (*N*-bromosuccinimide) in glacial AcOH. The use of NBS gave similar yields (83%) to when the reaction was carried out with bromine, but was safer and easier to handle. Initially, conversion of phenol **42** into chloride **22** was attempted by heating in neat $POCl_3$ at 110 °C, as had been reported, but this resulted in partial removal of the PMB group (Misra, Xiao, et al. 2003). Milder conditions were employed and key intermediate **22** was synthesised in 68% yield by heating with $POCl_3$ in dichloroethane at 75 °C.

The Chk1 inhibitor **16** was synthesised in two steps from **22** (Scheme 3.6).

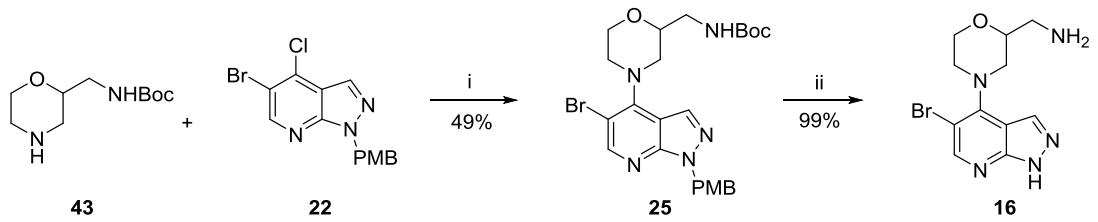

Scheme 3.6. Synthetic alterations in the final steps towards Chk1 inhibitor 1.
Nucleophilic aromatic substitution was optimised by change of solvent from *n*-butanol in the original procedure to NMP. Final deprotection was carried out in the presence of triisopropylamine for clean and full conversion to **1**. Conditions: i) 1.1 eq **28**, Et_3N , NMP, 130 °C, 7 h; ii) $^iPr_3SiH$, TFA, 40 °C, 18 h.

The nucleophilic aromatic substitution to form morpholine **25** was originally reported using 2.2 eq of the amine **43** in *n*-butanol as a solvent, and reaction times of 18 h (Matthews et al. 2009). When we performed this reaction in NMP (*N*-methyl-2-pyrolidone) , the amount of amine **43** could be reduced to 1.1 eq and the reaction time to 7 h, while still obtaining the same yield of **25** as had been reported in the original procedure (49% yield). In addition, unreacted starting material **7** could be recovered in 32% yield. Global deprotection of the Boc- and PMB-groups using neat TFA gave the Chk1 inhibitor **16**, along with some Boc-deprotected material, where the PMB-group was still intact. Addition of the cation scavenger triisopropylsilane solved this problem and the reaction went to completion. The product was purified by ion exchange chromatography using an ISOLUTE® SCX-2 cation exchange column and obtained in 99% yield.

3.3.2 Incorporation of the pyrazole substituents and synthesis of analogues **17-19**

Of the three opportunities we had identified earlier to introduce a substituent onto the pyrazole, we decided to focus on attaching the bioreductive

group at the step of pyrazole formation in the first instance (Scheme 3.7). We proposed that this strategy would allow us to completely avoid PMB-protection throughout the synthesis, making it shorter, faster and therefore potentially higher yielding.

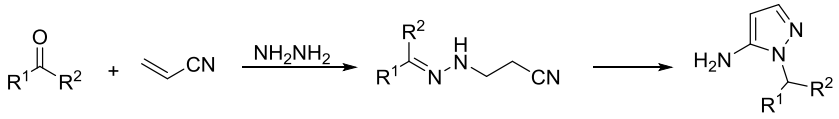

Scheme 3.7. Strategy A for the incorporation of the bioreductive group: Synthesis of different pyrazole building blocks.
Starting from the corresponding aldehydes (R^1=H, R^2=Ar-NO_2) and methyl ketones (R^1=Me, R^2=Ar-NO_2) of different nitro aromatic groups we proposed the synthesis of a variety of bioreductively substituted pyrazole building blocks.

In addition to nitroaromatic aldehydes, we intended to use methyl ketones in order to give rise to bioreductive agents with a germinal methyl group. Methyl groups aid bioreductive release (Thomson et al. 2007; Thomson et al. 2006; Hay et al. 1999).

Initially we explored conditions similar to those we had used for the formation of the PMB-protected pyrazole **21**, but instead of anisaldehyde we used 4-nitrobenzaldehyde **44a** and nitrobenzylmethyl ketone **44b** in order to incorporate the bioreductive group directly and avoid the use of a protecting group (Scheme 3.8). Once we had optimised conditions, we planned to apply them to the synthesis of the corresponding 2-nitroimidazole substituted pyrazoles.

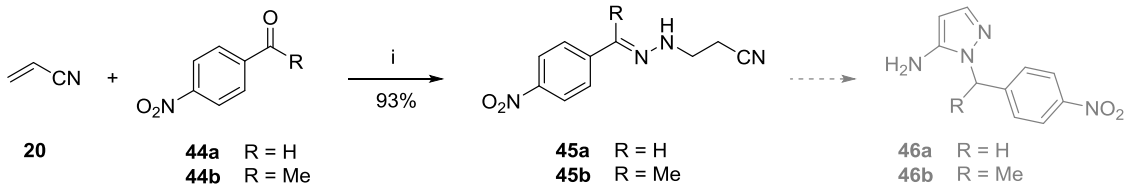

Scheme 3.8. Proposed synthesis of 4-nitrobenzyl pyrazole building blocks.
Imine formation with carbonyl compounds **44a** and **44b** proceeded rapidly, while subsequent heterocycle formation to form **46a** and **46b** was unsuccessful. Conditions: i) NH_2NH_2, THF, RT, 2 h. Then 4-nitroacetophenone, 0 °C to RT, 6 h.

Condensation to the imines **45a** and **45b** was rapid, but despite exploring a range of conditions involving different solvents and bases, formation of pyrazoles **46a** and **46b** could not be achieved.

Instead of exploring alternative routes to synthesise the bioreductive pyrazoles **46a** and **46b** we decided to incorporate the bioreductive groups later in the synthesis of the prodrug. Our alternative strategy involved incorporation of the bioreductive group before introduction of the morpholine substituent (Scheme 3.9). We predicted that simultaneous deprotection and conversion of intermediate **42** into the corresponding chloride **24** using $POCl_3$ would allow *N*-alkylation, followed by nucleophilic aromatic substitution and final deprotection of the primary amine.

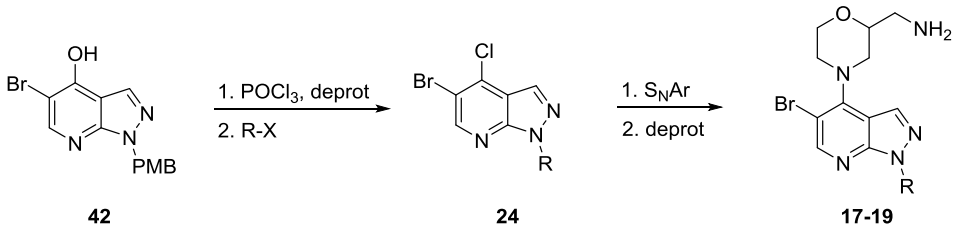

42 **24** **17-19**

Scheme 3.9. Strategy B for bioreductive group incorporation.
Following chlorination and PMB-deprotection (deprot.) of **42**, incorporation of the bioreductive group R was proposed prior to S_NAr and final Boc-deprotection (deprot).

Matthews and coworkers reported clorination and PMB-deprotection of compound **42** in one step using neat $POCl_3$ at 110 °C (Matthews et al. 2009). Following this procedure, however, we obtained a mixture of the three products **22**, the deprotected analogue **23** and the 2-*N*-PMB regioisomer **47** (Scheme 3.10).

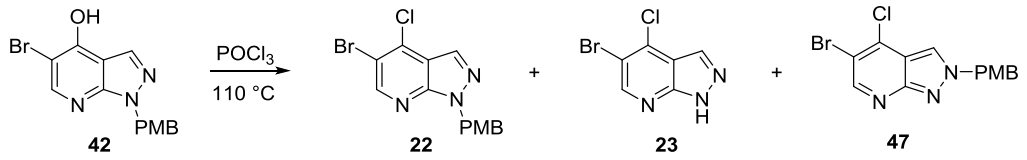

Scheme 3.10. Products obtained from an attempted one-step procedure to achieve chlorination and PMB-deprotection of 42.
Using reported conditions, a mixture of **22**, deprotected analogue **23** and regioisomer **47** was obtained (Matthews et al. 2009). Conditions: $POCl_3$, 110 °C, 2 h.

Addition of the PMB-cation scavenger anisol had been shown to result in cleaner and more rapid deprotection, but in this case did not improve the outcome (Muro et al. 2009). Consequently, we decided to first convert **42** into the corresponding chloride and carry out the PMP-deprotection in a second and separate step. Key intermediate **22** was synthesised as described above (Scheme 3.5) and then deprotected to generate **23** using neat TFA in the presence of the scavenger triisopropylsilane (Scheme 3.11). This way the formation of byproducts was avoided, resulting in higher yields and simpler purification.

In addition to the bioreductive prodrugs **17** and **18**, we intended to synthesise an inactive analogue **19** as a negative control compound. All of these analogues could be obtained from intermediate **22** using the same strategy (Scheme 3.11).

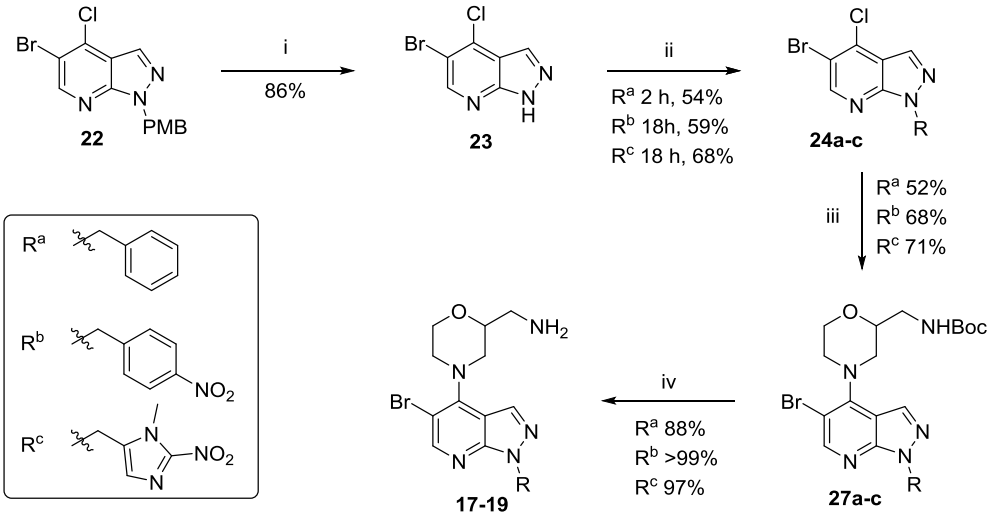

Scheme 3.11. Synthesis of the analogues 17, 18 and 19 from key intermediate 22.
Conditions: i) TFA, $^{i}Pr_3SiH$, 60 °C, 5 h; ii) X-R, TBAI, K_2CO_3, DMF, RT; iii) amine **43**, Et_3N, NMP, 120 °C, 7 h; iv) TFA, $^{i}Pr_3SiH$, 40 °C, 2 h.

After the PMB-deprotection (step i, Scheme 3.11) different pyrazole substituents were incorporated for which reaction conditions were optimised as summarised in Table 3.3.

All reactions were carried out in DMF. K_2CO_3 served as a base, when Cs_2CO_3 was used, the ratio of desired to undesired regioisomer was reversed (Table 3.3, entry 2). Higher temperatures resulted in some increase in regioselectivity but not an increased yield (Table 3.3, compare entries 3 and 4 and entries 7 and 8). We directly compared the reaction outcome between the use of 2-nitroimidazole chloride and 2-nitroimidazole bromide under otherwise identical conditions (Table 3.3, compare entries 3 and 5). Using bromide resulted in an improved regioselectivity and also overall yield. However, since the synthesis of bromide **37** had proceeded in poor yields (see 3.2.2, Table 3.1), chloride **38** was used for the prodrug synthesis. Tetrabutylammonium iodide (TBAI) has been shown to accelerate alkylation reactions with alkyl chlorides or bromides through *in situ* halogen exchange, similar to NaI in the classic Finkelstein reaction (Klapars and Buchwald 2002). When we combined

2-nitroimidazole chloride with TBAI, the regioselectivity increased to 9:1 in favour of the desired product and yields improved to 68% (Table 3.3, entry 6).

Overall, optimised conditions were found to give 54-68% yield of 1-*N*-substituted analogues **24a-c** from **23** when the reaction was carried out in DMF using K_2CO_3 and TBAI at RT.

Table 3.3. Optimisation of pyrazole substituent incorporation

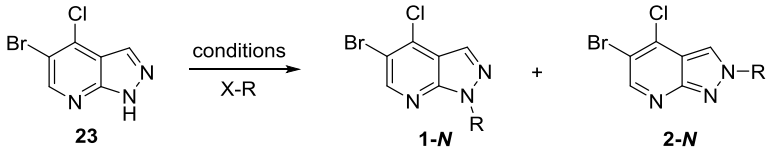

Entry	X-R	Conditions	1-*N* : 2-*N*[a]	1-*N* : 2-*N* [%][b]
1	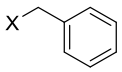	Br-R, K_2CO_3, 60 °C	2:1	54:nd
2		Br-R, Cs_2CO_3, RT	3:5	29:51
3	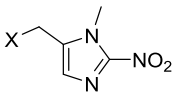	Cl-R, K_2CO_3, RT	2:1	50:16
4		Cl-R, K_2CO_3, 60 °C	4:1	40:11
5		Br-R, K_2CO_3, RT	4:1	56:nd
6		Cl-R, TBAI, K_2CO_3, RT	9:1	68:nd
7	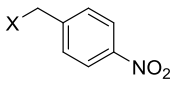	Br-R, TBAI, K_2CO_3, RT	6:1	59:11, 7% **48**[c]
8		Br-R, TBAI, K_2CO_3, 0 °C	nd	50:25

[a] Ratio from crude reaction mixture. [b] Isolated yield. All reactions were carried out in DMF. [c] See Figure 3.3 for the structure of disubstituted product **48**.

When these optimised conditions (Table 3.3, entry 7) were applied to the synthesis of 4-nitrobenzyl analogue **24b**, formation of the disubstituted compound

48 (Figure 3.3) was observed, which was difficult to separate from the desired product. The reaction was consequently carried out at 0 °C, which prevented formation of **48** but also lowered the isolated yield of the desired product from 59% to 50% due to diminished regioselectivity (Table 3.3, compare entries 7 and 8).

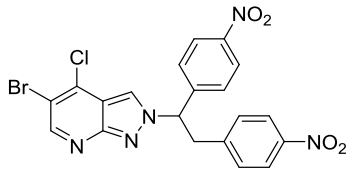

48

Figure 3.3. Structure of the disubstituted compound 48.
Compound **48** was obtained as a byproduct during the optimisation of reaction conditions for the alkylation of **23**.

With these optimised conditions, analogues **24a-c** were readily available and attachment of the morpholine ring could be carried out as had been optimised previously (see Scheme 3.6) with good yields in all three cases. Deprotection of the Boc group was rapid for the three compounds, and the final products **17-19** were isolated in high yields (Scheme 3.11).

3.4 *In vitro* testing of analogues 16-19

*3.4.1 The Chk1 inhibitor **16** sensitises cancer cells to severe hypoxia*

The chosen Chk1 inhibitor **16** was published with a comprehensive structural study and enzyme inhibition data demonstrating its potency and selectivity for Chk1 over Chk2 and CDK1 (Matthews et al. 2009). However, only limited cell-based *in vitro* data of the compound as a Chk1 inhibitor in human cancer cells had been published at that point. Inhibitor **16** has been shown to abrogate an etoposide-induced G_2 checkpoint in HT29 colon cancer cells with an

IC_{50} value of 5 µM, and further demonstrated cytotoxicity in an SRB (sulforhodamine B) assay (GI_{50} 16 µM) in the same cell line (Matthews et al. 2009).

In order to investigate Chk1 inhibition following treatment with **16** in RKO cells, we employed western blotting using Chk1 autophosphorylation (S296) as readout for Chk1 activity. Gemcitabine was used to induce Chk1 activity and this treatment combined with a range of doses of inhibitor **16**. The Chk1 inhibitor Gö6976 was used as a positive control (Figure 3.4) (Kohn, Yoo, and Eastman 2003).

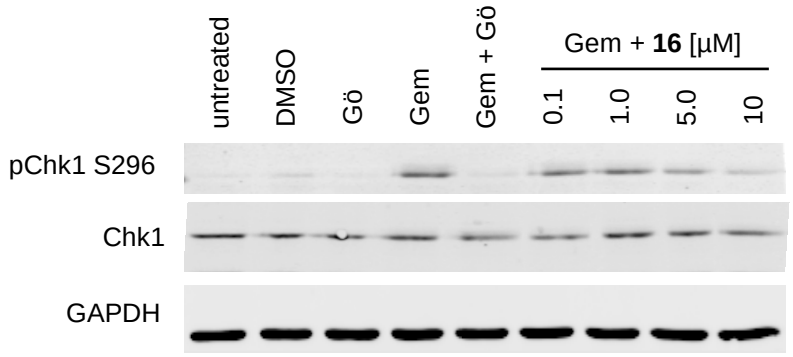

Figure 3.4. Compound 16 inhibits gemcitabine-induced Chk1 autophosphorylation on S296.
RKO cells were treated as indicated with the following doses: Gö6976 100 nM, gemcitabine 100 nM, **16** as indicated. Cells were treated with inhibitor as indicated or DMSO for 4 h followed by 6 h exposure to gemcitabine where shown. Chk1 autophosphorylation (S296) levels are shown as readout for Chk1 activity, and total Chk1 protein levels are shown for comparison. GAPDH is shown as a loading control.

Chk1 autophosphorylation was markedly induced following gemcitabine treatment for 6 h and could be inhibited using Gö6976 as expected. Inhibitor **16** markedly reduced gemcitabine-induced Chk1 autophosphorylation only when used at 5 µM or above, indicating a relatively low potency in RKO cells.

Next we tested the effect of **16** on clonogenic survival following hypoxia treatment and reoxygenation in two cancer cell lines. In particular, we examined if

RKO and H1299 cells were more sensitive to **16** when exposed to severe hypoxia (<0.1% O_2) in comparison with normoxia (21% O_2) (Figure 3.5).

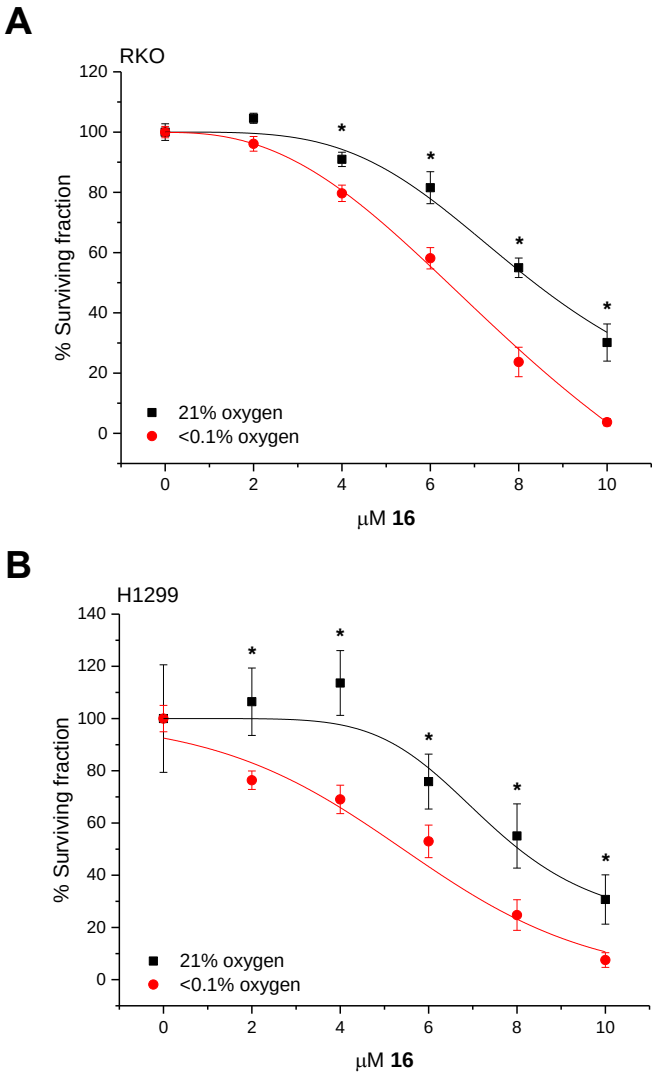

Figure 3.5. Clonogenic survival curves of H1299 and RKO cells treated with inhibitor 16 in severe hypoxia and normoxia.
A) H1299 cells were seeded in 6-well plates (300 cells/well), after 2 h cells were treated with drug and exposed to the indicated O_2 concentration for 16 h. Colonies were left to form for 10 days. ED_{50} (21% O_2) 8.1 μM, ED_{50} (<0.1% O_2) 5.5 μM. B) RKO cells were seeded in 6-well plates (350 cells/well), after 2 h treated with drug and exposed to the indicated O_2 concentration for 16 h. Colonies were left to form for 8 days. ED_{50} (21% O_2) 8.3 μM, ED_{50} (<0.1% O_2) 6.4 μM. Curves were fitted in OriginPro using a logistic model ($y = A_2+(A_1-A_2)/(1+x/x_0)^p$). Error bars represent the standard error between at least three technical replicates for the represented experiment, n=3. * indicates $p<0.05$.

Given the dose of **16** required for inhibition of gemcitabine-induced Chk1 activity in RKO cells, we expected similarly high doses to be necessary for a reduction in clonogenic survival. In both cell lines investigated, ED_{50} values were

in the micro molar range. Sensitivity to **16** was significantly increased after exposure to severe hypoxia/reoxygenation as was expected for treatment with a Chk1 inhibitor (Figure 3.5) (Hammond, Dorie, and Giaccia 2004; Hasvold et al. 2013; Pires, Bencokova, McGurk, et al. 2010). These results demonstrate that treatment with **16** results in biological responses that are characteristic for Chk1 inhibition.

3.4.2 Initial validation of the analogues **16-19**

We postulated that the formation of 1-*N*-substituted analogues of the Chk1 inhibitor **16** resulted in a significantly reduced Chk1 affinity of these analogues until prodrug activation in hypoxia had occurred. Analogues **17-19** were designed to disrupt hydrogen bonding between the pyrazole of the inhibitor and the amide of Glu85 in the ATP-binding site of Chk1. This interaction had been shown to be one of three major interactions between **16** and the active site of the enzyme (Matthews et al. 2009) (see Figure 3.1).

In order to validate the expected differences in binding affinity, IC_{50} values against purified Chk1 were determined using a radioactive (^{33}P-ATP) filter-binding assay comparing all four analogues, including the active Chk1 inhibitor (Figure 3.6).

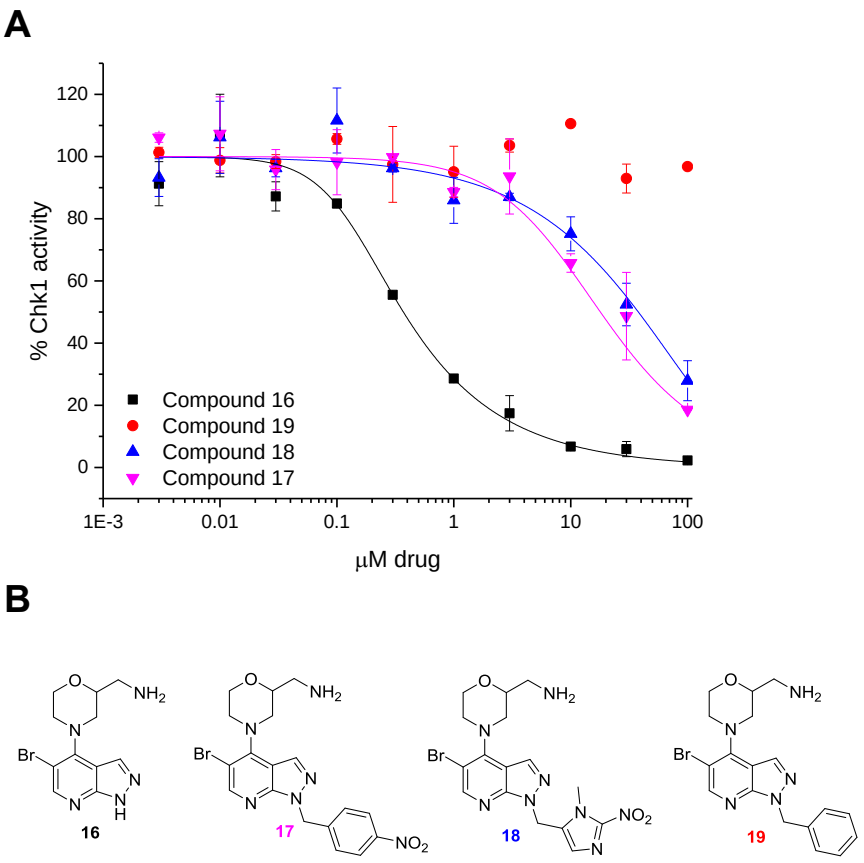

Figure 3.6. IC_{50} determination for compounds 16-19 against purified Chk1.
A) IC_{50} values were obtained using a radioactive (^{33}P-ATP) filter-binding assay. IC_{50} values: **16** 0.37 µM; **17** 17.95 µM; **18** 37.80 µM; **19** no inhibition. This analysis was carried out in duplicate by The International Centre for Kinase Profiling, University of Dundee. Curves were fitted in OriginPro using a logistic5 model model ($y = A_{min}+(A_{max}-A_{min})/(1+x_0/x)^s$). Error bars represent the standard deviation between four technical replicates for the represented experiment. B) Structures of the analogues **16-19**.

As expected, the benzyl-substituted analogue **19** showed no inhibition of Chk1 in the investigated dose range, of up to 100 µM. The active inhibitor had an IC_{50} value of 0.37 µM which corresponds well with the reported IC_{50} value of 0.39 µM (Matthews et al. 2009). Affinity of the 4-nitrobenzyl bioreductive analogue **17** was decreased by 49-fold in comparison to **16**, with an IC_{50} values of 17.95 µM. The 2-nitroimidazole analogue **18** showed an IC_{50} value of 37.80 µM, equivalent to a 102-fold decreased affinity relative to **16**. Considering this difference in IC_{50} between the active compound and the prodrugs, we

expected to see hypoxia-selectivity for both prodrugs, given rapid activation at reduced O_2 concentrations.

We had synthesised **19** as a negative control compound and proposed that the presence of the benzyl substituent resulted in an inactive analogue of Chk1 inhibitor **16**. Following the IC_{50} data which supported this hypothesis, RKO cells were treated with **19** and Chk1 activity assessed using western blotting (Figure 3.7, A). No reduction of Chk1 autophosphorylation (S296) was detected at doses up to 10 μM. Together with the IC_{50} data, this demonstrates that **19** showed no Chk1 affinity.

To further evaluate **19** as a negative control for our studies, we carried out a clonogenic survival assay in H1299 cells, using **19** at a range of doses in normoxia (21% O_2) and severe hypoxia (<0.1% O_2). We expected to see no effect on cell survival under both conditions over the entire dose range. Despite the previously proven inactivity of **19** as a Chk1 inhibitor, a clear reduction in clonogenic survival of H1299 cells was observed under both oxygen concentrations. With ED_{50} values of 1.7 μM (21% O_2) and 1.9 μM (<0.1% O_2) the H1299 cells were even more sensitive to **19** than to the Chk1 inhibitor **16**, (Figure 3.7, B and compare with Figure 3.5, B). This result suggests that compound **19** might have off-target cytotoxic effects, and was consequently considered unsuitable as a negative control compound in cell experiments.

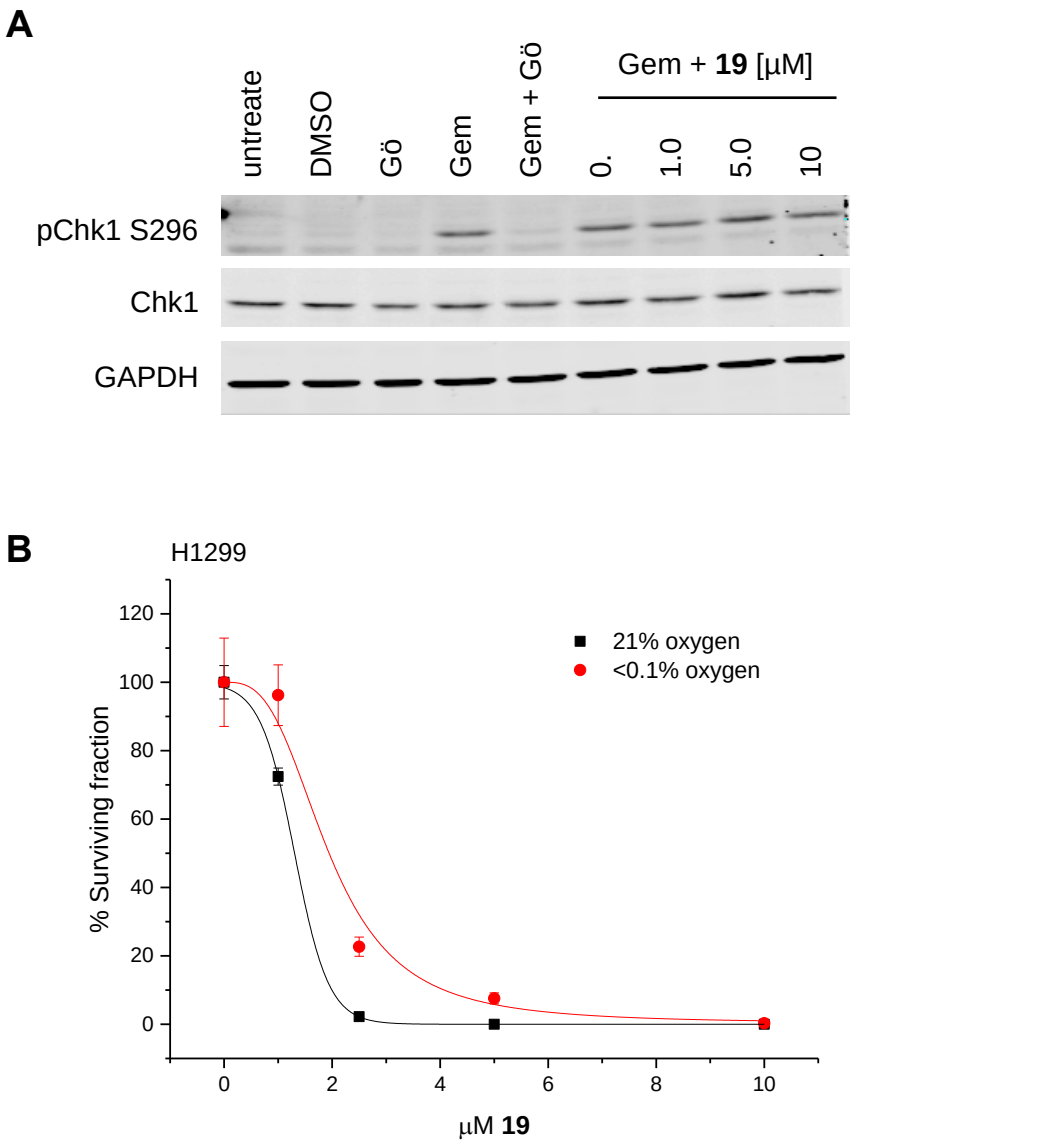

Figure 3.7. Effect of benzyl substituted analogue 19 on gemcitabine induced Chk1 activity and clonogenic survival.
A) RKO cells were treated as indicated with the following doses: Gö6976 100 nM, gemcitabine 100 nM, **19** as indicated. Cells were treated for 6 h. Chk1 autophosphorylation (S296) levels are shown as readout for Chk1 activity and total Chk1 protein levels shown for comparison. GAPDH is shown as a loading control. B) H1299 cells were seeded in 6-well plates (300 cells/well), after 2 h treated with drug and exposed to the indicated O_2 concentration for 16 h. Colonies were left to form for 10 days. ED_{50} (21% O_2) 1.7 µM, ED_{50} (<0.1% O_2) 1.9 µM. Error bars represent the standard error between technical replicates for the represented experiment, n=3.

Due to the unexpected toxicity observed with **19**, we next tested the two bioreductive analogues **17** and **18** in a similar manner. Clonogenic assays in H1299 and RKO cells were carried out at 21% O_2 in order to preclude any off-target toxicities. Neither cell line showed significant sensitivity to treatment with

the prodrug **18** (Figure 3.8), with ED_{50} values of 10.7 µM in H1299 cells and >40 µM in RKO cells. Similar to what we had observed previously with **19**, treatment with the 4-nitrobenzyl prodrug **17** significantly decreased cell viability in both cell lines. With ED_{50} values of 3.1 µM (H1299) and 6.9 µM (RKO), toxicity was not as marked as with **19**, but still greater than with the active Chk1 inhibitor **16** (compare to Figure 3.5).

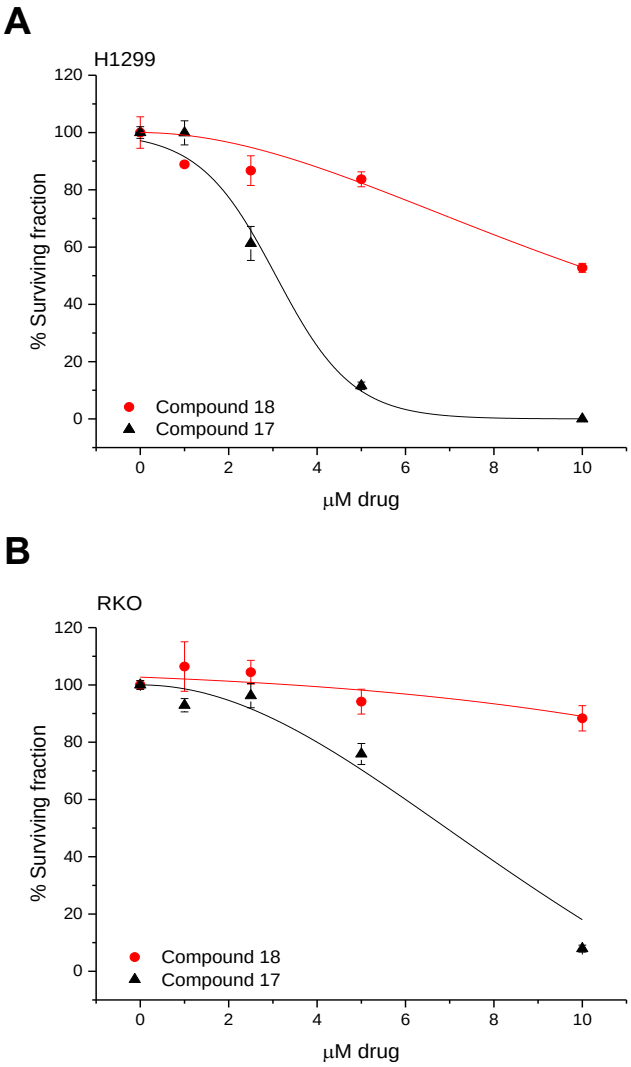

Figure 3.8. Clonogenic survival curves of H1299 and RKO cells treated with bioreductive analogues 17 and 18.
A) H1299 cells were seeded in 6-well plates (300 cells/well) and after 2 h treated with drug as indicated. Colonies were left to form for 10 days. ED_{50} (**18**) 10.7 µM, ED_{50} (**17**) 3.1 µM. B) RKO cells were seeded in 6-well plates (350 cells/well) and after 2 h treated with drug as indicated. Colonies were left to form for 8 days. ED_{50} (**18**) >40 µM, ED_{50} (**17**) 6.9 µM. Curves were fitted in OriginPro using a logistic model ($y = A_2+(A_1-A_2)/(1+x/x_0)^p$). Error bars represent the standard error between three technical replicates for the represented experiment, n=3.

Consequently, **19** and **17** were excluded from further *in vitro* testing and only **18** and the active inhibitor **16** taken forward.

3.4.3 Investigation of the mechanism of activation of prodrug **18**

In the process of validating the 2-nitroimidazole bioreductive prodrug **18** we next focused on studying its mechanism of activation in a reducing environment. We had proposed that following, enzymatic reduction of the nitro group in hypoxia, the presence of an electron-donating amine or hydroxylamine would result in prodrug fragmentation and release of Chk1 inhibitor **16.**

In the first instance, we carried out a simple chemical reduction of **18** using zinc and ammonium chloride. Shigenaga and coworkers have previously reported activation of a peptide by zinc-mediated reduction of a 4-nitrobenzyl group and we had employed this method in the reduction of CH-01 (Shigenaga et al. 2012; Cazares-Körner et al. 2013). Using the reported conditions, we planned to reduce the 2-nitroimidazole prodrug **18** to the corresponding amine **49** which was expected to fragment and release the active inhibitor **16** upon exposure to aqueous conditions (Figure 3.9, A). Reduction of **18** to the corresponding amine **49** occurred rapidly, with approximately 86% of the starting material converted to **49** (69%) and **16** (17%) after 1 h (Figure 3.9, C).

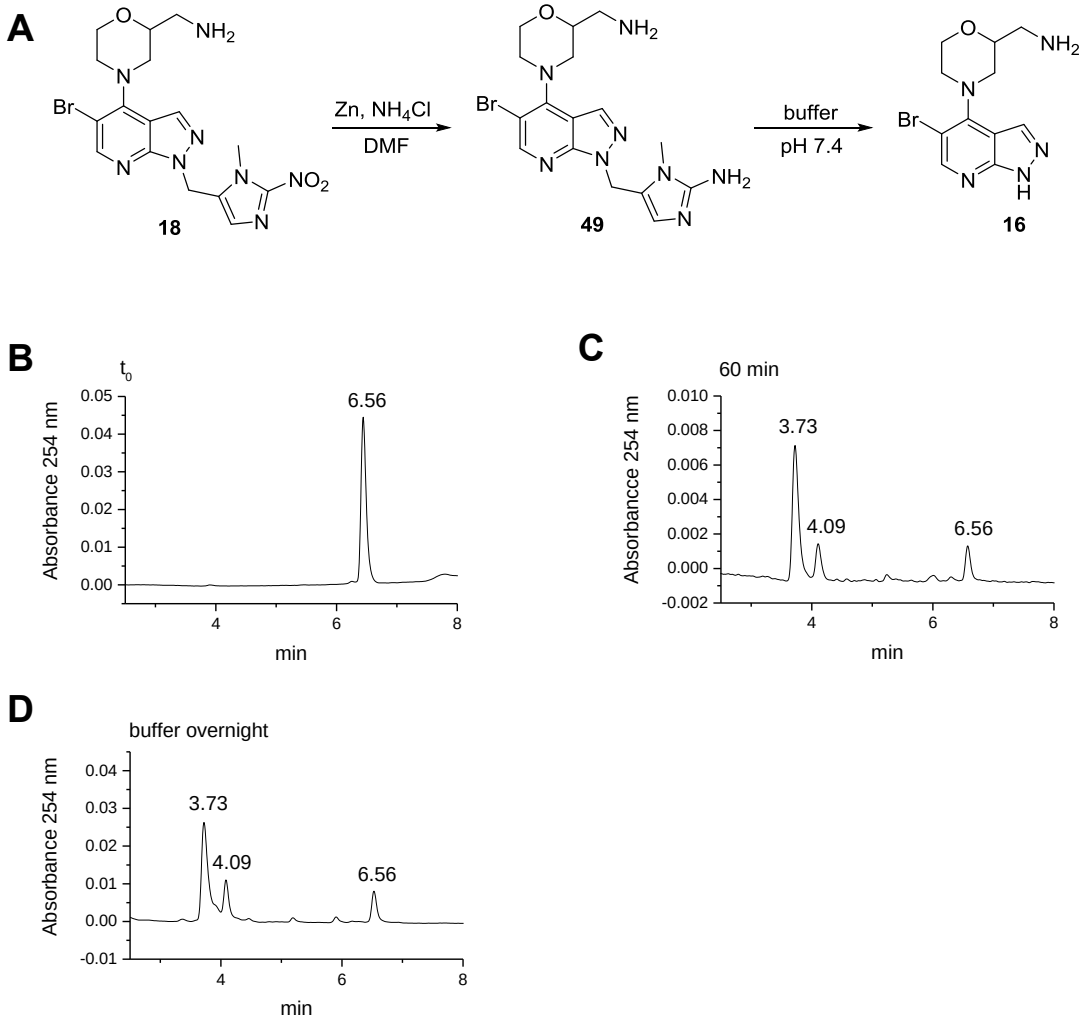

Figure 3.9. Chemical reduction of 18 using zinc and NH_4Cl.
A) Proposed reaction scheme for reduction of **18** and exposure to PPB. Compound **18** was subjected to zinc reduction (10 eq) in DMF and 10% *w/v aqueous* NH_4Cl (ratio 100:1) and samples taken for LCMS analysis, B) UV-trace for starting material **18** at t_0. C) After 60 min most starting material has reacted to amine **49** (3.73 min) and inhibitor **16** (4.09 min). D) An aliquot (5 µl) was taken after 60 min reaction time, injected into 95 µl PPB and left at 37 °C overnight. LCMS analysis reveals no further reaction.

At this stage (after 1 h) an aliquot of the reaction was taken and injected into PPB (potassium phosphate buffer, pH 7.4) in order to evaluate fragmentation of the reduced prodrug. LCMS analysis revealed no increase in the production of **16** from **49**, even after a reaction time of 18 h at 37 °C (Figure 3.9, D), demonstrating that fragmentation of **49** did not occur spontaneously following reduction.

In order to validate these results in an independent experiment, we used sodium dithionite ($Na_2S_2O_4$) as a reducing agent, following a method reported by Heeres and coworkers where $Na_2S_2O_4$ was used for the reduction of 2-nitropropyl starch (Heeres et al. 2001). The product of dithionite oxidation is sulfite and 3 eq of $Na_2S_2O_4$ are required for the full reduction of a nitro group to the corresponding amine (Figure 3.10, A). From a deoxygenated $Na_2S_2O_4$ solution in PPB, 3 eq of dithionite were added to a 50 µM solution of **18** in PPB in six portions, corresponding to 0.5 eq each. Five minutes after each addition, a sample was taken for LCMS analysis to monitor prodrug reduction step by step.

In contrast to the clean conversion observed in the zinc-mediated reduction of **18**, this method resulted in a range of new products none of which corresponded to the active inhibitor **16**. The major products were identified as amine **49** and most likely amide **50**, eluting at 3.38 min and 3.73 min, respectively (Figure 3.10, D and E). Amide **50** could have formed following decomposition of dithionite (Figure 3.10, B and E). Solutions of $Na_2S_2O_4$ are unstable and decompose in the presence of oxygen to $NaHSO_4$ and $NaHSO_3$. Consistent with our previous observations, fragmentation and release of active inhibitor **16** did not take place following reduction to the amine **49**.

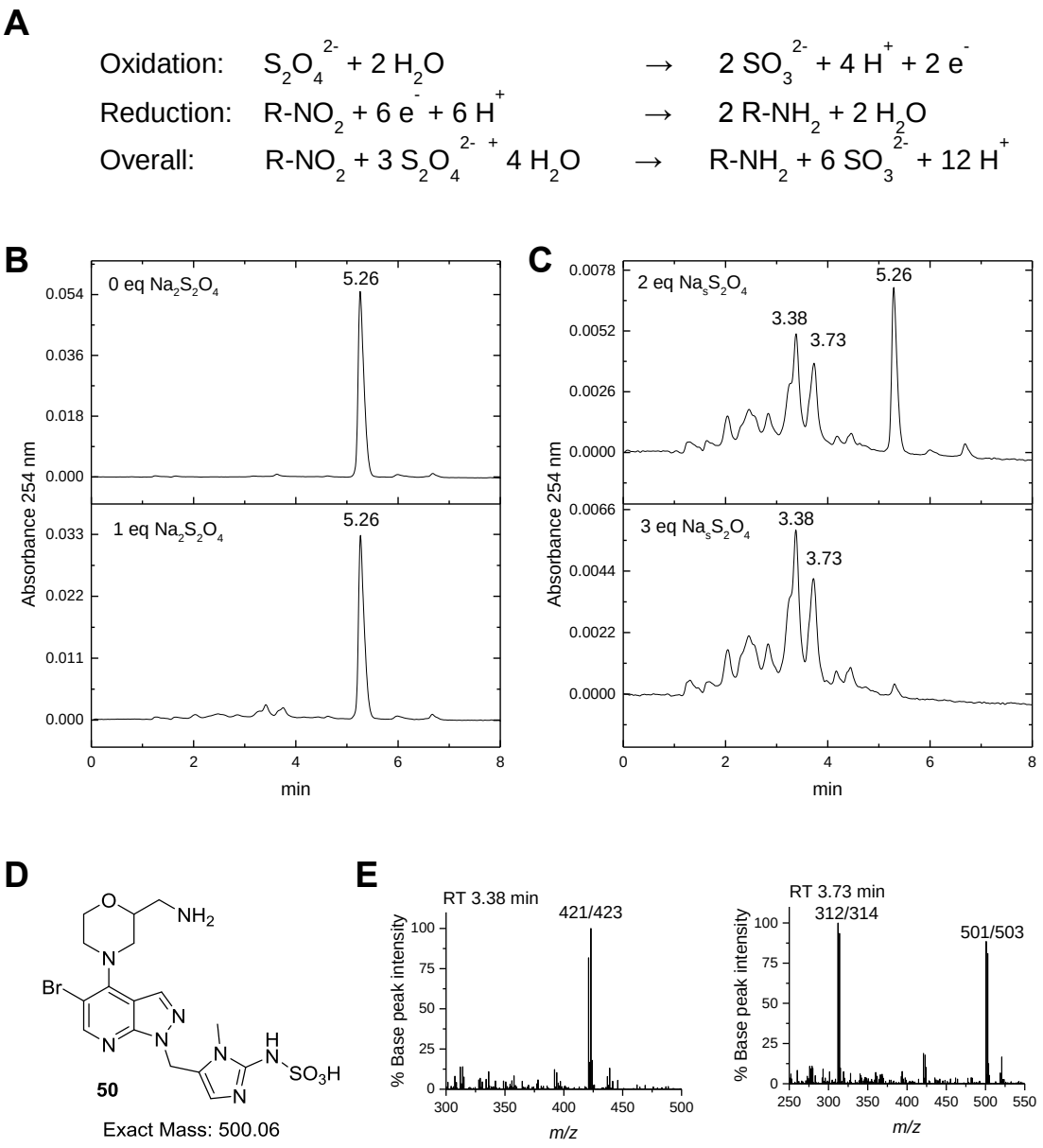

Figure 3.10. Sodium dithionite reduction of prodrug 18.
A) Redox reaction scheme for the reduction of an organo-nitro compound to the corresponding amine using dithionite as a reducing agent. B and C) UV traces of the reaction, with the starting material **18** eluting at 5.26 min and two major metabolites at 3.38 min and 3.73 min. D) Proposed structure of the product eluting at RT 3.73 min. E) Mass spectra of the two major metabolites, corresponding to amine **49** (RT 3.38 min, $[M+H]^+$ 421/423) and amide **50** (RT 3.73 min, $[M+H]^+$ 501/503).

Although we had previously excluded the 4-nitrobenzyl compound **17** from further studies, we used **17** in this experiment as a control compound. Given the wide range of products formed when **18** was subjected to dithionite reduction, we asked whether this was also the case for **17** and a potential characteristic of the method. The reaction was carried out under the same conditions as described

above for **18**, and proceeded cleanly towards formation of the corresponding amine **51**, no other products were detected (Figure 3.11).

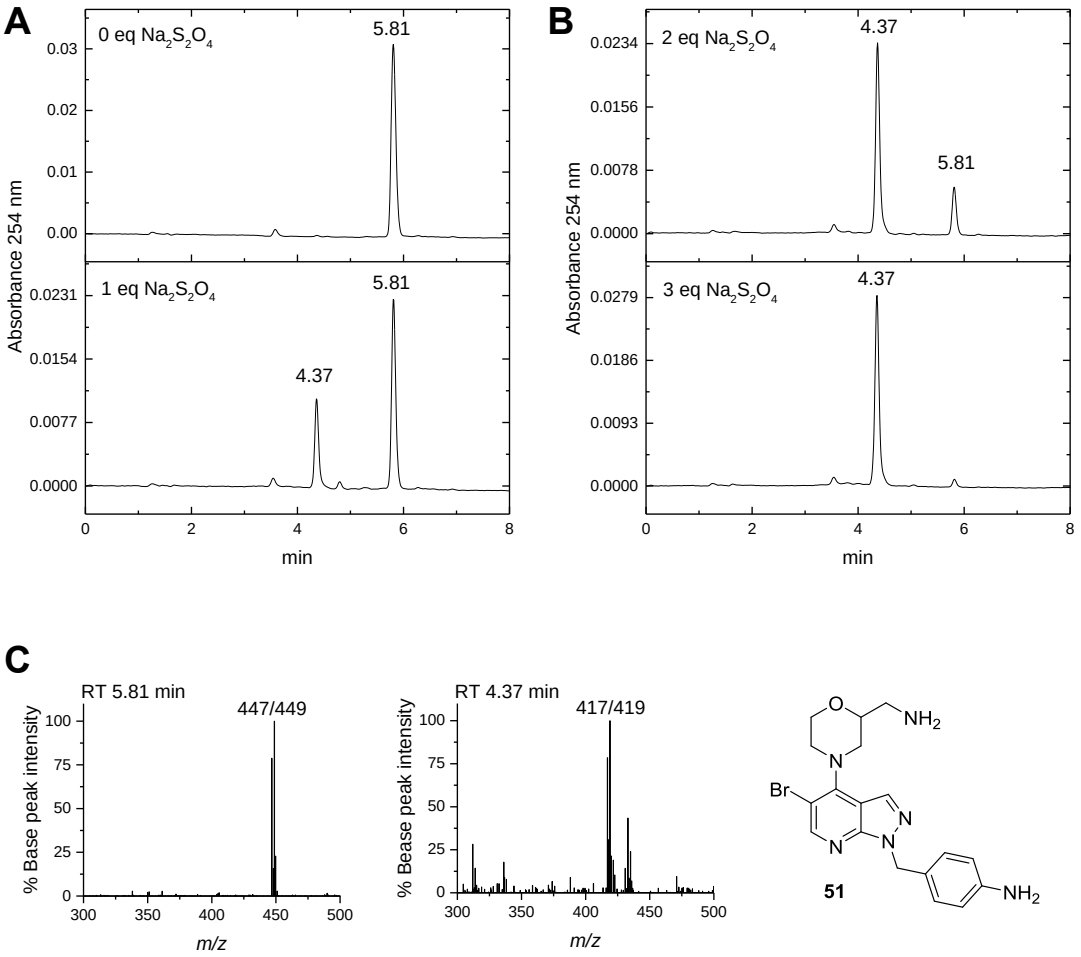

Figure 3.11. Sodium dithionite reduction of prodrug 17.
A and B) UV traces of the reaction, with the starting material **17** eluting at 5.81 min and the product at 4.37 min. C) Mass spectra of starting material **2** (RT 5.81 min, $[M+H]^+$ 447/449) and product **51** (RT 4.37 min, $[M+H]^+$ 417/419).

The clean formation of amine **51** from **17** and the formation of a range of products from **18**, suggest that dithionite might not be suitable for the reduction 2-nitroimidazoles. There is no example in the literature of a 2-nitroimidazole reduction to the corresponding amine using $Na_2S_2O_4$. Despite the formation of multiple products, the presence of amine **49** and absence of active inhibitor **16** point towards the fact that the reduced prodrug might be too stable to fragment.

Observation of a similar issue for the 4-nitrobenzyl prodrug **17**, with reduction taking place but fragmentation failing, strengthens this hypothesis.

As a third way to trigger activation of prodrug **18**, we used live cancer cells as enzymatic systems. This experiment was considered to be the most accurate model system to examine prodrug activation in hypoxia. Colorectal RKO cells were treated with **18** and exposed to either normoxia (21% O_2) or severe hypoxia (<0.1% O_2) and cell lysates analysed by LCMS (Figure 3.12).

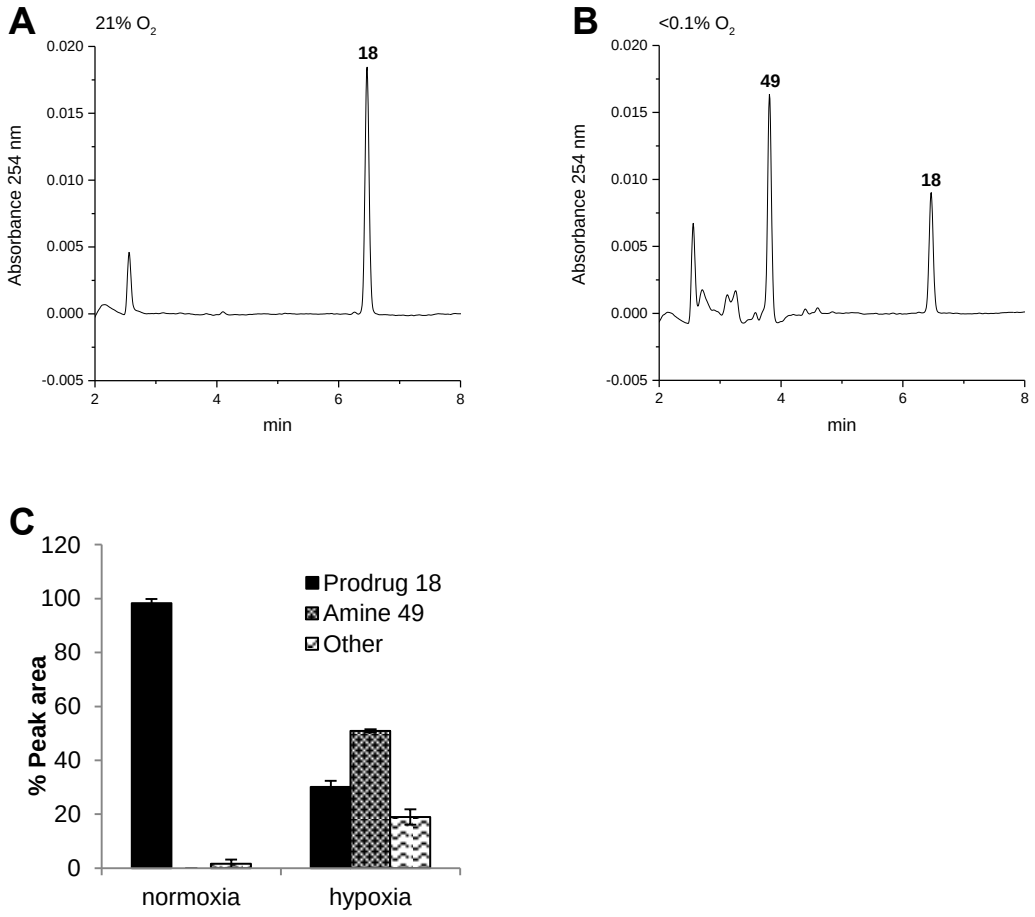

Figure 3.12. Formation of metabolites from 18 in RKO cells.
RKO cells were treated with 10 µM **18** and exposed to either normoxia (21% O_2) or severe hypoxia (<0.1% O_2) for 6 h. Cell lysates were analysed by LCMS. A) Representative UV-trace for lysates from normoxia treated cells, showing intact prodrug and no metabolites present. B) Representative UV-trace for lysate from hypoxia-treated cells. The major metabolite is amine **49**, together with some minor, unidentified metabolites. C) Comparison of the peak areas from A) and B), representing three independent experiments. Error bars represent the standard error between technical replicates for the represented experiment, n=3.

Consistent with the results from previous reductions of **18**, metabolite analysis from RKO cells demonstrated stability of the prodrug to normoxia (21% O_2) (Figure 3.12, A) and formation of amine **49** when cells were exposed to severe hypoxia (<0.1% O_2) (Figure 3.12, B). A minor amount of other metabolites were detected, none of which corresponded to the active inhibitor **16**.

Taken together, the results from these three reduction experiments show that prodrug **18**, although undergoing reduction to the corresponding amine **49**, is unsuitable for release of active inhibitor **16**.

3.5 Discussion

We chose a Chk1 inhibitor for the development of a set of bioreductive and control analogues. The set was comprised of the active Chk1 inhibitor **16**, an inactive analogue **19** and two bioreductive prodrugs **17** and **18**. All four compounds were synthesised following a previously published route for the synthesis of **16**. Modifications to the synthetic route were made to improve yields and selectivity, and the route adapted for the incorporation of different pyrazole substituents. We found a convenient synthetic route towards the bioreductive 2-nitroimidazole building block. This synthetic route has recently been further optimised by others in our research group and additional functional analogues were synthesised (O'Connor et al. 2015). Pyrazole formation using the aldehyde of the corresponding bioreductive group did not succeed following imine formations. It is likely that the presence of the mesomerically electron withdrawing nitro group resulted in decreased nucleophilicity of the imine, and hence rendered heterocycle formation unfavourable. Alternatively, we could have attempted to form the hydrazine of the bioreductive group first followed by

pyrazole formation with this more nucleophilic system as had been reported for other molecule with electron withdrawing groups (Sakya and Rast 2003; Quiroga et al. 2008). Given that incorporation of the pyrazole substituents at a later stage in the synthesis was successful this strategy was not pursued further.

Despite being a potent inhibitor against purified Chk1, the active Chk1 inhibitor **16** showed relatively low potency when used in RKO and H1299 cells both, in western blotting and clonogenic survival assays. **16** had to be used at micro molar doses in order to show an inhibitory effect and reduced cell survival. Survival of RKO and H1299 cells following treatment with **16** in conjunction with exposure to severe hypoxia and reoxygenation was decreased in comparison to when cells were treated with **16** only. We chose these cell lines in order to study **16** in a p53 wt (RKO) and a p53 null (H1299) background (Smith et al. 1995). H1299 cells have a homozygous partial deletion of TP53 gene and lack p53 protein expression. Inhibition of Chk1 as a therapeutic strategy has been widely indicated in combination with DNA damaging agents in a p53-mutant background, where lack of functional p53 renders cells reliant on the G_2/M and S phase checkpoints (Ma, Janetka, and Piwnica-Worms 2011; McNeely, Beckmann, and Bence Lin 2014). Reoxygenation after chronic exposure to severe hypoxia leads to accumulation of damage and Chk2-dependent cell cycle arrest and Chk1 has been suggested to contribute to this response (Freiberg, Hammond, et al. 2006; Pires, Bencokova, McGurk, et al. 2010). Inhibition of Chk1 prevents cell cycle arrest in G_2 and can cause premature entry into mitosis in the presence of DNA damage. Acutely severely hypoxic cells were shown to be sensitive to Chk1 inhibition, especially following reoxygenation-induced replication restart. This was attributed to the role Chk1 plays in delaying origin

firing and maintaining replication fork stability under these conditions. In consequence, Chk1 inhibition leads to increased origin firing in the presence of reoxygenation-induced DNA damage. As a result, p53-proficient cells undergo p53-dependent apoptosis and p53-mutant cells are likely to accumulate increased genomic instability over the course of several cell cycles, ultimately resulting in cell death due to checkpoint impairment (Pires, Bencokova, Milani, et al. 2010; Pires, Bencokova, McGurk, et al. 2010).

Despite the promising IC_{50} data we obtained, the benzyl and 4-nitrobenzyl substituted compounds **19** and **17** were excluded from further *in vitro* studies. They both showed increased toxicity in cells in comparison to the active Chk1 inhibitor **16**. There have been numerous examples of pyrazolopyridine-based inhibitors and it is likely that compounds **19** and **17** hit off-target effects. In particular, compounds with non-polar pyrazole substituents, such as alkyl chains or benzyl groups have been documented as phosphodiesterase-4 (PDE4) inhibitors (Hamblin et al. 2008). Inhibition of PDE4 leads to augmentation of cAMP levels, which in turn can cause a range of cellular responses such as altered gene regulation, proliferation or apoptosis. The exact cause for toxicity arising from **19** and **17** is unclear.

We have demonstrated in three different experiments that spontaneous fragmentation of the 2-nitroimidazole prodrug **18** following reduction did not occur. Additionally, dithionite reduction of the 4-nitrobenzyl prodrug **17** generated the reduced prodrug exclusively, without further fragmentation even after prolonged periods of time. The high stability of both of these reduced intermediates which were designed to release the same Chk1 inhibitor, suggests strongly that fragmentation of the prodrug was prevented by a poor leaving group

ability of the active inhibitor. Initial fragmentation studies on model systems resembling a similar leaving group situation would have been of great value and potentially prevented the choice of inhibitor **16**. Alternatively we considered changing the linker moiety between Chk1 inhibitor and bioreductive group from a methylene to a carbamate linker. A method for the incorporation of the nitroimidazole carbamate building had been reported before but after taking into account the poor potency of **16** in cells we decided to choose a different inhibitor (Hay, Wilson, and Denny 2000; Hay et al. 2003; Hay, Wilson, and Denny 2005).

CHAPTER 4

DEVELOPMENT OF A 2-NITROIMIDAZOLE BIOREDUCTIVE PRODRUG BASED ON A POTENT AND SELECTIVE CHK1-INHIBITOR

4.1 Introduction

Inhibitor **16**, which built the basis of the analogues **17-19** in Chapter 3, has recently been further developed into the potent and highly selective Chk1 inhibitor SAR020106 (Matthews et al. 2009; Reader et al. 2011; Matthews et al. 2010). SAR020106 has now undergone extensive *in vitro* and *in vivo* testing. The drug radiosensitised p53-mutant cells and potentiated gemcitabine- and irinotecan-induced toxicity in SW620 colon cancer cells and tumour xenografts (Walton et al. 2010; Reader et al. 2011; Borst et al. 2013; Touchefeu et al. 2013).

Using x-ray crystallography Reader and coworkers showed binding of SAR020106 to the hinge region of Chk1 through Glu85 and Cys87, as was the case for the preceding molecule **16** (Figure 4.1, A) (Reader et al. 2011). The ribose pocket of the kinase was occupied by the dimethylamine side chain and the nitrile group formed a hydrogen bond with Lys38. Excellent selectivity for Chk1 over Chk2 (>3000-fold) was achieved by substitution of the isoquinoline to an 8-chloroisoquinoline.

We proposed to synthesise the 2-nitroimidazole prodrug **52** directly from SAR020106 and 5-(chloromethyl)-2-nitroimidazole **38** (Figure 4.1, B). Positioning of the bioreductive group on the inhibitor aniline was expected to disrupt

interaction with the Chk1 hinge region resulting in significantly reduced binding affinity of prodrug **52** in comparison with the active inhibitor SAR020106.

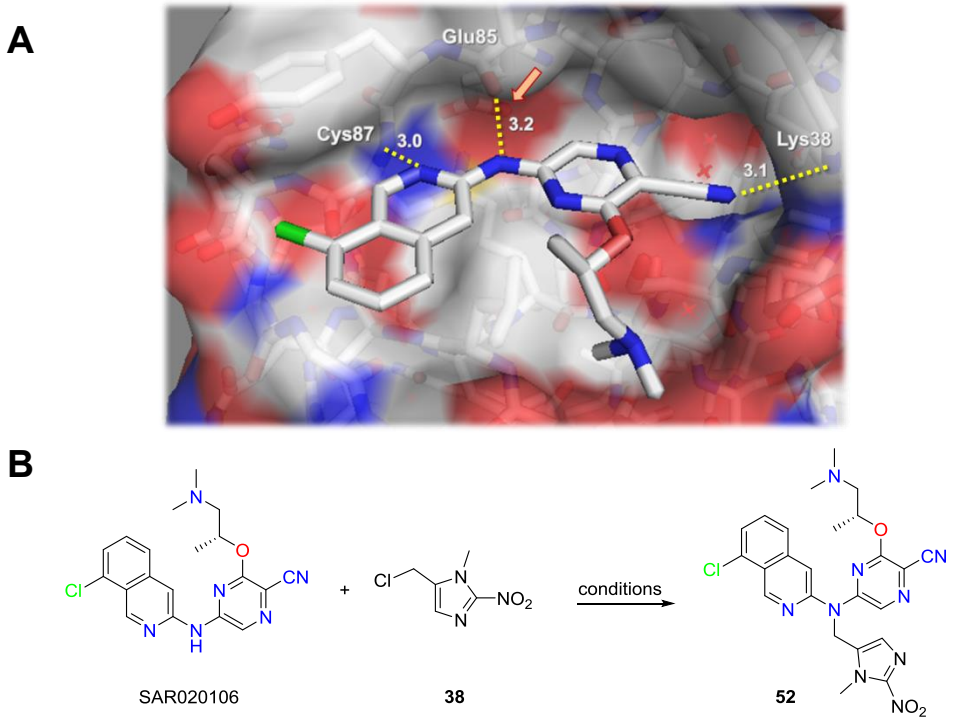

Figure 4.1. Design of the bioreductive Chk1 inhibitor 52 based on SAR020106.
A) X-Ray crystal structure of SAR020106 in the ATP-binding site of Chk1 (PDB 2ym8). Hydrogen bonds are shown as dashed yellow lines with their length given in Å. Selected interacting amino acid residues are depicted. An arrow indicates the chosen site of substitution. B) Proposed synthesis of 2-nitroimidazole prodrug **52** by direct alkylation of SAR020106.

4.2 *In vitro* testing of SAR020106 in hypoxia

A small amount (20 mg) of the Chk1 inhibitor SAR020106 was kindly provided (Professors Michelle Garrett and Ian Collins, The Institute of Cancer Research, London) for our studies. We tested SAR020106 in the context of hypoxia, in particular regarding its effect on cell viability and carried out clonogenic survival assays. Due to the limited amount of SAR020106 available for *in vitro* testing and the synthesis of a bioreductive analogue, clonogenic survival assays were scaled down to a 96- to 12-well format, depending on the

cell line. Using HeLa cells, the assay could be carried out in 96-well plates (Figure 4.2). In order to maximise the number of colonies obtained in this format, cell numbers were optimised by seeding different cell densities (Figure 4.2, A) and determining the plating efficiency (Figure 4.2, B). HeLa cells form discrete colonies and an optimal number of 200 cells could be plated per well with a plating efficiency of 52%. At higher plating densities, the colonies overlapped and could not be resolved. Colonies were an appropriate size (>50 cells per colony) after 6 days, making this format of the clonogenic assay relatively quick in comparison to the typical 6-well setup.

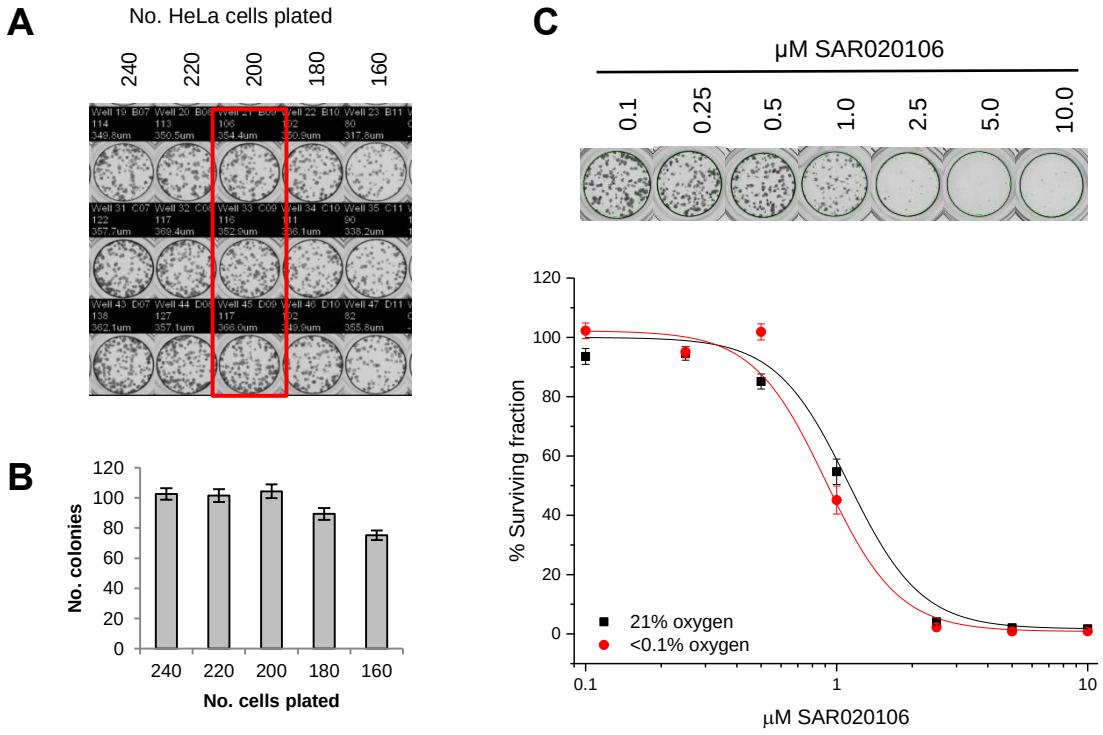

Figure 4.2. Optimisation of a 96-well clonogenic assay and dose-response curve for SAR020106 in HeLa cells.
A) HeLa cells were seeded in a 96-well plate at the indicated densities and colonies left to form for 6 days. Cells were then fixed with Crystal Violet stain and colonies counted using a GelCount colony counter. B) The optimal cell density was determined as 200 per well, considering the plating efficiency. C) Using the 96-well assay, a dose-response curve was determined with SAR020106 in 21% O_2 and <0.1% O_2 (24 h exposure). Curves were fitted in OriginPro using a logistic model (y = A_2+(A_1-A_2)/(1+x/x_0)^p) and ED_{50} values determined: ED_{50} (21% O_2) 1.11 mM, ED_{50} (<0.1% O_2) 0.90 mM. Error bars represent the standard error between technical replicates for the represented experiment, n=3.

A dose-response curve for SAR020106 in HeLa cells was determined in this format, comparing normoxia (21% O_2) with severe hypoxia (<0.1% O_2) (Figure 4.2, C). Cells were treated at the indicated O_2 concentration for 24 h and then colonies left to form. The dose-response curves for both O_2 concentrations are almost overlapping with ED_{50} values of 1.11 mM (21% O_2) and 0.90 mM (<0.1% O_2), indicating a comparable sensitivity of HeLa cells to SAR020106 in normoxia and severe hypoxia. Given that inhibition or deletion of Chk1 sensitises cells to severe hypoxia/reoxygenation (Hammond, Dorie, and Giaccia 2004; Pires, Bencokova, McGurk, et al. 2010), this result was surprising. We had expected to see a greater sensitisation to SAR020106 in severe hypoxia than in normoxia. It is possible that the prolonged drug exposure (6 days) in this experiment impaired normal DNA replication and cell cycle progression to such an extent that any increased sensitivity due to hypoxia/reoxygenation were masked by this effect.

Preclinical *in vitro* data in SW620 colon carcinoma cells showed that SAR020106 caused abrogation of an SN38-induced S phase arrest and an etoposide-induced G_2/M arrest at low micro molar concentrations. Western blotting for SN38- and gemcitabine-induced biomarker changes of Chk1 activity following treatment with a range of SAR020106 concentrations further demonstrated inhibition of Chk1 activity at >1 µM SAR020106 (Walton et al. 2010). We carried out western blotting for Chk1 activity (autophosphorylation on S296) in RKO colorectal cancer cells in order to demonstrate inhibition of Chk1 by SAR020106 following severe hypoxia/reoxygenation. To determine an appropriate drug concentration for inhibition of Chk1 in RKO cells following replication stress (100 nM gemcitabine) and severe hypoxia/reoxygenation (7 h

severe hypoxia followed by 1 h reoxygenation), we exposed cells to increasing concentrations of SAR020106. In response to gemcitabine-induced replication stress and following severe hypoxia/reoxygenation, Chk1 autophosphorylation on S296 was increased relative to the untreated controls, and a marked decrease in pChk1 S296 levels was seen at an SAR020106 concentration of 500 nM or above (Figure 4.3).

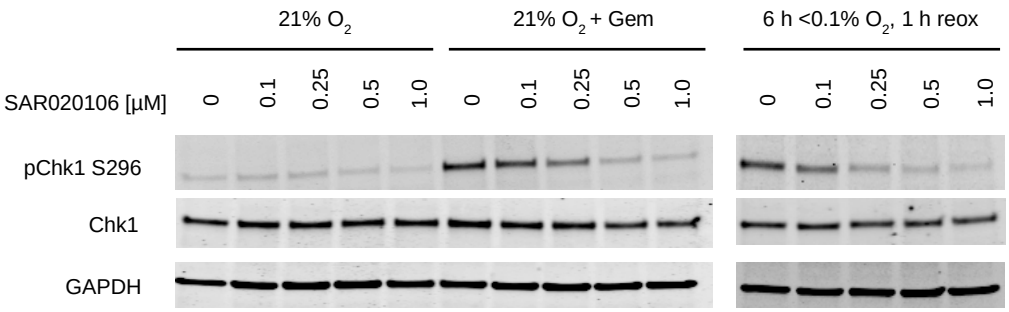

Figure 4.3. Inhibition of Chk1 autophosphorylation by SAR020106 in RKO cells.
RKO cells were treated with the indicated doses of SAR020106 and exposed to either 21% O_2 for 7 h, 100 nM gemcitabine at 21% O_2 for 7 h or <0.1% O_2 followed by 1 h of reoxygenation at 21% O_2. Western blotting was carried out. Chk1 autophosphorylation (S296) levels are shown as readout for Chk1 activity and total Chk1 protein levels are shown for comparison. GAPDH is shown as a loading control.

For numerous reasons we decided to continue our study in two oesophageal cancer cell lines. Firstly, carcinomas of the oesophagus are known to form hypoxic tumours. Secondly, it has often been noted that the efficacy of Chk1 inhibitors depends on the functional status of the p53 pathway (Garrett and Collins 2011; Chen et al. 2012; McNeely, Beckmann, and Bence Lin 2014) and we therefore chose to study cell lines with mutations in the *P53* gene. Thirdly, amplification of the *MYC* oncogene causes replication stress and is frequently found in carcinoma of the oesophagus (Tselepis et al. 2003; von Rahden et al. 2006) indicating that targeting the replicative stress response could be a promising strategy to target oesophageal cancer cells.

Hypoxia-induced Chk1 signalling had not previously been studied in oesophageal cancer cells. We chose two oesophageal cancer cell lines for our study, the adenocarcinoma cell line FLO-1 and the squamous carcinoma cell line OE21. We initially investigated the previously seen ATR-mediated Chk1 activation in response to severe hypoxia in FLO-1 cells. Upon exposure of FLO-1 cells to severe hypoxia (<0.1% O_2), increased Chk1 phosphorylation levels were detected as early as 2 h on residues S296, S317 and S345. ATR-induced phosphorylation (S317, S345) and Chk1 autophosphorylation (S296) levels peaked at 6 h (Figure 4.4, A), indicating Chk1 activity to be highest after 6 h exposure to <0.1% O_2.

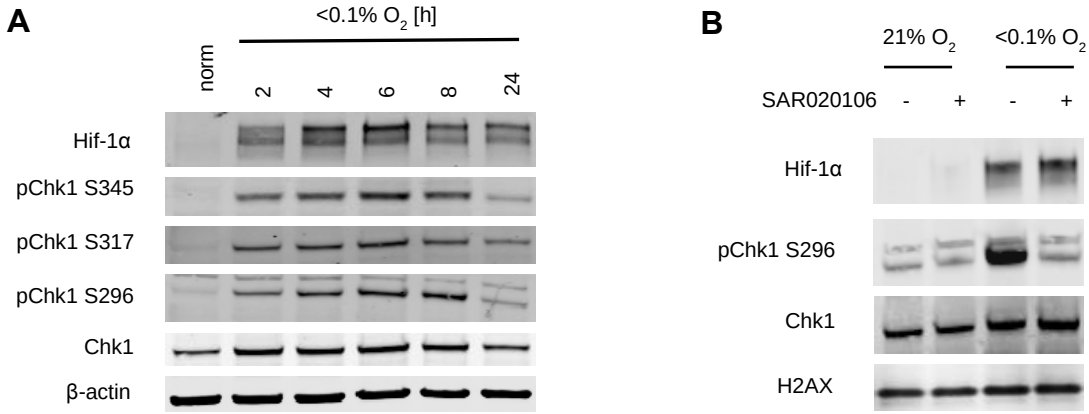

Figure 4.4. Chk1 is phosphorylated and active in response to severe hypoxia in FLO-1 cells and SAR020106 inhibits this activity.
A) FLO-1 cells were treated with hypoxia (<0.1% O_2) for the indicated times. Rapid phosphorylation of Chk1 at its ATR (S317 and S345) and autophosphorylation sites (S296) was seen. Hif-1α is shown as a hypoxia marker. Total Chk1 protein levels are shown for comparison. β-Actin is shown as a loading control B) Hypoxia-induced (<0.1% O_2) Chk1 activity in FLO-1 cells was inhibited using SAR020106 (500 nM). Cells were treated with drug and severe hypoxia for 6 h. Hif1α is shown as a hypoxia marker. Total Chk1 protein levels are shown for comparison. H2A is shown as a loading control.

Hypoxia-induced Chk1 autophosphorylation on S296 could be inhibited in FLO-1 cells using 500 nM SAR020106 (Figure 4.4, B).

Given the clear inhibitory effect SAR020106 showed in FLO-1 cells, we decided to study its effect on cell survival in severe hypoxia (<0.1% O_2) and normoxia (21% O_2) and carried out clonogenic assays in both, FLO-1 and OE21

cells. These assays could not be performed in a 96-well format due to the larger size of colonies formed by FLO-1 and OE21 cells, but they could be scaled down to 24-well (FLO-1) and 12-well (OE21) assays in order to use as little drug as possible. Surprisingly, as we had seen before for HeLa cells, both cell lines showed a similar sensitivity to SAR020106 in normoxia and severe hypoxia (<0.1% O_2, 16 h) with both dose response curves overlapping (Figure 4.5). OE21 cells were more sensitive to SAR020106 than FLO-1, with ED_{50} values of 0.44 µM (normoxia) and 0.56 µM (severe hypoxia) for OE21, and 1.37 µM (normoxia) and 1.35 µM (severe hypoxia) for FLO-1.

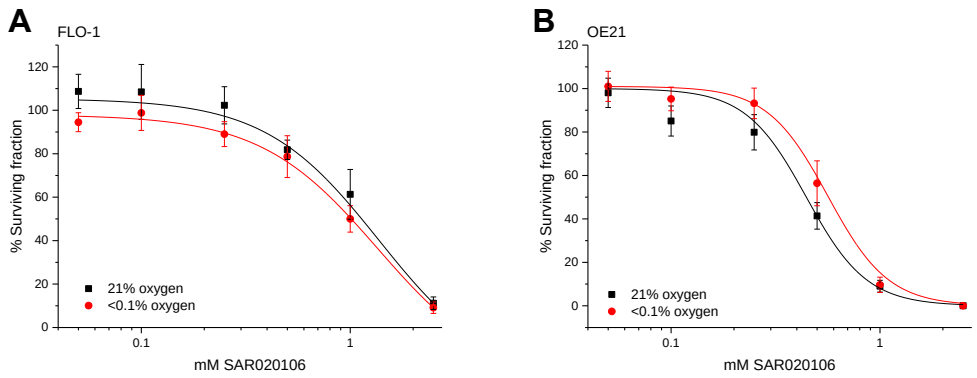

Figure 4.5. Dose-response curve for SAR020106 in FLO-1 and OE21 cells.
A) FLO-1 cells were seeded in 24-well plates (100 cells/well) after 2 h treated with drug and exposed to the indicated O_2 concentration for 16 h. Colonies were left to form for 10 days. B) OE21 cells were seeded in 12-well plates (100 cells/well) after 2 h treated with drug and exposed to the indicated O_2 concentration for 16 h. Colonies were left to form for 8 days. Curves were fitted in OriginPro using a logistic model ($y = A_2+(A_1-A_2)/(1+x/x_0)^p$) and ED_{50} values determined. FLO-1: ED_{50} (21% O_2) 1.37 µM, ED_{50} (<0.1% O_2) 1.35 µM. OE21: ED_{50} (21% O_2) 0.44 µM, ED_{50} (<0.1% O_2) 0.56 µM. Error bars represent the standard error between replicates for the shown experiment, n=3.

It is well established that inhibition of Chk1 results in accumulation of DNA damage and genomic instability (Syljuåsen et al. 2005; Lam et al. 2004). After having demonstrated inhibition of Chk1 signalling and loss of cell viability in OE21 and FLO-1 cells following treatment with SAR020106, we investigated whether treatment with SAR020106 resulted in an increased accumulation of DNA damage. OE21 cells were seeded in chamber slides and the following day

treated with either 500 nM SAR020106 or DMSO for 6 h while exposed to normoxia (21% O_2) or severe hypoxia (<0.1% O_2). Cells were fixed while still at the O_2 tension of treatment, *i.e.* without the induction of reoxygenation-induced damage, and were then processed for immunofluorescence microscopy. Since the DNA damage indicator and marker of replication stress γH2AX is robustly induced in severe hypoxia, we chose to analyse the formation of 53BP1 foci to evaluate DNA damage in response to SAR020106. Cells were scored as positive or negative for 53BP1 according to their total number of foci (Figure 4.6). Given the basal levels of DNA damage in this cell line, cells with more than 6 foci were considered 53BP1 positive and those with 6 or less foci as 53BP1 negative.

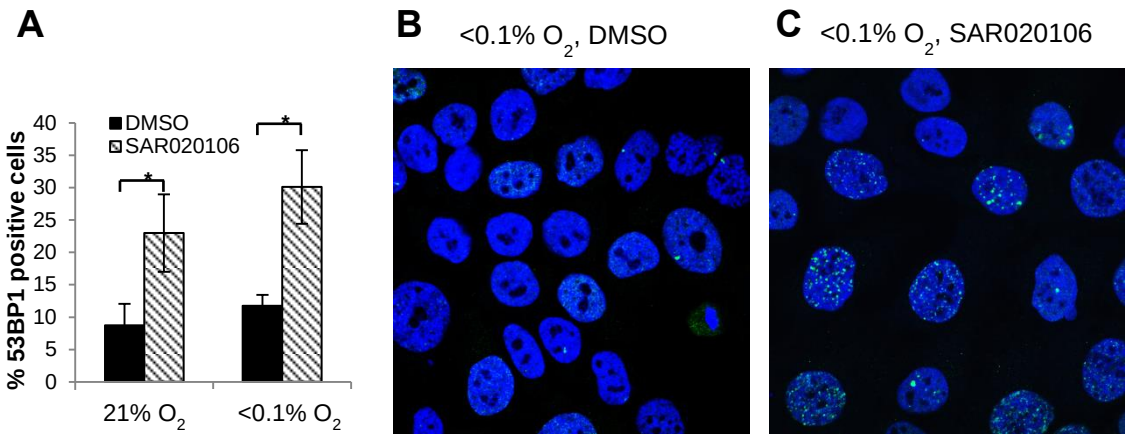

Figure 4.6. SAR020106 treatment leads to DNA damage in OE21 cells in normoxia and severe hypoxia.
OE21 cells were seeded in chamber slides, treated with either DMSO or SAR020106 (500 nM) and severe hypoxia (<0.1% O_2) or normoxia (21% O_2) for 6 h. A) Cells were stained for 53BP1 and scored according to their number of foci, where 53BP1 positive cells contained >6 foci. At least 100 cells from 8-10 different fields of view were scored per condition and experiment. B) and C) representative images of OE21 cells. Error bars represent the standard error between technical replicates, n=4. * indicates $p<0.05$.

A significant increase in 53BP1 foci formation was seen in the SAR020106 treated cells in comparison with the DMSO treated controls and this increase was comparable between severe hypoxia and normoxia. Together with the clonogenic survival data, these results surprisingly suggest that sensitivity of FLO-1 and

OE21 cells towards SAR020106 was not altered upon exposure to severe hypoxia or severe hypoxia/reoxygenation.

4.3 Optimisation of synthesis and purification of 52

4.3.1 Synthesis of **52**

We planned to synthesise the bioreductive prodrug **52** from the known inhibitor SAR020106 in one step by alkylation of the secondary aniline using 5-(chloromethyl)-2-nitroimidazole **38**. Given the small amount of material we had to find optimal reaction conditions, optimisation had to be carried out on an analytical scale (<0.5 mg scale, monitoring by HPLC). HPLC conditions were optimised to the method outlined in Chapter 6. The optimal detection wavelength for both reactants was 360 nm and any product formed was assumed to show similar absorbance properties. An initial test reaction to couple SAR020106 and **38** was carried out in DMF at RT with 2 eq of the chloride **38** relative to SAR020104 and 1 eq Cs_2CO_3. The same reaction was also set up using substoichiometric amounts (10 mol%) of TBAI which, similar to NaI, had been shown to accelerate alkylations using alkyl chlorides or bromides through *in situ* halogen exchange (Klapars and Buchwald 2002). Both reactions showed the same pattern of product formation, indicating that the use of TBAI did not accelerate the reaction (Figure 4.7).

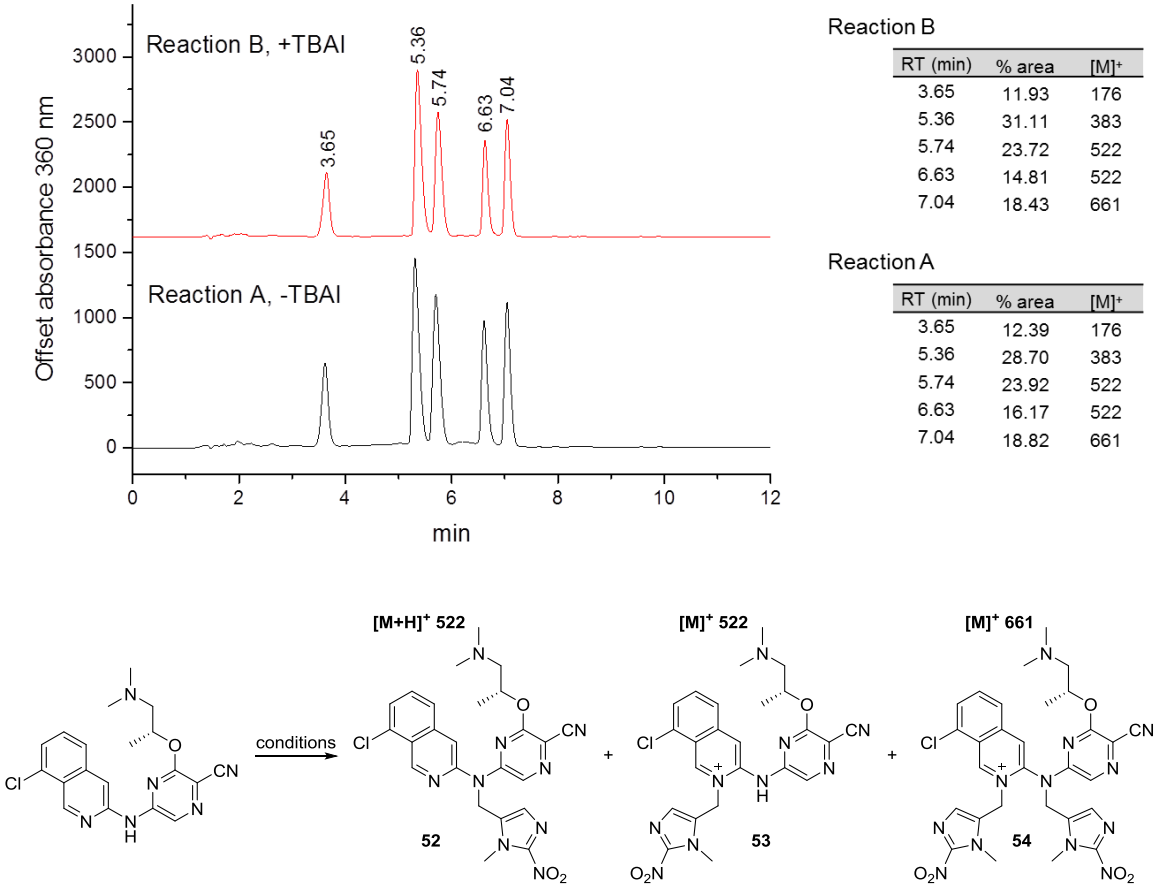

Figure 4.7. Initial test reactions for the formation of 52.
Two test reactions (A and B) were monitored by HPLC. *Conditions for reaction A*: 2 eq **38**, 1 eq Cs_2CO_3, DMF, RT. *Conditions for reaction B*: like A, with additional 0.1 eq TBAI. The HPLC traces and area analyses shown were taken after 24 h reaction time. Formation of three new products was seen, two of which showed an ion $[M]^+$ 522 (peaks at RT 5.74 and 6.63 mins) and one an ion $[M]^+$ 661 in ESI+ MS. Ions $[M]^+$ 522 were expected to be the desired product **52** and regioisomer **53**, ion $[M]^+$ 661 to be a doubly-alkylated form **54**.

The formation of three products was seen, two of which showed a signal of *m/z* 522 Da and a third peak corresponding to *m/z* 661 Da. Assuming that one of the products with *m/z* 522 Da was the desired prodrug **52**, we reasoned the other to be a regioisomer **53** where alkylation took place on a different nitrogen atom. The mass of the third product corresponded to a double-alkylation product **54**.

In order to optimise reaction conditions towards the desired product, the two possible products had to be clearly identified. Given the restricted amount of material available, we attempted to distinguish them by mass spectrometry. If the

molecules fragmented by breakage between the aniline nitrogen and the aromatic substituents, characteristically different fragments could be expected for **52** and **53**, but no such fragmentation pattern could be observed (with Dr James Wickens, Department of Chemistry, Oxford). Further, while the byproduct **53** was expected to always show as $[M]^+$, the desired product **52** would be able to form different positively charged species, *i.e.* $[M+H]^+$, $[M+Na]^+$, $[M+K]^+$. $[M+NH_4]^+$. We attempted to favour formation of these specific molecular ions using sodium citrate, potassium citrate and ammonium acetate as additives for mass spectrometry. Neither of the two products showed formation of those ions in ESI+ mode.

To clearly identify the two products, we decided to find optimal reaction conditions to favour the formation of either and then isolate enough material for NMR analysis. A range of reaction conditions were investigated, as summarised in Table 4.1.

Table 4.1. Optimisation of synthesis of the regioisomers 52 and 53.

Entry	Conditions[a]	Time	%**52**[b]	%**53**[b]	%**54**[b]
1	1 eq Cs_2CO_3, 2 eq **38**, RT	90 min	10.0	8.1	1.5
2	1 eq Cs_2CO_3, 2 eq **38**, 50 °C	15 min	12.9	10.5	2.8
3	1 eq **38**, RT	2 d	0	33.6	0
4	1 eq **38**, 50 °C	7 h	0	76.4	0
5	1 eq Cs_2CO_3, 0.75 eq **38**, 100 °C	2 h	22.6	1.5	0
6	1 eq Cs_2CO_3, 1 eq **38**, 50 °C	2 h	49.0	3.2	5.2

[a] All reactions were carried out in DMF. [b] %Product corresponds to the % peak area relative to the peak area of the limiting starting material.

The initial test reaction seen in Figure 4.7 was repeated (Table 4.1, entry 1) and monitored. Both products **52** and **53** formed at a similar rate. The temperature was increased to 50 °C in order to determine whether this would favour formation of one product, but other than an overall faster turnover no difference was seen (Table 4.1, entry 2). In both reactions, formation of doubly-alkylated **54** was detected. To avoid generation of **54**, the amount of chloride **38** was reduced to 1 eq or less in subsequent reactions. Formation of the pyridinium product **53** was expected to take place and be favoured in the absence of base. The reaction was carried out in the absence of base at RT and showed selective but very slow formation of one product (Table 4.1, entry 3). An increase of the reaction temperature to 50 °C resulted in the much faster, selective formation of the same product, with 77% conversion after 7 h (Table 4.1, entry 4). The selective formation of this product in the absence of base together with the

previously seen absence of ions in ESI- mass spectrometry suggested it to be the pyridinium species **53**.

Formation of **52** over **53** or the double alkylated **54** was achieved in the presence of 1 eq of base and 0.75 eq of chloride **38**. Carried out at 100 °C (Table 4.1, entry 5), the reaction turned dark brown in colour after 2 h and HPLC showed the presence of several side products, but when the temperature was lowered to 50 °C and stoichiometric amounts of **38** used, 49% conversion was detected (entry 6).

We next decided to scale up this reaction in order to be able to carry out NMR analysis and unambiguously identify the major product. The reaction conditions were changed slightly from those in Table 4.1, entry 6. Small amounts of the two by products **53** and **54** had been seen with those conditions and we speculated that increasing the amount of base to 2 eq might solve this issue. The reaction was scaled up to 2.4 mg SAR020106 and conditions employed as shown in Scheme 4.1.

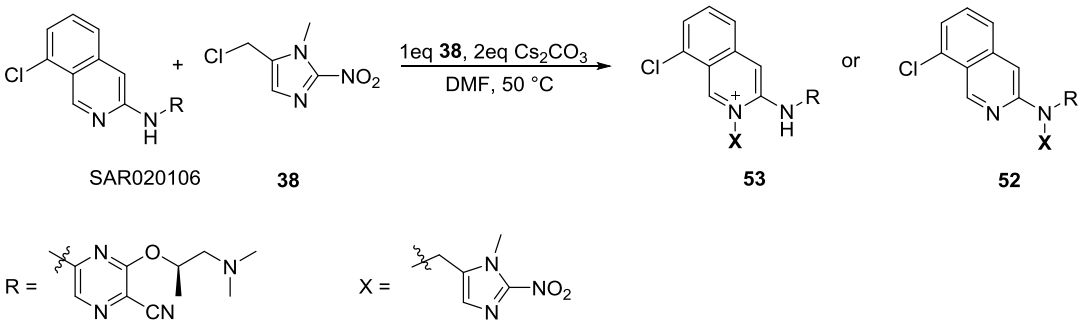

Scheme 4.1. Selective synthesis of either 52 or 53 for NMR analysis.
The reaction was carried out to selectively form either of the two analogues **52** and **53** for identification by NMR analysis.

After 6.5 h, conversion had gone up to 47% with still 51% of SAR020106 starting material left and almost no side products. At this stage the reaction was stopped to enable isolation of the product and recovery of starting material. Semi-

preparative HPLC as described in Chapter 6 was used to sufficiently separate starting material from product. The trifluoroacetate of the product was isolated in high purity (96% purity, 2.1 mg) along with recovered starting material (92% purity, 1.5 mg) (see appendix B).

Subsequently, 2D-NMR analysis was carried out in order to identify the product. In the HMBC NMR spectrum we were looking for a correlation between carbon C1' and protons C6'-*H* and C6''-*H* as a characteristic for analogue **52** (Figure 4.8). This correlation was not expected to be seen in the pyridinium regioisomer **53** and thus would prove the identity of the desired product **52**. As seen in Figure 4.8, this correlation was clearly present in the isolated product and proved that the compound was the desired product **52**.

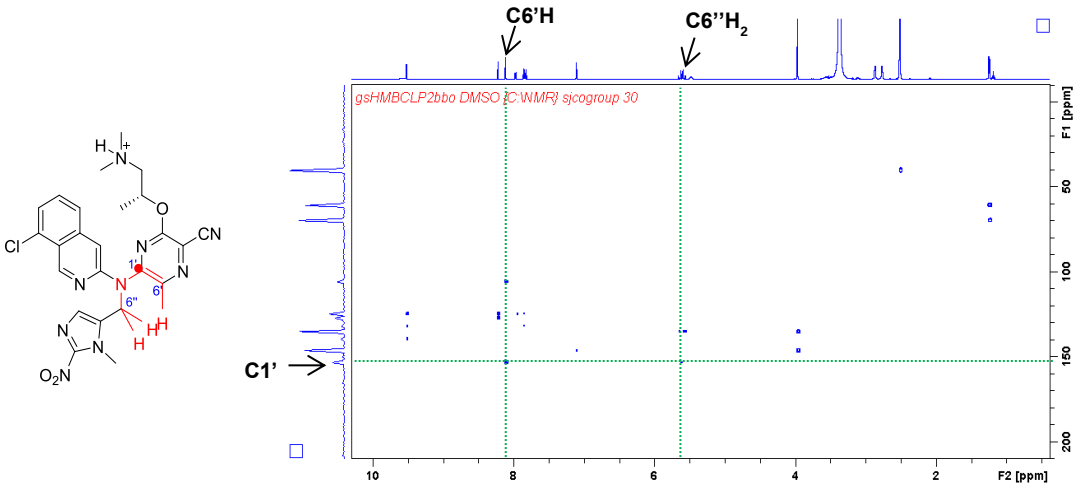

Figure 4.8. HMBC NMR spectrum of 52.
The correlation between carbon C1' and protons C6'-*H* and C6''-*H* prove identity of the compound as **52**. The spectrum was recorded on a Bruker AVII500 sprectrometer (500 MHz).

As another way to distinguish between the pyridinium salt **53** and product **52**, we tested their stability to hydrolysis in the presence of base (Peixoto et al. 2010; Burns, Jessing, and Baran 2009; Miyata et al. 2013; Rodenko et al. 2011). A crude mixture of a previously performed reaction, containing all three products, was treated with pyridine at 90 °C and monitored by HPLC. We anticipated that

pyridinium salts would hydrolyse under these conditions while **52** was expected to be stable. As shown in Figure 4.9, the ratio of the different species changed as expected with a decrease in **53** and **54**, while the amounts of starting material SAR020106 and product **52** increased over time.

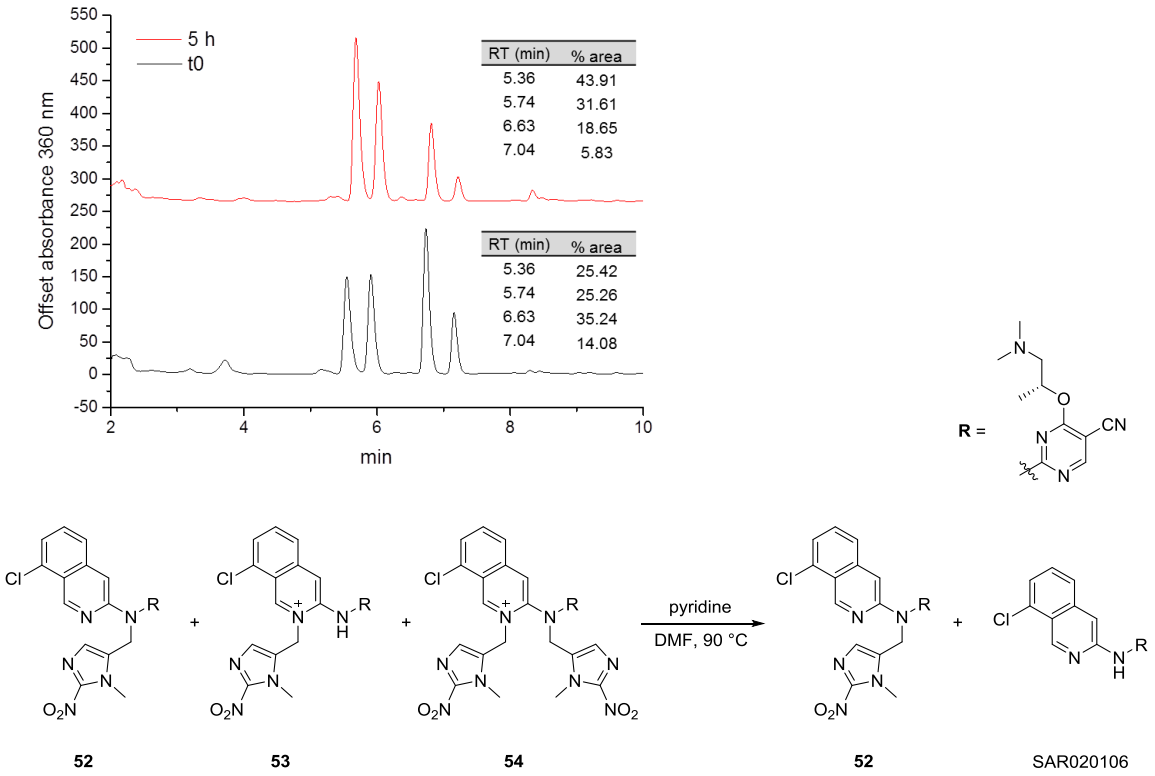

Figure 4.9. Selective hydrolysis of pyridinium species 53 and 54.
A crude mixture from a previous reaction was taken (25 µl in DMF), pyridine added (10 µl) (t_0 HPLC trace taken at this stage) and the reaction heated to 90 °C. A decrease in pyridinium species (6.63 and 7.04 mins) and an increase in their respective hydrolysis products (5.36 and 5.74 mins) was seen after 5 h.

Considering the previously described observations, we were confident at this point that we had resolved the identity of products **52** and **53**.

Previously, purification of **52** for NMR studies had been carried out in a semi-preparative fashion using a water/acetonitrile/0.1% TFA system. For testing in cells, however, trifluoroacetates are undesirable, since TFA has been shown to be toxic to osteoblasts, chondrocytes and different organisms (Ulhaq et al. 2013;

Wang et al. 2014). Consequently, we aimed to isolate **52** as the hydrochloride, acetate or the free base.

The simplest way to convert a trifluoroacetate into a hydrochloride is by lyophilising the sample several times with aqueous HCl (Andrushchenko, Vogel, and Prenner 2007). We took a small amount of **52** trifluoroacetate and lyophilised it three times with 0.1 M HCl. HPLC analysis after this process revealed partial degradation of **52** to SAR020106 and an additional, unidentified product. Next, we attempted to optimise semi-preparative HPLC conditions to a water/acetonitrile/1% AcOH system, but peaks appeared significantly broader under these conditions than when 0.1% TFA was used and separation of **52** and SAR020106 was not possible.

In collaboration with Dr. Michael Stratford (Department of Oncology, University of Oxford) a range of HPLC columns and systems were investigated for preparative separation of **52** from SAR020106. Excellent separation was achieved using a Gemini®-NX column and isocratic conditions (60% acetonitrile / 40% H_2O + 0.2% NH_3, pH 11) (Figure 4.10, A). With this column, systems with extreme pH values can be employed which is particularly useful for ionisable compounds like most drug-like molecules. At pH 11, as used in our method, both compounds (**52** and SAR020106) are expected to be completely deprotonated. This ensures higher retention times under reverse phase conditions and sharp peaks due to the single ionisation form. The synthesis of **52** was scaled up to 9.5 mg of SAR020106 starting material and the prodrug could be purified using the above column. Because of the excellent peak separation, this column could be loaded with approximately 200 µg of crude product per run and 6.2 mg of **52** were obtained for *in vitro* testing (>99% purity, 48% yield) (Figure 4.10).

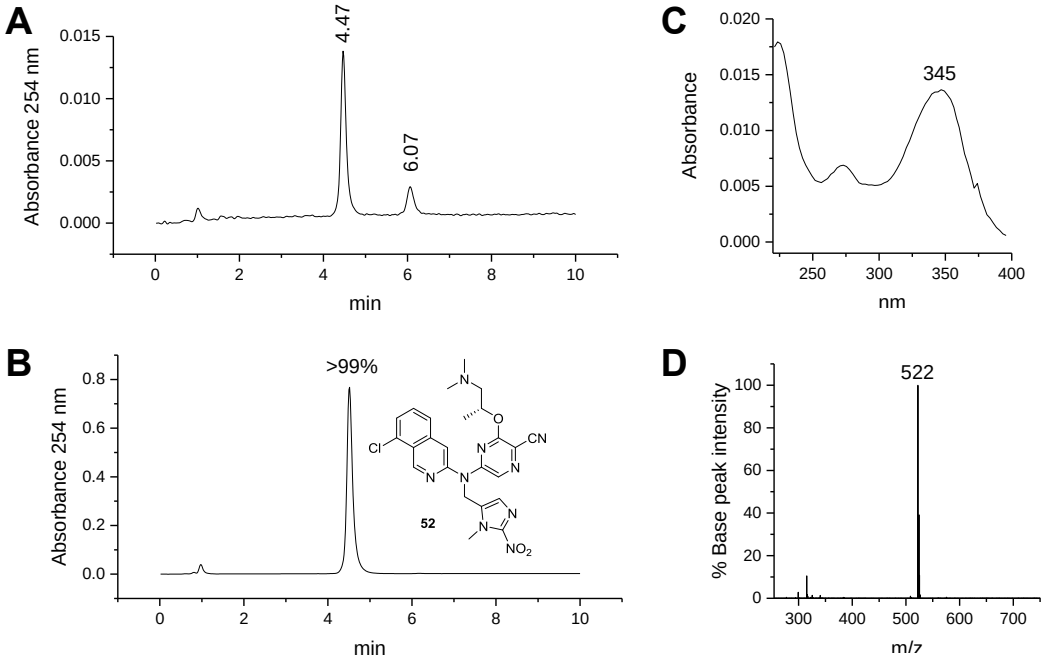

Figure 4.10. Purification of 52.
A) A Gemini®-NX column was used to separate **52** (4.47 min) from the starting material SAR020106 (6.07 min). The system was run isocratically (60% acetonitrile / 40% H_2O + 0.2% NH_3) at pH 11. B) **52** was isolated as the free base in excellent purity (>99%). C and D) **52** shows a maximum UV absorbance at 345 nm and a clean $[M+H]^+$ signal (100% abundance) in ESI+ mass spectrometry.

4.4 Validation of the bioreductive mechanism of action

4.4.1 The bioreductive prodrug **52** *shows decreased Chk1 affinity and cytotoxicity*

We had chosen the site of bioreductive group attachment on SAR020106 in such a way that an interaction between the secondary aniline of the inhibitor and the Glu85 residue in the hinge region of the Chk1 active site would be directly disrupted. We further hypothesized that this substitution also prevented hydrogen bonding between Cys87 and the isoquinoline moiety and an overall reduced binding affinity of the prodrug **52** to Chk1. In order to test this hypothesis, IC_{50} values of the active inhibitor SAR020106 and **52** against the purified kinase

were determined using a radioactive (^{33}P-ATP) filter-binding assay (Figure 4.11). The determined IC_{50} for SAR020106 was 0.005 µM (literature: 0.013 µM (Reader et al. 2011)) and the prodrug **52** had a 55-fold increased IC_{50} value of 0.274 µM.

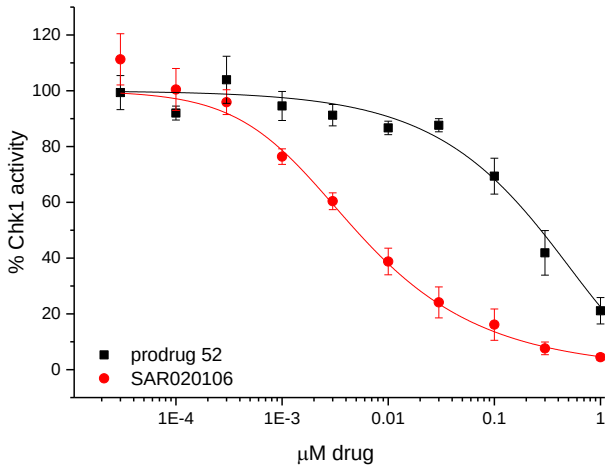

Figure 4.11. IC_{50} determination for 52 and SAR020106 against purified Chk1.
IC_{50} values for **52** and SAR020106 were obtained using a radioactive (^{33}P-ATP) filter-binding assay. SAR020106 had an IC_{50} value of 0.005 µM, while **52** showed a 55-fold decreased affinity with an IC_{50} value of 0.274 µM. This analysis was carried out three times in duplicates by The International Centre for Kinase Profiling, University of Dundee. Curves were fitted in OriginPro using a logistic5 model ($y = A_{min}+(A_{max}-A_{min})/(1+x_0/x)^s$). Error bars indicate the standard error between technical replicates, n=4.

Having observed this significant difference in Chk1 affinity between prodrug and active inhibitor, we next tested **52** for its effect on cell viability in comparison with SAR020106 in a clonogenic survival assay (Figure 4.12). FLO-1 and OE21 cells were exposed to a dose range of either **52** or SAR020106 and colonies counted. As expected, **52** showed no effect on clonogenic survival over the investigated dose range (up to 2.5 µM).

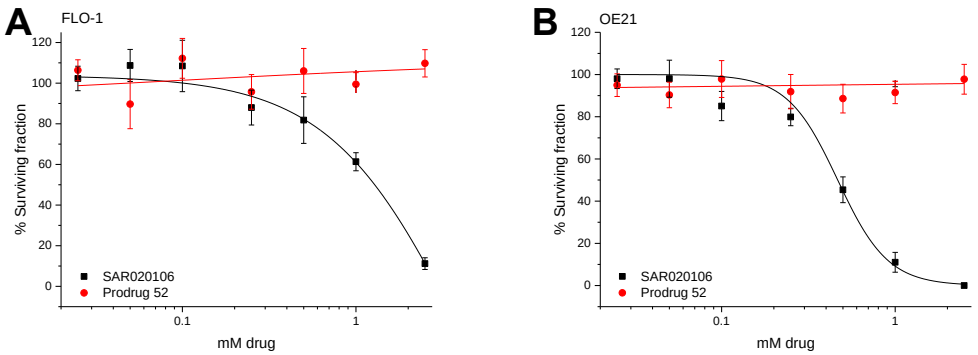

Figure 4.12. The bioreductive prodrug 52 has no effect on clonogenic survival in FLO-1 and OE21 cell at 21% O_2.
Clonogenic survival assays were performed at 21% O_2. A) FLO-1 cells were seeded in 24-well plates (100 cells/well), after 2 h treated with drug and colonies were left to form for 10 days. B) OE21 cells were seeded in 12-well plates (100 cells/well), after 2 h treated with drug and colonies were left to form for 8 days. Curves were fitted in OriginPro using a logistic model ($y = A_2+(A_1-A_2)/(1+x/x_0)^p$). Error bars indicate the standard error between technical replicates, n=3.

Together with the IC_{50} data, this result shows that substitution of SAR020106 with the 2-nitroimidazole group resulted in the generation of the truly inactive prodrug **52**. We had shown previously by western blotting that SAR020106 could be used at doses as low as 500 nM to achieve inhibition of Chk1 signalling (Figures 4.3 and 4.4). In addition, cell survival in three cancer cell lines was severely compromised when cells were treated with SAR020106 at concentrations as high as 2.5 µM or above (Figures 4.2 and 4.5). Assuming prodrug **52** was going to be used at concentrations similar to the active inhibitor SAR020106, Figure 4.12 demonstrates that **52** showed no cytotoxicity at biologically relevant doses.

4.4.1 Inhibition of Chk1 by **52** *requires reduction of the prodrug*

After compound **52** had been validated as a non-toxic prodrug in OE21 and FLO-1 cells with a 55-fold reduced affinity to Chk1 compared to its active analogue, we next studied the mechanism of prodrug activation. With the

2-nitroimidazole group as a bioreductive trigger, we expected **52** to become irreversibly reduced and activated at a partial O_2 pressure of approximately 10 mmHg (1.3% O_2) and below (Arteel, Thurman, and Raleigh 1998; Kizaka-Kondoh et al. 2003). It has been shown that the 2-nitroimidazole prodrug TH-302 undergoes activation at O_2 concentrations below 1.5% (Hu et al. 2010). In addition, similar to TH-302, we expected the activation of **52** to be CYP450 dependent (Meng et al. 2012).

We carried out the CYP450 reductase assay at a range of O_2 concentrations. Samples were taken up to 6 h after initiation of the reaction and analysed by LCMS. A detection wavelength of 360 nm was employed, which gave high absorbance for SAR020106 and **52** while other components of the assay (*i.e.* NADHP, G6P) did not interfere. Any metabolites derived from **52** were expected to show similar absorbance properties. LCMS analysis revealed the formation of one major metabolite, which showed an absorption maximum at 345 nm and was identified as the hydroxylamine **55** (Figure 4.13).

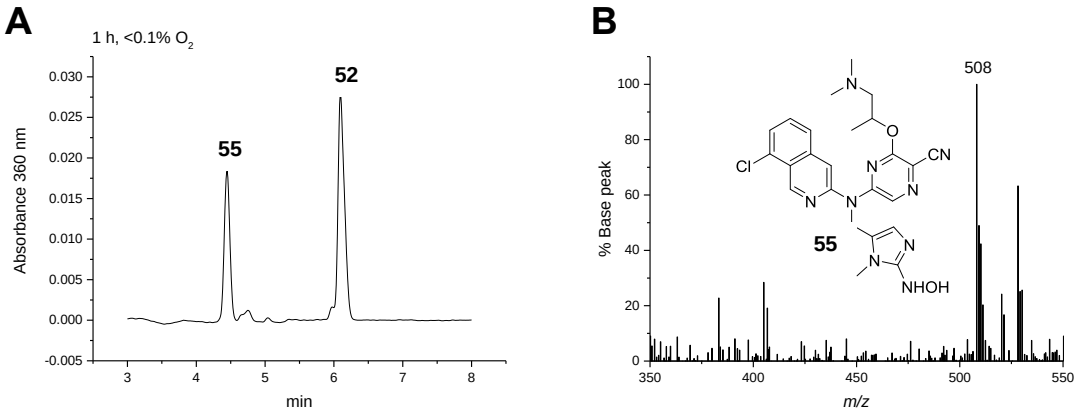

Figure 4.13. CYP450 reduces 52 to the hydroxylamine 55.
A) A representative HPLC trace is shown for CYP450 reduction of **52** at <0.1% O_2 after 1 h. Beside prodrug **52**, the major metabolite at 4.45 min is hydroxylamine **55**. B) ESI+ mass spectrometry for the metabolite eluting at 4.45 min shows the characteristic $[M+H]^+$ of the hydroxylamine **55**.

We carried out the CYP450 reductase assay at four different O_2 concentrations to investigate the O_2 dependency of prodrug activation (<0.1%, 1%, 3% and 21% O_2) (Figure 4.14). Samples were taken up to 6 h after initiation (CYP450 addition) of the reaction and analysed by LCMS. Consumption of prodrug and generation of hydroxylamine **55** from **52** was rapid at <0.1% O_2. Although we had anticipated a short half-life for the reduced prodrug and *in situ* release of SAR020106, only slow release of the active inhibitor from **52** was observed (Figure 4.14, A). With increased O_2 concentration, the hydroxylamine production rate slowed down, but even at 3% O_2 as much as 60% of the total metabolite amount corresponded to **55** after 6 h (Figure 4.14, C). When the assay was performed at 21% O_2 on the other hand, the prodrug **52** was stable and showed no reduction (Figure 4.14, D).

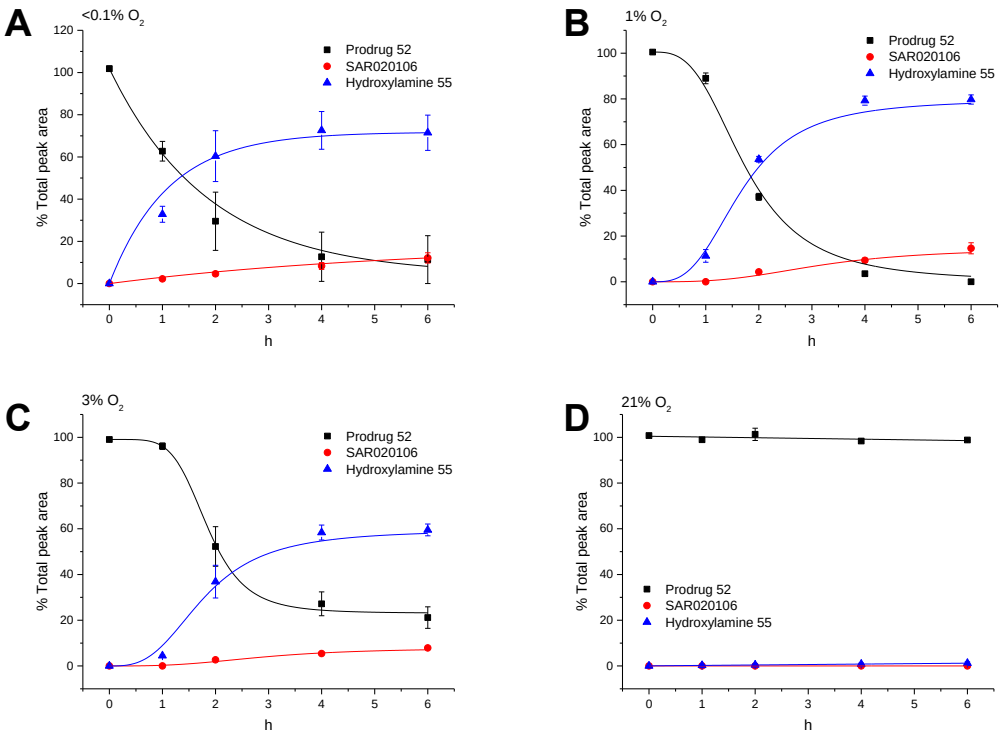

Figure 4.14. CYP450 reduction of 52 at different O_2 concentrations.
Prodrug **52** was incubated with CYP450 enzyme and an enzymatic NADPH-regenerating system (Becton Dickinson Biosciences) at the indicated O_2 concentrations at 37 °C. 50 µl samples were taken at designated times, quenched with 50 µl acetonitrile and analysed by LCMS. Absorbance was measured at 360 nm. Curves were fitted in OriginPro using an asymptotic model (A) (y = a-b*c^x) or a logistic model (B-D) (y = A_2+(A_1-A_2)/(1+x/x_0)^p). Error bars represent the standard error between technical replicates of the experiment, n=3.

The relatively rapid generation of hydroxylamine **55** at 3% O_2 was unexpected and a potential reason for concern considering the O_2 levels found in some healthy organs (McKeown 2014; E M Hammond et al. 2014). Fragmentation of **55** and release of inhibitor SAR020106 was slow and independent of the O_2 concentration.

We next asked if reduction of **52**, as we had seen in the CYP450 assay, was representative for the reductive metabolism of **52** in live cells. A multitude of one-electron reductases can be found in cells and CYP450 only represents one example. The direct analysis of cell lysates from cells treated with **52** in hypoxia allowed us to identify the **52**-derived metabolites, and show whether **52** was able to penetrate cell membranes. FLO-1 and OE21 cells were treated with 500 nM **52**

for 6 h at four different O_2 concentrations (<0.1%, 1%, 3% and 21% O_2). Cells were lysed and the lysates processed for metabolite analysis by LCMS (Figure 4.15).

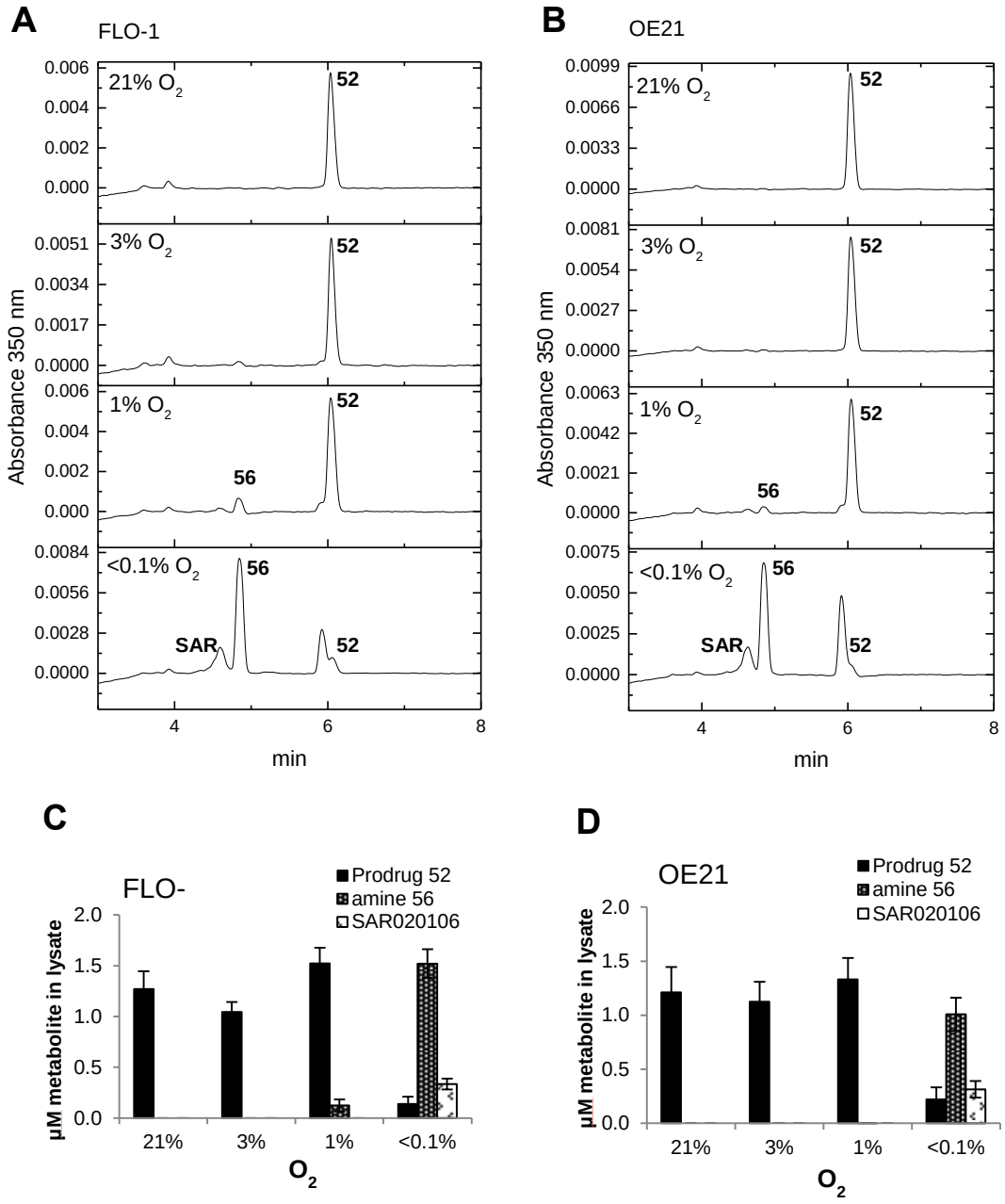

Figure 4.15. Metabolite analysis for 52 in FLO-1 and OE21 cells at various O_2 concentrations.
Cells were treated with 500 nM of **52** at the indicated O_2 concentration for 6 h, harvested, lysed with 3% *v/v* TCA and lysates analysed by LCMS. A) and B) Representative sets of HPLC traces for the four different O_2 concentrations in both cell lines. Quantification of metabolites for C) FLO-1 and D) OE21 using calibration curves as in appendix C. Error bars indicate the standard error between technical replicates of the experiment, n=3. SAR indicates SAR020106.

Prodrug **52** was stable at 21% and 3% O_2 in both cell lines, analysis of the cell lysates showed no evidence of reduction (Figure 4.15). Some reduction of **52** to the amine **56** occurred at 1% O_2 but the majority after 6 h was the parent prodrug in both cell lines. In FLO-1 cells, 93% (1.52 μM) of the drug was still in the form of prodrug **52** after exposure to 1% O_2 and 7% (0.12 μM) had been reduced to the amine. In OE21 cells, minimal reduction to the amine **56** was detectable by LCMS but accurate quantification was not possible because of the small amount of **56**. An estimated ~2% of the drug was present as amine and ~98% (1.33 μM) detected in the form of **52** (Figure 4.15). At <0.1% O_2, most of the prodrug was reduced to **56**, of which some (17-20%) fragmented to release inhibitor SAR020106. In FLO-1 cells, 7% (0.14 μM) of the prodrug was still present in its original form **52**, 76% (1.52 μM) had been reduced to amine **56** and 17% (0.33 μM) had fragmented to active inhibitor SAR020106. Similarly, in OE21 cells, exposure to <0.1% O_2 resulted in 14% (0.22 μM) of the drug still in the form of **52**, 66% (1.01 μM) in the form of amine **56** and 20% (0.31 μM) as SAR020106.

In contrast to the CYP450 reduction assay where the hydroxylamine **55** had been detected as an intermediate species, enzymatic reduction of prodrug **52** in FLO-1 and OE21 cells generated amine **56**. In addition, the metabolism of **52** in these cell lines appears to be more selective toward a lower O_2 concentration than what had been observed in the CYP450 assay. These two observations suggest that the CYP450 assay is not an accurate system to model the metabolism of **52** in cells.

4.4.2 Activation of **52** *is not only CYP450-dependent*

To expand on the previous results, we reasoned that if the major enzyme responsible for **52** reduction in hypoxia was indeed CYP450, as we had previously assumed, the rate of prodrug turnover could be expected to be dependent on cellular CYP450 levels. A set of cell lines derived from the HCT116 cell line was used to test this hypothesis. The set was provided by Prof. William R. Wilson (Auckland University, New Zealand) and consisted of the HCT116 wt cell line and two mutants (HKO1 and HKO1/POR) derived from it. In the HKO1 cell line, mutations were introduced into the 8^{th} exon of both CYP450 alleles using custom-designed zinc finger nucleases. One allele carries a 15 bp deletion and the other a 26 bp deletion. HKO1 has lower CYP450 enzyme activity than the parental line (Su et al. 2013). HKO1/POR is a derivative of HKO1 in which the human CYP450 gene has been re-expressed by transfecting with a F527.V5 plasmid which carries a puromycin resistance marker (Guise et al. 2012). HKO1/POR expresses a higher CYP450 enzyme activity than HCT116 as was verified by western blotting (Figure 4.16, A).

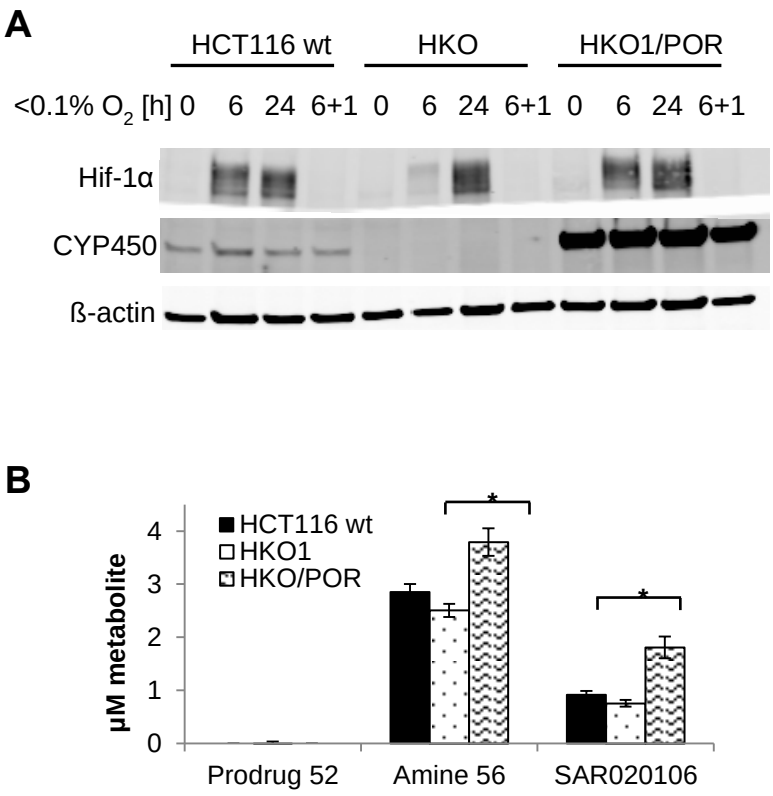

Figure 4.16. Comparison of 52 metabolism in a set of CYP450 mutant cell lines.
A) The three cell lines HCT116 wt, HKO1 and HKO1/POR express different levels of CYP450 reductse and this is independent of the O_2 concentration. Cells were exposed to severe hypoxia (<0.1% O_2) for the indicated time or for 6 h and then reoxygenated for 1 h at 21% O_2 (indicated as 6+1). β-Actin was used as a loading control and Hif1α as a hypoxia marker. B) Cells as indicated were treated with **52** (1 µM) and exposed to <0.1% O_2 for 6 h. They were lysed with 3% *v/v* TCA and lysates analysed by LCMS. Quantification of metabolites was carried out using calibration curves as in appendix C. Error bars indicate the standard error between technical replicates of the experiment. * denotes $p<0.05$.

Su and coworkers tested sensitivity of CYP450 clones to 11 different bioreductive prodrugs, including nitroaromatics, N-oxides and quinones. Their reports shows that, while CYP450 overexpression potentiated cytotoxicity of most bioreductive prodrugs, CYP450 knockout had little or no effect on the cytotoxicity of most compounds (Su et al. 2013). Similarly to the findings of Su and coworkers, we only saw limited CYP450-dependence in the metabolism of **52**. In the mutant cell line HKO1, which shows markedly reduced CYP450 levels compared to the parental line, no significant differences in metabolite pattern compared to the HCT116 wt cell line were detected. We could, however, see an

increase in both, amine **56** and active Chk1 inhibitor SAR020106, in lysates from the CYP450 overexpressing cell line HKO1/POR. The overall amount of **56** increased from 2.8 µM in HCT116 to 3.8 µM in HKO1/POR and the amount of SAR020106 doubled from 0.9 µM in HCT116 to 1.8 µM in the overexpressing mutant. This indicates that **52** metabolism does indeed proceed faster in the presence of increased CYP450 reductase. Although CYP450 overexpression potentiated reduction and activation of **52**, CYP450 knockout showed no effect on **52** metabolism and other one-electron reductases are likely to be primarily responsible for prodrug activation in cells.

4.5 Biological evaluation of prodrug 52

4.5.1 The prodrug **52** *is a hypoxia-selective Chk1 inhibitor*

After we had shown that **52** undergoes hypoxia-selective reduction and activation, we studied its effect on Chk1 signalling, DNA damage induction and cell survival. In particular, we tested whether biological responses following treatment with **52** occurred in a hypoxia-selective fashion. First we carried out western blotting for Chk1 activity. FLO-1 cells were treated with **52** and exposed to <0.1% O_2 for up to 10 h (Figure 4.17, A). Different exposure times to severe hypoxia allowed us to determine the duration of hypoxia treatment that was required for prodrug activation and Chk1 inhibition. In the DMSO treated control cells, Chk1 activity (shown by Chk1 autophosphorylation on S296) could be seen after 3 h exposure to <0.1% O_2. A marked decrease in pChk1 S296 levels could already be seen in the **52**-treated cells after 3 h severe hypoxia and after 10 h

exposure to severe hypoxia, S296 levels were further decreased. SAR020106 showed Chk1 inhibition as expected.

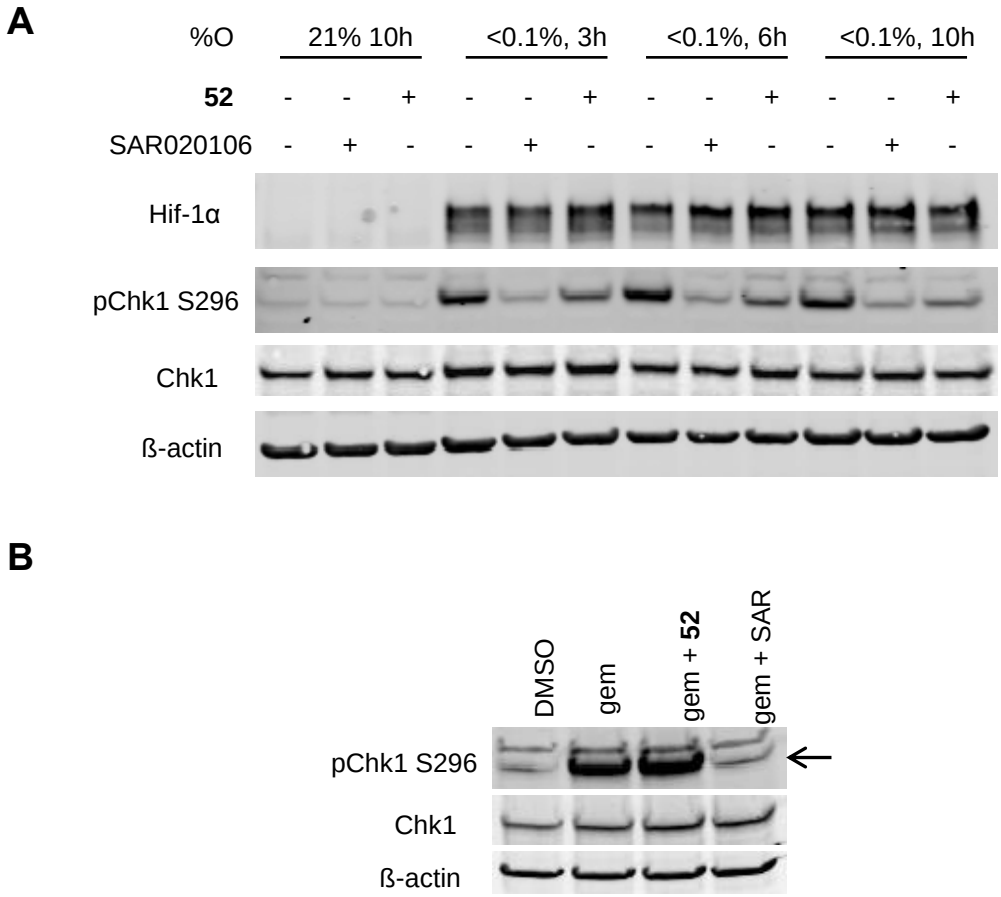

Figure 4.17. Prodrug 52 inhibits Chk1 selectively in severe hypoxia.
A) FLO-1 cells were treated with either **52** (500 nM), SAR020106 (500 nM) or DMSO and exposed to 21% O_2 or <0.1% O_2 for the indicated times. Hif1α is shown as a hypoxia marker. Total Chk1 protein levels are shown for comparison. β-Actin is shown as a loading control. B) FLO-1 cells were treated with the following or a combination thereof, as indicated: DMSO, gemcitabine (100 nM), SAR020106 (SAR) (500 nM), **52** (500 nM). Cells were exposed to the drugs for 6 h at 21% O_2. Total Chk1 protein levels are shown for comparison. β-Actin is shown as a loading control.

Since Chk1 activity in the unstressed control cells at 21% O_2 is very low (Figure 4.17, A), we carried out a control experiment in order to demonstrate that Chk1 inhibition by **52** was hypoxia selective (Figure 4.17, B). Chk1 activation was induced by treatment of FLO-1 cells with 100 nM gemcitabine. Exposure of gemcitabine-treated cells to **52** at 21% O_2 did not result in reduced pChk1 S296 levels in comparison to the gemcitabine treated control cells. As expected,

SAR020106 reduced gemcitabine-induced Chk1 phosphorylation to control levels. These results demonstrate that **52** inhibits Chk1 autophosphorylation selectively in severe hypoxia.

4.5.2 Treatment with **52** *leads to an increased accumulation of DNA damage selectively in hypoxia*

We had previously observed that treatment with the Chk1 inhibitor SAR020106 resulted in a significant accumulation of DNA damage as judged by the formation of 53BP1 foci in OE21 cells in both, normoxia and severe hypoxia (<0.1% O_2) (Figure 4.6). We now investigated whether prodrug **52** showed a similar effect selectively in severe hypoxia. FLO-1 cells were seeded in chamber slides and treated the following day with DMSO, SAR020106 or **52** for 6 h while exposed to either 21% O_2 or <0.1% O_2. Cells were fixed under the experimental O_2 tension in order to avoid reoxygenation-induced damage, and processed for 53BP1 immunofluorescence. Cells were scored as 53BP1 positive or negative according to their total number of foci (Figure 4.18), while cells with more than 6 foci were considered 53BP1 positive and those with 6 or less foci as negative.

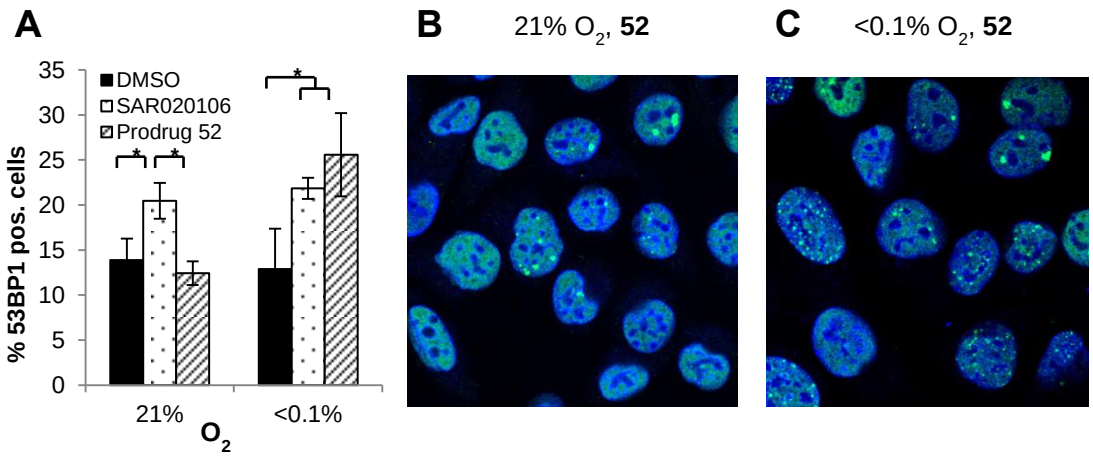

Figure 4.18. Treatment of FLO-1 cells with 52 results in increased accumulation of 53BP1 foci selectively in severe hypoxia.
FLO-1 cells were seeded in chamber slides. Cells were treated with either DMSO, SAR020106 (500 nM) or **52** (500 nM) and exposed to 21% O_2 or <0.1% O_2 for 6 h. Cells were scored according to their number of 53BP1 foci as negative (≤6 foci) or positive (>6 foci). Per condition, at least 100 cells taken from 8-10 different fields of view were scored. A) The relative amount of 53BP1 positive cells comparing the different drug treatments in 21% O_2 and <0.1% O_2 was plotted. Error bars indicate the standard error of technical replicates. * denotes $p<0.05$. B) and C) Cells were stained for DAPI and 53BP1, and visualised using a LSM780 confocal microscope.

Upon exposure to normoxia only cells treated with SAR020106 showed a significant increase in the number of 53BP1 foci. Treatment with **52** at 21% O_2 did not result in increased DNA damage in comparison to the control cells. When combined with severe hypoxia (<0.1% O_2) both drug treatments, SAR020106 and **52**, significantly increased the number of 53BP1 positive cells. DNA damage induction by **52** was thus hypoxia-selective in FLO-1 cells. Although not statistically significant, there is an indication that DNA damage in response to **52** in severe hypoxia might be greater than the amount of DNA damage induced by SAR020106 under the same conditions (Figure 4.18, A). If this increase is indeed real, it could have its origin in additional DNA damage caused by the release of the 2-nitroimidazole bioreductive group, but this speculation requires additional experiments with a control compound similar to **12** (Chapter 2).

4.5.3 Clonogenic survival in response to **52**

After we had shown that the prodrug **52** undergoes reduction and fragmentation selectively in hypoxia, resulting in Chk1 inhibition and accumulation of DNA damage we studied its effect on clonogenic survival. We initially performed a clonogenic survival experiment in HeLa cells due to the possibility of scaling the assay down to a 96-well format in this cell line. As in previous experiments we expected a Chk1 inhibitor specific response, in this case reduced clonogenic survival, selectively in hypoxia. Surprisingly, **52** had no effect on clonogenic survival of HeLa cells in severe hypoxia (Figure 4.19, A).

We had earlier studied reduction and activation of **52** in FLO-1 and OE21 and knew from the identification of metabolites in these cell lines that 17-20% of the prodrug undergoes reduction and activation to the Chk1 inhibitor SAR020106 (compare Figure 4.15). Given this knowledge, we next performed a clonogenic survival assay in these cell lines using a drug dose of up to 2.5 µM. At this dose the amount of active inhibitor was expected to be high enough to detect some effect even if only partial activation of about 20% took place. The result seen in the HeLa cells, however, was also observed in the two oesophageal cell lines. Treatment with **52** did not affect clonogenic survival in either of the two cell lines and this was the case at 21% O_2 (as expected) as well as <0.1% O_2 (Figure 4.19, B and C).This result was surprising, since treatment with the active compound SAR020106 resulted in a marked decrease of cell survival at sub micro molar doses (Figure 4.5).

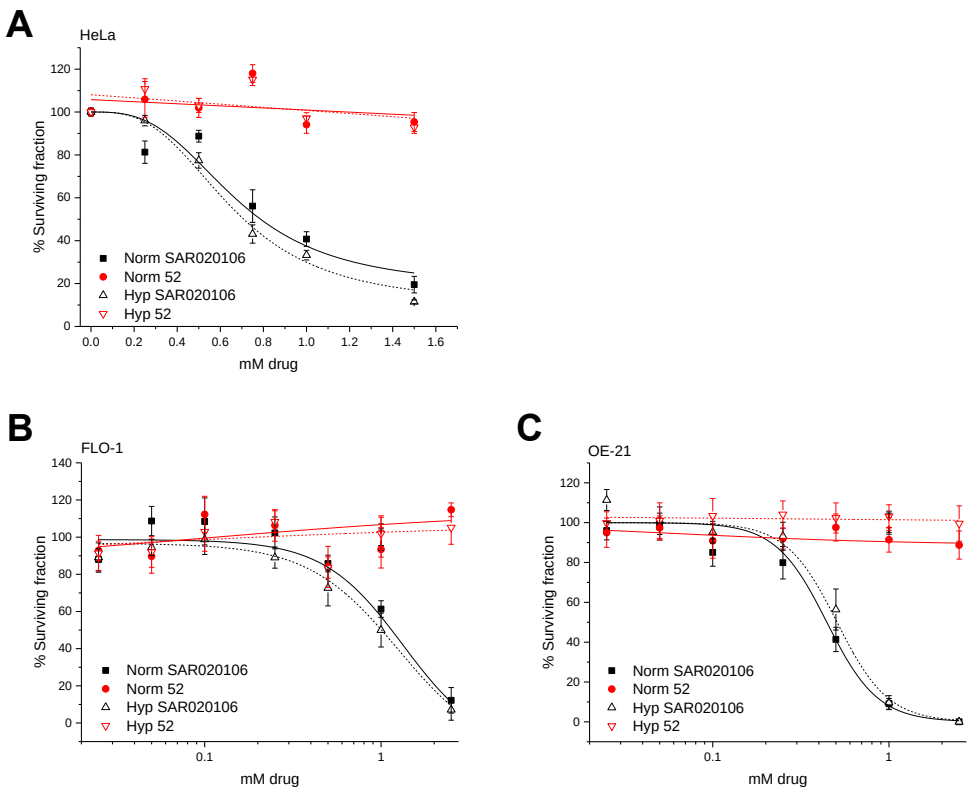

Figure 4.19. Clonogenic survival assays comparing SAR020106 and 52 at two O_2 concentrations in three cell lines.
A) HeLa cells were seeded in 96-well plates (200 cells/well) after 2 h treated with drug and exposed to the indicated O_2 concentration for 18 h. Colonies were left to form for 6 days, stained with Crystal Violet and analysed using a GelCount colony counter. B) FLO-1 cells were seeded in 24-well plates (100 cells/well) after 2 h treated with drug and exposed to the indicated O_2 concentration for 16 h. Colonies were left to form for 10 days. C) OE21 cells were seeded in 12-well plates (100 cells/well) after 2 h treated with drug and exposed to the indicated O_2 concentration for 16 h. Colonies were left to form for 8 days. (Curves were fitted in OriginPro using a logistic5 model ($y = A_{min}+(A_{max}-A_{min})/(1+x_0/x)^s$). Error bars indicate the standard error between technical replicates, n=3.

In the clonogenic survival assay only extremely low cell densities are seeded, prodrug activation however relies on the presence of cellular reductases. This is of no concern if the prodrug is rapidly reduced and undergoes *in situ* fragmentation. In the case of **52**, on the other hand, we have seen that amine **56** was very stable, possibly allowing the cell enough time to clear **56** before fragmentation takes place. This way the effective concentration of amine **56** and consequently inhibitor SAR020106 becomes extremely low in the culture media resulting in no detectable effect on cell survival.

4.5.4 Spheroid studies

Following the results from the clonogenic survival assays and our hypothesis, that the low cell density in those experiments was to account for the lack of cytotoxicity observed with **52**, we initially changed the way clonogenic survival assays were carried out. Instead of seeding single cells and treating those with the respective drug doses and hypoxia exposure times, exponentially growing cells (80% confluency) were treated in 6 cm glass dishes and then trypsinised, counted and reseeded as single cells for colony formation (Franken et al. 2006). However, this way to set up a clonogenic survival experiment is more prone to errors. In particular, the counting and reseeding of multiple dishes of cells bears a high risk for experimental errors. Despite several attempts, we never obtained reproducible results from these experiments and decided to study **52** in 3D cell cultures instead. 3D cultures also offer a way to avoid the extremely low cell densities of a colony survival assay. It is further well established that they resemble the gene expression profiles, cell signalling and pathophysiological gradients of tumours more accurately than 2D culture monolayers (Abbott 2003; Hirschhaeuser et al. 2010). In particular, one report indicated that expression levels of CYP450 decreased over several days in cell culture monolayers, while remaining more stable when cells were grown as spheroids (Niwa et al. 1996). Testing novel treatment strategies in spheroids is considered highly advantageous in the drug development process and could result in elimination of unsuitable candidates before testing in animal models. For the activation of bioreductive prodrugs it is crucial that the molecule can diffuse through multiple layers of cells from a functional blood vessel into the hypoxic area of a tumour. This situation is well resembled in spheroids.

Both oesophageal cancer cell lines that were used before in this study were unsuitable for spheroid formation. FLO-1 cells did not form spheroids and OE21 cells formed only very small spheroids which stopped growing after a few days. Instead we used the glioblastoma derived U87-MG cells for this study which had been used for 3D cultures before in our laboratory. Cells were grown into spheroids in agarose-coated 24-well plates. Four days after seeding the cells (10^5 per well), they had grown into spheroids with an average radius of approximately 400 µm. At this stage the medium was replaced with drug-containing medium and hypoxia (3% O_2) treatment started, if indicated (day 0 of treatment). Spheroids were measured and treated on days 0, 2, and 4 by replacing the medium with fresh drug-containing medium. On day 7, spheroids were measured, treated with 200 µM pimonidazole for 6 h and harvested. They then processed for metabolite analysis, western blotting or immunofluorescence microscopy.

We grew the spheroids at two different O_2 concentrations (21% and 3% O_2) to examine whether the exposure to a lower O_2 concentration would affect prodrug activation and spheroid growth. Spheroids grown at 21% O_2 developed a hypoxic core which could be visualised on spheroid sections, using a monoclonal antibody towards pimonidazole adducts (Figure 4.20, A). Spheroids grown at 3% O_2 were hypoxic through the entire section. Pimonidazole staining in these spheroids revealed a hypoxic and pimonidazole positive outer rim. The centre of the spheroid showed reduced pimonidazole staining and this is likely to indicate necrosis in this area (Figure 4.20, B) (Hoogsteen et al. 2009). In addition, it is possible that most of the pimonidazole bound to the hypoxic cells in the core,

reducing the likelihood of pimonidazole reaching the core. Longer exposure times to the marker or higher concentrations could help in preventing this effect.

Western blotting from whole spheroid lysates for the hypoxic marker Hif1α showed stabilisation of Hif1α in the spheroids grown at 21% O_2 (Figure 4.20, C). In those spheroids grown at 3% O_2, Hif-1α levels where significantly higher, indicating an overall greater hypoxic fraction within the spheroid. Interestingly, we detected lower Hif-1α protein levels in the SAR020106- and **52**-treated spheroids at both O_2 concentrations (Figure 4.20, C). This might be an indication for increased cell kill in the hypoxic (Hif-1α-expressing) fraction of the spheroid, but this is only a speculation.

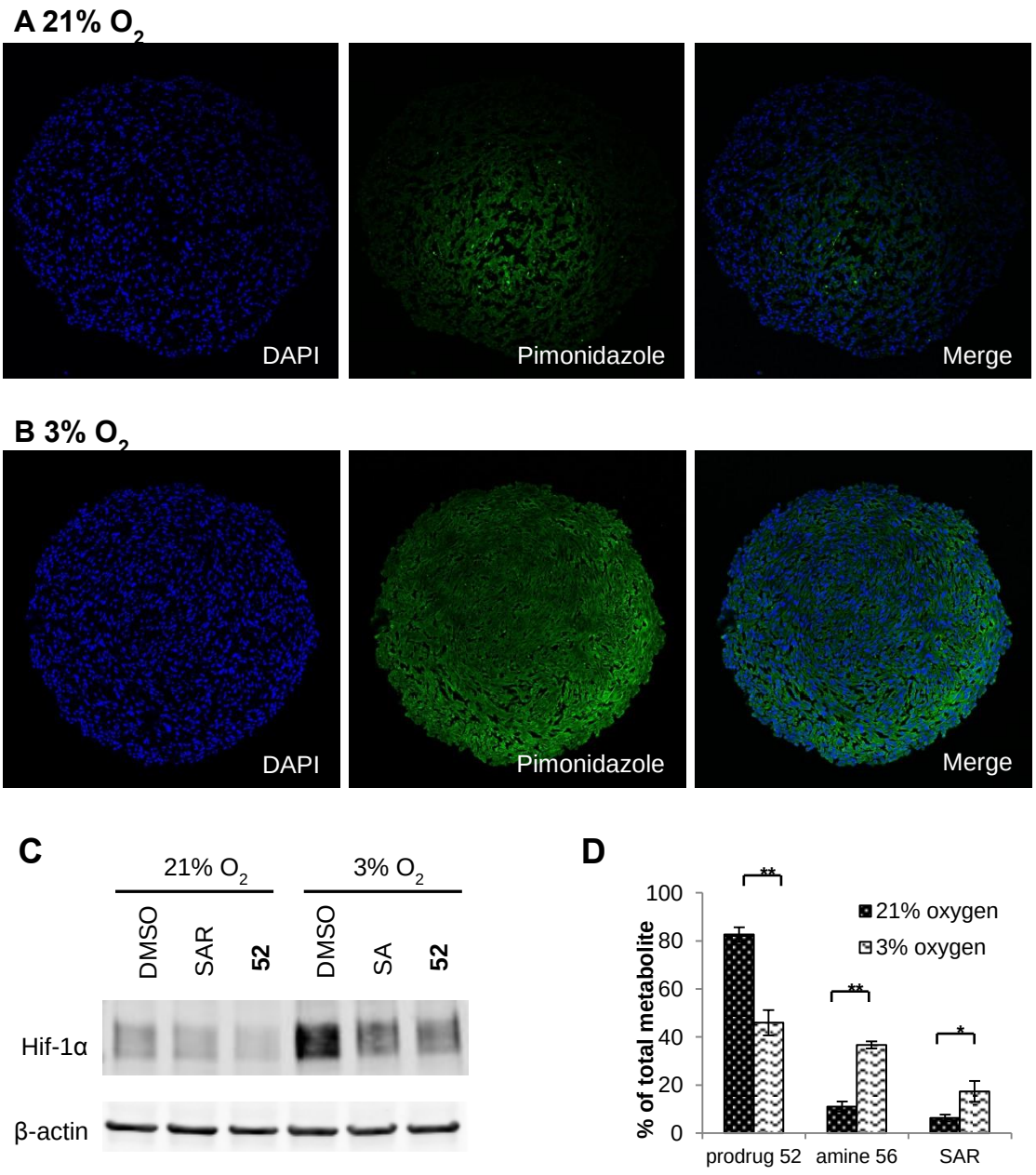

Figure 4.20. O_2-dependency of 52 metabolism and growth reduction in U87-MG spheroids. U87-MG cells (10^5 per well) were seeded into agarose-coated 24-well plates. Spheroids were left to form for 4 days (average radius 400 µm) and treatment started as indicated (DMSO, 500 nM SAR020106 (SAR) or 500 nM **52**; 21% or 3% O_2) (day 0 of treatment). Spheroids were measured and treated with fresh drug-containing medium on days 0, 2, and 4. On day 7, spheroids were measured, treated with 200 µM pimonidazole for 6 h and harvested. A) and B) Immunofluorescence images of 5 µm sections from DMSO-treated spheroid, antibodies used as indicated. C) Western blotting from whole spheroid lysates. Spheroids were treated as indicated. Hif1α is shown as a hypoxia marker and β-actin as a loading control. D) Spheroids were treated as indicated, lysed with 3% *v/v* TCA and lysates analysed by LCMS. Quantification of metabolites was carried out using calibration curves as in appendix C. Error bars indicate the standard error between technical replicates of the experiment, n=3. * denotes $p<0.1$, ** denotes $p>0.05$

We further lysed and prepared spheroids for metabolite analysis by LCMS (Figure 4.20, D). At both O_2 concentrations, prodrug **52** was taken up by the cells.

As expected, treatment with 3% O_2 resulted in increased prodrug activation. Overall comparison of drug metabolites shows that, while 6.3% SAR020106 and 11.1% amine **56** were detected in the spheroids grown at 21% O_2 (the remaining 82.6% were unmetabolised prodrug **52)**, 17.3% SAR020106 and 36.7% **56** resulted when spheroids were grown at 3% O_2.

Spheroid growth was monitored over the course of treatment and the radius of individual spheroids measured on days 0, 2, 4 and 7. Assuming an ideal sphere, the increase in spheroid volume was then calculated relative to day 0, (Figure 4.21, A and B).

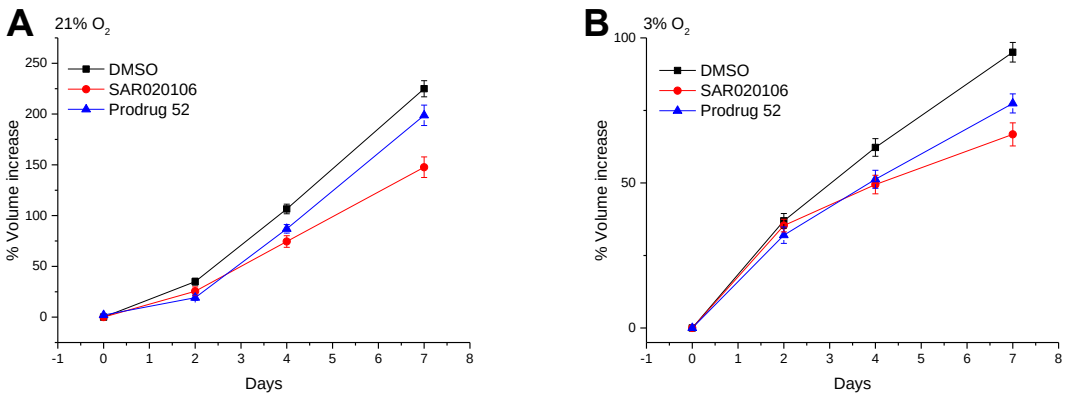

Figure 4.21. Growth reduction in U87-MG spheroids following treatment with 52 and SAR020106.
U87-MG cells (10^5 per well) were seeded into agarose-coated 24-well plates. Spheroids were left to form for 4 days (average radius 400 µm) and treatment started as indicated (DMSO, 500 nM SAR020106 or 500 nM **52**; 21% or 3% O_2) (day 0 of treatment). Spheroids were measured and treated with fresh drug-containing medium on days 0, 2, and 4. On day 7, spheroids were measured, treated with 200 µM pimonidazole for 6 h and harvested. A) and B) Spheroid growth over 7 days for treatment as indicated. The spheroid radius was measured and the volume calculated assuming an ideal sphere. Error bars indicate the standard error between technical replicates of the experiment, n=3.

Spheroids grown in hypoxia did not increase in volume as much as those exposed to 21% O_2 (95% *versus* 225%) pointing towards an overall smaller fraction of proliferating cells probably due to a large necrotic centre (see Figure 4.20, B). A significant growth reduction after treatment with SAR020106 and also **52** in comparison with the DMSO treated controls was seen after 7 days under

both O_2 concentrations. Treatment with SAR020106 resulted in a comparable reduction in growth at both O_2 concentrations (33% reduction at 21% O_2 and 30% at 3% O_2). Spheroids treated with **52** showed an 11% growth reduction in normoxia and 19% when exposed to hypoxia.

We have demonstrated that spheroids grown from U87-MG cells exhibit an O_2 gradient within the sphere, resulting in a hypoxic centre. Spheroids grown at 3% O_2 show an overall greater hypoxic fraction as evidenced by immunofluorescence staining and western blotting for the hypoxic markers pimonidazole and Hif-1α. Reductive metabolism of the prodrug **52** and reduction in spheroid growth was O_2 dependent.

4.6 Discussion

We have shown that the potent and selective Chk1 inhibitor SAR020106 reduced clonogenic survival in HeLa, FLO-1 and OE21 cells and caused accumulation of DNA damage (53BP1 foci) when used as a single agent and in combination with severe hypoxia (<0.1% O_2). Surprisingly, exposure to severe hypoxia (<0.1% O_2) did not potentiate the cytotoxicity of SAR020106 in any of the three cell lines.

We successfully synthesised **52**, a bioreductive 2-nitroimidazole analogue of the Chk1 inhibitor SAR020106. Two reactive sites, prone to alkylation by 5-(chloromethyl)-2-nitroimidazole, were observed. Alkylation took place on either the inhibitor aniline as anticipated, the isoquinoline N-atom to generate a pyridinium-like product, or on both centres giving a double-alkylation product. The pyridine N-atom is very prone to electrophilic attack since the lone pair is separated from the aromatic system and not delocalised. It lies in the molecular

plane of the molecule, projecting outward and thereby being very exposed to electrophiles.

Selective alkylation of the aniline over isoquinoline N-alkylation was achieved by using Cs_2CO_3 as a base and the selectivity was inverted if the reaction was carried out in the absence of base. Purification of **52** was optimised using a Gemini®-NX column at pH 11 and 6.2 mg of highly pure **52** obtained for *in vitro* testing.

As predicted, based on the X-ray crystal structure of SAR020106 bound to the ATP-binding site of Chk1, the bioreductive prodrug **52** showed reduced Chk1 affinity. A 55-fold higher IC_{50} value than the active analogue SAR020106 was determined in a Chk1 binding assay. Moreover, treatment with **52** at 21% O_2 did not result in increased clonogenic cell kill in two oesophageal cancer cell lines and gemcitabine-induced Chk1 autophosphorylation was not altered by **52**-treatment at 21% O_2.

Metabolite studies in the oesophageal cell lines OE21 and FLO-1 at different O_2 concentrations revealed a requirement for 1% O_2 or less for prodrug reduction to the corresponding amine **56** and activation to inhibitor SAR020106. At >3% O_2 **52** was stable, indicating hypoxia-selectivity for an optimal O_2 concentration in order to spare healthy tissue.

Interestingly, although **52** was reduced by CYP450 to the corresponding hydroxylamine **55** in a biochemical assay, metabolite analysis in a set of CYP450 wt and mutant cell lines suggested only limited CYP450-dependence in the reductive metabolism of **52**. While prodrug reduction and activation were significantly increased in the CYP450 overexpressing mutant HKO1/POR, no difference was seen between the parental HCT116 cell line and the knockout

mutant HKO1. This suggests other one-electron reductases are also responsible for reductive metabolism of **52** in cells. A variety of flavoproteins capable of one-electron prodrug reduction other than CYP450 have been reported, including inducible nitric oxide synthase (iNOS) (Chandor et al. 2008; Guise et al. 2012), methionine synthase reductase (MTRR) (Guise et al. 2012) and aldo-keto reductase 1C3 (AKR1C3) (Guise et al. 2010). The identification of the specific reductases accountable for reduction of **52**, however, was beyond the scope of this study.

These metabolite studies further revealed that amine **56** was the major metabolite arising from prodrug **52** in hypoxia, demonstrating a relatively high stability of this intermediate. Consequently, a mere 17-20% conversion into the active drug was observed in FLO-1 and OE21 cells. This presents an obvious problem for the overall efficacy of the prodrug and we speculate that it also resulted in a technical problem when assessing the effect of **52** on clonogenic cell survival. The long half live of intermediate amine **56** most likely lead to clearance of **56** from the cells before conversion into the active drug SAR020106 could take place, leading to extremely low concentrations of amine **56** in the culture media and as a result, no overall effect of **52** on clonogenic survival in severe hypoxia could be seen.

Due to technical problems with a different setup of the clonogenic assay, we then studied **52** in 3D cultures. Metabolite studies in U87-MG spheroids grown at 21% O_2 revealed that some prodrug reduction and activation took place but most of the drug (82.6%) was recovered in the unmetabolised form **52**. This was surprising since these spheroids formed large hypoxic cores which stained positive for pimonidazole adducts, an indicator for <1.3% O_2 (Gross et al. 1995;

Chou et al. 2004). We had shown before that an O_2 concentration of 1% or less was required for prodrug reduction. Possibly, **52** diffuses poorly to the centre of the spheroid and only reaches the outer rim of the hypoxic core without actually reaching regions of low O_2 efficiently. When spheroids were grown in hypoxia (3% O_2), more amine **56** and inhibitor SAR020106 was recovered from spheroid lysates and only 45.9% remained in the form of **52**, most likely due to the overall greater hypoxic fraction in these spheroids. It is worth noting that the spheroids exposed to normoxia were much larger than those grown at 3% O_2, possibly due to the formation of large necrotic centres at low O_2 concentrations. The greater diffusion distances across a large spheroid reduce the likelihood of **52** reaching the hypoxic core. In addition to being smaller, the spheroids grown at 3% O_2 also have their hypoxic cells much closer to the surface, as evident by pimonidazole staining, making them more accessible for a prodrug like **52**.

CHAPTER 5

DISCUSSION

In accordance with previous finding we confirmed that Chk1 is phosphorylated on its ATR-targeted and autophosphorylation sites in response to severe hypoxia and that it phosphorylates its downstream target TLK1. This shows that Chk1 is involved in the hypoxia-induced DDR. Hypoxia-induced Chk1 signalling was shown to be a transient response and protein levels of phosphorylated Chk1 decreased after exposure to severe hypoxia for longer than 6 h. This is in line with a previously observed decline in RPA foci upon prolonged exposure to severe hypoxia (Pires, Bencokova, Milani, et al. 2010; Pires, Bencokova, McGurk, et al. 2010). Inhibition of Chk1 resulted in the accumulation of DNA damage in normal human lung fibroblasts, highlighting a potential for genomic instability, as had been reported before (Lam et al. 2004; Syljuåsen et al. 2005). Based on these findings, we reasoned that the intrinsic sensitivity of hypoxic cells to Chk1 inhibition could be exploited and simultaneously normal tissue protected if Chk1 inhibition was hypoxia selective.

Consequently, we synthesised two 4-nitrobenzyl (compounds **2** and **17**) and two 2-nitroimidazole (compounds **18** and **52**) bioreductive analogues of three previously published Chk1 inhibitors. In all cases, prodrug design was rationalised through published X-ray crystal structures of the respective Chk1 inhibitors bound to the ATP-site of Chk1. In the case of compound **2**, docking studies were performed to further validate the site of substitution. In general, substitution sites were chosen such that the prodrug would show substantially

reduced Chk1 binding affinity in comparison with the biologically active inhibitor, and the validity of our design was confirmed for all four bioreductive compounds (**2**, **17**, **18** and **52**) in a radioactive (^{33}P-ATP) filter-binding assay. Synthesis of the prodrugs required optimisation at various stages. Most notably, we established a protocol for the synthesis of a precursor to the bioreductive 2-nitroimidazole group, which has recently been further optimised and expanded (O'Connor et al. 2015). This bioreductive group has received attention in the field as a trigger unit in the clinically advanced candidate TH-302 (Meng et al. 2012).

The mechanism of activation of the bioreductive prodrugs was evaluated following a sequence of reduction assays which proceeded in an increasingly biologically relevant fashion (Figure 5.1). Chemical reduction of the bioreductive group nitro moiety to the corresponding amine was achieved using zinc and ammonium chloride, and fragmentation assessed by incubation in PPB (Figure 5.1, step 1). This initial chemical reduction is an inexpensive and quick way to determine the fragmentation propensity of a bioreductive group and make necessary chemical adjustments before proceeding to biochemical and *in vitro* testing. It is important to note that other reducible functionalities, such as aryl halides, may also undergo reduction in this assay. Adjusting the reaction conditions can avoid this problem. Alternatively, prodrug activation can directly be assessed using a biochemical assay (Figure 5.1, step 2). Based on the assumption that most nitro(hetero)aromatic prodrugs are substrates of CYP450 (Wilson and Hay 2011), step 2 of our protocol for bioreductive prodrug testing consisted of a CYP450 reductase assay.

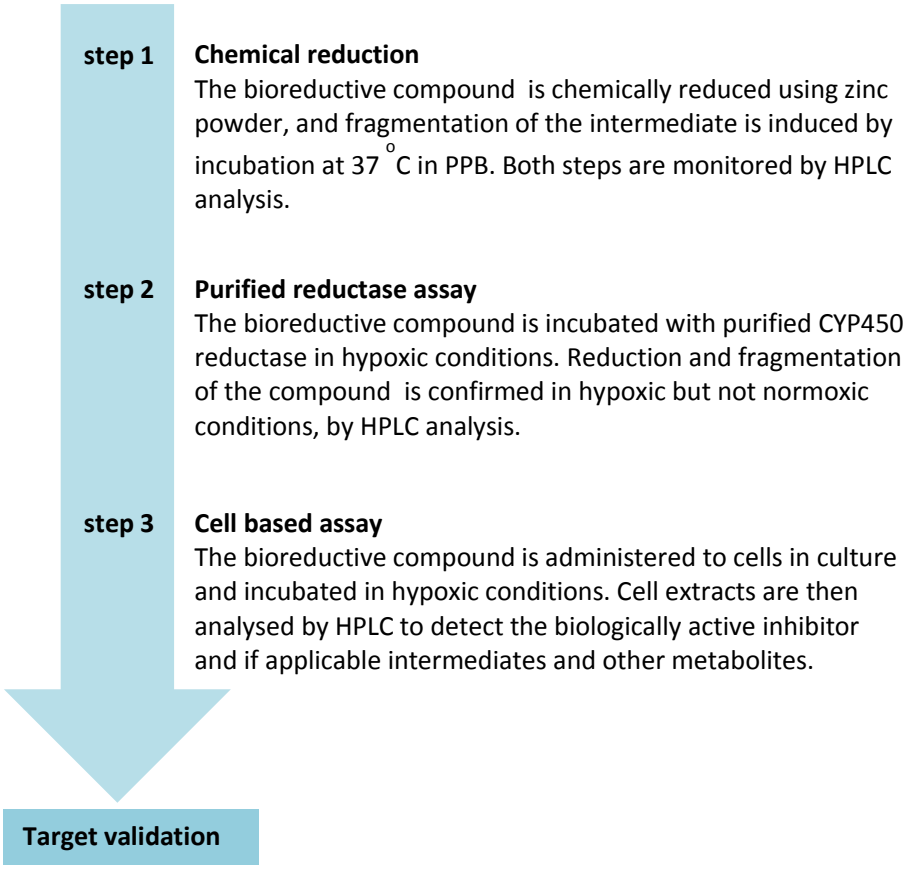

Figure 5.1. How we test bioreductive prodrugs.
Sequential strategy for the evaluation of the bioreductive mechanism of activation of a hypoxia-activated prodrug. Testing of the bioreductive prodrug is carried out in three steps of increasing biological relevance.

Importantly, although compound **52** underwent reduction to the corresponding hydroxylamine in the CYP450 assay, we saw only limited CYP450 dependence in the reductive metabolism of **52** in a set of CYP450 knockout and overexpressing cell lines. A variety of other one-electron reductases accountable for activation of bioreductive prodrugs have been reported (Guise et al. 2012; Guise et al. 2010; Chandor et al. 2008) and in order to accurately predict prodrug metabolism *in vivo*, those will have to be considered as well. In that respect, experiments in isogenic cell lines, which differ only in the expression of the protein of interest, will be invaluable.

We tested our compounds following the protocol shown in Figure 5.1 and discovered that most prodrugs were reduced in hypoxia. However, fragmentation

following reduction was generally either slow (occurring over several hours in the case of **2** and **52**) or did not take place (in case of **17** and **18**). This was probably due to a poor leaving group ability of the active inhibitors. Since it is desirable to design bioreductive prodrugs with a short half-life following reduction in order to ensure rapid and complete release of the active molecule, simple chemical model systems similar to the prodrug could be used to assess the leaving group ability of an inhibitor scaffold. In addition, a linker can be introduced between the bioreductive group and the inhibitor moiety of the prodrug to facilitate fragmentation (Hay et al. 1999; Hay, Wilson, and Denny 2005).

Despite slow fragmentation, compounds **2** and **52** were shown to inhibit their targets AURKA and Chk1 in a hypoxia-selective fashion. Moreover, treatment with these bioreductive prodrugs resulted in the accumulation of DNA damage and reduction in clonogenic survival or spheroid growth in an O_2-dependent fashion. We speculate that the potency of the bioreductive prodrugs could be greatly improved if fragmentation was more rapid and propose that *in situ* release of the biologically active inhibitor is desirable upon reduction. In accordance with previous findings, our studies suggest that cell lines with high levels of replication stress are particularly sensitive to hypoxia-activated Chk1 inhibition (Murga et al. 2011; Ferrao et al. 2012; Bryant, Rawlinson, and Massey 2014). In conclusion, we propose that the selective *in situ* activation of a Chk1 inhibitor within the hypoxic tumour microenvironment is a promising strategy to target hypoxic tumour cells. Moreover, since inhibition of Chk1 has previously been shown to radiosensitise, this strategy would allow potentiation of radiotherapy in a tumour fraction that is highly radio resistant.

CHAPTER 6

EXPERIMENTAL

6.1 Materials

6.1.1 General laboratory materials and reagents

Cell culture plastic ware was obtained from Costar. The chemicals and reagents outlined in Table 6.1 were used.

Table 6.1. Chemicals and reagents

Name	Supplier
Acetonitrile	Sigma-Aldrich UK
Acrylamide/Bis Solution, 30%, 29:1	BioRad
Agarose	Sigma-Aldrich UK
Ammonium chloride (NH_4Cl)	Sigma-Aldrich UK
APS	Fisher Scientific
ß-Mercaptoethanol	Fisher Scientific
Blocking buffer LiCor	LiCor
Bromophenol blue	Fisher Scientific
BSA	Fisher Scientific

Crystal Violet	Sigma-Aldrich UK
CYP450 reductase	Cypex
DMEM	Sigma-Aldrich UK
DMSO	Sigma-Aldrich UK
Ethanol	Fisher Scientific
FBS	Autogen Bioscience
Formic acid	Fisher Scientific
Goat serum	Sigma-Aldrich UK
Methanol	Fisher Scientific
Methylene Blue	Fisher Scientific
OCT compound	Tissue-Tek
PBS	Fisher Scientific
Penicillin	Sigma-Aldrich UK
PFA	Fisher Scientific
Ponceau S solution	Sigma-Aldrich UK
PPB, 0.5 M, pH 7.4	Becton Dickinson Biosciences
ProLong® Gold	Invitrogen/Life technologies
Puromycin	Fisher Scientific
RPMI	Sigma-Aldrich UK

Sodium dithionite ($Na_2S_2O_4$)	Sigma-Aldrich UK
Solution A	Becton Dickinson Biosciences
Solution B	Becton Dickinson Biosciences
Streptomycin	Sigma-Aldrich UK
Sucrose	Sigma-Aldrich UK
TCA	Fisher Scientific
TEMED	Fisher Scientific
Trypsin 0.05% EDTA	Sigma-Aldrich UK
Tris-Glycine	Fisher Scientific
Tris-HCl	Fisher Scientific
Triton-X-100	Fisher Scientific
Tween 20	Fisher Scientific
Urea	Fisher Scientific
Zinc powder	Sigma-Aldrich UK

6.1.2 Drugs (commercially available and in-house)

Drugs were obtained from suppliers as outlined in Table 6.2 or synthesised as described in Chapters 2-4.

Table 6.2. Drugs used in this study

Name	Supplier
AZD1152	Selleckchem, S1147
Analogue **19**	In house (Chapter 3)
Chk1 inhibitor **16**	In house (Chapter 3)
Gemcitabine hydrochloride	Sigma-Aldrich UK, G6423
Gö6976	Sigma-Aldrich UK, G1171
HU	Sigma-Aldrich UK, H8627
MLN8237	Selleckchem, S1133
Prodrug **2**	In house (Cazares-Körner et al. 2013)
Prodrug **17**	In house (Chapter 3)
Prodrug **18**	In house (Chapter 3)
Prodrug **52**	In house (Chapter 4)
Pimonidazole hydrochloride	Hypoxyprobe, HP-100mg
SAR020106	ICR, London
UCN01	Sigma-Aldrich UK, U6508

6.1.3 Antibodies

Table 6.3. Primary antibodies used for western blotting (WB) or immunofluorescence (IF)

Name	Species	Dilution	Application	Producer, Cat. number
53BP1	Rabbit	1:500	IF	Novus Biologicals, NB100-904
ß-Actin	Mouse	1:10000	WB	Santa Cruz Biotechnology, sc-69879
CAIX	Mouse	1:100	IF	Prof. Adrian Harris, Oxford UK
Chk1	Mouse	1:1000	WB	Santa Cruz Biotechnology, sc-8408
Phospho-Chk1 (S296)	Rabbit	1:500	WB	Cell Signaling/New England Biolabs, #2349
Phospho-Chk1 (S317)	Rabbit	1:500	WB	Cell Signaling/New England Biolabs, #2344
Phospho-Chk1 (S345)	Rabbit	1:500	WB	Cell Signaling/New England Biolabs, #2341
CYP450	Mouse	1:1000	WB	Santa Cruz Biotechnology, sc-25263
GAPDH	Mouse	1:4000	WB	Novus Biologicals, NB600-502
Glut1	Rabbit	1:500	IF	Abcam, ab652

H2AX	Rabbit	1:2500	WB	Merck Millipore, Calbiochem, DR1016
Phospho-H2AX (S139, γ-H2AX)	Mouse	1:5000	WB	Upstate/Millipore, #05-636
H3	Mouse	1:5000	WB	Cell Signaling/New England Biolabs, #3638S
Phospho-H3 (S10)	Rabbit	1:1000	WB	Cell Signaling/New England Biolabs, #9701
Hif-1α	Mouse	1:500	WB	Becton Dickinson Biosciences, #610959
Pimonidazole adducts	Mouse	1:1000	IF	Hypoxyprobe, HP1-100

Table 6.4. Secondary antibodies used for western blotting (WB) or immunofluorescence (IF)

Name	Dilution	Application	Producer, Cat. number
Alexa Fluor 680 goat anti-mouse IgG (H+L)	1:10000	WB	Invitrogen, #A21057
Alexa Fluor 680 goat anti-rabbit IgG (H+L)	1:10000	WB	Invitrogen, #A21076
IRDye 800CW donkey anti-mouse IgG	1:5000	WB	LiCor, #926-32212
IRDye 800CW donkey	1:5000	WB	LiCor, #926-32213

anti-rabbit IgG			
Alexa Fluor 488-conjugated goat anti rabbit IgG	1:250	IF	Invitrogen, #A11070
Alexa Fluor 594-conjugated goat anti rabbit IgG	1:250	IF	Invitrogen, #A11007

6.2 Methods

6.2.1 Cell lines and tissue culture

Cell lines were obtained from ATCC (American Type Culture Collection) unless otherwise indicated. A549, FLO-1 (Dr. Ricky Sharma, Oxford, UK), H1299, H1975, HCT116 (Prof. William Wilson, Auckland, NZ), HKO1 (Prof. William Wilson, Auckland, NZ), HKO1/POR (Prof. William Wilson, Auckland, NZ), OE21 (Dr. Ricky Sharma, Oxford, UK), RKO, U87-MG (Prof. Adrian Harris, Oxford, UK) and WI38 (Dr. Grigory Dianov, Oxford, UK) cells were used in this study.

HKO1 and HKO1/POR are derivatives of HCT116. In HKO1 mutations were introduced into the 8th exon of both CYP450 alleles using custom-designed zinc finger nucleases. One allele carries a 15 bp deletion and the other a 26 base pair deletion. HKO1 has lower CYP450 enzyme activity than the parental HCT116 line (Su et al. 2013). HKO1/POR is a derivative of HKO1 in which the human CYP450 gene has been re-expressed by transfecting with a F527.V5 plasmid which carries a puromycin resistance marker (Guise et al. 2012). It is

maintained in 3 µM puromycin and expresses CYP450 enzyme activity approximately 10-fold higher than HCT116.

Unless otherwise stated, cells were cultured in DMEM supplemented with 10% FBS, penicillin (100 units/ml) and streptomycin (100 µg/ml), in a standard humidified incubator at 37 °C and 5% CO_2. Culture medium for HKO1/POR additionally contained 3 µM puromycin. OE21 were cultured in RPMI medium supplemented with 10% FBS, penicillin (100 units/ml) and streptomycin (100 µg/ml). WI38 were cultured in DMEM containing 15% FBS. Cells were passaged three times a week. Routine tissue culture involved the preparation of a cell suspension by removal of the medium, washing with PBS and trypsinising with trypsin-EDTA. Trypsin was deactivated by addition of fresh culture medium. The cell density was determined by addition of 10 µl of cell suspension to a Neuenbauer haemocytometer and cell counting. Cells were seeded at desired densities in fresh medium prior to all experiments.

Cell lines were routinely tested for mycoplasma using a PlasmoTest^{TM} kit (InvivoGen). Cells were grown in antibiotic free medium and harvested when 90-100% confluent. Cells were heated for 15 min at 100 °C, 50 µl of the above suspension was added to 200 µl of HEK-Blue^{TM} cells (1-3.5 × 10^5 cells/ml) in HEK-Blue^{TM} detection medium (InvivoGen). The cells were plated in duplicate in a 96-well plate, together with positive and negative controls provided by the manufacturer and incubated for 24 h under normal tissue culture conditions. Appearance of a blue colour indicated the presence of lipoprotein expressed by all types of bacteria and mycoplasma. A pink colour indicated a negative result and absence of mycoplasma.

6.2.2 Cryopreservation of cell lines

Exponentially growing cells (approximately 70% confluency) were trypsinised, resuspended in 5 ml of medium and centrifuged at 400 × g for 5 min at ambient temperature. The supernatant was removed, cells resuspended in 1 ml of medium containing 10% FBS and 10% DMSO and placed in a 1.5 ml cryovial (Thermo Scientific Nunc, 363401). The vial was placed in a Mr. Frosty^{TM} freezing container (Nalgene, #CRY-OFF-700C) containing 2-propanol and stored at -80 °C for 24 h before being stored in liquid nitrogen.

Cells were recovered from liquid nitrogen by thawing quickly at 37 °C, transferred into 5 ml pre warmed medium, centrifuged at 400 × g for 5 min at ambient temperature and the supernatant removed. The pellet was resuspended in fresh medium and seeded into a 25 cm^2 culture flask.

6.2.3 Drug treatments

Solid drugs were stored in darkness at -20 °C. All drugs were dissolved in DMSO to 10 mM stock solutions and stored at -20 °C unless otherwise stated. Gemcitabine was dissolved in sterile water to 100 µM stock solutions. HU was dissolved in sterile water to 1 mM stock solutions. Pimonidazole was dissolved to a 1 mg/ml stock in saline which was stored at 4 °C. Drugs were used at concentrations indicated for every experiment while the final concentration of DMSO in the culture medium was not to exceed 1%.

6.2.4 Hypoxia treatment

Hypoxia treatment was carried out in a Bactron II anaerobic chamber (Shell Labs) (for experiments at >0.1% O_2), an *in vivo* 400 Ruskin hypoxic chamber (for experiments at 0.5-5% O_2) or a standard tissue culture incubator set at 3% O_2. The Bactron II anaerobic chamber is supplied with a gas mixture of 5% CO_2, 5% H_2 and 90% N_2. A complete absence of oxygen cannot be guaranteed due to passing in and out of material and potential small leakages. The O_2 concentration for experiments performed in this chamber will be stated as >0.1% O_2. The *in vivo* 400 Ruskinn chamber is supplied with compressed air, CO_2 and N_2. The chamber features a gas mixer and oxygen concentrations were adjustable while the CO_2 concentration was kept constant at 5% in all experiments.

6.2.5 γ-Irradiation

Cells were irradiated using a Gamma Service® GSR D1 irradiator containing a ^{137}Cs source at a constant distance from the source (shelf 1) and a dose rate of 1.938 Gy/min, as stated by the manufacturer. Exposure times were calculated according to the required dose.

6.2.6 Analytical HPLC

HPLC (Waters 2695 system) comprised an RPB column (100 × 3.2 mm, 35 °C). Separation was achieved at a flow rate of 0.5 ml/min with a gradient of acetonitrile in 10 mM aqueous formic acid over 6 min (details in Table 6.5).

Detection used a photodiode array (PDA) spectrophotometer (Waters 2996) and a mass spectrometer (MS) (Waters Micromass ZQ mass spectrometer) or a fluorescence spectrophotometer (FS) (Waters 474) with λ_{ex} 320 nm, λ_{em} 380 nm. 10-20 µl injections were made. Samples were injected in DMSO, acetonitrile, water or a mixture thereof.

Table 6.5. HPLC conditions

Compound	Gradient % acetonitrile	Detection
2	60-95	PDA/MS or FS
16	5-70	PDA/MS
17	10-80	PDA/MS
18	5-70	PDA/MS
52	5-95	PDA/MS

6.3 Drug metabolism

6.3.1 Zinc reduction

The substrate (1 mg) was dissolved in DMF (2 ml), aqueous NH_4Cl (20 µl, 10% *w/v*) and zinc powder (10 eq) were added and the resulting mixture stirred at ambient temperature. Samples (200 µl) were taken at designated times (t_0 refers to before the addition of zinc) and analysed by HPLC.

To determine stability of the reduced species to aqueous conditions, a time point from the above reaction was chosen that showed sufficient amounts of that species. This sample was diluted 1:19 with 100 mM PPB (pH 7.4) and

incubated at 37 °C. At designated times samples were taken and centrifuged for 5 min at 16200 × g. The supernatant was collected and any precipitate formed dissolved in acetonitrile. Both fractions were analysed by HPLC.

6.3.2 Sodium dithionite reduction

From a 50 mM substrate stock in DMSO, a 50 µM substrate solution in PPB (100 mM, pH 7.4, 3 ml) was prepared and deoxygenated by bubbling nitrogen for 5 min. A 25 mM sodium dithionite ($Na_2S_2O_4$) solution in PPB (100 mM, pH 7.4) was deoxygenated by bubbling nitrogen for 5 min. For full reduction of one equivalent of nitro-compound, three equivalents of $Na_2S_2O_4$ are required. The $Na_2S_2O_4$ solution was added in six portions of 0.5 eq and a sample (100 µl) taken 5 min after every addition for HPLC analysis. Samples were injected into the HPLC without further preparation.

6.3.3 CYP450 reductase assay

Unless otherwise indicated the assay was carried out using the reagents and volumes outlined in Table 6.6. Bactosomal human NADPH-CYP450 reductase (Cypex, Cyp004) was used in combination with an enzymatic NADPH-regenerating system (solutions A and B, Becton Dickinson Biosciences). For different batches of CYP450 enzyme, the amount used in the assay was adjusted according to the activity of the enzyme. All reagents were mixed in a glass vial and the reaction initiated by final addition of CYP450. For experiments in hypoxia, vials were either deoxygenated by bubbling nitrogen prior to CYP450

addition or by allowing the solution to equilibrate in the hypoxia chamber for 10 min.

Table 6.6. Reaction components and volumes for CYP450 reductase assay

Reagent	Volume (µl) for 500 µl incubation	Final conc./activity
0.5 M PPB pH 7.4	100	100 mM
Solution A	25	1.3 mM $NADP^-$ 3.3 mM G6P 3.3 mM $MgCl_2$
Solution B	5	0.4 units/ml G6PDH
H_2O	365	-
10 mM substrate	0.5	10 µM
CYP450	Batch dependent	278 nmol/min

At different times, 50 µl samples were taken and quenched with 50 µl acetonitrile. The samples could be stored at -80 °C until analysis. Prior to HPLC analysis, the samples were centrifuged for 10 min at 16200 × g and 4 °C and the supernatant analysed.

6.3.5 Metabolite analysis from cell lysates

Cells were seeded in 6 cm glass dishes. The next day the medium was replaced for drug containing medium and the cells exposed to hypoxia as described for each experiment. Cells were washed with PBS, removed from the

dishes by scraping into 1 ml of PBS and centrifuged briefly to form a pellet. The supernatant was removed, the pellet resuspended in 50 µl 3% v/v TCA and the sample kept at -20 °C until analysis. For HPLC analysis, the sample was centrifuged for 10 min at 16200 × g and the supernatant analysed (20 µl injection volume).

6.4 Protein analysis

6.4.1 Protein sample preparation

Cells were used at approximately 60-70% confluency and treated as indicated for each experiment. Cells were washed with PBS, scraped into 1 ml of PBS and centrifuged briefly to form a pellet. The supernatant was removed and the cells lysed with 40-100 µl UTB (9 M urea, 75 mM Tris-HCl, pH 7.5, 0.1 M ß-mercaptoethanol). The samples were sonicated on ice for 2 × 15 seconds and centrifuged for 15 min at 16200 × g, the supernatant was used as protein sample. The protein concentration of the sample was measured in duplicates at 280 nm using a NanoDrop meter (UTB served as blank). The average of both measurements was taken as the protein concentration of each sample.

6.4.2 SDS-PAGE (SDS-Polyacrylamide Gel Electophoresis)

Gels were either obtained as precast gels (Mini-PROTEAN® TGX^{TM}, 10% or 4-20%, BioRad) or prepared following the recipe in Tables 6.7 and 6.8 (Sambrook and Russell 2001).

Table 6.7. Recipe for stacking gel

Reagent	Volume
H_2O	6.1 ml
0.5 M Tris-HCl pH 6.8	2.5 ml
Acrylamide	1.3 ml
10% SDS	100 µl
10% APS	100 µl
TEMED	20 µl

Table 6.8. Recipe for separating gel (7.5-15%)

Reagent	Volume in accordance with gel %		
	7.5	10	15
H_2O	7.40 ml	6.07 ml	3.75 ml
1.5 M Tris-HCl pH 8.8	3.75 ml	3.75 ml	3.75 ml
Acrylamide	3.65 ml	4.95 ml	7.25 ml
10% SDS	150 µl	150 µl	150 µl
10% APS	75 µl	75 µl	75 µl
TEMED	18 µl	18 µl	18 µl

Typically 50 µg of protein was used per sample, 80-100 µg were used when assessing phosphorylation of Chk1 on residues S317 and S345. The required amount of sample was diluted with 5 µl of sample buffer (3.3% SDS, 6 M urea, 17 mM Tris-HCl, pH 7.5, 0.07 M ß-mercaptoethanol, 0.01% bromophenol blue), heated at 100 °C for 5 min, centrifuged briefly to remove air bubbles and loaded onto the gel. Protein ladder (4 µl, Precision plus protein standards, BioRad) allowed assessment of the molecular weight of the bands. Precast gels were electrophoresed at 150 V for 40-45 min and self-cast gels at 100 V for 60-90 min in Tris-glycine running buffer (25 mM Tris base, 192 mM glycine, 0.1% *w/v* SDS).

6.4.3 Western Blotting

Protein bands in the electrophoresed gels were electro-transferred onto nitrocellulose membranes using either a Trans-Blot® Turbo™ transfer system (BioRad, 7 min Turbo protocol) and Trans-Blot® Turbo™ PVDF Transfer Packs (BioRad, #170-4157) or a transfer onto nitrocellulose membranes (BioRad) at 100 V for 1 h in transfer buffer (25 mM Tris base, 150 mM glycine, 20% v/v methanol).

Proteins were visualised with Ponceau S solution and membranes cut to probe with several antibodies if indicated. The membranes were washed twice in TBS and blocked while shaking for at least 1 h at ambient temperature in a 1:1 mixture of LiCor and TBS (50 mM Tris-HCl, pH 7.6, 150 mM NaCl). Membranes were probed with primary antibody (see list and dilutions in Table 6.3) diluted in a 1:1 mixture of LiCor and TBS-Tween (0.1% v/v Tween) overnight at 4 °C while shaking. Membranes were then washed three times with TBS-Tween for 10 min

and probed with secondary antibody (see list and dilutions in Table 6.4) diluted in a 1:1 mixture of LiCor and TBS-Tween for 1-2 h at ambient temperature while shaking. The membranes were washed twice with TBS-Tween for 10 min and once with TBS. Protein bands were visualised using the Odyssey® infrared imaging system.

6.4.4. Immunofluorescence microscopy

Immunofluorescence was carried out on glass slides or 4-well chamber slides. Cells were seeded such as to reach approximately 80% confluence by the start of the treatment. Treated cells were washed with PBS and fixed with 4% fixation buffer (4% *w/v* paraformaldehyde, 2% *w/v* sucrose in PBS) for 15 min at ambient temperature. Cells were washed twice with PBS and could then be stored for a week at 4 °C in PBS.

Cells were permeabilised by incubating with PBS-Triton-X-100 (PBS-T) (1% *v/v* Triton-X-100) for 10 min at ambient temperature and blocked for 1-2 h with 2% *w/v* BSA in PBS-T (0.1% *v/v* Triton-X-100). Cells were washed once with ice-cold PBS-T (0.25% *v/v* Triton-X-100) and incubated for 1-2 h with primary antibody (see list and dilutions in Table 6.3) diluted in 2% w/v BSA in PBS-T (0.1% *v/v* Triton-X-100) at 37 °C in a humidified chamber. The cells were washed twice with ice-cold PBS-T (0.25% *v*/v Triton-X-100), once with PBS and incubated for 1 h with secondary antibody (see list and dilutions in Table 6.4) diluted in 2% *w/v* BSA in PBS-T (0.1% *v/v* Triton-X-100) at 37 °C in a humidified chamber in darkness. After two washes with ice-cold PBS-T (0.25% *v/v* Triton-X-100) and a final wash with PBS the slides were mounted using ProLong® Gold mounting medium with DAPI. Slides were left overnight at ambient temperature in the dark

before sealing with nail varnish. The slides were imaged using a Bio-radiance confocal, Nikon 90i or LSM780 (Carl Zeiss Microscopy LtD) confocal microscope.

6.5 Clonogenic survival

According to a cell line's plating efficiency, cells were plated in 6-well plates such that at least 100 colonies were obtained in the control wells. Cells were allowed to settle for 2-3 h and then treated as indicated in each experiment. Colonies (>50 cells) were allowed to form for 8-12 days (cell line dependent) and stained with Crystal Violet (5 mg/l Crystal Violet, 50% *v/v* methanol, 20% *v/v* ethanol, 30% *v/v* H_2O) or Methylene Blue (1 mg/l Methylene Blue, 70% *v/v* methanol, 30% *v/v* PBS) staining solution. Colonies (>50 cells) were counted and the surviving fraction determined.

6.6 Spheroids

Spheroids were grown from U87-MG cells in agarose-coated 24-well plates. Wells were coated with 250 µl of hot 1 % *w/v* agarose in PBS. Plates were left open to cool for 5-10 min and 400 µl DMEM medium added to each well. The plates were incubated at 37 °C for 2 h, the medium removed and replaced with 350 µl of cell suspension, seeding 10000 cells per well. Spheroids were left to form undisturbed for 4 days.

On day 4 after seeding (day 0 of treatment) the average radius of the spheroids was measured, using a Nikon TE2000 microscope with incubator set at 37 °C. The medium was replaced with drug containing medium and spheroids left to grow at a defined oxygen concentration, as described for each experiment.

This procedure (measurement, medium replacement, hypoxia treatment) was repeated on days 2 and 4. On day 7 spheroids were measured, harvested and processed following either of the following procedures:

Protein analysis as described in 6.4.1 - 6.4.3,

Metabolite analysis as described in 6.3.5,

Immunofluorescence microscopy as described as follows.

For immunofluorescence microscopy, spheroids were washed with PBS and fixed with fixation buffer (4% *w/v* paraformaldehyde, 2% *w/v* sucrose in PBS) at 4 °C overnight. They were washed twice with PBS and left in 30% *w/v* sucrose in PBS for at least 48 h but up to two weeks.

Spheroids were embedded in OCT compound and could be left at -80 °C until cutting into 5 µm thick sections using a Bright cryostat. Sections were taken up onto microscopy slides and left to dry for 1-2 h. A hydrophobic barrier was drawn around each sample set of sections and sections rehydrated twice for 5 min using TBS. Sections were incubated for 20 min with 50 mM aqueous NH_4Cl, washed twice for 5 min with TBS-Triton-X-100 (0.25% *v/v*) and blocked for 1-2 h in 10% *v/v* goat serum, 1% *w/v* BSA in TBS. The sections were washed briefly with TBS and probed overnight at 4 °C with primary antibody (see list and dilutions in Table 6.3) diluted in 1% *w/v* BSA in TBS. They were washed twice for 5 min with TBS, incubated with secondary antibody (see list and dilutions in Table 6.4) diluted in 1% *w/v* BSA in TBS for 1 h and washed three times for 5 min with TBS. After a brief wash in water, slides were mounted with ProLong® Gold mounting medium with DAPI, left in darkness overnight at ambient temperature and then sealed with nail varnish.

Samples were imaged using a LSM780 (Carl Zeiss Microscopy LtD) confocal microscope.

6.7 Analysis

Statistical analysis was carried out using Microsoft Excel. Standard errors (SE) were calculated as SE = standard deviation (SD)/√number of samples (n). Each data point indicates means ± SE from at least three independent experiments. A statistical significant difference of $p < 0.05$ between two sets of data was calculated using student t-test.

HPLC data was analysed using OriginPro 9.1 for baseline correction, peak integration and graphing.

Immunofluorescence data was analysed using ImageJ or Zeiss Zen2011 black software. Per sample at least 150 cells where counted from 8-10 different and randomly chosen fields of view.

6.8 General chemical experimental procedures

^{1}H NMR spectra were recorded on Bruker AV400 (400 MHz), Bruker DRX500 (500 MHz) or Bruker AVII500 (500 MHz) spectromers using the deuterated solvent specified as a reference for internal deuterium lock. Chemical shift data for each signal are given as δ_H in units of parts per million (ppm) relative to tetramethylsilane (TMS) where δ_H (TMS) = 0.00 ppm. The multiplicity of each signal is indicated by: s (singlet); d (doublet); t (triplet); q (quartet); dd (doublet of doublets); combinations thereof or m (multiplet). A broadened signal is denoted by the prefix br (broad). The number of protons (n) for a given resonance

signal is indicated by nH. Coupling constants (*J*) are averaged in each spectrum and reported to the nearest 0.1 Hz. The coupling constants are determined by analysis using Bruker TopSpin software.

^{13}C NMR spectra were recorded on Bruker AV400 (100 MHz), Bruker DRX500 (126 MHz) or Bruker AVII500 (126 MHz) spectrometers with broadband proton decoupling and internal deuterium lock. Chemical shift data for each signal are given as δ_C in units of parts per million (ppm) relative to tetramethylsilane (TMS) where δ_C (TMS) = 0.00 ppm.

Numbering of carbon atoms is to aid reading of the NMR data and does not conform to IUPAC nomenclature. In compounds with more than one ring system, additional systems are numbered with primes (‘) and double primes (‘’).

NMR spectra were assigned using 2D NMR experiments (COSY, HSQC, HMBC) and analysed using Bruker TopSpin software.

High-resolution mass spectra were acquired in a Bruker MicroTOF spectrometer from solutions of methanol, water or acetonitrile (ESI), or a Waters GCT TOF spectrometer with a temperature-programmed solids probe inlet (FI), operating in positive or negative mode.

Low-resolution mass spectra were acquired on a Waters LCT Premier spectrometer or an Agilent 6120 Quadrupole LC/MS spectrometer from solutions of methanol, water or acetonitrile (ESI). *m/z* values are reported in Daltons and followed by their percentage abundance in parentheses.

Melting points on recrystallised samples were determined using a Kofler hot stage microscope and are uncorrected. The solvent of crystallisation is shown in parentheses.

Infrared spectra were obtained from neat samples as solids or from solutions as thin films on an NaCl plate using a Diamond ATR module. The spectra were recorded on a Bruker Tensor 27 spectrometer. Absorption maxima (ν_{max}) are reported in wavenumbers (cm^{-1}).

Microanalyses were obtained at the Elemental Analysis Service, London Metropolitan University, London. Elemental analysis was carried out in duplicate; average values are reported.

Analytical thin layer chromatography (TLC) was carried out on Merck silica gel 60 F_{254} aluminium-supported thin layer chromatography sheets. Visualisation was by absorption of UV light (λ_{max} 254 nm), or thermal development after dipping in one of: **a** ethanolic solutions of: phosphomolybdic acid (PMA) or Ninhydrin; **b** aqueous solution of potassium permanganate.

Flash column chromatography was carried out manually on VWR Prolabo silica gel 60 (240-400 mesh) eluting with solvents as supplied, under a positive pressure of compressed air.

Analytical HPLC to monitor reactions and compound purity, was carried out on a PerkinElmer Flexar system with a Binary LC Pump and UV/VIS LC Detector and a Dionex Acclaim® 120 column (5 µm, 150 × 4.6 mm). A 10-minute gradient as described in Table 6.9 was employed, where solvent A refers to 95% H_2O / 5 % acetonitrile + 0.1% TFA and solvent B refers to 5% H_2O / 95 % acetonitrile + 0.1% TFA. The flow rate was 1 ml/min and detection at 254 nm or 360 nm unless otherwise stated. Samples of were injected in DMSO (20 µl injections).

Table 6.9. PerkinElmar Flexar, Dionex Acclaim® method

Step length (min)	Elapsed time (min)	%A	%B
2	2	60	40
10	12	0	100
2	14	0	100
1	15	60	40
5	20	60	40

For determination of compound purity, HPLC was carried out on a Waters 2695 system using a Hichrom RPB column (100 × 3.2 mm, 35 °C) or a Gemini NX column (150 × 3.0 mm, 35 °C). Separation was achieved at a flow rate of 0.5 ml/min with a gradient of acetonitrile in 10 mM aqueous formic acid over 6 min when using the RPB column and an isocratic method (60% acetonitrile / 40% H_2O + 0.2% NH_3, pH 11) when using the Gemini NX column. Details of the gradient systems are included in the synthetic procedures for relevant compounds. Detection used a photodiode array spectrophotometer (Waters 2996) and a mass spectrometer (Waters Micromass ZQ mass spectrometer). 10 µl injections were made. Samples were injected in DMSO, acetonitrile, water or a mixture thereof.

Preparative HPLC for purification of compound 52 (Dr. Michael Stratford, Department of Oncology, University of Oxford) was carried out on a Waters 2695 system using a Gemini NX column (150 × 3.0 mm, 35 °C). Separation was achieved using an isocratic method (60% acetonitrile / 40% H_2O

+ 0.2% NH_3, pH 11). Detection used a photodiode array spectrophotometer (Waters 2996) and a mass spectrometer (Waters Micromass ZQ mass spectrometer). 20 µl injections were made, loading 200-300 µg of material per run.

Anhydrous solvents were obtained under the following conditions: anhydrous DMF and anhydrous MeOH were purchased from Sigma-Aldrich UK in SureSeal™ bottles and used without further purification; CH_2Cl_2 and THF were dried by passing through a column of activated basic alumina according to Grubbs' procedure (Pangborn et al. 1996) and stored over activated 3 Å molecular sieves under an argon or nitrogen atmosphere.

Chemicals were purchased from ABCR Chemicals, Acros UK, Sigma-Aldrich UK, Alfa Aesar UK or Fisher UK. All non-aqueous reactions were performed in a flame-dried flask or microwave vial under an atmosphere of argon or nitrogen. Where required, K_2CO_3 and Cs_2CO_3 were dried in an oven prior to use.

Reactions with microwave irradiation were carried out in a Biotage Initiator microwave synthesiser.

In vacuo refers to removal of volatile components under reduced pressure using a Buchi™ rotary evaporator.

Brine refers to a saturated aqueous solution of sodium chloride.

Petroleum ether refers to the fraction boiling between 30-40 °C unless otherwise stated.

Lyophilisation refers to the removal of water or a water/acetonitrile mixture from solutions by freezing and sublimation under high vacuum using a Christ Alpha 2-4-LD lyophiliser.

6.9 Synthetic Procedures

6.9.1 2-Nitroimidazole analogues

Ethyl 2-amino-1-methyl-1H-imidazole-5-carboxylate **32**

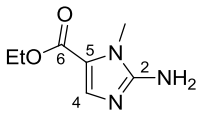

Ethylformate (6.0 ml, 74.5 mmol) was added to a suspension of sarcosine methylester hydrochloride (2.08 g, 14.9 mmol) in anhydrous THF (20 ml). The mixture was cooled with an ice/water bath, NaH (1.79 g, 44.7 mmol, 60 % in mineral oil) added in portions and the reaction left to slowly warm up to the ambient temperature. It was left for an additional 4 h, concentrated *in vacuo* and triturated with petroleum ether (2 × 20 ml). The resulting residue was dissolved in EtOH (60 ml), concentrated HCl (12 ml) slowly added and the mixture heated to 85 °C for 1 h. The cooled mixture was filtered, the filtrate concentrated *in vacuo* and the residual oil dissolved in 10% *v/v* aq. AcOH (50 ml). Following addition of sodium acetate trihydrate (4.06 g, 29.8 mmol) and cyanamide (2.62 g, 29.8 mmol) the reaction was left at 100 °C for 18 h, concentrated to approximately half the original volume and basified to pH 8-9 using solid K_2CO_3. The formed precipitate was isolated by filtration and a second batch obtained by further concentrating the mother liquor. The combined batches were dried under reduced pressure to yield **32** as a pale yellow solid (948 mg, 38 % over three steps): $\mathbf{R_f}$**;** 0.4 (CH_2Cl_2, 10% MeOH); ***mp*** 130–133 °C (H_2O); $\mathbf{\nu_{max}}$ (neat) cm^{-1}: 3389, 3338, 3125, 1648, 1479, 1350; **^{1}H NMR** (500 MHz, $CDCl_3$): δ_H 7.45 (s, 1H, C4-*H*), 4.27 (q, *J* = 7.1, 2H, C*H*$_2$), 3.69 (s, 3H, NC*H*$_3$), 1.34 (t, *J* = 7.1, 3H, CH_2CH_3); **^{13}C NMR** (126 MHz, $CDCl_3$): δ_C 160.6 (*C6*), 151.8 (*C*2), 135.2 (*C4*-H),

119.0 (*C*5), 59.8 (*C*H_2), 30.5 (N*C*H_3), 14.4 (CH_2*C*H_3); **HRMS** *m/z* (ES+): [Found; $(M+Na)^+$ 192.0743. $C_7H_{11}N_3NaO_2$ requires $(M+Na)^+$, 192.0743], **LRMS** *m/z* (ESI+): 192.06 ($[M+Na]^+$, 100%), 170.08 ($[M+H]^+$, 70%); **Elem. anal.** calcd. for $C_7H_{11}N_3O_2$: C, 49.7; H, 6.6; N, 24.8. Found C, 49.7; H, 6.5; N 24.7.

Ethyl 1-methyl-2-nitro-1H-imidazole-5-carboxylate **34**

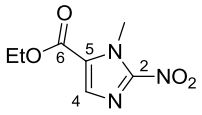

A solution of amine **32** (1.05 g, 6.2 mmol) in glacial AcOH (10 ml) was added drop wise to an ice-cooled solution of $NaNO_2$ (4.29 g, 62.1 mmol) in water (5 ml) and the reaction left at the ambient temperature for 2 h. The mixture was extracted with CH_2Cl_2 (3×15 ml), the combined organic layers washed with water (40 ml), saturated aqueous Na_2CO_3 solution (40 ml) and brine (40 ml). The solution was dried over anhydrous $MgSO_4$, filtered, concentrated *in vacuo* and purified by column chromatography eluting with CH_2Cl_2 to give **34** as pale yellow crystals (908 mg, 73 %). $\mathbf{R_f}$; 0.9 (CH_2Cl_2, 10% MeOH); **mp** 56-57 °C (CH_2Cl_2/petroleum ether) (lit. 65-66 °C) (Cavalleri, Ballotta, and Lancini 1972); $\boldsymbol{\nu_{max}}$ (neat) cm^{-1}: 3016, 1739, 1437, 1367; **^{1}H NMR** (400 MHz, $CDCl_3$): δ_H 7.75 (s, 1H, C4-*H*), 4.41 (q, *J* = 7.2, 2H, C*H*$_2$), 4.35 (s, 3H, NC*H*$_3$), 1.41 (t, *J* = 7.2, 3H, CH_2C*H*$_3$); **^{13}C NMR** (126 MHz, $CDCl_3$): δ_C 159.1 (1C, *C*6), 147.4 (1C, *C*2), 134.7 (1C, *C4*-H), 126.3 (1C, *C*5), 61.8 (1C, *C*H_2), 35.4 (1C, N*C*H_3), 14.2 (1C, CH_2*C*H_3); **HRMS** *m/z* (ES+): [Found; $(M+Na)^+$ 222.0485. $C_7H_9N_3NaO_4$ requires $(M+Na)^+$, 222.0485], **LRMS** *m/z* (ESI+) 222.03 ($[M+Na]^+$, 100%), 200.06 ($[M+H]^+$, 48%); **Elem. anal.** calcd. for $C_7H_9N_3O_4$: C, 42.2; H, 4.6; N, 21.1. Found C, 42.3; H, 4.5; N 21.1.

1-Methyl-2-nitro-1H-imidazole-5-carboxylic acid **36**

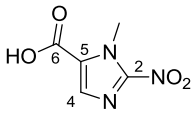

A suspension of ethylester **34** (43 mg, 0.22 mmol) in 1 M aqueous NaOH (1 ml) was stirred for 18 h at ambient temperature. The solution was acidified to pH 1 using 1 M aqueous HCl, extracted with EtOAc (3 × 3 ml), the combined organic layers dried over anhydrous $MgSO_4$, filtered and concentrated *in vacuo*. The residual solid was recrystalised from $CHCl_3$ to yield **36** as pale yellow crystals (16 mg, 43 %): ***mp*** 155-157 °C ($CHCl_3$) (lit. 161–163 °C) (Cavalleri, Ballotta, and Lancini 1972); $\mathbf{\nu_{max}}$ (neat) cm^{-1}: 1712, 1497, 1362; **^{1}H NMR** (400 MHz, MeOD-d_4): δ_H 7.73 (s, 1H, C4-*H*), 4.33 (s, 3H, NCH_3); **^{13}C NMR** (126 MHz, MeOD-d_4): δ_C 161.6 (*C*6), 149.0 (*C*2), 134.8 (*C4*-H), 128.5 (*C5*), 35.8 (N*C*H_3); **HRMS** *m/z* (ES+): [Found; $(M-H)^-$ 170.0207. $C_5H_4N_3O_4$ requires $(M-H)^-$ 170.0207]; **LRMS** *m/z* (ESI-) 170.02 ($[M-H]^-$, 68%); **Elem. anal.** calcd. for $C_5H_5N_3O_4$: C, 35.1; H, 3.0; N, 24.6. Found C, 35.2; H, 2.8; N 24.4.

5-(Hydroxymethyl)-1-methyl-2-nitro-1H-imidazole **35**

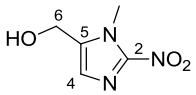

A solution of ethylester **34** (230 mg, 1.16 mmol) in anhydrous THF (6 ml) and MeOH (0.5 ml) was cooled with an ice/water bath and $NaBH_4$ (131 mg, 3.47 mmol) added in portions. The reaction was left at 0 °C for an additional 45 min and then at ambient temperature for 1 h. It was cooled with ice, quenched by addition of ice followed by 1 M aqueous HCl until pH 7. The mixture was saturated with NaCl to aid extraction, extracted with EtOAc (5 × 15 ml), washed

with saturated aqueous $NaHCO_3$ solution, dried over anhydrous $MgSO_4$, filtered and concentrated *in vacuo*. The crude product was purified by column chromatography, eluting with petroleum ether/EtOAc (1:1 to 100% EtOAc) to give **35** as pale yellow crystals (109 mg, 66%): **R_f;** 0.5 (CH_2Cl_2, 10% MeOH); **mp** 141-143 °C (EtOAc) (lit. 142-144 °C) (Cavalleri, Ballotta, and Lancini 1972); **ν_{max}** (neat) cm^{-1}: 3226, 3017, 1492, 1394; **^{1}H NMR** (400 MHz, DMSO-d_6): δ_H 7.12 (s, 1H, C4-*H*), 5.50 (t, *J* = 5.4, 1H, O*H*), 4.54 (d, *J* = 5.4, 2H, C6-*H_2*), 3.92 (s, 3H, NC*H_3*); **^{13}C NMR** (126 MHz, DMSO-d_6): δ_C 146.7 (*C*2), 138.6 (*C5*), 126.5 (*C4*-H), 53.0 (*C6*-H_2), 34.1 (N*C*H_3); **HRMS** *m/z* (ES+): [Found; $(M-H)^-$ 156.0412. $C_5H_6N_3O_3$ requires $(M-H)^-$ 156.0414]; **LRMS** *m/z* (ESI-) 156.04 ($[M-H]^-$, 100%), 192.2 ($[M+Cl]^-$, 34%); **Elem. anal.** calcd. for $C_5H_7N_3O_3$: C, 38.2; H, 4.5; N, 26.7. Found C, 38.2; H, 4.5; N 26.6.

5-(Chloromethyl)-1-methyl-2-nitro-1H-imidazole **38**

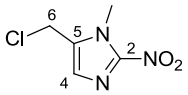

A solution of $SOCl_2$ (0.28 ml, 3.90 mmol) in dry CH_2Cl_2 (2 ml) was added drop wise to an ice-cooled solution of alcohol **35** (200 mg, 1.27 mmol) and distilled pyridine (Armarego and Chai 2003) (0.30 ml, 3.63 mmol) in dry CH_2Cl_2 (8 ml). The reaction was left stirring at 0 °C for 1 h followed by another hour at ambient temperature. It was quenched by addition of ice, followed by saturated aqueous $NaHCO_3$ solution (5 ml). It was extracted with CH_2Cl_2 (2 × 15 ml), the combined organic layers washed with brine (30 ml), dried over anhydrous $MgSO_4$, filtered and concentrated *in vacuo*. The crude product was purified by column chromatography, eluting with petroleum ether/EtOAc (1:1 to 100% EtOAc) to give **38** as pale yellow crystals (147 mg, 66%): **R_f;** 0.4 (1:1 EtOAc :

petroleum ether); **mp** 87-90 °C (EtOAc) (lit. 94-96 °C) (Parveen et al. 1999); $\mathbf{\nu_{max}}$ (neat) cm^{-1}: 3029, 1483, 1360; **^{1}H NMR** (500 MHz, $CDCl_3$): δ_H 7.17 (s, 1H, C4-*H*), 4.63 (s, 2H, C6-H_2), 4.06 (s, 3H, NCH_3); **^{13}C NMR** (126 MHz, $CDCl_3$): δ_C 146.3 (*C*2), 132.9 (C_5), 128.5 (*C4*-H), 34.2 (N*C*H_3), 33.9 (*C*H_2); **HRMS** *m/z* (ES+): [Found; $(M+Na)^+$ 198.0041. $C_5H_6ClN_3NaO_2$ requires $(M+Na)^+$ 198.0041]; **LRMS** *m/z* (ESI+) 198.1 ($[M+Na]^+$, 100%); **Elem. anal.** calcd. for $C_5H_6ClN_3O_2$: C, 34.2; H, 3.4; N, 23.9. Found C, 34.3; H, 3.5; N 23.8.

5-(Bromomethyl)-1-methyl-2-nitro-1H-imidazole **37**

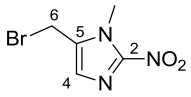

A solution of alcohol **35** (37 mg, 0,24 mmol) in dry CH_2Cl_2 (3 ml) was cooled to -10 °C with an ice/NaCl bath and PBr_3 (0.03 ml, 0.31 mmol) added drop wise. The reaction was left at -10 °C for an additional 30 min and then stirred at ambient temperature for 1 h. Ice was added to quench the reaction, followed by saturated aqueous $NaHCO_3$ solution (4 ml) and extracted with CH_2Cl_2 (2 × 5 ml). The combined organic layers were dried over anhydrous $MgSO_4$, filtered and concentrated *in vacuo*. The crude product was purified by column chromatography, eluting with petroleum ether/EtOAc (2:1 to 100% EtOAc) to give **37** as pale yellow crystals (15 mg, 29%) and recovered starting material **NN** (6 mg, 16%): **R_f;** 0.6 (1:1 EtOAc : petroleum ether); **mp** 89-94 °C (EtOAc) (lit. 84-87 °C) (Parveen et al. 1999); $\mathbf{\nu_{max}}$ (neat) cm^{-1}: 3041, 1483, 1359; **^{1}H NMR** (400 MHz, $CDCl_3$): δ_H 7.22 (s, 1H, C4-*H*), 4.48 (s, 2H, C6-H_2), 4.06 (s, 3H, NCH_3); **^{13}C NMR** (126 MHz, $CDCl_3$): δ_C 146.9 (*C*2), 133.5 (*C5*), 129.0 (*C4*-H), 34.7 (N*C*H_3), 19.5 (*C6*-H_2); **HRMS** *m/z* (ES+): [Found; $(M+Na)^+$ 241.9538. $C_5H_6BrN_3NaO_2$ requires $(M+Na)^+$ 241.9536]; **LRMS** *m/z* (ESI+) 242.0 ($[M+Na]^+$,

100%), 222.0 ([M+H]$^+$, 30%). **HPLC** (Dionex Acclaim®, 254 nm): Retention time 3.65 min, 99% purity.

6.9.2 The pyrazolo-pyridine-based Chk1 inhibitor **16** *and analogues* **17-19**

3-(2-(1-(4-Nitrophenyl)ethylidene)hydrazinyl)propanenitrile **45b**

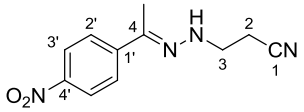

Hydrazine monohydrate (180 µl, 3.7 mmol) was added drop wise to an ice-cooled solution of acrylonitrile **20** (250 µl, 3.7 mmol) in THF (4 ml) and the resulting solution stirred at ambient temperature. After 2 h, the mixture was cooled with an ice bath and 4-nitroacetophenone (612 mg, 3.7 mmol) added slowly. The reaction was left to stir at ambient temperature for 6 h. All volatiles were removed *in vacuo* and the product purified by flash column chromatography (gradient: EtOAc : petroleum ether, 1:4 to 1:1), yielding **45b** as a bright orange solid (795 mg, 93%): $\mathbf{R_f}$; 0.2 (5:1 EtOAc : MeOH); **mp** 76-78 °C (EtOAc); $\mathbf{\nu_{max}}$ (neat) cm^{-1}: 3320, 2252, 1544, 1325; **^{1}H NMR** (400 MHz, $CDCl_3$): δ_H 8.19 (d, *J* = 9.0, 2H, C3'-*H*), 7.81 (d, *J* = 9.0, 2H, C2'-*H*), 5.60 (t, *J* = 4.6, 1H, N*H*), 3.66 (dt, *J* = 4.6, 6.3, 2H, C3-H_2), 2.75 (t, *J* = 6.3, 2H, C2-H_2), 2.16 (s, 3H, CH_3); **^{13}C NMR** (400 MHz, $CDCl_3$): δ_C 147.1 (*C*), 144.8 (*C*), 141.7 (*C*), 125.8 (*C3'*-H), 123.6 (*C2'*-H), 118.4 (*C*1), 46.3 (*C3*-H_2), 19.0 (*C2*-H_2), 11.9 (*C*H_3); **HRMS** *m/z* (ES+): [Found (M+Na)$^+$ 255.0854. $C_{11}H_{12}N_4NaO_2$ requires (M+Na)$^+$, 255.0852]; **LRMS** *m/z* (ESI-) 231.09 ([M-H]$^-$, 100%); **Elem. anal.** calcd. for $C_{11}H_{12}N_4O_2$: C, 56.9; H, 5.2; N, 24.2. Found C, 56.8; H, 5.3; N 24.0.

Ethyl 4-hydroxy-1-(4-methoxybenzyl)-1H-pyrazolo[3,4-b]pyridine-5-carboxylate **40**

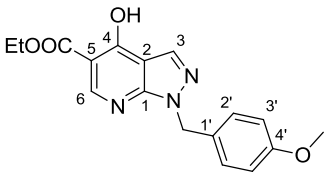

Hydrazine monohydrate (1.3 ml, 25.2 mmol) was added drop wise to an ice-cooled solution of acrylonitrile **20** (1.7 ml, 25.2 mmol) in THF (20 ml) and the resulting solution stirred at ambient temperature. After 2 h, the mixture was cooled with an ice bath and 4-anisaldehyde (3.1 ml, 25.2 mmol) added slowly. The reaction was left to stir at ambient temperature for 6 h. All volatiles were removed *in vacuo* and the resulting intermediate imine **39** was used for the subsequent step without further purification:

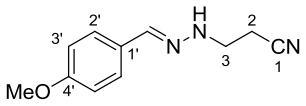

R_f; 0.6 (1:1 EtOAc : petroleum ether); **^{1}H NMR (400 MHz, $CDCl_3$):** δ_H 7.70 (s, 1H, C*H*N), 7.50 (d, *J* = 8.9, 2H, C2'-*H*), 6.89 (d, *J* = 8.9, 2H, C3'-*H*), 5.44 (br, 1H, N*H*), 3.83 (s, 3H, OCH_3), 3.52 (t, *J* = 6.4, 2H, C2-H_2), 2.71 (t, *J* = 6.4, 2H, C3-H_2).

Imine **39** was dissolved in ^{i}PrOH (125 ml), solid NaOH (0.76 g, 18.9 mmol) added and the mixture heated under reflux to 100 °C oil-bath temperature. After 6 h all volatiles were removed *in vacuo*, the residue redissolved in EtOAc, washed with water, brine and dried over anhydrous $MgSO_4$. Pyrazole **21** was concentrated and used in the next step without further purification:

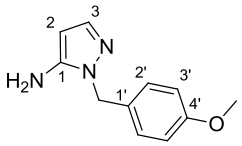

R_f; 0.3 (1:1 EtOAc : petroleum ether); **^{1}H NMR (400 MHz, $CDCl_3$):** δ_H 7.30 (d, *J* = 1.5, 1H, C3-*H*), 7.12 (d, *J* = 8.6, 2H, C2'-*H*), 6.86 (d, *J* = 8.6, 2H, C3'-*H*), 5.56 (d, *J* = 1.5, 1H, C2'-*H*), 5.15 (2, 2H, CH_2), 3.78 (s, 3H, OCH_3), 3.41 (br s, 2H, NH_2).

A mixture of pyrazole **21** and diethyl ethoxymethylenemalonate (5.09 ml, 25.2 mmol) were heated to 120 °C under reflux. After 3 h the reaction was left to cool to ambient temperature. Diphenylether (40 ml) was added and the reaction mixture heated to 240 °C for 24 h, the mixture was left to cool down and 50 ml petroleum ether added. The solution was left at -20 °C overnight for **40** to crystallise as brown crystals (2.55 g, 31% over 5 steps): **R_f;** 0.8 (3:2 EtOAc : petroleum ether); **mp** 139-140 °C (EtOAC); **ν_{max}** (neat) cm^{-1}: 3083, 1751; **^{1}H NMR** (500 MHz, $CDCl_3$): δ_H 12.25 (s, 1H, O*H*), 8.92 (s, 1H, C6-*H*), 8.16 (s, 1H, C3-*H*), 7.32 (d, *J* = 8.7, 2H, C2'-*H*), 6.84 (d, *J* = 8.7, 2H, C3'-*H*), 5.60 (s, 2H, NCH_2), 4.48 (q, *J* = 7.1, 2H, CH_2CH$_3$), 3.77 (s, 3H, OCH_3), 1.46 (t, *J* = 7.1, 3H, CH_2CH_3); **^{13}C NMR** (126 MHz, $CDCl_3$): δ_C 170.5 (*C*OOEt), 164.2 (*C5*), 159.3(*C4'*), 153.7 (*C1*), 151.6 (*C6*-H), 132.2 (*C3*-H), 129.5 (*C2'*-H), 128.7 (*C1'*), 114.0 (*C3'*-H), 106.2 (*C2*), 102.5 (*C4*), 61.7 (CH_2CH_3), 55.2 (OCH_3), 50.4 (NCH_2), 14.2 (CH_2CH_3); **HRMS** m/z (ES+): [Found; $(M+Na)^+$ 350.1109. $C_{17}H_{17}N_3NaO_4$ requires $(M+Na)^+$, 350.1111]; **LRMS** *m/z* (ESI-) 326.11 ($[M-H]^-$, 100%); **Elem. anal.** calcd. for $C_{17}H_{17}N_3O_4$: C, 62.4; H, 5.2; N, 12.8. Found C, 62.5; H, 5.1; N 12.8.

1-(4-Methoxybenzyl)-1H-pyrazolo[3,4-b]pyridin-4-ol **41**

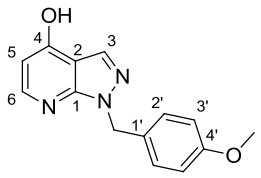

Ethylester **40** (504 mg, 1.54 mmol) was dissolved in warm EtOH (50 ml), 3 ml of 15% *w/v* aqueous NaOH added and the solution heated to 90 °C for 6 h. The mixture was concentrated *in vacuo* to approximately 5 ml, water (15 ml) was added, the mixture stirred at ambient temperature for 30 min and extracted with EtOAc (3 × 15 ml). The pH of the aqueous layer was adjusted to pH 3-4 with conc. HCl to precipitate the corresponding carboxylic acid. The precipitate was filtered, washed with 1M aqueous HCl and dried under reduced pressure. The carboxylic acid was heated to 240 °C in diphenylether (30 ml) for 18 h. Petroleum ether (50 ml) was added and the solution left to crystallise, yielding **41** (315 mg, 80% over 2 steps) as colourless crystals: $\mathbf{R_f}$**;** 0.3 (2:1 EtOAc : petroleum ether with 10% MeOH); **mp** 149-154 °C (EtOAC); $\mathbf{\nu_{max}}$ (neat) cm^{-1}: 2938, 1249; **^{1}H NMR** (400 MHz, $CDCl_3$): δ_H 9.29 (br, 1H, O*H*), 8.05 (s, 1H, C3-*H*), 7.65 (d, *J* = 6.8, 1H, C6-*H*), 7.17 (d, *J* = 8.7, 2H, C2'-*H*), 6.72 (d, *J* = 8.7, 2H, C3'-*H*), 6.24 (d, *J* = 6.8, 1H, C5-*H*), 5.49 (s, 2H, CH_2), 3.70 (s, 3H, OCH_3); **^{13}C NMR** (100 MHz, $CDCl_3$): δ_H 161.3 (*C*4), 159.4 (*C*4'), 145.6 (*C1*), 140.1 (1C, *C6*-H), 133.7 (*C3*-H), 129.0 (*C2'*-H), 127.7 (*C1'*), 114.1 (*C3'*-H), 112.0 (*C*2), 108.0 (*C5*-H), 55.2 (OCH_3), 51.4 (CH_2); **HRMS** *m/z* (ES+): [Found; $(M+H)^+$ 256.1081. $C_{14}H_{14}N_3O_2$ requires $(M+H)^+$, 256.1081, **LRMS** *m/z* (ESI+) 256.11 ($[M+H]^+$, 100%), 278.09 ($[M+Na]^+$, 70%).

5-Bromo-1-(4-methoxybenzyl)-1H-pyrazolo[3,4-b]pyridin-4-ol **42**

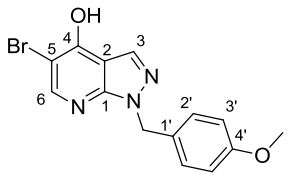

Phenol **41** (118 mg, 0.46 mmol) was dissolved in glacial AcOH (1.7 ml), *N*-bromosuccinimide added (99 mg, 0.56 mmol) and the mixture heated to 60 °C for 2 h. Water (2 ml) was added, the mixture stirred for 20 min, filtered and the precipitate washed with water. The solid was dried *in vacuo*, washed twice with cold $CHCl_2$ and dried, yielding **41** as an off-white solid (0.129 g, 83%): $\mathbf{R_f}$; 0.2 (4:1 EtOAc : petroleum ether); **mp** 167-168 °C (AcOH/H_2O) ; $\mathbf{\nu_{max}}$ (neat) cm^{-1}: 3082; **^{1}H NMR** (400 MHz, MeOD-d_4): δ_H 8.24 (s, 1H, C6-*H*), 8.11 (s, 1H, C3-*H*), 7.18 (d, *J* = 8.8, 2H, C2'-*H*), 6.87 (d, *J* = 8.8, 2H, C3'-*H*), 5.48 (s, 2H, CH_2), 3.76 (s, 3H, OCH_3); **^{13}C NMR** (126 MHz, MeOD-d_4): δ_C 166.6 (*C*5), 161.0 (*C4'*), 146.8 (*C*1), 143.5 (*C6*-H), 134.1 (*C2*-H), 129.8 (*C2'*-H), 129.3 (*C1'*), 115.2 (*C3'*-H), 111.9 (*C2*), 104.4 (*C*4), 55.7 (OCH_3), 52.1 (CH_2); **HRMS** *m/z* (ES+): [Found; $(M+Na)^+$ 356.0009. $C_{14}H_{12}BrN_3NaO_2$ requires $(M+Na)^+$, 356.0005], **LRMS** *m/z* (ESI-) 332.0 ($[M-H]^-$, 100%); **Elem. anal.** calcd. for $C_{14}H_{12}BrN_3O_2$: C, 50.3; H, 3.6; N, 12.6. Found C, 50.1; H, 3.5; N 12.4.

5-Bromo-4-chloro-1-(4-methoxybenzyl)-1H-pyrazolo[3,4-b]pyridine **22**

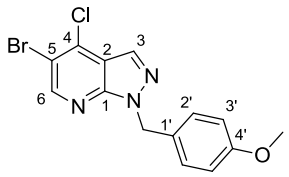

A solution of phenol **42** (1.75 g, 5.24 mmol) in dichloroethane (20 ml) and $POCl_3$ (20 ml) was heated to 75 °C for 2 h. The cooled reaction was poured on

ice, neutralised with solid Na_2CO_3 and extracted with CH_2Cl_2 (3 × 30 ml). The combined organic layers were washed with saturated aqueous $NaHCO_3$ solution (50 ml) and brine (50 ml), dried over anhydrous $MgSO_4$, filtered and concentrated *in vacuo*. The crude product was purified by column chromatography eluting with petroleum ether/EtOAc (9:1) to give **22** as colourless crystals (1.26 g, 68%): **R_f;** 0.6 (1:1 EtOAc : petroleum ether); **mp** 128-132 °C (EtOAc); **ν_{max}** (neat) cm^{-1}: 3058; **^{1}H NMR** (400 MHz, $CDCl_3$): δ_H 8.62 (s, 1H, C6-*H*), 8.05 (s, 1H, C3-*H*), 7.32 (d, *J* = 8.7, 2H, C2'-*H*), 6.83 (d, *J* = 8.7, 2H, C3'-*H*), 5.61 (s, 2H, CH_2), 3.77 (s, 3H, OCH_3); **^{13}C NMR** (126 MHz, $CDCl_3$): δ_C 159.4 (*C*4'), 150.8 (*C6*-H), 149.2 (*C1*), 137.1 (*C4*), 130.9 (*C3*-H), 129.5 (*C2'*-H), 128.3 (*C1'*), 116.7 (C*2*), 114.1 (*C3'*-H), 112.9 (*C5*-Br), 55.2 (O*C*H_3), 50.9 (*C*H_2); **HRMS** *m/z* (ES+): [Found; $(M+H)^+$ 351.9845. $C_{14}H_{12}BrClN_3O$ requires $(M+H)^+$, 351.9847]; **LRMS** *m/z* (ESI+) 353.98 ($[M+H]^+$, 100%); **Elem. anal.** calcd. for $C_{14}H_{11}BrClN_3O$: C, 47.7; H, 3.1; N, 11.9. Found C, 47.8; H, 3.2; N 12.1.

Tert-butyl ((4-(5-bromo-1-(4-methoxybenzyl)-1H-pyrazolo[3,4-b]pyridin-4-yl) morpholin-2-yl)methyl)carbamate **25**

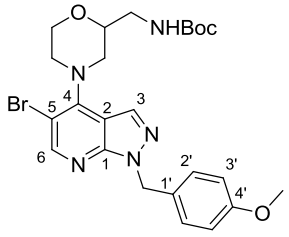

Et_3N (0.03 ml, 0.19 mmol) was added to a solution of **22** (34 mg, 0.10 mmol) and *tert*-butyl (morpholin-2-ylmethyl) carbamate **43** (23 mg, 0.11 mmol) in NMP (1 ml) and the mixture heated to 130 °C for 7 h. Water (3 ml) was added to the cooled reaction and the mixture extracted with EtOAc (3 × 5 ml). The combined organic layers were washed with brine (3 × 15 ml), dried over

anhydrous $MgSO_4$, filtered, concentrated *in vacuo* and purified by column chromatography eluting with petroleum ether/EtOAc (4:1 to 1:1). Carbamate **25** was obtained as a colourless solid (25 mg, 49%), together with recovered starting material **22** (11 mg, 32%): **R_f;** 0.6 (1:1 EtOAc : petroleum ether); **mp** 139-141 °C (EtOAc); **ν_{max}** (neat) cm^{-1}: 3384, 3011, 1739; **^{1}H NMR** (500 MHz, CD_2Cl_2): δ_H 8.46 (s, 1H, C6-*H*), 8.11 (s, 1H, C3-*H*), 7.29 (d, *J* = 8.7, 2H, C2'-*H*), 6.85 (d, *J* = 8.7, 2H, C3'-*H*), 5.58 (s, 2H, NCH_2), 4.97 (br, 1H, N*H*), 4.06 (m, 1H, OCH_aH$_b$), 3.90 (ddd, *J* = (11.3, 11.3, 2.5), 1H, OCH$_a$$H_b$), 3.88-3.85 (m, 1H, OCHCH_aH$_b$), 3.84-8.79 (m, 2H, OCH & OCH$_2$CH_aH$_b$), 3.78 (s, 3H, OCH_3), 3.40-3.35 (m, 2H, OCH$_2$CH$_a$$H_b$ & CH_aH$_b$NHBoc), 3.26 (ddd, *J* = 14.0, 5.7, 5.7, 1H, CH$_a$$H_b$NHBoc), 3.16 (dd, *J* = 10.8, 10.8, 1H, OCHCH$_a$$H_b$), 1.47 (s, 9H, C(C$H_3$)$_3$); **^{13}C NMR** (126 MHz, CD_2Cl_2): δ_C 159.7 (*C4'*), 156.3 (*C*OO^{t}Bu), 152.8 (*C6*-H), 151.5 (*C1*), 150.8 (*C4*), 131.8 (*C3*-H), 129.6 (*C2'*-H), 129.6 (*C1'*), 114.2 (*C3'*-H), 111.7 (*C2*), 105.1 (*C5*), 79.6 (*C*(CH$_3$)$_3$), 75.4 (O*C*H), 67.2 (O*C*H$_2$), 55.6 (O*C*H$_3$), 54.0 (OCH*C*H$_2$), 51.3 (OCH$_2$*C*H$_2$), 43.1 (*C*H$_2$NH$_2$), 28.5 (C(*C*H$_3$)$_3$). **HRMS** *m/z* (ES+): [Found; $(M+H)^+$ 532.1538. $C_{24}H_{31}BrN_5O_4$ requires $(M+H)^+$, 532.1554]; **LRMS** *m/z* (ESI+) 534.16 ($[M+H]^+$, 84%); **Elem. anal.** calcd. for $C_{24}H_{30}BrN_5O_4$: C, 54.1; H, 5.7; N, 13.2. Found C, 54.1; H, 5.7; N 13.0.

(4-(5-Bromo-1H-pyrazolo[3,4-b]pyridin-4-yl)morpholin-2-yl)methanamine **16**

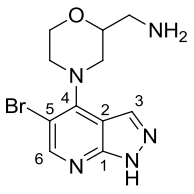

Carbamate **25** (25 mg, 0.05 mmol) was dissolved in TFA (2 ml) and ^{i}Pr$_3$SiH (0.03 ml, 0.14 mmol) added. The resulting solution was stirred at 40 °C for 18 h and concentrated *in vacuo*. The crude product was dissolved in 5 ml

MeOH and the solution loaded onto an ISOLUTE® SCX-2 cation exchange column (500 mg resin), washed with 10 ml MeOH and then eluted with 1 M NH_3 in MeOH to give **16** as colourless crystals (15 mg, >99%): **R_f;** 0.2 (4:1 $CHCl_3$: MeOH); **mp** 93–98 °C (MeOH) ; **ν_{max}** (neat) cm^{-1}: 3360; **^{1}H NMR** (500 MHz, MeOD-d_4): δ_H 8.40 (s, 1H, C6-*H*), 8.31 (s, 1H, C3-*H*), 4.13 - 4.10 (m, 1H, OCH_aH$_b$), 3.92 (ddd, *J* = 11.4, 11.4, 2.4, 1H, OCH$_a$$H_b$), 3.92 – 3.90 (m, 1H, OCH$_2$CH_aH$_b$), 3.86 – 3.80 (m, 2H, OCHCH_aH$_b$ & OC*H*), 3.44 (ddd, *J* = 11.6, 11.6, 2.8, 1H, OCH$_2$CH$_a$$H_b$), 3.17 (dd, *J* = 12.0, 10.1, 1H, OCHCH$_a$$H_b$), 2.88 – 2.86 (m, 2H, C$H_2NH_2$); **^{13}C NMR** (126 MHz, MeOD-d_4): δ_C 154.0 (*C1*), 153.8 (*C6*-H), 152.5 (*C4*), 134.1 (*C3*-H), 111.9 (*C2*), 105.2 (*C5*), 78.1 (O*C*H), 67.9 (O*C*H$_2$), 55.0 (OCH*C*H$_2$), 52.2 (OCH$_2$*C*H$_2$), 44.7 (*C*H$_2$NH$_2$); **HRMS** *m/z* (ES+): [Found; $(M+H)^+$ 312.0450. $C_{11}H_{15}BrN_5O$ requires $(M+H)^+$, 312.0454]; **LRMS** *m/z* (ESI+) 312.1 ($[M+H]^+$, 100%). **HPLC** (Hichrom RPB column, 5-70% acetonitrile, 254 nm): Retention time 4.51 min, 98% purity.

5-Bromo-4-chloro-1H-pyrazolo[3,4-b]pyridine **23**

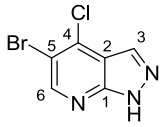

Pyrazolo pyridine **22** (289 mg, 0.82 mmol) was dissolved in TFA (5 ml), ^{i}PrSiH added (0.34 ml, 1.64 mmol) and heated to 60 °C for 5 h. Water (10 ml) was added to the cold reaction mixture and extracted with EtOAc (3 × 10 ml). The combined organic layers were washed with saturated aqueous Na_2CO_3 solution (2 × 30 ml), brine (30 ml), dried over anhydrous $MgSO_4$, filtered and concentrated *in vacuo*. The crude product was purified by column chromatography eluting with petroleum ether/EtOAc (gradient: 10:1 to 4:1) to give **23** as fine colourless

crystals (164 mg, 86%): **R_f;** 0.4 (4:1 EtOAc : petroleum ether); ***mp*** 138-154 °C (decomposition, EtOAc); **ν_{max}** (neat) cm^{-1}: 3457, 3016; **^{1}H NMR** (500 MHz, DMSO-d_6): δ_H 14.23 (br, 1H, N*H*), 8.73 (s, 1H, C6-*H*), 8.27 (s, 1H, C3-*H*); **^{13}C NMR** (126 MHz, DMSO-d_6): δ_C 151.1 (*C1*), 150.8 (*C6*-H), 135.4 (*C4*), 131.6 (*C3*-H), 115.3 (*C5*), 112.0 (*C2*); **HRMS** *m/z (ES+):* [Found; $(M-H)^-$ 229.9127. $C_6H_2BrClN_3O$ requires $(M-H)^-$, 229.9126]; **LRMS** *m/z* (ESI-) 231.91 ($[M-H]^-$, 100%); **Elem. anal.** calcd. for $C_6H_3BrClN_3$: C, 31.0; H, 1.3; N, 18.1. Found C, 31.2; H, 1.4; N 17.9.

1-Benzyl-5-bromo-4-chloro-1H-pyrazolo[3,4-b]pyridine **24a** (1-*N* regioisomer)

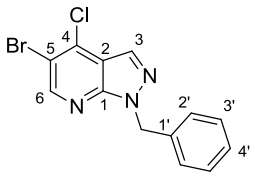

Benzylbromide (0.034 ml, 0.28 mmol) was added to a solution of **23** (45 mg, 0.19 mmol) and anhydrous K_2CO_3 (80 mg, 0.58 mmol) in anhydrous DMF (5 ml) and the resulting mixture stirred at ambient temperature for 2 h. Water (10 ml) was added and the reaction extracted with EtOAc (2 × 10 ml). The combined organic layers were washed with brine (3 × 15 ml), dried over anhydrous $MgSO_4$, filtered and concentrated *in vacuo*. The crude product was purified by column chromatography eluting with petroleum ether/Et_2O (gradient: 100 % petroleum ether to 9:1), yielding **24a** as colourless crystals (34 mg, 54%): **R_f;** 0.4 (1:9 Et_2O : petroleum ether); **mp** 89-90 °C (Et_2O/ petroleum ether); **ν_{max}** (neat) cm^{-1}: 3029; **^{1}H NMR** (400 MHz, $CDCl_3$): δ_H 8.62 (s, 1H, C6-*H*), 8.08 (s, 1H, C3-*H*), 7.36-7.28 (m, 5H, C2'-*H*, C3'-*H*, C4'-*H*), 5.69 (s, 2H, CH_2); **^{13}C NMR** (126 MHz, $CDCl_3$): δ_C 150.9 (*C6*-H), 149.5 (*C1*), 137.0 (*C4*), 136.2 (*C*H_2), 131.0 (*C3*-H), 128.7 & 128.0 (*C2'*-H & *C3'*-H), 128.0 (*C4'*-H), 116.7 (*C2*), 113.0 (*C5*), 51.3

(*C*H_2); **HRMS** *m/z (ES+):* [Found; $(M+Na)^+$ 343.9555. $C_{13}H_9BrClN_3Na$ requires $(M+Na)^+$, 343.9561]; **LRMS** *m/z* (ESI+) 344.0 ($[M+Na]^+$, 100%); **Elem. anal.** calcd. for $C_{13}H_9BrClN_3$: C, 48.4; H, 2.8; N, 13.0. Found C, 48.5; H, 2.7; N 12.9.

2-Benzyl-5-bromo-4-chloro-2H-pyrazolo[3,4-b]pyridine **24a** (2-*N* regioisomer)

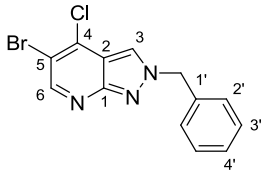

Benzylbromide (0.028 ml, 0.24 mmol) was added to a solution of **23** (37 mg, 0.16 mmol) and anhydrous Cs_2CO_3 (87 mg, 0.27 mmol) in anhydrous DMF (4 ml) and the resulting mixture stirred at ambient temperature for 3 h. Water (10 ml) was added to the reaction and extracted with EtOAc (2 × 10 ml). The combined organic layers were washed with brine (3 × 15 ml), dried over anhydrous $MgSO_4$, filtered and concentrated *in vacuo*. The crude product was purified by column chromatography eluting with petroleum ether/Et_2O (9:1) followed by petroleum ether/EtOAc (4:1), yielding **24a** (2-*N* regioisomer) as colourless crystals (33 mg, 64%) and the regioisomer **24a** (1-*N* regioisomer) (15 mg, 29%): $\mathbf{R_f}$**;** 0.7 (1:1 EtOAc : petroleum ether); **mp** 162-163 °C (EtOAc); $\mathbf{\nu_{max}}$ (neat) cm^{-1}: 3097, 3031; ^{1}**H NMR** (500 MHz, $CDCl_3$): δ_H 8.72 (s, 1H, C6-*H*), 7.92 (s, 1H, C3-*H*), 7.41-7.37 (m, 5H, C2'-*H*, C3'-*H*, C4'-*H*), 5.62 (s, 2H, CH_2); ^{13}**C NMR** (126 MHz, $CDCl_3$): δ_C 157.1 (*C1*), 153.2 (*C6*-H), 135.9 (*C4*), 134.2 (*C*H_2), 129.2 & 128.5 (*C2'*-H & *C3'*-H), 129.0 (*C4'*-H), 122.1 (1C, *C3*-H), 116.1 (*C5*), 113.4 (*C2*), 58.5 (*C*H_2); **HRMS** *m/z* (ES+): [Found; $(M+Na)^+$ 343.9555. $C_{13}H_9BrClN_3Na$ requires $(M+Na)^+$, 343.9561]; **LRMS** *m/z* (ESI+) 344.0 ($[M+Na]^+$, 100%) 322.0 ($[M+H]^+$, 95%); **Elem. anal.** calcd. for $C_{13}H_9BrClN_3$: C, 48.4; H, 2.8; N, 13.0. Found C, 48.5; H, 2.9; N 13.4.

5-Bromo-4-chloro-1-((1-methyl-2-nitro-1H-imidazol-5-yl)methyl)-1H-pyrazolo[3,4-b]pyridine **24c** (1-*N* regioisomer)

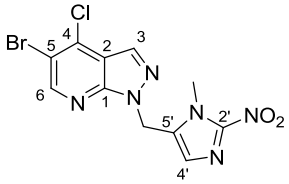

Representative procedure A: Pyrazolo pyridine **23** (143 mg, 0.62 mmol), chloride **38** (119 mg, 0.68 mmol), TBAI (227 mg, 0.62 mmol) and anhydrous K_2CO_3 (255 mg, 1.86 mmol) were dissolved in anhydrous DMF (6 ml) and stirred at ambient temperature for 18 h. Water (10 ml) was added to the mixture and extracted with EtOAc (2 × 10 ml). The combined organic layers were washed with brine (3 × 30 ml), dried over anhydrous $MgSO_4$, concentrated *in vacuo* and the residue purified by column chromatography, eluting with petroleum ether/EtOAc (gradient: 4:1 to 1:4). Compound **24c** (1-*N* regioisomer) was obtained as colourless needles (156 mg, 68%): $\mathbf{R_f}$**;** 0.4 (1:1 EtOAc : petroleum ether); **mp** 193-194 °C (CH_2Cl_2/petroleum ether); $\mathbf{\nu_{max}}$ (neat) cm^{-1}: 1480, 1342; **^{1}H NMR** (500 MHz, CD_2Cl_2): δ_H 8.69 (s, 1H, C6-*H*), 8.13 (s, 1H, C3-*H*), 7.28 (s, 1H, C4'-*H*), 5.75 (s, 2H, C*H*$_2$), 4.10 (s, 3H, NC*H*$_3$); **^{13}C NMR** (126 MHz, CD_2Cl_2): δ_C 151.7 (1C, *C6*-H), 149.8 (*C1*), 146.6 (*C2'*), 137.7 (*C4*), 132.7 (*C5'*), 132.2 (*C3*-H), 129.6 (*C4'*-H), 117.2 (*C5*), 114.0 (*C2*), 41.2 (*C*H$_2$), 35.0 (N*C*H$_3$); **HRMS** *m/z* (ES+): [Found; $(M+Na)^+$ 394.9474. $C_{11}H_8BrClN_6NaO_2$ requires $(M+Na)^+$, 394.9473]; **LRMS** *m/z* (ESI-) 368.9 ($[M-H]^-$, 100%); **Elem. anal.** calcd. for $C_{11}H_8BrClN_6O_2$: C, 35.6; H, 2.2; N, 22.6. Found C, 35.7; H, 2.2; N 22.6.

5-Bromo-4-chloro-2-((1-methyl-2-nitro-1H-imidazol-5-yl)methyl)-2H-pyrazolo[3,4-b]pyridine **24c** (2-*N* regioisomer)

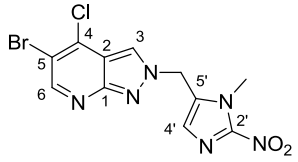

Pale yellow crystals (5 mg, 16%), obtained as a side product in the synthesis of **24c** (1-*N* regioisomer): **R_f;** 0.4 (1:9 EtOAc : petroleum ether); **mp** 189-192 °C (CH_2Cl_2); **ν_{max}** (neat) cm^{-1}: 3010, 1488, 1321; **^{1}H NMR** (500 MHz, CD_2Cl_2): δ_H 8.74 (s, 1H, C6-*H*), 8.10 (s, 1H, C3-*H*), 7.37 (s, 1H, C4'-*H*), 5.73 (s, 2H, CH_2), 4.07 (s, 3H, NCH_3); **^{13}C NMR** (126 MHz, CD_2Cl_2): δ_C 157.6 (*C1*), 154.3 (*C6*-H), 146.5 (*C2'*), 136.5 (*C4*), 130.9 (*C5'*), 130.0 (*C4'*-H), 122.9 (*C3*-H), 116.6 (*C2*), 114.4 (*C5*), 48.2 (CH_2), 35.3 (NCH_3); **HRMS** *m/z* (ES+): [Found; $(M+Na)^+$ 394.9472. $C_{11}H_8BrClN_6NaO_2$ requires $(M+Na)^+$, 394.9473]; **LRMS** *m/z* (ESI-) 368.9 ($[M-H]^-$, 100%).

5-Bromo-4-chloro-1-(4-nitrobenzyl)-1H-pyrazolo[3,4-b]pyridine **24b** (1-*N* regioisomer)

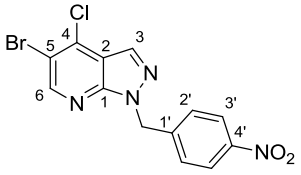

Preparation according to representative procedure A. Colourless needles (82 mg, 56%): **R_f;** 0.7 (4:1 petroleum ether : EtOAc); **mp** 144-145 °C (EtOAc); **ν_{max}** (neat) cm^{-1}: 3008, 1539, 1347; **^{1}H NMR** (500 MHz, $CDCl_3$): δ_H 8.62 (s, 1H, C6-*H*), 8.18 (d, *J* = 8.7, 2H, C3'-*H*), 8.11 (s, 1H, C3-*H*), 7.48 (d, *J* = 8.7, 2H, C2'-*H*), 5.78 (s, 2H, CH_2); **^{13}C NMR** (126 MHz, $CDCl_3$): δ_C 151.3 (*C6*-H), 149.6 (*C1*), 147.6 (*C4'*), 143.2 (*C1'*), 137.4 (*C4*), 131.7 (*C3*-H), 128.7 (*C2'*-H), 124.0 (*C3'*-H),

116.8 (*C2*), 113.5 (*C5*), 50.5 (CH_2).; **HRMS** *m/z* (FI+): [Found; $(M)^+$ 365.9528. $C_{13}H_8BrClN_4O_2$ requires $(M)^+$ 365.9519]; **LRMS** *m/z* (FI+) 367.9 ($[^{81}Br^{35}ClM]^+$ & $[^{79}Br^{37}ClM]^+$, 100%), 366.0 ($[^{79}Br^{35}ClM]^+$, 53%). **Elem. anal.** calcd. for $C_{13}H_8BrClN_4O_2$: C, 42.5; H, 2.2; N, 15.2. Found C, 42.3; H, 2.2; N, 15.2.

5-Bromo-4-chloro-2-(4-nitrobenzyl)-1H-pyrazolo[3,4-b]pyridine **24b** (2-*N* regioisomer)

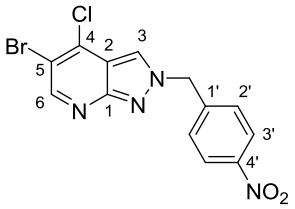

Colourless needles (6 mg, 11%), obtained as a side product in the synthesis of **24b** (1-*N* regioisomer): **R_f;** 0.4 (1:1 petroleum ether : EtOAc); **mp** 192 °C (EtOAc); **ν_{max}** (neat) cm^{-1}: 3006; **^{1}H NMR** (500 MHz, $CDCl_3$): δ_H 8.75 (s, 1H, C6-*H*), 8.24 (d, *J* = 8.5, 2H, C3'-*H*), 8.06 (s, 1H, C3-*H*), 7.51 (d, *J* = 8.5, 2H, C2'-*H*), 5.72 (s, 2H, CH_2); **^{13}C NMR** (126 MHz, $CDCl_3$): δ_C 157.3 (*C1*), 153.8 (*C6*-H), 148.1 (*C4'*), 141.4 (*C1'*), 136.1 (*C4*), 128.9 (*C2'*-H), 124.3 (*C3'*-H), 122.8 (*C3*-H), 116.3 (*C2*), 114.0 (*C5*), 57.5 (CH_2); **HRMS** *m/z* (FI+): [Found; $(M)^+$ 365.9523. $C_{13}H_8BrClN_4O_2$ requires $(M)^+$ 365.9519]; **LRMS** *m/z* (FI+) 367.9 ($[^{81}Br^{35}ClM]^+$ & $[^{79}Br^{37}ClM]^+$, 100%), 366.0 ($[^{79}Br^{35}ClM]^+$, 47%).

2-(1,2-Bis(4-nitrophenyl)ethyl)-5-bromo-4-chloro-2H-pyrazolo[3,4-b]pyridine **48**

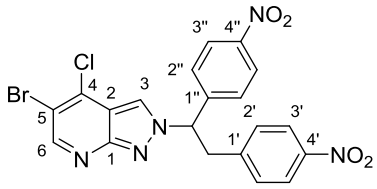

Off white solid (5 mg, 7%), obtained as a side product in the synthesis of **24b**: **R_f;** 0.3 (4:1 petroleum ether : EtOAc); **mp** 176-179 °C (EtOAc); **ν_{max}** (neat) cm^{-1}: 1517, 1281; **^{1}H NMR** (500 MHz, $CDCl_3$): δ_H 8.77 (s, 1H, C6-*H*), 8.23 (d, *J* = 8.7, 2H, C3‘‘-*H*), 8.07 (d, *J* = 8.6, 2H, C3‘-*H*), 7.91 (s, 1H, C3-*H*), 7.72 (d, *J* = 8.7, 2H, C2‘‘-*H*), 7.29 (d, *J* = 8.6, 2H, C2‘-*H*), 5.76 (dd, *J* = (9.9, 5.3), 1H, C*H*CH_2), 4.26 (dd, *J* = (9.9, 14.0), 1H, C$H_a$$H_b$), 3.64 (dd, *J* = (5.3, 14.0), 1H, $CH_a$$H_b$); **^{13}C NMR** (126 MHz, $CDCl_3$): δ_C 157.2 (*C1*), 154.0 (*C6*-H), 148.2 (*C4‘‘*), 147.2 (*C4‘*), 144.6 (*C1‘‘*), 143.8 (*C1‘*), 138.7 (*C5*), 136.1 (*C4*), 129.9 (*C2‘*-H), 128.2 (*C2‘‘*-H), 124.3 (*C3‘‘*-H), 124.0 (*C3‘*-H), 122.9 (*C3*), 115.7 (*C2*), 105.6 (*C4*), 69.3 (*C*HCH_2), 41.4 (*C*H_2); **HRMS** *m/z* (ES-): [Found; $(M-H)^-$ 499.9764. $C_{20}H_{12}BrClN_5O_4$ requires $(M-H)^-$ 499.9767]; **LRMS** *m/z* (ESI-) 502.0 ($[M-H]^-$, 100%), 499.9 ($[M-H]^-$, 70%), 537.9 ($[M+Cl]^-$, 55%), 536.0 ($[M+Cl]^-$, 30%).

Tert-butyl ((4-(1-benzyl-5-bromo-1H-pyrazolo[3,4-b]pyridin-4-yl)morpholin-2-yl) methyl)carbamate **27a**

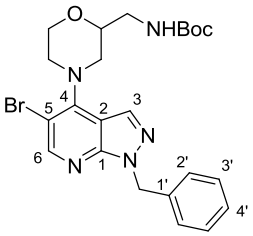

Representative procedure B: Et_3N (0.03 ml, 0.18 mmol) was added to a solution of **24a** (1-*N* regioisomer) (27 mg, 0.08 mmol) and *tert*-butyl (morpholin-2-

ylmethyl) carbamate (20 mg, 0.09 mmol) in NMP (1 ml) and the mixture heated to 130 °C for 7 h. Water (3 ml) was added to the cooled reaction vessel and the mixture extracted with EtOAc (3 × 5 ml). The combined organic layers were washed with brine (3 × 15 ml), dried over anhydrous $MgSO_4$, filtered, concentrated *in vacuo* and purified by column chromatography eluting with petroleum ether/EtOAc (gradient: 5:1 to 2:1). Carbamate **27a** was obtained as a colourless solid (22 mg, 52%), together with recovered starting material **24a** (12 mg, 44%). Carbamate **27a** was recrystallised from Et_2O/ petroleum ether: $\mathbf{R_f}$**;** 0.3 (1:2 EtOAc : petroleum ether); **mp** 120-123 °C (Et_2O/petroleum ether); $\mathbf{\nu_{max}}$ (neat) cm^{-1}: 3374, 1690; **^{1}H NMR** (500 MHz, $CDCl_3$): δ_H 8.44 (s, 1H, C6-*H*), 8.09 (s, 1H, C3-*H*), 7.32-7.23 (m, 5H, C2'-*H.* C3'-*H*, C4'-*H*), 5.64 (s, 2H, NCH_2), 4.94 (br, 1H, N*H*), 4.06 – 4.03 (m, 1H, OCH_aH$_b$), 3.89 (ddd, *J* = 11.1, 11.1, 2.3, 1H, OCH$_a$$H_b$), 3.86 – 3.80 (m, 2H, CHCH_aH$_b$N & OC*H*), 3.78 – 3.75 (m, 1H, OCH$_2$CH_aH$_b$), 3.42-3.34 (m, 2H, CH_aH$_b$NHBoc & OCH$_2$CH$_a$$H_b$), 3.26 (ddd, *J* = 14.0, 5.7, 5.7, 1H, CH$_a$$H_b$NHBoc), 3.13 (dd, *J* = 11.2, 11.2, 1H, OCHCH$_a$$H_b$), 1.46 (s, 9H, C(C$H_3$)$_3$); **^{13}C NMR** (126 MHz, $CDCl_3$): δ_C 156.0 (*C*OO^{t}Bu), 152.6 (*C6*-H), 151.2 (*C1*), 150.3 (*C4*), 136.7 (*C1'*), 131.2 (*C3*-H), 128.6 & 127.8 (*C2'*-H & *C3'*-H), 127.8 (*C4'*-H), 111.3 (*C2*), 105.0 (*C5*), 79.6 (*C*(CH$_3$)$_3$), 74.9 (O*C*H), 66.8 (O*C*H$_2$), 53.6 (OCH*C*H$_2$), 50.8 (N*C*H$_2$), 50.8 (OCH$_2$*C*H$_2$), 42.7 (*C*H$_2$NHBoc), 28.4 (C(*C*H$_3$)$_3$); **HRMS** *m/z* (ES+): [Found; (M+Na)$^+$ 524.1268. $C_{23}H_{28}BrN_5NaO_3$ requires (M+Na)$^+$, 524.1268]; **LRMS** *m/z* (ESI+) 307.2 ([M-Br-NHBoc]$^+$, 100%), 524.1 ([M+Na]$^+$, 35%), 502.1 ([M+H]$^+$, 7%); **Elem. anal.** calcd. for $C_{23}H_{28}BrN_5O_3$: C, 55.0; H, 5.6; N, 13.9. Found C, 55.1; H, 5.7; N 13.9.

Tert-butyl ((4-(5-bromo-1-((1-methyl-2-nitro-1H-imidazol-5-yl)methyl)-1H-pyrazolo[3,4-b]pyridin-4-yl)morpholin-2-yl)methyl)carbamate **27c**

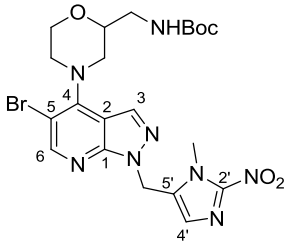

Procedure according to representative procedure B. Bright yellow crystals (230 mg, 71%): **R_f;** 0.3 (2:1 EtOAc : petroleum ether); **mp** 72-75 °C (EtOAc); **ν_{max}** (neat) cm^{-1}: 3343, 1705, 1487, 1365; **^{1}H NMR** (500 MHz, CD_2Cl_2): δ_H 8.48 (s, 1H, C6-*H*), 8.15 (s, 1H, C3-*H*), 7.24 (s, 1H, C4'-*H*), 5.69 (s, 2H, NCH_2), 4.98 (br, 1H, N*H*), 4.09 (s, 3H, NCH_3), 4.08 – 4.05 (m, 1H, OCH_aH$_b$), 3.91 (ddd, *J* = 11.3, 11.3, 2.4, 1H, OCH$_a$$H_b$), 3.89 – 3.86 (m, 1H, OCHCH_aH$_b$), 3.85-3.80 (m, 2H, OC*H*, OCH$_2$CH_aH$_b$), 3.41-3.35 (m, 2H, OCH$_2$CH$_a$$H_b$ & CH_aH$_b$NHBoc), 3.26 (ddd, *J* = 14.0, 5.9, 5.9, 1H, CH$_a$$H_b$NHBoc), 3.18 (dd, *J* = 10.8, 10.8, 1H, OCHCH$_a$$H_b$), 1.46 (s, 9H, C(C$H_3$)$_3$); **^{13}C NMR** (126 MHz, CD_2Cl_2): δ_C 156.3 (*C*OO^{t}Bu), 153.2 (*C6*-H), 151.5 & 151.1 (*C4* & *C1*), 146.5 (*C2'*), 133.3 (*C5'*), 132.9 (*C3*-H), 129.4 (*C4'*-H), 111.6 (*C2*), 105.5 (*C5*), 79.6 (*C*(CH$_3$)$_3$), 75.4 (O*C*H), 67.1 (O*C*H$_2$), 54.1 (OCH*C*H$_2$), 51.2 (OCH$_2$*C*H$_2$), 43.1 (*C*H$_2$NHBoc), 40.7 (N*C*H$_2$), 35.0 (N*C*H$_3$), 28.5 (C(*C*H$_3$)$_3$); **HRMS** *m/z* (ES+): [Found; $(M+Na)^+$ 573.1197. $C_{21}H_{27}BrN_8NaO_5$ requires $(M+Na)^+$, 573.1180]; **LRMS** *m/z* (ESI+) 573.0 ($[M+Na]^+$, 87%). **Elem. anal.** calcd. for $C_{21}H_{27}BrN_8O_5$: C, 45.7; H, 4.9; N, 20.3. Found C, 45.9; H, 5.0; N 20.2.

Tert-butyl ((4-(5-bromo-1-(4-nitrobenzyl)-1H-pyrazolo[3,4-b]pyridin-4-yl)morpholin-2-yl)methyl)carbamate **27b**

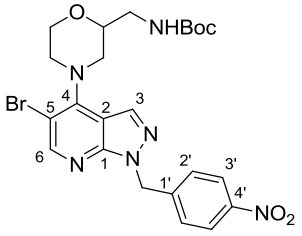

Procedure according to representative procedure for B. Orange crystals (56 mg, 68%): $\mathbf{R_f}$**;** 0.3 (2:1 EtOAc : petroleum ether); **mp** 164-165 °C (EtOAc); $\mathbf{\nu_{max}}$ (neat) cm^{-1}: 3380, 1739, 1522, 1307; **^{1}H NMR** (500 MHz, $CDCl_3$): δ_H 8.42 (s, 1H, C6-*H*), 8.14 (d, *J* = 8.7, 2H, C3'-*H*), 8.12 (s, 1H, C3-*H*), 7.43 (d, *J* = 8.7, 2H, C2'-*H*), 5.72 (s, 2H, NCH_2), 4.95 (br, 1H, N*H*), 4.06–4.03 (m, 1H, OCH_aH$_b$), 3.98 (ddd, *J* = 11.3, 11.3, 2.2, 1H, OCH$_a$$H_b$), 3.87 – 3.79 (m, 3H, OCHCH_aH$_b$, OCH$_2$CH_aH$_b$, OC*H*), 3.42-3.34 (m, 2H, OCH$_2$CH$_a$$H_b$ & CH_aH$_b$NHBoc), 3.26 (ddd, *J* = 14.0, 5.7, 5.7, 1H, CH$_a$$H_b$NHBoc), 3.17 (dd, *J* = 10.7, 10.7, 1H, OCHCH$_a$$H_b$), 1.45 (s, 9H, C(C$H_3$)$_3$); **^{13}C NMR** (126 MHz, $CDCl_3$): δ_C 156.1 (*C*OO^{t}Bu), 152.8 (*C6*-H), 151.2 (*C1*), 150.5 (*C4*), 147.5 (*C4'*), 143.8 (*C1'*),132.2 (*C3*-H), 128.6 (*C2'*-H), 123.9 (*C3'*-H), 111.3 (*C2*), 105.1 (*C5*), 79.7 (*C*(CH$_3$)$_3$), 75.0 (O*C*H), 66.7 (O*C*H$_2$), 53.6 (OCH*C*H$_2$), 50.7 (OCH$_2$*C*H$_2$), 50.0 (N*C*H$_2$), 42.7 (*C*H$_2$NHBoc), 28.4 (C(*C*H$_3$)$_3$); **HRMS** *m/z* (ES+): [Found; (M+Na)$^+$ 569.1140. $C_{23}H_{27}BrN_6NaO_5$ requires (M+Na)$^+$, 569.1119]; **LRMS** *m/z* (ESI+) 569.2 ([M+Na]$^+$, 82%). **Elem. anal.** calcd. for $C_{23}H_{27}BrN_6O_5$: C, 50.5; H, 5.0; N, 15.4. Found C, 50.4; H, 4.9; N 15.3.

(4-(1-Benzyl-5-bromo-1H-pyrazolo[3,4-b]pyridin-4-yl)morpholin-2-yl)methanamine **19**

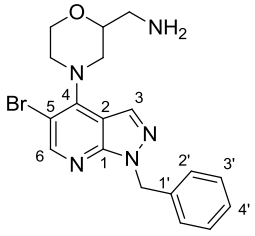

Representative procedure C**:** Carbamate **27a** (50 mg, 0.10 mmol) was dissolved in TFA (5 ml) and $^{i}Pr_3SiH$ (0.06 ml, 0.30 mmol) added. The resulting solution was stirred at 40 °C for 1 h and concentrated *in vacuo*. The crude product was dissolved in MeOH and the solution loaded onto a SCX-2 column, washed with MeOH and eluted with 1 M NH_3 in MeOH to give **19** as a colourless gum (35 mg, 88%): $\mathbf{R_f}$**;** 0.4 (9:1 $CHCl_3$: MeOH); $\mathbf{\nu_{max}}$ (neat) cm^{-1}: 3456, 3370, 3028; **^{1}H NMR** (500 MHz, MeOD-d_4): δ_H 8.44 (s, 1H, C6-*H*), 8.31 (s, 1H, C3-*H*), 7.30 - 7.23 (m, 5H, C2'-*H*, C3'-*H*, C4'-*H*), 5.63 (s, 2H, NCH_2), 4.10 – 4.08 (m, 1H, OCH_aH$_b$), 3.90 (ddd, *J* = 11.1, 11.1, 2.5, 1H, OCH$_a$$H_b$), 3.92 – 3.89 (m, 1H, OCHCH_aH$_b$), 3.86 – 3.84 (m, 1H, OCH$_2$CH_aH$_b$), 3.77 (dtd, *J* = 9.8, 5.7, 2.1, 1H, OC*H*), 3.42 (ddd, *J* = 11.5, 11.5, 2.5, 1H, OCH$_2$CH$_a$$H_b$), 3.18 (dd, *J* = 11.6, 9.8, 1H, OCHCH$_a$$H_b$), 2.80 (d, *J* = 5.7, 2H, CH_2NH$_2$); **^{13}C NMR** (126 MHz, MeOD-d_4): δ_C 153.7 (*C6*-H), 152.5 (*C1*), 152.3 (*C4*), 138.3 (NCH$_2$), 133.3 (*C3*-H), 129.6 (*C4'*-H), 128.8 & 128.7 (*C2'*-H & *C3'*-H), 112.5 (*C2*), 105.5 (*C5*), 78.1 (OCH), 67.9 (OCH$_2$), 54.9 (OCHCH$_2$), 52.2 (OCH$_2$CH$_2$), 51.6 (NCH$_2$), 44.7 (CH$_2$NH$_2$); **HRMS** *m/z* (ES+): [Found; $(M+H)^+$ 402.0919. $C_{18}H_{21}BrN_5O$ requires $(M+H)^+$ 402.0924]; **LRMS** *m/z* (ESI+) 402.1 ($[M+H]^+$, 100%). **HPLC** (Hichrom RPB column, 10-80% acetonitrile, 254 nm): Retention time 5.83 min, 99% purity.

(4-(5-Bromo-1-((1-methyl-2-nitro-1H-imidazol-5-yl)methyl)-1H-pyrazolo[3,4-b]pyridin-4-yl)morpholin-2-yl)methanamine **18**

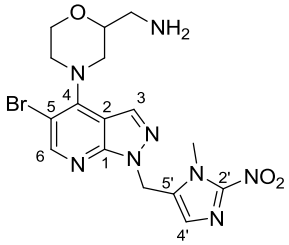

Preparation according to representative procedure C. Bright yellow crystals (92 mg, 97%): $\mathbf{R_f}$; 0.2 ($CHCl_3$ 5% MeOH); **mp** 70-73 °C (MeOH); $\mathbf{\nu_{max}}$ (neat) cm^{-1}: 3376, 1485, 1336; **^{1}H NMR** (500 MHz, MeOD-d_4): δ_H 8.45 (s, 1H, C6-*H*), 8.31 (s, 1H, C3-*H*), 7.17 (s, 1H, C4'-*H*), 5.76 (s, 2H, NCH_2), 4.09 (s, 3H, NCH_3), 4.09 - 4.07 (m, 1H, OCH_aH$_b$), 3.91 - 3.86 (m, 2H, OCH$_a$$H_b$ & OCHCH_aH$_b$), 3.85 – 3.81 (m, 1H, OCH$_2$CH_aH$_b$), 3.76 (dtd, *J* = 10.0, 5.8, 2.3, 1H, OC*H*), 3.40 (ddd, *J* = 12.0, 12.0, 2.9, 1H, OCH$_2$CH$_a$$H_b$), 3.15 (dd, *J* = 12.0, 10.0, 1H, OCHCH$_a$$H_b$), 2.80 (d, *J* = 5.8, 2H, CH_2NH$_2$). ; **^{13}C NMR** (126 MHz, MeOD-d_4): δ_C 153.9 (*C6*-H), 152.6 (*C4*), 152.3 (*C1*), 147.2 (*C2'*), 134.9 (*C5'*), 134.2 (*C3*-H), 129.1 (*C4'*-H), 112.5 (*C2*), 105.8 (*C5*), 78.1 (O*C*H), 67.9 (O*C*H$_2$), 54.9 (OCH*C*H$_2$), 52.2 (OCH$_2$*C*H$_2$), 44.7 (*C*H$_2$NH$_2$), 41.3 (N*C*H$_2$), 35.3 (N*C*H$_3$); **HRMS** *m/z* (ES+): [Found; $(M+H)^+$ 451.0825. $C_{16}H_{20}BrN_8O_3$ requires $(M+H)^+$ 451.0836]; **LRMS** *m/z* (ESI+) 451.1 ($[M+H]^+$, 100%). **Elem. anal.** calcd. for $C_{16}H_{19}BrN_8O_3$: C, 42.5; H, 4.2; N, 24.8. Found C, 42.4; H, 4.3; N 24.8.

(4-(5-Bromo-1-(4-nitrobenzyl)-1H-pyrazolo[3,4-b]pyridin-4-yl)morpholin-2-yl)methanamine **17**

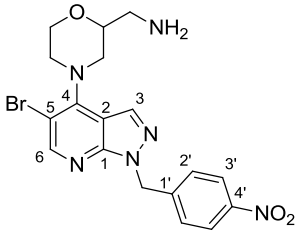

Preparation according to representative procedure C. Orange crystals (56 mg, 68%): **R_f;** 0.2 ($CHCl_3$, 5% MeOH); **mp** 59-62 °C (MeOH); **ν_{max}** (neat) cm^{-1}: 3457, 3370, 1518, 1344; **^{1}H NMR** (500 MHz, MeOD-d_4): δ_H 8.41 (s, 1H, C6-*H*), 8.33 (s, 1H, C3-*H*), 8.13 (d, *J* = 8.8, 2H, C3'-*H*), 7.44 (d, *J* = 8.8, 2H, C2'-*H*), 5.73 (s, 2H, NCH_2), 4.10 – 4.07 (m, 1H, OC$H_a$$H_b$), 3.91 – 3.89 (m, 1H, OCHC$H_a$$H_b$), 3.98 (ddd, *J* = 11.2, 11.2, 2.4, 1H, OC$H_a$$H_b$), 3.85 – 3.82 (m, 1H, OCH_2C$H_a$$H_b$), 3.76 (dtd, *J* = 10.0, 5.7, 2.3, 1H, OC*H*), 3.41 (ddd, *J* = 11.5, 11.5, 2.9, 1H, OCH_2C$H_a$$H_b$), 3.16 (dd, *J* = 12.0, 10.0, 1H, OCHC$H_a$$H_b$), 2.80 (d, *J* = 5.7, 2H, C$H_2$$NH_2$); **^{13}C NMR** (126 MHz, MeOD-d_4): δ_C 153.9 (*C6*-H), 152.5 (*C1*), 152.5 (*C4*), 148.9 (*C4'*), 145.7 (*C1'*),134.0 (*C3*-H), 129.7 (*C2'*-H), 124.7 (*C3'*-H), 112.5 (*C2*), 105.7 (*C5*), 78.1 (O*C*H), 67.9 (OCH_2), 55.0 (OCH*C*H_2), 52.2 (OCH_2*C*H_2), 50.9 (N*C*H_2), 44.7 (*C*H_2NH_2); **HRMS** *m/z* (ES+): [Found; $(M+H)^+$ 447.0769. $C_{18}H_{20}BrN_6O_3$ requires $(M+H)^+$, 447.0775]; **LRMS** *m/z* (ESI+) 447.1 ($[M+H]^+$, 100%). **Elem. anal.** calcd. for $C_{18}H_{19}BrN_6O_3$: C, 48.3; H, 4.3; N, 18.8. Found C, 48.2; H, 4.2; N 18.7.

6.9.3 Synthesis of the bioreductive Chk1 inhibitor **52**

5-((8-Chloroisoquinolin-3-yl)((1-methyl-2-nitro-1H-imidazol-5-yl)methyl)amino)-3-((1-(dimethylamino)propan-2-yl)oxy)pyrazine-2-carbonitrile **52**

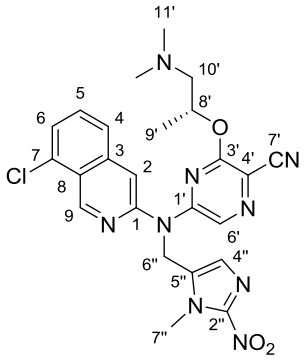

SAR020106 (9.5 mg, 0.025 mmol) was dissolved in DMF (1.5 ml), Cs_2CO_3 (16.4 mg, 0.05 mmol) added and stirred for 2 min. Chloride **38** was added (4.4 mg, 0.025 mmol), the reaction heated to 50 °C and monitored by HPLC. After 30 min the mixture was filtered and dried using a Genevac HT vaccum evaporator. The residue was purified by HPLC (see general experimental) and lyophilised to give **52** as a pale yellow solid (6.2 mg, 48%): **mp** 149-151 °C (H_2O); $\mathbf{\nu_{max}}$ (neat) cm^{-1}: 3661, 2979, 2889; **^{1}H NMR** (500 MHz, MeCN-d_3): δ_H 9.57 (s, 1H, C9-*H*), 7.88-7.86 (m, 3H, C6-*H*, C2-*H*, C6'-*H*), 7.76-7.71 (m, 2H, C4-*H*, C5-*H*), 6.99 (s, 1H, C4''-*H*), 5.55 (d, 1H, *J* = 16.6, C6''-H_a), 5.50 (d, 1H, *J* = 16.6, C6''-H_b), 5.36 (qdd, *J* = (4.7, 7.3, 6.3), 1H, C8'-*H*), 3.95 (s, 3H, C7''-H_3), 2.63 (dd, *J* = (12.9, 7.5), 1H, C10'-H_a), 2.41 (dd, *J* = (12.9, 3.5), 1H, C10'-H_b), 2.23 (s, 6H, N(C11'-$H_3)_2$), 1.32 (d, *J* = 6.3, 3H, C9'-H_3). **^{13}C NMR** (126 MHz, MeCN-d_3): δ_C 160.7 (*C3'*), 153.2 (*C1'*), 149.8 (*C9*-H), 149.3 (*C1*), 145.7 (*C2'*), 139.3 (*C7*), 134.4 (*C5''*), 132.0 (*C8*), 131.7 (*C5*-H), 128.1 (*C4*-H), 127.7 (*C4''*-H), 126.6 (*C6'*-H), 126.3 (*C6*-H), 124.6 (*C3*), 115.9 (*C7'*), 115.8 (*C2*-H), 105.8 (*C4'*), 72.3 (*C8'*-H), 63.4 (*C10'*-H_2), 45.2 (2 × *C11'*-H_3), 43.2 (*C6''*-H_2), 34.3 (*C7''*-H_3), 17.5 (*C9'*-H_3) ;

HRMS *m/z* (ES+): [Found; $(M+H)^+$ 522.1687. $C_{24}H_{24}ClN_9O_3$ requires $(M+H)^+$, 522.1763]; **LRMS** *m/z* (ESI+) 522.2 ($[M+H]^+$, 100%). **HPLC** (gemini NX column, 254 nm): Retention time 4.57 min, >99.9% purity.

APPENDIX A

Published papers

1) Reprinted with permission from ACS chemical biology, 8,7, **Cazares-Körner C**., Pires I.M., Swallow I.D., Grayer S.C., O'Connor L.J., Olcina M.M., Christlieb M., Conway S.J. and Hammond E.M., CH-01 is a hypoxia-activated prodrug that sensitizes cells to hypoxia/reoxygenation through inhibition of Chk1 and Aurora A, 1451-1459. Copyright 2013 American Chemical Society.[1]
2) Reproduced from Organic Chemistry Frontiers, 2, 9, O'Connor L.J., **Cazares-Körner C**., Saha J., Evans C.N.G., Stratford M.R.L., Hammond E.M., and Conway S.J., Efficient synthesis of 2-nitroimidazole derivatives and the bioreductive clinical candidate Evofosfamide (TH-302), 1026-1029. With permission from the Chinese Chemical Society (CCS), Shanghai Institute of Organic Chemistry (SIOC), and the Royal Society of Chemistry.[2]

[1] The data published in this paper is part of Chapter 2.
[2] Some of the data published in this paper is part of Chapter 3.

APPENDIX B

Synthesis and purification of compound **52** for NMR analysis

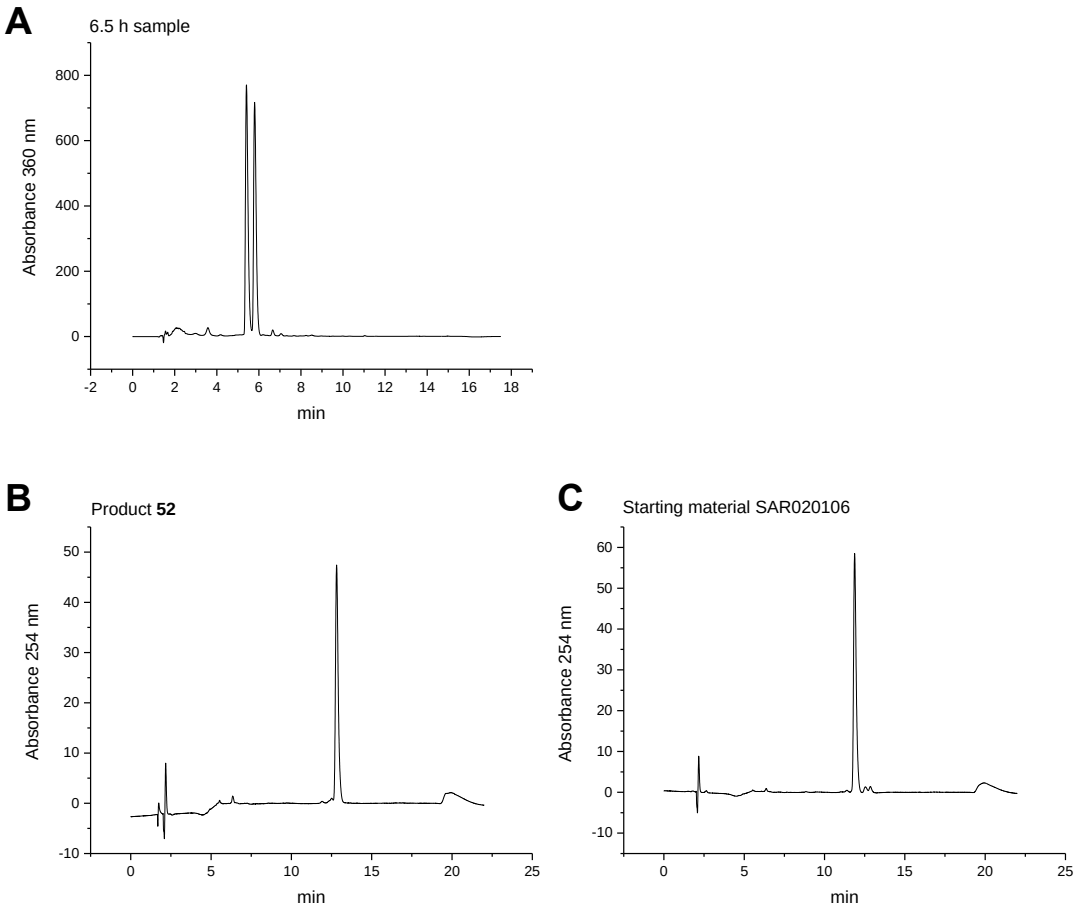

Figure B. HPLC traces of synthesis and purification of 52 for NMR analysis.
A) HPLC trace of the reaction mixture after 6.5 h. At this stage 47% conversion into product **52** (retention time 5.80 min) had taken place and 51% starting material SAR020106 (retention time 5.41 min) was left, as judged by peak integration. B) HPLC trace of product **52** after purification. C) HPLC trace of recovered SAR020106.

APPENDIX C

Calibration curves

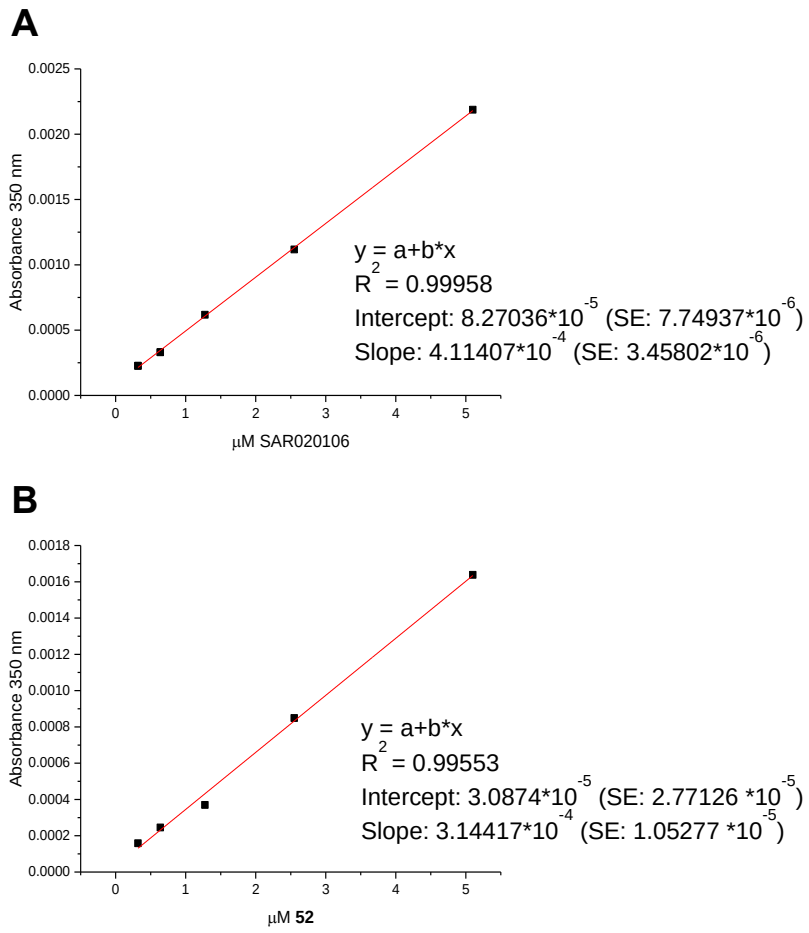

Figure C. Calibration curves for quantification of SAR020106, amine 56 and compound 52.
Calibration curves for A) SAR020106 and B) **52** were obtained in order to quantify **52** and metabolites. Amine **56** was quantified using the calibration for **52**, based on the identical UV spectrum (C).

REFERENCES

Abbott, Alison. 2003. “Cell Culture: Biology’s New Dimension.” *Nature* 424 (6951): 870–72. doi:10.1038/424870a.

Aebersold, D M, P Burri, K T Beer, J Laissue, V Djonov, R H Greiner, and G L Semenza. 2001. “Expression of Hypoxia-Inducible Factor-1alpha: A Novel Predictive and Prognostic Parameter in the Radiotherapy of Oropharyngeal Cancer.” *Cancer Research* 61 (7): 2911–16.

Al-Ahmadie, Hikmat, Gopa Iyer, Marcel Hohl, Saurabh Asthana, Akiko Inagaki, Nikolaus Schultz, Aphrothiti J Hanrahan, et al. 2014. “Synthetic Lethality in ATM-Deficient RAD50-Mutant Tumors Underlies Outlier Response to Cancer Therapy.” *Cancer Discovery* 4 (9): 1014–21. doi:10.1158/2159-8290.CD-14-0380.

Andrushchenko, Valery V, Hans J Vogel, and Elmar J Prenner. 2007. “Optimization of the Hydrochloric Acid Concentration Used for Trifluoroacetate Removal from Synthetic Peptides.” *Journal of Peptide Science : An Official Publication of the European Peptide Society* 13 (1): 37–43. doi:10.1002/psc.793.

Anglana, Mauro, Françoise Apiou, Aaron Bensimon, and Michelle Debatisse. 2003. “Dynamics of DNA Replication in Mammalian Somatic Cells: Nucleotide Pool Modulates Origin Choice and Interorigin Spacing.” *Cell* 114 (3): 385–94.

Armarego, W. L. F., and C. L. L. Chai. 2003. *Purification of Laboratory Chamicals*. 5th ed. Butterworth-Heinemann.

Arteel, Gavin E., Ronald G. Thurman, and James A. Raleigh. 1998. “Reductive Metabolism of the Hypoxia Marker Pimonidazole Is Regulated by Oxygen Tension Independent of the Pyridine Nucleotide Redox State.” *European Journal of Biochemistry* 253 (3): 743–50. doi:10.1046/j.1432-1327.1998.2530743.x.

Asato, Goro, and Gerald Berkelhammer. 1972. “Nitroheterocyclic Antimicrobial Agents. 1-Methyl-2-Nitro-5-Imidazolyl Derivatives.” *Journal of Medicinal Chemistry* 15 (10). American Chemical Society: 1086–88. doi:10.1021/jm00280a030.

Asby, D J, F Cuda, F Hoakwie, E Miranda, and A Tavassoli. 2014. “HIF-1 Promotes the Expression of Its A-Subunit via an Epigenetically Regulated Transactivation Loop.” *Molecular bioSystems* 10 (10): 2505–8. doi:10.1039/c4mb00351a.

Aylon, Yael, Batia Liefshitz, and Martin Kupiec. 2004. “The CDK Regulates Repair of Double-Strand Breaks by Homologous Recombination during the Cell Cycle.” *The EMBO Journal* 23 (24): 4868–75. doi:10.1038/sj.emboj.7600469.

Bahassi, E M, J L Ovesen, A L Riesenberg, W Z Bernstein, P E Hasty, and P J Stambrook. 2008. “The Checkpoint Kinases Chk1 and Chk2 Regulate the Functional Associations between hBRCA2 and Rad51 in Response to DNA Damage.” *Oncogene* 27 (28): 3977–85. doi:10.1038/onc.2008.17.

Bartek, J, and J Lukas. 2001. “Mammalian G1- and S-Phase Checkpoints in Response to DNA Damage.” *Current Opinion in Cell Biology* 13 (6): 738–47.

Bartkova, Jirina, Zuzana Horejsí, Karen Koed, Alwin Krämer, Frederic Tort, Karsten Zieger, Per Guldberg, et al. 2005. “DNA Damage Response as a Candidate Anti-Cancer Barrier in Early Human Tumorigenesis.” *Nature* 434 (7035). Macmillian Magazines Ltd.: 864–70. doi:10.1038/nature03482.

Bartkova, Jirina, Nousin Rezaei, Michalis Liontos, Panagiotis Karakaidos, Dimitris Kletsas, Natalia Issaeva, Leandros-Vassilios F Vassiliou, et al. 2006. “Oncogene-Induced Senescence Is Part of the Tumorigenesis Barrier Imposed by DNA Damage Checkpoints.” *Nature* 444 (7119): 633–37. doi:10.1038/nature05268.

Bayer, Christine, Kuangyu Shi, Sabrina T Astner, Constantin-Alin Maftei, and Peter Vaupel. 2011. “Acute versus Chronic Hypoxia: Why a Simplified Classification Is Simply Not Enough.” *International Journal of Radiation Oncology, Biology, Physics* 80 (4): 965–68. doi:10.1016/j.ijrobp.2011.02.049.

Beck, Halfdan, Viola Nähse-Kumpf, Marie Sofie Yoo Larsen, Karen A O’Hanlon, Sebastian Patzke, Christian Holmberg, Jakob Mejlvang, et al. 2012. “Cyclin-Dependent Kinase Suppression by WEE1 Kinase Protects the Genome through Control of Replication Initiation and Nucleotide Consumption.” *Molecular and Cellular Biology* 32 (20): 4226–36. doi:10.1128/MCB.00412-12.

Bencokova, Zuzana, Muriel R Kaufmann, Isabel M Pires, Philip S Lecane, Amato J Giaccia, and Ester M Hammond. 2009. “ATM Activation and Signaling under Hypoxic Conditions.” *Molecular and Cellular Biology* 29 (2): 526–37. doi:10.1128/MCB.01301-08.

Bendell, Johanna C., Cathy Eng, Kathleen N. Moore, Howard A. Burris, Funda Meric-Bernstam, Suzanne Fields Jones, Sarina Anne Piha-Paul, et al. 2015. “Checkpoint Kinase (CHK) 1/2 Inhibitor LY2606368 in a Phase I, Dose-Expansion Study in Patients (pts) with Metastatic Squamous Cell Carcinoma (mSCC) of the Anus.” *ASCO Meeting Abstracts* 33 (15_suppl): 3520.

Bergers, Gabriele, and Laura E Benjamin. 2003. “Tumorigenesis and the Angiogenic Switch.” *Nature Reviews. Cancer* 3 (6): 401–10. doi:10.1038/nrc1093.

Berra, Edurne, Emmanuel Benizri, Amandine Ginouvès, Véronique Volmat, Danièle Roux, and Jacques Pouysségur. 2003. “HIF Prolyl-Hydroxylase 2 Is the Key Oxygen Sensor Setting Low Steady-State Levels of HIF-1alpha in Normoxia.” *The EMBO Journal* 22 (16): 4082–90. doi:10.1093/emboj/cdg392.

Bertoni, F, A M Codegoni, D Furlan, M G Tibiletti, C Capella, and M Broggini. 1999. “CHK1 Frameshift Mutations in Genetically Unstable Colorectal and Endometrial Cancers.” *Genes, Chromosomes & Cancer* 26 (2): 176–80.

Bester, Assaf C., Maayan Roniger, Yifat S. Oren, Michael M. Im, Dan Sarni, Malka Chaoat, Aaron Bensimon, Gideon Zamir, Donna S. Shewach, and Batsheva Kerem. 2011. “Nucleotide Deficiency Promotes Genomic Instability in Early Stages of Cancer Development.” *Cell* 145 (3): 435–46. doi:10.1016/j.cell.2011.03.044.

Bindra, Ranjit S, Paul J Schaffer, Alice Meng, Jennifer Woo, Kårstein Måseide, Matt E Roth, Paul Lizardi, David W Hedley, Robert G Bristow, and Peter M Glazer. 2004. “Down-Regulation of Rad51 and Decreased Homologous Recombination in Hypoxic Cancer Cells.” *Molecular and Cellular Biology* 24 (19): 8504–18. doi:10.1128/MCB.24.19.8504-8518.2004.

Blasina, Alessandra, Jill Hallin, Enhong Chen, Maria Elena Arango, Eugenia Kraynov, James Register, Stephan Grant, et al. 2008. “Breaching the DNA Damage Checkpoint via PF-00477736, a Novel Small-Molecule Inhibitor of Checkpoint Kinase 1.” *Molecular Cancer Therapeutics* 7 (8): 2394–2404. doi:10.1158/1535-7163.MCT-07-2391.

Borst, Gerben R, Martin McLaughlin, Joan N Kyula, Sari Neijenhuis, Aadil Khan, James Good, Shane Zaidi, et al. 2013. “Targeted Radiosensitization by the Chk1 Inhibitor SAR-020106.” *International Journal of Radiation Oncology, Biology, Physics* 85 (4): 1110–18. doi:10.1016/j.ijrobp.2012.08.006.

Bos, Reinhard, Petra van der Groep, Astrid E. Greijer, Avi Shvarts, Sybren Meijer, Herbert M. Pinedo, Gregg L. Semenza, Paul J. van Diest, and Elsken van der Wall. 2003. “Levels of Hypoxia-Inducible Factor-1? Independently Predict Prognosis in Patients with Lymph Node Negative Breast Carcinoma.” *Cancer* 97 (6): 1573–81. doi:10.1002/cncr.11246.

Boutros, Rose, Christine Dozier, and Bernard Ducommun. 2006. “The When and Wheres of CDC25 Phosphatases.” *Current Opinion in Cell Biology* 18 (2): 185–91. doi:10.1016/j.ceb.2006.02.003.

Boutros, Rose, Valérie Lobjois, and Bernard Ducommun. 2007. “CDC25 Phosphatases in Cancer Cells: Key Players? Good Targets?” *Nature Reviews Cancer* 7 (7). Nature Publishing Group: 495–507. doi:10.1038/nrc2169.

Branzei, Dana, and Marco Foiani. 2010. “Maintaining Genome Stability at the Replication Fork.” *Nature Reviews. Molecular Cell Biology* 11 (3). Nature Publishing Group: 208–19. doi:10.1038/nrm2852.

Brega, N., G. A. McArthur, C. Britten, S. G. Wong, E. Wang, K. D. Wilner, A. Blasina, G. K. Schwartz, J. Gallo, and A. N. Tse. 2010. “Phase I Clinical Trial of Gemcitabine (GEM) in Combination with PF-00477736 (PF-736), a Selective Inhibitor of CHK1 Kinase.” *ASCO Meeting Abstracts* 28 (15_suppl): 3062.

Bristow, Robert G., and Richard P. Hill. 2008. “Hypoxia and Metabolism: Hypoxia, DNA Repair and Genetic Instability.” *Nature Reviews Cancer* 8 (3): 180–92. doi:10.1038/nrc2344.

Brnardic, Edward J, Robert M Garbaccio, Mark E Fraley, Edward S Tasber, Justin T Steen, Kenneth L Arrington, Vadim Y Dudkin, et al. 2007. “Optimization of a Pyrazoloquinolinone Class of Chk1 Kinase Inhibitors.” *Bioorganic & Medicinal Chemistry Letters* 17 (21): 5989–94. doi:10.1016/j.bmcl.2007.07.051.

Brooks, K, V Oakes, B Edwards, M Ranall, P Leo, S Pavey, A Pinder, et al. 2013. “A Potent Chk1 Inhibitor Is Selectively Cytotoxic in Melanomas with High Levels of Replicative Stress.” *Oncogene* 32 (6): 788–96. doi:10.1038/onc.2012.72.

Brough, Rachel, Jessica R Frankum, Sara Costa-Cabral, Christopher J Lord, and Alan Ashworth. 2011. “Searching for Synthetic Lethality in Cancer.” *Current Opinion in Genetics & Development* 21 (1): 34–41. doi:10.1016/j.gde.2010.10.009.

Brown, J M. 1979. “Evidence for Acutely Hypoxic Cells in Mouse Tumours, and a Possible Mechanism of Reoxygenation.” *The British Journal of Radiology* 52 (620): 650–56. doi:10.1259/0007-1285-52-620-650.

———. 1984. “Clinical Trials of Radiosensitizers: What Should We Expect?” *International Journal of Radiation Oncology, Biology, Physics* 10 (3): 425–29.

Brown, J M, and M J Lemmon. 1991. “Tumor Hypoxia Can Be Exploited to Preferentially Sensitize Tumors to Fractionated Irradiation.” *International Journal of Radiation Oncology, Biology, Physics* 20 (3): 457–61.

Brugarolas, J, C Chandrasekaran, J I Gordon, D Beach, T Jacks, and G J Hannon. 1995. “Radiation-Induced Cell Cycle Arrest Compromised by p21 Deficiency.” *Nature* 377 (6549): 552–57. doi:10.1038/377552a0.

Bruick, R K, and S L McKnight. 2001. “A Conserved Family of Prolyl-4-Hydroxylases That Modify HIF.” *Science (New York, N.Y.)* 294 (5545): 1337–40. doi:10.1126/science.1066373.

Bryant, Christopher, Rebecca Rawlinson, and Andrew J Massey. 2014. “Chk1 Inhibition as a Novel Therapeutic Strategy for Treating Triple-Negative Breast and Ovarian Cancers.” *BMC Cancer* 14 (January): 570. doi:10.1186/1471-2407-14-570.

Bryant, Christopher, Kirsten Scriven, and Andrew J Massey. 2014. “Inhibition of the Checkpoint Kinase Chk1 Induces DNA Damage and Cell Death in Human Leukemia and Lymphoma Cells.” *Molecular Cancer* 13 (January): 147. doi:10.1186/1476-4598-13-147.

Burgess, Rebecca C, Bharat Burman, Michael J Kruhlak, and Tom Misteli. 2014. “Activation of DNA Damage Response Signaling by Condensed Chromatin.” *Cell Reports* 9 (5): 1703–17. doi:10.1016/j.celrep.2014.10.060.

Burns, Noah Z, Mikkel Jessing, and Phil S Baran. 2009. “Total Synthesis of Haouamine A: The Indeno-Tetrahydropyridine Core.” *Tetrahedron* 65 (33): 6600–6610. doi:10.1016/j.tet.2009.05.075.

Burri, Philipp, Valentin Djonov, Daniel M Aebersold, Katja Lindel, Ueli Studer, Hans J Altermatt, Luca Mazzucchelli, Richard H Greiner, and Günther Gruber. 2003. “Significant Correlation of Hypoxia-Inducible Factor-1alpha with Treatment Outcome in Cervical Cancer Treated with Radical Radiotherapy.” *International Journal of Radiation Oncology, Biology, Physics* 56 (2): 494–501.

Busby, Ericka C., Dru F. Leistritz, Robert T. Abraham, Larry M. Karnitz, and Jann N. Sarkaria. 2000. “The Radiosensitizing Agent 7-Hydroxystaurosporine (UCN-01) Inhibits the DNA Damage Checkpoint Kinase hChk1.” *Cancer Research* 60 (8): 2108–12.

Busino, Luca, Maddalena Donzelli, Massimo Chiesa, Daniele Guardavaccaro, Dvora Ganoth, N Valerio Dorrello, Avram Hershko, Michele Pagano, and Giulio F Draetta. 2003. “Degradation of Cdc25A by Beta-TrCP during S Phase and in Response to DNA Damage.” *Nature* 426 (6962): 87–91. doi:10.1038/nature02082.

Byun, Tony S, Marcin Pacek, Muh-ching Yee, Johannes C Walter, and Karlene A Cimprich. 2005. “Functional Uncoupling of MCM Helicase and DNA Polymerase Activities Activates the ATR-Dependent Checkpoint.” *Genes & Development* 19 (9): 1040–52. doi:10.1101/gad.1301205.

Calvo, Emiliano, Victor J Chen, Mark Marshall, Ute Ohnmacht, Scott M Hynes, Elizabeth Kumm, H Bruce Diaz, et al. 2014. “Preclinical Analyses and Phase I Evaluation of LY2603618 Administered in Combination with Pemetrexed and Cisplatin in Patients with Advanced Cancer.” *Investigational New Drugs* 32 (5): 955–68. doi:10.1007/s10637-014-0114-5.

Cavalleri, Bruno, Roberto Ballotta, and Gian Carlo Lancini. 1972. “Synthesis of 1-Alkyl-2-Nitroimidazole-5-Carboxaldehydes.” *Journal of Heterocyclic Chemistry* 9 (5): 979–84. doi:10.1002/jhet.5570090502.

Cavelier, Cindy, Christine Didier, Naïs Prade, Véronique Mansat-De Mas, Stéphane Manenti, Christian Recher, Cécile Demur, and Bernard Ducommun. 2009. “Constitutive Activation of the DNA Damage Signaling Pathway in Acute Myeloid Leukemia with Complex Karyotype: Potential Importance for Checkpoint Targeting Therapy.” *Cancer Research* 69 (22): 8652–61. doi:10.1158/0008-5472.CAN-09-0939.

Cazares-Körner, Cindy, Isabel M Pires, I Diane Swallow, Samuel C Grayer, Liam J O’Connor, Monica M Olcina, Martin Christlieb, Stuart J Conway, and Ester M Hammond. 2013. “CH-01 Is a Hypoxia-Activated Prodrug That Sensitizes Cells to Hypoxia/reoxygenation through Inhibition of Chk1 and Aurora A.” *ACS Chemical Biology* 8 (7): 1451–59. doi:10.1021/cb4001537.

Celli, Claudia M., Namphuong Tran, Richard Knox, and Anil K. Jaiswal. 2006. “NRH:quinone Oxidoreductase 2 (NQO2) Catalyzes Metabolic Activation of Quinones and Anti-Tumor Drugs.” *Biochemical Pharmacology* 72 (3): 366–76. doi:10.1016/j.bcp.2006.04.029.

Chan, Denise A, and Amato J Giaccia. 2011. “Harnessing Synthetic Lethal Interactions in Anticancer Drug Discovery.” *Nature Reviews. Drug Discovery* 10 (5): 351–64. doi:10.1038/nrd3374.

Chan, N., I. M. Pires, Z. Bencokova, C. Coackley, K. R. Luoto, N. Bhogal, M. Lakshman, et al. 2010. “Contextual Synthetic Lethality of Cancer Cell Kill Based on the Tumor Microenvironment.” *Cancer Research* 70 (20): 8045–54. doi:10.1158/0008-5472.CAN-10-2352.

Chan, Norman, Marianne Koritzinsky, Helen Zhao, Ranjit Bindra, Peter M Glazer, Simon Powell, Abdellah Belmaaza, Brad Wouters, and Robert G Bristow. 2008. “Chronic Hypoxia Decreases Synthesis of Homologous Recombination Proteins to Offset Chemoresistance and Radioresistance.” *Cancer Research* 68 (2): 605–14. doi:10.1158/0008-5472.CAN-07-5472.

Chan, T A, H Hermeking, C Lengauer, K W Kinzler, and B Vogelstein. 1999. “14-3-3Sigma Is Required to Prevent Mitotic Catastrophe after DNA Damage.” *Nature* 401 (6753): 616–20. doi:10.1038/44188.

Chandor, Alexia, Sylvie Dijols, Booma Ramassamy, Yves Frapart, Daniel Mansuy, Dennis Stuehr, Nuala Helsby, and Jean-Luc Boucher. 2008. “Metabolic Activation of the Antitumor Drug 5-(Aziridin-1-Yl)-2,4-Dinitrobenzamide (CB1954) by NO Synthases.” *Chemical Research in Toxicology* 21 (4): 836–43. doi:10.1021/tx7004234.

Chen, Clark C, Richard D Kennedy, Samuel Sidi, A Thomas Look, and Alan D’Andrea. 2009. “CHK1 Inhibition as a Strategy for Targeting Fanconi Anemia (FA) DNA Repair Pathway Deficient Tumors.” *Molecular Cancer* 8 (January): 24. doi:10.1186/1476-4598-8-24.

Chen, Mei-Shya, Christine E Ryan, and Helen Piwnica-Worms. 2003. “Chk1 Kinase Negatively Regulates Mitotic Function of Cdc25A Phosphatase through 14-3-3 Binding.” *Molecular and Cellular Biology* 23 (21): 7488–97.

Chen, Ping, Chun Luo, Yali Deng, Kevin Ryan, James Register, Stephen Margosiak, Anna Tempczyk-Russell, et al. 2000. “Implications for Chk1 Regulation: The 1.7 Å Crystal Structure of Human Cell Cycle Checkpoint Kinase Chk1.” *Cell* 100 (6): 681–92. doi:10.1016/S0092-8674(00)80704-7.

Chen, Tao, Peter A Stephens, Fiona K Middleton, and Nicola J Curtin. 2012. “Targeting the S and G2 Checkpoint to Treat Cancer.” *Drug Discovery Today* 17 (5-6): 194–202. doi:10.1016/j.drudis.2011.12.009.

Chen, Yu, and Longqin Hu. 2009. “Design of Anticancer Prodrugs for Reductive Activation.” *Medicinal Research Reviews* 29 (1): 29–64. doi:10.1002/med.20137.

Chou, Danny M, and Stephen J Elledge. 2006. “Tipin and Timeless Form a Mutually Protective Complex Required for Genotoxic Stress Resistance and Checkpoint Function.” *Proceedings of the National Academy of Sciences of the United States of America* 103 (48): 18143–47. doi:10.1073/pnas.0609251103.

Chou, S-C, Y Azuma, M A Varia, and J A Raleigh. 2004. “Evidence That Involucrin, a Marker for Differentiation, Is Oxygen Regulated in Human Squamous Cell Carcinomas.” *British Journal of Cancer* 90 (3): 728–35. doi:10.1038/sj.bjc.6601585.

Ciccia, Alberto, and Stephen J Elledge. 2010. “The DNA Damage Response: Making It Safe to Play with Knives.” *Molecular Cell* 40 (2): 179–204. doi:10.1016/j.molcel.2010.09.019.

Cobb, Jennifer A, Lotte Bjergbaek, Kenji Shimada, Christian Frei, and Susan M Gasser. 2003. “DNA Polymerase Stabilization at Stalled Replication Forks Requires Mec1 and the RecQ Helicase Sgs1.” *The EMBO Journal* 22 (16): 4325–36. doi:10.1093/emboj/cdg391.

Cole, Kristina A, Jonathan Huggins, Michael Laquaglia, Chase E Hulderman, Mike R Russell, Kristopher Bosse, Sharon J Diskin, et al. 2011. “RNAi Screen of the Protein Kinome Identifies Checkpoint Kinase 1 (CHK1) as a Therapeutic Target in Neuroblastoma.” *Proceedings of the National Academy of Sciences of the United States of America* 108 (8): 3336–41. doi:10.1073/pnas.1012351108.

Conti, Chiara, Barbara Saccà, John Herrick, Claude Lalou, Yves Pommier, and Aaron Bensimon. 2007. “Replication Fork Velocities at Adjacent Replication Origins Are Coordinately Modified during DNA Replication in Human Cells.” *Molecular Biology of the Cell* 18 (8): 3059–67. doi:10.1091/mbc.E06-08-0689.

Converso, Antonella, Timothy Hartingh, Robert M Garbaccio, Edward Tasber, Keith Rickert, Mark E Fraley, Youwei Yan, et al. 2009. “Development of Thioquinazolinones, Allosteric Chk1 Kinase Inhibitors.” *Bioorganic & Medicinal Chemistry Letters* 19 (4): 1240–44. doi:10.1016/j.bmcl.2008.12.076.

Coumar, Mohane Selvaraj, Chang-Ying Chu, Cheng-Wei Lin, Hui-Yi Shiao, Yun-Lung Ho, Randheer Reddy, Wen-Hsing Lin, et al. 2010. “Fast-Forwarding Hit to Lead: Aurora and Epidermal Growth Factor Receptor Kinase Inhibitor Lead Identification.” *Journal of Medicinal Chemistry* 53 (13): 4980–88. doi:10.1021/jm1000198.

Coumar, Mohane Selvaraj, Ming-Tsung Tsai, Chang-Ying Chu, Biing-Jiun Uang, Wen-Hsing Lin, Chun-Yu Chang, Teng-Yuan Chang, et al. 2010. “Identification, SAR Studies, and X-Ray Co-Crystallographic Analysis of a Novel Furanopyrimidine Aurora Kinase A Inhibitor.” *ChemMedChem* 5 (2): 255–67. doi:10.1002/cmdc.200900339.

Crosio, Claudia, Gian Maria Fimia, Romain Loury, Masashi Kimura, Yukio Okano, Hongyi Zhou, Subrata Sen, C David Allis, and Paolo Sassone-Corsi. 2002. “Mitotic Phosphorylation of Histone H3: Spatio-Temporal Regulation by Mammalian Aurora Kinases.” *Molecular and Cellular Biology* 22 (3): 874–85.

Cui, Shi-Yun, Jia-Yuan Huang, Yi-Tian Chen, Hai-Zhu Song, Gui-Chun Huang, Wei De, Rui Wang, and Long-Bang Chen. 2013. “The Role of Aurora A in Hypoxia-Inducible Factor 1α-Promoting Malignant Phenotypes of Hepatocelluar Carcinoma.” *Cell Cycle (Georgetown, Tex.)* 12 (17): 2849–66. doi:10.4161/cc.25916.

Danson, S, T H Ward, J Butler, and M Ranson. 2004. “DT-Diaphorase: A Target for New Anticancer Drugs.” *Cancer Treatment Reviews* 30 (5): 437–49. doi:10.1016/j.ctrv.2004.01.002.

Dar, Altaf A, Laura W Goff, Shahana Majid, Jordan Berlin, and Wael El-Rifai. 2010. “Aurora Kinase Inhibitors--Rising Stars in Cancer Therapeutics?” *Molecular Cancer Therapeutics* 9 (2): 268–78. doi:10.1158/1535-7163.MCT-09-0765.

Daud, Adil I, Michelle T Ashworth, Jonathan Strosberg, Jonathan W Goldman, David Mendelson, Gregory Springett, Alan P Venook, et al. 2015. “Phase I Dose-Escalation Trial of Checkpoint Kinase 1 Inhibitor MK-8776 as Monotherapy and in Combination with Gemcitabine in Patients with Advanced Solid Tumors.” *Journal of Clinical Oncology : Official Journal of the American Society of Clinical Oncology* 33 (9): 1060–66. doi:10.1200/JCO.2014.57.5027.

De Souza, C P, K A Ellem, and B G Gabrielli. 2000. “Centrosomal and Cytoplasmic Cdc2/cyclin B1 Activation Precedes Nuclear Mitotic Events.” *Experimental Cell Research* 257 (1): 11–21. doi:10.1006/excr.2000.4872.

Deng, Chuxia, Pumin Zhang, J. Wade Harper, Stephen J. Elledge, and Philip Leder. 1995. “Mice Lacking p21CIP1/WAF1 Undergo Normal Development, but Are Defective in G1 Checkpoint Control.” *Cell* 82 (4): 675–84. doi:10.1016/0092-8674(95)90039-X.

Denny, W A. 2000. “The Role of Hypoxia-Activated Prodrugs in Cancer Therapy.” *The Lancet. Oncology* 1 (1): 25–29. doi:10.1016/S1470-2045(00)00006-1.

Dewhirst, Mark W, Yiting Cao, and Benjamin Moeller. 2008. “Cycling Hypoxia and Free Radicals Regulate Angiogenesis and Radiotherapy Response.” *Nature Reviews. Cancer* 8 (6): 425–37. doi:10.1038/nrc2397.

Di Micco, Raffaella, Marzia Fumagalli, Angelo Cicalese, Sara Piccinin, Patrizia Gasparini, Chiara Luise, Catherine Schurra, et al. 2006. “Oncogene-Induced Senescence Is a DNA Damage Response Triggered by DNA Hyper-Replication.” *Nature* 444 (7119): 638–42. doi:10.1038/nature05327.

Doi, Toshihiko, Takayuki Yoshino, Kohei Shitara, Nobuaki Matsubara, Nozomu Fuse, Yoichi Naito, Kazunori Uenaka, Takashi Nakamura, Scott M Hynes, and Aimee Bence Lin. 2015. “Phase I Study of LY2603618, a CHK1 Inhibitor, in Combination with Gemcitabine in Japanese Patients with Solid Tumors.” *Anti-Cancer Drugs*, August. doi:10.1097/CAD.0000000000000278.

Duan, Jian-Xin, Hailong Jiao, Jacob Kaizerman, Timothy Stanton, James W Evans, Leslie Lan, Gustavo Lorente, et al. 2008. “Potent and Highly Selective Hypoxia-Activated Achiral Phosphoramidate Mustards as Anticancer Drugs.” *Journal of Medicinal Chemistry* 51 (8): 2412–20. doi:10.1021/jm701028q.

Eklund, Hans, Ulla Uhlin, Mathias Färnegårdh, Derek T. Logan, and Pär Nordlund. 2001. “Structure and Function of the Radical Enzyme Ribonucleotide Reductase.” *Progress in Biophysics and Molecular Biology* 77 (3): 177–268. doi:10.1016/S0079-6107(01)00014-1.

Engelke, Carl G, Leslie A Parsels, Yushen Qian, Qiang Zhang, David Karnak, Jordan R Robertson, Daria M Tanska, et al. 2013. “Sensitization of Pancreatic Cancer to Chemoradiation by the Chk1 Inhibitor MK8776.” *Clinical Cancer Research : An Official Journal of the American Association for Cancer Research* 19 (16): 4412–21. doi:10.1158/1078-0432.CCR-12-3748.

Errico, Alessia, Vincenzo Costanzo, and Tim Hunt. 2007. “Tipin Is Required for Stalled Replication Forks to Resume DNA Replication after Removal of Aphidicolin in Xenopus Egg Extracts.” *Proceedings of the National Academy of Sciences of the United States of America* 104 (38): 14929–34. doi:10.1073/pnas.0706347104.

Evans, S M, W T Jenkins, M Shapiro, and C J Koch. 1997. “Evaluation of the Concept of ‘Hypoxic Fraction’ as a Descriptor of Tumor Oxygenation Status.” *Advances in Experimental Medicine and Biology* 411 (January): 215–25.

Ferrao, P T, E P Bukczynska, R W Johnstone, and G A McArthur. 2012. “Efficacy of CHK Inhibitors as Single Agents in MYC-Driven Lymphoma Cells.” *Oncogene* 31 (13): 1661–72. doi:10.1038/onc.2011.358.

Fishler, T, Y-Y Li, R-H Wang, H-S Kim, K Sengupta, A Vassilopoulos, T Lahusen, et al. 2010. “Genetic Instability and Mammary Tumor Formation in Mice Carrying Mammary-Specific Disruption of Chk1 and p53.” *Oncogene* 29 (28). Macmillan Publishers Limited: 4007–17. doi:10.1038/onc.2010.163.

Flashman, Emily, Lee M Hoffart, Refaat B Hamed, J Martin Bollinger, Carsten Krebs, and Christopher J Schofield. 2010. “Evidence for the Slow Reaction of Hypoxia-Inducible Factor Prolyl Hydroxylase 2 with Oxygen.” *The FEBS Journal* 277 (19): 4089–99. doi:10.1111/j.1742-4658.2010.07804.x.

Foloppe, Nicolas, Lisa M. Fisher, Rob Howes, Peter Kierstan, Andrew Potter, Alan G. S. Robertson, and Allan E. Surgenor. 2005. “Structure-Based Design of Novel Chk1 Inhibitors: Insights into Hydrogen Bonding and Protein−Ligand Affinity.” *Journal of Medicinal Chemistry* 48 (13): 4332–45. doi:10.1021/jm049022c.

Forment, Josep V, Melanie Blasius, Ilaria Guerini, and Stephen P Jackson. 2011. “Structure-Specific DNA Endonuclease Mus81/Eme1 Generates DNA Damage Caused by Chk1 Inactivation.” *PloS One* 6 (8): e23517. doi:10.1371/journal.pone.0023517.

Franken, Nicolaas A P, Hans M Rodermond, Jan Stap, Jaap Haveman, and Chris van Bree. 2006. “Clonogenic Assay of Cells in Vitro.” *Nature Protocols* 1 (5). Nature Publishing Group: 2315–19. doi:10.1038/nprot.2006.339.

Freiberg, Rachel A, Ester M Hammond, Mary Jo Dorie, Scott M Welford, and Amato J Giaccia. 2006. “DNA Damage during Reoxygenation Elicits a Chk2-Dependent Checkpoint Response.” *Molecular and Cellular Biology* 26 (5): 1598–1609. doi:10.1128/MCB.26.5.1598-1609.2006.

Freiberg, Rachel A, Adam J Krieg, Amato J Giaccia, and Ester M Hammond. 2006. “Checking in on Hypoxia/reoxygenation.” *Cell Cycle (Georgetown, Tex.)* 5 (12): 1304–7.

Furuta, T, R L Hayward, L-H Meng, H Takemura, G J Aune, W M Bonner, M I Aladjem, K W Kohn, and Y Pommier. 2006. “p21CDKN1A Allows the Repair of Replication-Mediated DNA Double-Strand Breaks Induced by Topoisomerase I and Is Inactivated by the Checkpoint Kinase Inhibitor 7-Hydroxystaurosporine.” *Oncogene* 25 (20): 2839–49. doi:10.1038/sj.onc.1209313.

Fuse, E, H Tanii, N Kurata, H Kobayashi, Y Shimada, T Tamura, Y Sasaki, et al. 1998. “Unpredicted Clinical Pharmacology of UCN-01 Caused by Specific Binding to Human alpha1-Acid Glycoprotein.” *Cancer Research* 58 (15): 3248–53.

Fuse, Eiichi, Takashi Kuwabara, Alex Sparreboom, Edward A Sausville, and William D Figg. 2005. “Review of UCN-01 Development: A Lesson in the Importance of Clinical Pharmacology.” *Journal of Clinical Pharmacology* 45 (4): 394–403. doi:10.1177/0091270005274549.

Garrett, Michelle D, and Ian Collins. 2011. “Anticancer Therapy with Checkpoint Inhibitors: What, Where and When?” *Trends in Pharmacological Sciences* 32 (5): 308–16. doi:10.1016/j.tips.2011.02.014.

Ge, Xin Quan, and J Julian Blow. 2010. “Chk1 Inhibits Replication Factory Activation but Allows Dormant Origin Firing in Existing Factories.” *The Journal of Cell Biology* 191 (7): 1285–97. doi:10.1083/jcb.201007074.

Ge, Xin Quan, Dean A Jackson, and J Julian Blow. 2007. “Dormant Origins Licensed by Excess Mcm2-7 Are Required for Human Cells to Survive Replicative Stress.” *Genes & Development* 21 (24): 3331–41. doi:10.1101/gad.457807.

Giaccia, Amato, Bronwyn G Siim, and Randall S Johnson. 2003. “HIF-1 as a Target for Drug Development.” *Nature Reviews. Drug Discovery* 2 (10): 803–11. doi:10.1038/nrd1199.

Gibson, Shannon L, Ranjit S Bindra, and Peter M Glazer. 2005. “Hypoxia-Induced Phosphorylation of Chk2 in an Ataxia Telangiectasia Mutated-Dependent Manner.” *Cancer Research* 65 (23): 10734–41. doi:10.1158/0008-5472.CAN-05-1160.

Gibson, Shannon L., Ranjit S. Bindra, and Peter M. Glazer. 2009. “CHK2-Dependent Phosphorylation of BRCA1 in Hypoxia,” July.

Gilad, Oren, Barzin Y Nabet, Ryan L Ragland, David W Schoppy, Kevin D Smith, Amy C Durham, and Eric J Brown. 2010. “Combining ATR Suppression with Oncogenic Ras Synergistically Increases Genomic Instability, Causing Synthetic Lethality or Tumorigenesis in a Dosage-Dependent Manner.” *Cancer Research* 70 (23): 9693–9702. doi:10.1158/0008-5472.CAN-10-2286.

Glazer, Peter M, Denise C Hegan, Yuhong Lu, Jennifer Czochor, and Susan E Scanlon. 2013. “Hypoxia and DNA Repair.” *The Yale Journal of Biology and Medicine* 86 (4): 443–51.

González Besteiro, Marina A, and Vanesa Gottifredi. 2015. “The Fork and the Kinase: A DNA Replication Tale from a CHK1 Perspective.” *Mutation Research. Reviews in Mutation Research* 763 (January): 168–80. doi:10.1016/j.mrrev.2014.10.003.

Görgün, Güllü, Elisabetta Calabrese, Teru Hideshima, Jeffrey Ecsedy, Giulia Perrone, Mala Mani, Hiroshi Ikeda, et al. 2010. “A Novel Aurora-A Kinase Inhibitor MLN8237 Induces Cytotoxicity and Cell-Cycle Arrest in Multiple Myeloma.” *Blood* 115 (25): 5202–13. doi:10.1182/blood-2009-12-259523.

Graeber, T G, C Osmanian, T Jacks, D E Housman, C J Koch, S W Lowe, and A J Giaccia. 1996. “Hypoxia-Mediated Selection of Cells with Diminished Apoptotic Potential in Solid Tumours.” *Nature* 379 (6560): 88–91. doi:10.1038/379088a0.

Granchi, Carlotta, Tiziana Funaioli, Janine T. Erler, Amato J. Giaccia, Marco Macchia, and Filippo Minutolo. 2009. “Bioreductively Activated Lysyl Oxidase Inhibitors against Hypoxic Tumours.” *ChemMedChem* 4 (10): 1590–94. doi:10.1002/cmdc.200900247.

Graves, P R, L Yu, J K Schwarz, J Gales, E A Sausville, P M O’Connor, and H Piwnica-Worms. 2000. “The Chk1 Protein Kinase and the Cdc25C Regulatory Pathways Are Targets of the Anticancer Agent UCN-01.” *The Journal of Biological Chemistry* 275 (8): 5600–5605.

GRAY, L H, A D CONGER, M EBERT, S HORNSEY, and O C SCOTT. 1953. “The Concentration of Oxygen Dissolved in Tissues at the Time of Irradiation as a Factor in Radiotherapy.” *The British Journal of Radiology* 26 (312): 638–48. doi:10.1259/0007-1285-26-312-638.

Gross, M W, U Karbach, K Groebe, A J Franko, and W Mueller-Klieser. 1995. “Calibration of Misonidazole Labeling by Simultaneous Measurement of Oxygen Tension and Labeling Density in Multicellular Spheroids.” *International Journal of Cancer. Journal International Du Cancer* 61 (4): 567–73.

Groth, Anja, Jiri Lukas, Erich A Nigg, Herman H W Silljé, Christer Wernstedt, Jiri Bartek, and Klaus Hansen. 2003. “Human Tousled like Kinases Are Targeted by an ATM- and Chk1-Dependent DNA Damage Checkpoint.” *The EMBO Journal* 22 (7): 1676–87. doi:10.1093/emboj/cdg151.

Guise, Chris P, Anderson T Wang, Anke Theil, David J Bridewell, William R Wilson, and Adam V Patterson. 2007. “Identification of Human Reductases That Activate the Dinitrobenzamide Mustard Prodrug PR-104A: A Role for NADPH:cytochrome P450 Oxidoreductase under Hypoxia.” *Biochemical Pharmacology* 74 (6): 810–20. doi:10.1016/j.bcp.2007.06.014.

Guise, Christopher P, Maria R Abbattista, Rachelle S Singleton, Samuel D Holford, Joanna Connolly, Gabi U Dachs, Stephen B Fox, et al. 2010. “The Bioreductive Prodrug PR-104A Is Activated under Aerobic Conditions by Human Aldo-Keto Reductase 1C3.” *Cancer Research* 70 (4): 1573–84. doi:10.1158/0008-5472.CAN-09-3237.

Guise, Christopher P, Maria R Abbattista, Smitha R Tipparaju, Neil K Lambie, Jiechuang Su, Dan Li, William R Wilson, Gabi U Dachs, and Adam V Patterson. 2012. “Diflavin Oxidoreductases Activate the Bioreductive Prodrug PR-104A under Hypoxia.” *Molecular Pharmacology* 81 (1): 31–40. doi:10.1124/mol.111.073759.

Guise, Christopher P, Alexandra M Mowday, Amir Ashoorzadeh, Ran Yuan, Wan-Hua Lin, Dong-Hai Wu, Jeff B Smaill, Adam V Patterson, and Ke Ding. 2014. “Bioreductive Prodrugs as Cancer Therapeutics: Targeting Tumor Hypoxia.” *Chinese Journal of Cancer* 33 (2): 80–86. doi:10.5732/cjc.012.10285.

Guo, Cai, Akiko Kumagai, Katharina Schlacher, Anna Shevchenko, Andrej Shevchenko, and William G Dunphy. 2015. “Interaction of Chk1 with Treslin Negatively Regulates the Initiation of Chromosomal DNA Replication.” *Molecular Cell* 57 (3): 492–505. doi:10.1016/j.molcel.2014.12.003.

Guzi, Timothy J, Kamil Paruch, Michael P Dwyer, Marc Labroli, Frances Shanahan, Nicole Davis, Lorena Taricani, et al. 2011. “Targeting the Replication Checkpoint Using SCH 900776, a Potent and Functionally Selective CHK1 Inhibitor Identified via High Content Screening.” *Molecular Cancer Therapeutics* 10 (4): 591–602. doi:10.1158/1535-7163.MCT-10-0928.

Hamblin, J Nicole, Tony D R Angell, Stuart P Ballantine, Caroline M Cook, Anthony W J Cooper, John Dawson, Christopher J Delves, et al. 2008. “Pyrazolopyridines as a Novel Structural Class of Potent and Selective PDE4 Inhibitors.” *Bioorganic & Medicinal Chemistry Letters* 18 (14): 4237–41. doi:10.1016/j.bmcl.2008.05.052.

Hammond, E M, M-C Asselin, D Forster, J P B O’Connor, J M Senra, and K J Williams. 2014. “The Meaning, Measurement and Modification of Hypoxia in the Laboratory and the Clinic.” *Clinical Oncology (Royal College of Radiologists (Great Britain))* 26 (5): 277–88. doi:10.1016/j.clon.2014.02.002.

Hammond, Ester M, Nicholas C Denko, Mary Jo Dorie, Robert T Abraham, and Amato J Giaccia. 2002. “Hypoxia Links ATR and p53 through Replication Arrest.” *Molecular and Cellular Biology* 22 (6): 1834–43.

Hammond, Ester M, Mary Jo Dorie, and Amato J Giaccia. 2003. “ATR/ATM Targets Are Phosphorylated by ATR in Response to Hypoxia and ATM in Response to Reoxygenation.” *The Journal of Biological Chemistry* 278 (14): 12207–13. doi:10.1074/jbc.M212360200.

———. 2004. “Inhibition of ATR Leads to Increased Sensitivity to Hypoxia/reoxygenation.” *Cancer Research* 64 (18): 6556–62. doi:10.1158/0008-5472.CAN-04-1520.

Hanada, Katsuhiro, Magda Budzowska, Sally L Davies, Ellen van Drunen, Hideo Onizawa, H Berna Beverloo, Alex Maas, Jeroen Essers, Ian D Hickson, and Roland Kanaar. 2007. “The Structure-Specific Endonuclease Mus81 Contributes to Replication Restart by Generating Double-Strand DNA Breaks.” *Nature Structural & Molecular Biology* 14 (11): 1096–1104. doi:10.1038/nsmb1313.

Hanahan, D, and R A Weinberg. 2000. “The Hallmarks of Cancer.” *Cell* 100 (1): 57–70.

Hanahan, Douglas, and Robert A Weinberg. 2011. “Hallmarks of Cancer: The next Generation.” *Cell* 144 (5): 646–74. doi:10.1016/j.cell.2011.02.013.

Hannak, E, M Kirkham, A A Hyman, and K Oegema. 2001. “Aurora-A Kinase Is Required for Centrosome Maturation in Caenorhabditis Elegans.” *The Journal of Cell Biology* 155 (7): 1109–16. doi:10.1083/jcb.200108051.

Hao, Jing, Christelle de Renty, Yongming Li, Haijie Xiao, Michael G Kemp, Zhiyong Han, Melvin L DePamphilis, and Wenge Zhu. 2015. “And-1 Coordinates with Claspin for Efficient Chk1 Activation in Response to Replication Stress.” *The EMBO Journal* 34 (15). EMBO Press: 2096–2110. doi:10.15252/embj.201488016.

Harper, J Wade, and Stephen J Elledge. 2007. “The DNA Damage Response: Ten Years After.” *Molecular Cell* 28 (5): 739–45. doi:10.1016/j.molcel.2007.11.015.

Harris, Adrian L. 2002. “Hypoxia--a Key Regulatory Factor in Tumour Growth.” *Nature Reviews. Cancer* 2 (1): 38–47. doi:10.1038/nrc704.

Hasvold, Grete, Viola Nähse-Kumpf, Kinga Tkacz-Stachowska, Einar K Rofstad, and Randi G Syljuåsen. 2013. “The Efficacy of CHK1 Inhibitors Is Not Altered by Hypoxia, but Is Enhanced after Reoxygenation.” *Molecular Cancer Therapeutics* 12 (5): 705–16. doi:10.1158/1535-7163.MCT-12-0879.

Hay, Michael P, Robert F Anderson, Dianne M Ferry, William R Wilson, and William A Denny. 2003. “Synthesis and Evaluation of Nitroheterocyclic Carbamate Prodrugs for Use with Nitroreductase-Mediated Gene-Directed Enzyme Prodrug Therapy.” *Journal of Medicinal Chemistry* 46 (25). American Chemical Society: 5533–45. doi:10.1021/jm030308b.

Hay, Michael P, William R Wilson, and William A Denny. 2005. “Nitroarylmethylcarbamate Prodrugs of Doxorubicin for Use with Nitroreductase Gene-Directed Enzyme Prodrug Therapy.” *Bioorganic & Medicinal Chemistry* 13 (12): 4043–55. doi:10.1016/j.bmc.2005.03.055.

Hay, Michael P., Bridget M. Sykes, William A. Denny, and Charmian J. O’Connor. 1999. “Substituent Effects on the Kinetics of Reductively-Initiated Fragmentation of Nitrobenzyl Carbamates Designed as Triggers for Bioreductive Prodrugs.” *Journal of the Chemical Society, Perkin Transactions 1*, no. 19 (January). The Royal Society of Chemistry: 2759–70. doi:10.1039/a904067f.

Hay, Michael P., William R. Wilson, and William A. Denny. 2000. “Design, Synthesis and Evaluation of Imidazolylmethyl Carbamate Prodrugs of Alkylating Agents.” *Tetrahedron* 56 (4): 645–57. doi:10.1016/S0040-4020(99)01031-5.

Heeres, André, Henk A van Doren, Kees F Gotlieb, Ido P Bleeker, Jack Bergsma, and Richard M Kellogg. 2001. “Synthesis, Analysis and Reduction of 2-Nitropropyl Starch.” *Carbohydrate Research* 330 (2): 191–204. doi:10.1016/S0008-6215(00)00288-3.

Helleday, Thomas, Eva Petermann, Cecilia Lundin, Ben Hodgson, and Ricky A Sharma. 2008. “DNA Repair Pathways as Targets for Cancer Therapy.” *Nature Reviews. Cancer* 8 (3). Nature Publishing Group: 193–204. doi:10.1038/nrc2342.

Hermeking, Heiko, and Anne Benzinger. 2006. “14-3-3 Proteins in Cell Cycle Regulation.” *Seminars in Cancer Biology* 16 (3): 183–92. doi:10.1016/j.semcancer.2006.03.002.

Hewitson, Kirsty S, Luke A McNeill, Madeline V Riordan, Ya-Min Tian, Alex N Bullock, Richard W Welford, Jonathan M Elkins, et al. 2002. “Hypoxia-Inducible Factor (HIF) Asparagine Hydroxylase Is Identical to Factor Inhibiting HIF (FIH) and Is Related to the Cupin Structural Family.” *The Journal of Biological Chemistry* 277 (29): 26351–55. doi:10.1074/jbc.C200273200.

Hills, Stephanie A, and John F X Diffley. 2014. “DNA Replication and Oncogene-Induced Replicative Stress.” *Current Biology : CB* 24 (10): R435–44. doi:10.1016/j.cub.2014.04.012.

Hirota, Toru, Naoko Kunitoku, Takashi Sasayama, Tomotoshi Marumoto, Dongwei Zhang, Masayuki Nitta, Katsuyoshi Hatakeyama, and Hideyuki Saya. 2003. “Aurora-A and an Interacting Activator, the LIM Protein Ajuba, Are Required for Mitotic Commitment in Human Cells.” *Cell* 114 (5): 585–98.

Hirschhaeuser, Franziska, Heike Menne, Claudia Dittfeld, Jonathan West, Wolfgang Mueller-Klieser, and Leoni A Kunz-Schughart. 2010. “Multicellular Tumor Spheroids: An Underestimated Tool Is Catching up Again.” *Journal of Biotechnology* 148 (1): 3–15. doi:10.1016/j.jbiotec.2010.01.012.

Ho, A. L., J. C. Bendell, J. M. Cleary, G. K. Schwartz, H. A. Burris, P. Oakes, F. Agbo, P. N. Barker, A. M. Senderowicz, and G. Shapiro. 2011. “Phase I, Open-Label, Dose-Escalation Study of AZD7762 in Combination with Irinotecan (irino) in Patients (pts) with Advanced Solid Tumors.” *ASCO Meeting Abstracts* 29 (15_suppl): 3033.

Hockel, M, K Schlenger, B Aral, M Mitze, U Schaffer, and P Vaupel. 1996. “Association between Tumor Hypoxia and Malignant Progression in Advanced Cancer of the Uterine Cervix.” *Cancer Research* 56 (19): 4509–15.

Hoeijmakers, Jan H J. 2009. “DNA Damage, Aging, and Cancer.” *The New England Journal of Medicine* 361 (15): 1475–85. doi:10.1056/NEJMra0804615.

Höglund, Andreas, Lisa M Nilsson, Somsundar Veppil Muralidharan, Lisa A Hasvold, Philip Merta, Martina Rudelius, Viktoriya Nikolova, Ulrich Keller, and Jonas A Nilsson. 2011. “Therapeutic Implications for the Induced Levels of Chk1 in Myc-Expressing Cancer Cells.” *Clinical Cancer Research : An Official Journal of the American Association for Cancer Research* 17 (22): 7067–79. doi:10.1158/1078-0432.CCR-11-1198.

Hollstein, M, D Sidransky, B Vogelstein, and C C Harris. 1991. “p53 Mutations in Human Cancers.” *Science (New York, N.Y.)* 253 (5015): 49–53.

Hoogsteen, Ilse J, Jasper Lok, Henri A M Marres, Robert P Takes, Paul F J W Rijken, Albert J van der Kogel, and Johannes H A M Kaanders. 2009. “Hypoxia in Larynx Carcinomas Assessed by Pimonidazole Binding and the Value of CA-IX and Vascularity as Surrogate Markers of Hypoxia.” *European Journal of Cancer (Oxford, England : 1990)* 45 (16): 2906–14. doi:10.1016/j.ejca.2009.07.012.

Hu, Jinsong, Damian R Handisides, Els Van Valckenborgh, Hendrik De Raeve, Eline Menu, Isabelle Vande Broek, Qian Liu, et al. 2010. “Targeting the Multiple Myeloma Hypoxic Niche with TH-302, a Hypoxia-Activated Prodrug.” *Blood* 116 (9): 1524–27. doi:10.1182/blood-2010-02-269126.

Ilves, Ivar, Tatjana Petojevic, James J Pesavento, and Michael R Botchan. 2010. “Activation of the MCM2-7 Helicase by Association with Cdc45 and GINS Proteins.” *Molecular Cell* 37 (2): 247–58. doi:10.1016/j.molcel.2009.12.030.

Ira, Grzegorz, Achille Pellicioli, Alitukiriza Balijja, Xuan Wang, Simona Fiorani, Walter Carotenuto, Giordano Liberi, et al. 2004. “DNA End Resection, Homologous Recombination and DNA Damage Checkpoint Activation Require CDK1.” *Nature* 431 (7011): 1011–17. doi:10.1038/nature02964.

Isaacs, Jennifer S, Yun-Jin Jung, Edward G Mimnaugh, Alfredo Martinez, Frank Cuttitta, and Leonard M Neckers. 2002. “Hsp90 Regulates a von Hippel Lindau-Independent Hypoxia-Inducible Factor-1 Alpha-Degradative Pathway.” *The Journal of Biological Chemistry* 277 (33): 29936–44. doi:10.1074/jbc.M204733200.

Ivan, M, K Kondo, H Yang, W Kim, J Valiando, M Ohh, A Salic, J M Asara, W S Lane, and W G Kaelin. 2001. “HIFalpha Targeted for VHL-Mediated Destruction by Proline Hydroxylation: Implications for O2 Sensing.” *Science (New York, N.Y.)* 292 (5516): 464–68. doi:10.1126/science.1059817.

Jaakkola, P, D R Mole, Y M Tian, M I Wilson, J Gielbert, S J Gaskell, A von Kriegsheim, et al. 2001. “Targeting of HIF-Alpha to the von Hippel-Lindau Ubiquitylation Complex by O2-Regulated Prolyl Hydroxylation.” *Science (New York, N.Y.)* 292 (5516): 468–72. doi:10.1126/science.1059796.

Jackson, Stephen P, and Jiri Bartek. 2009. “The DNA-Damage Response in Human Biology and Disease.” *Nature* 461 (7267): 1071–78. doi:10.1038/nature08467.

Jaffar, M, M A Naylor, N Robertson, S D Lockyer, R M Phillips, S A Everett, G E Adams, and I J Stratford. 1998. “5-Substituted Analogues of 3-Hydroxymethyl-5-Aziridinyl-1-Methyl-2-[1H-Indole-4,7-Dione]prop-2-En- 1-Ol (EO9, NSC 382459) and Their Regioisomers as Hypoxia-Selective Agents: Structure-Cytotoxicity in Vitro.” *Anti-Cancer Drug Design* 13 (2): 105–23.

Janetka, James W, Lynsie Almeida, Susan Ashwell, Patrick J Brassil, Kevin Daly, Chun Deng, Thomas Gero, et al. 2008. “Discovery of a Novel Class of 2-Ureido Thiophene Carboxamide Checkpoint Kinase Inhibitors.” *Bioorganic & Medicinal Chemistry Letters* 18 (14): 4242–48. doi:10.1016/j.bmcl.2008.05.016.

Janetka, James W, and Susan Ashwell. 2009. “Checkpoint Kinase Inhibitors: A Review of the Patent Literature.” *Expert Opinion on Therapeutic Patents* 19 (2): 165–97. doi:10.1517/13543770802653622.

Jeong, Woondong, Annamaria Rapisarda, Sook Ryun Park, Robert J Kinders, Alice Chen, Giovanni Melillo, Baris Turkbey, et al. 2014. “Pilot Trial of EZN-2968, an Antisense Oligonucleotide Inhibitor of Hypoxia-Inducible Factor-1 Alpha (HIF-1α), in Patients with Refractory Solid Tumors.” *Cancer Chemotherapy and Pharmacology* 73 (2): 343–48. doi:10.1007/s00280-013-2362-z.

Jin, Jianping, Takahiro Shirogane, Lai Xu, Grzegorz Nalepa, Jun Qin, Stephen J Elledge, and J Wade Harper. 2003. “SCFbeta-TRCP Links Chk1 Signaling to Degradation of the Cdc25A Protein Phosphatase.” *Genes & Development* 17 (24): 3062–74. doi:10.1101/gad.1157503.

Johnson, Louise N, Edward D Lowe, Martin E.M Noble, and David J Owen. 1998. “The Structural Basis for Substrate Recognition and Control by Protein Kinases 1.” *FEBS Letters* 430 (1-2): 1–11. doi:10.1016/S0014-5793(98)00606-1.

Jones, Rebecca M, and Eva Petermann. 2012. “Replication Fork Dynamics and the DNA Damage Response.” *The Biochemical Journal* 443 (1). Portland Press Limited: 13–26. doi:10.1042/BJ20112100.

Jordan, Bénédicte F, and Pierre Sonveaux. 2012. “Targeting Tumor Perfusion and Oxygenation to Improve the Outcome of Anticancer Therapy.” *Frontiers in Pharmacology* 3 (January): 94. doi:10.3389/fphar.2012.00094.

Kaelin, William G. 2008. “The von Hippel-Lindau Tumour Suppressor Protein: O2 Sensing and Cancer.” *Nature Reviews. Cancer* 8 (11): 865–73. doi:10.1038/nrc2502.

Karp, Judith E, Brian M Thomas, Jacqueline M Greer, Christopher Sorge, Steven D Gore, Keith W Pratz, B Douglas Smith, et al. 2012. “Phase I and Pharmacologic Trial of Cytosine Arabinoside with the Selective Checkpoint 1 Inhibitor Sch 900776 in Refractory Acute Leukemias.” *Clinical Cancer*

Research : An Official Journal of the American Association for Cancer Research 18 (24): 6723–31. doi:10.1158/1078-0432.CCR-12-2442.

Kasahara, Kousuke, Hidemasa Goto, Masato Enomoto, Yasuko Tomono, Tohru Kiyono, and Masaki Inagaki. 2010. "14-3-3gamma Mediates Cdc25A Proteolysis to Block Premature Mitotic Entry after DNA Damage." *The EMBO Journal* 29 (16). EMBO Press: 2802–12. doi:10.1038/emboj.2010.157.

Katsha, Ahmed, Abbes Belkhiri, Laura Goff, and Wael El-Rifai. 2015. "Aurora Kinase A in Gastrointestinal Cancers: Time to Target." *Molecular Cancer* 14 (January): 106. doi:10.1186/s12943-015-0375-4.

Kawabata, Tsuyoshi, Spencer W Luebben, Satoru Yamaguchi, Ivar Ilves, Ilze Matise, Tavanna Buske, Michael R Botchan, and Naoko Shima. 2011. "Stalled Fork Rescue via Dormant Replication Origins in Unchallenged S Phase Promotes Proper Chromosome Segregation and Tumor Suppression." *Molecular Cell* 41 (5): 543–53. doi:10.1016/j.molcel.2011.02.006.

Kemp, Michael G, Zafer Akan, Seçil Yilmaz, Mary Grillo, Stephanie L Smith-Roe, Tae-Hong Kang, Marila Cordeiro-Stone, et al. 2010. "Tipin-Replication Protein A Interaction Mediates Chk1 Phosphorylation by ATR in Response to Genotoxic Stress." *The Journal of Biological Chemistry* 285 (22): 16562–71. doi:10.1074/jbc.M110.110304.

Kennedy, K A, S Rockwell, and A C Sartorelli. 1980. "Preferential Activation of Mitomycin C to Cytotoxic Metabolites by Hypoxic Tumor Cells." *Cancer Research* 40 (7): 2356–60.

Khanna, A., O. Kauko, C. Bockelman, A. Laine, I. Schreck, J. I. Partanen, A. Szwajda, et al. 2013. "Chk1 Targeting Reactivates PP2A Tumor Suppressor Activity in Cancer Cells." *Cancer Research* 73 (22): 6757–69. doi:10.1158/0008-5472.CAN-13-1002.

Kim, C Y, M H Tsai, C Osmanian, T G Graeber, J E Lee, R G Giffard, J A DiPaolo, D M Peehl, and A J Giaccia. 1997. "Selection of Human Cervical Epithelial Cells That Possess Reduced Apoptotic Potential to Low-Oxygen Conditions." *Cancer Research* 57 (19): 4200–4204.

King, Constance, H Bruce Diaz, Samuel McNeely, Darlene Barnard, Jack Dempsey, Wayne Blosser, Richard Beckmann, David Barda, and Mark S Marshall. 2015. "LY2606368 Causes Replication Catastrophe and Anti-Tumor Effects through CHK1-Dependent Mechanisms." *Molecular Cancer Therapeutics*, July. doi:10.1158/1535-7163.MCT-14-1037.

King, Constance, Henry Diaz, Darlene Barnard, David Barda, David Clawson, Wayne Blosser, Karen Cox, Sherry Guo, and Mark Marshall. 2014. "Characterization and Preclinical Development of LY2603618: A Selective and Potent Chk1 Inhibitor." *Investigational New Drugs* 32 (2): 213–26. doi:10.1007/s10637-013-0036-7.

Kizaka-Kondoh, Shinae, Masahiro Inoue, Hiroshi Harada, and Masahiro Hiraoka. 2003. “Tumor Hypoxia: A Target for Selective Cancer Therapy.” *Cancer Science* 94 (12): 1021–28. doi:10.1111/j.1349-7006.2003.tb01395.x.

Klapars, Artis, and Stephen L. Buchwald. 2002. “Copper-Catalyzed Halogen Exchange in Aryl Halides: An Aromatic Finkelstein Reaction.” *Journal of the American Chemical Society* 124 (50). American Chemical Society: 14844–45. doi:10.1021/ja028865v.

Klein, Alexandra, Daniela Flügel, and Thomas Kietzmann. 2008. “Transcriptional Regulation of Serine/threonine Kinase-15 (STK15) Expression by Hypoxia and HIF-1.” *Molecular Biology of the Cell* 19 (9): 3667–75. doi:10.1091/mbc.E08-01-0042.

Klimovskaia, Ilnaz M, Clifford Young, Caroline B Strømme, Patrice Menard, Zuzana Jasencakova, Jakob Mejlvang, Katrine Ask, et al. 2014. “Tousled-like Kinases Phosphorylate Asf1 to Promote Histone Supply during DNA Replication.” *Nature Communications* 5 (January). Nature Publishing Group: 3394. doi:10.1038/ncomms4394.

Knox, R J, M P Boland, F Friedlos, B Coles, C Southan, and J J Roberts. 1988. “The Nitroreductase Enzyme in Walker Cells That Activates 5-(aziridin-1-Yl)-2,4-Dinitrobenzamide (CB 1954) to 5-(aziridin-1-Yl)-4-Hydroxylamino-2-Nitrobenzamide Is a Form of NAD(P)H Dehydrogenase (quinone) (EC 1.6.99.2).” *Biochemical Pharmacology* 37 (24): 4671–77.

Kohn, Ethan A, Carolyn J Yoo, and Alan Eastman. 2003. “The Protein Kinase C Inhibitor Gö6976 Is a Potent Inhibitor of DNA Damage-Induced S and G2 Cell Cycle Checkpoints.” *Cancer Research* 63 (1): 31–35.

Kong, Xianguo, Zhao Lin, Dongming Liang, Donna Fath, Nianli Sang, and Jaime Caro. 2006. “Histone Deacetylase Inhibitors Induce VHL and Ubiquitin-Independent Proteasomal Degradation of Hypoxia-Inducible Factor 1alpha.” *Molecular and Cellular Biology* 26 (6): 2019–28. doi:10.1128/MCB.26.6.2019-2028.2006.

Koslowski, M, U Luxemburger, O Türeci, and U Sahin. 2011. “Tumor-Associated CpG Demethylation Augments Hypoxia-Induced Effects by Positive Autoregulation of HIF-1α.” *Oncogene* 30 (7): 876–82. doi:10.1038/onc.2010.481.

Krämer, Alwin, Niels Mailand, Claudia Lukas, Randi G Syljuåsen, Christopher J Wilkinson, Erich A Nigg, Jiri Bartek, and Jiri Lukas. 2004. “Centrosome-Associated Chk1 Prevents Premature Activation of Cyclin-B-Cdk1 Kinase.” *Nature Cell Biology* 6 (9): 884–91. doi:10.1038/ncb1165.

Krause, Darren R, Jyoti C Jonnalagadda, Magtouf H Gatei, Herman H W Sillje, Bin-Bing Zhou, Erich A Nigg, and Kumkum Khanna. 2003. “Suppression of Tousled-like Kinase Activity after DNA Damage or Replication Block

Requires ATM, NBS1 and Chk1." *Oncogene* 22 (38): 5927–37. doi:10.1038/sj.onc.1206691.

Krude, T, M Jackman, J Pines, and R A Laskey. 1997. "Cyclin/Cdk-Dependent Initiation of DNA Replication in a Human Cell-Free System." *Cell* 88 (1): 109–19.

Kumagai, Akiko, and William G. Dunphy. 2000. "Claspin, a Novel Protein Required for the Activation of Chk1 during a DNA Replication Checkpoint Response in Xenopus Egg Extracts." *Molecular Cell* 6 (4): 839–49. doi:10.1016/S1097-2765(05)00092-4.

Lainchbury, Michael, Thomas P Matthews, Tatiana McHardy, Kathy J Boxall, Michael I Walton, Paul D Eve, Angela Hayes, et al. 2012. "Discovery of 3-Alkoxyamino-5-(pyridin-2-Ylamino)pyrazine-2-Carbonitriles as Selective, Orally Bioavailable CHK1 Inhibitors." *Journal of Medicinal Chemistry* 55 (22): 10229–40. doi:10.1021/jm3012933.

Lam, Michael H, Qinghua Liu, Stephen J Elledge, and Jeffrey M Rosen. 2004. "Chk1 Is Haploinsufficient for Multiple Functions Critical to Tumor Suppression." *Cancer Cell* 6 (1): 45–59. doi:10.1016/j.ccr.2004.06.015.

Lando, David, Daniel J Peet, Jeffrey J Gorman, Dean A Whelan, Murray L Whitelaw, and Richard K Bruick. 2002. "FIH-1 Is an Asparaginyl Hydroxylase Enzyme That Regulates the Transcriptional Activity of Hypoxia-Inducible Factor." *Genes & Development* 16 (12): 1466–71. doi:10.1101/gad.991402.

Laronga, C, H Y Yang, C Neal, and M H Lee. 2000. "Association of the Cyclin-Dependent Kinases and 14-3-3 Sigma Negatively Regulates Cell Cycle Progression." *The Journal of Biological Chemistry* 275 (30): 23106–12. doi:10.1074/jbc.M905616199.

Lee, Joon, Akiko Kumagai, and William G Dunphy. 2007. "The Rad9-Hus1-Rad1 Checkpoint Clamp Regulates Interaction of TopBP1 with ATR." *The Journal of Biological Chemistry* 282 (38): 28036–44. doi:10.1074/jbc.M704635200.

Lehman, Norman L, James P O'Donnell, Lisa J Whiteley, Robert T Stapp, Trang D Lehman, Kathleen M Roszka, Lonni R Schultz, et al. 2012. "Aurora A Is Differentially Expressed in Gliomas, Is Associated with Patient Survival in Glioblastoma and Is a Potential Chemotherapeutic Target in Gliomas." *Cell Cycle (Georgetown, Tex.)* 11 (3): 489–502. doi:10.4161/cc.11.3.18996.

Lei, M, Y Kawasaki, M R Young, M Kihara, A Sugino, and B K Tye. 1997. "Mcm2 Is a Target of Regulation by Cdc7-Dbf4 during the Initiation of DNA Synthesis." *Genes & Development* 11 (24): 3365–74.

Leszczynska, Katarzyna B, Iosifina P Foskolou, Aswin G Abraham, Selvakumar Anbalagan, Céline Tellier, Syed Haider, Paul N Span, Eric E O'Neill, Francesca M Buffa, and Ester M Hammond. 2015. "Hypoxia-Induced p53

Modulates Both Apoptosis and Radiosensitivity via AKT." *The Journal of Clinical Investigation* 125 (6): 2385–98. doi:10.1172/JCI80402.

Lin, Nan-Horng, Ping Xia, Peter Kovar, Chang Park, Zehan Chen, Haiying Zhang, Saul H Rosenberg, and Hing L Sham. 2006. "Synthesis and Biological Evaluation of 3-Ethylidene-1,3-Dihydro-Indol-2-Ones as Novel Checkpoint 1 Inhibitors." *Bioorganic & Medicinal Chemistry Letters* 16 (2): 421–26. doi:10.1016/j.bmcl.2005.09.064.

Liu, Peijun, Laura R Barkley, Tovah Day, Xiaohui Bi, Damien M Slater, Mark G Alexandrow, Heinz-Peter Nasheuer, and Cyrus Vaziri. 2006. "The Chk1-Mediated S-Phase Checkpoint Targets Initiation Factor Cdc45 via a Cdc25A/Cdk2-Independent Mechanism." *The Journal of Biological Chemistry* 281 (41): 30631–44. doi:10.1074/jbc.M602982200.

Liu, Q, S Guntuku, X S Cui, S Matsuoka, D Cortez, K Tamai, G Luo, et al. 2000. "Chk1 Is an Essential Kinase That Is Regulated by Atr and Required for the G(2)/M DNA Damage Checkpoint." *Genes & Development* 14 (12): 1448–59.

Liu, Qian, Jessica D Sun, Jingli Wang, Dharmendra Ahluwalia, Amanda F Baker, Lee D Cranmer, Damien Ferraro, et al. 2012. "TH-302, a Hypoxia-Activated Prodrug with Broad in Vivo Preclinical Combination Therapy Efficacy: Optimization of Dosing Regimens and Schedules." *Cancer Chemotherapy and Pharmacology* 69 (6): 1487–98. doi:10.1007/s00280-012-1852-8.

Liu, Shizhou, Simon Bekker-Jensen, Niels Mailand, Claudia Lukas, Jiri Bartek, and Jiri Lukas. 2006. "Claspin Operates Downstream of TopBP1 to Direct ATR Signaling towards Chk1 Activation." *Molecular and Cellular Biology* 26 (16): 6056–64. doi:10.1128/MCB.00492-06.

Lopes, M, C Cotta-Ramusino, A Pellicioli, G Liberi, P Plevani, M Muzi-Falconi, C S Newlon, and M Foiani. 2001. "The DNA Replication Checkpoint Response Stabilizes Stalled Replication Forks." *Nature* 412 (6846): 557–61. doi:10.1038/35087613.

López-Contreras, Andres J, Paula Gutierrez-Martinez, Julia Specks, Sara Rodrigo-Perez, and Oscar Fernandez-Capetillo. 2012. "An Extra Allele of Chk1 Limits Oncogene-Induced Replicative Stress and Promotes Transformation." *The Journal of Experimental Medicine* 209 (3): 455–61. doi:10.1084/jem.20112147.

Luo, Yan, Shayna K. Rockow-Magnone, Paul E. Kroeger, Leigh Frost, Zehan Chen, Edward K.-H. Han, Shi-Chung Ng, Robert L. Simmer, and Vincent L. Giranda. 2001. "Blocking CHK1 Expression Induces Apoptosis and Abrogates the G2 Checkpoint Mechanism." *Neoplasia* 3 (5): 411–19. doi:10.1038/sj.neo.7900175.

Luoto, Kaisa R, Ramya Kumareswaran, and Robert G Bristow. 2013. "Tumor Hypoxia as a Driving Force in Genetic Instability." *Genome Integrity* 4 (1): 5. doi:10.1186/2041-9414-4-5.

Ma, Cynthia X, James W Janetka, and Helen Piwnica-Worms. 2011. “Death by Releasing the Breaks: CHK1 Inhibitors as Cancer Therapeutics.” *Trends in Molecular Medicine* 17 (2): 88–96. doi:10.1016/j.molmed.2010.10.009.

MacDougall, Christina A, Tony S Byun, Christopher Van, Muh-ching Yee, and Karlene A Cimprich. 2007. “The Structural Determinants of Checkpoint Activation.” *Genes & Development* 21 (8): 898–903. doi:10.1101/gad.1522607.

Mack, Philip C, David R Gandara, Alvin H Lau, Primo N Lara, Martin J Edelman, and Paul H Gumerlock. 2003. “Cell Cycle-Dependent Potentiation of Cisplatin by UCN-01 in Non-Small-Cell Lung Carcinoma.” *Cancer Chemotherapy and Pharmacology* 51 (4): 337–48. doi:10.1007/s00280-003-0571-6.

Majka, Jerzy, Sara K Binz, Marc S Wold, and Peter M J Burgers. 2006. “Replication Protein A Directs Loading of the DNA Damage Checkpoint Clamp to 5’-DNA Junctions.” *The Journal of Biological Chemistry* 281 (38): 27855–61. doi:10.1074/jbc.M605176200.

Majumder, Pradip K, Phillip G Febbo, Rachel Bikoff, Raanan Berger, Qi Xue, Louis M McMahon, Judith Manola, et al. 2004. “mTOR Inhibition Reverses Akt-Dependent Prostate Intraepithelial Neoplasia through Regulation of Apoptotic and HIF-1-Dependent Pathways.” *Nature Medicine* 10 (6): 594–601. doi:10.1038/nm1052.

Malumbres, Marcos, and Ignacio Pérez de Castro. 2014. “Aurora Kinase A Inhibitors: Promising Agents in Antitumoral Therapy,” November. Informa UK, Ltd.London.

Malumbres, Marcos, and Ignacio Pérez de Castro. 2014. “Aurora Kinase A Inhibitors: Promising Agents in Antitumoral Therapy.” *Expert Opinion on Therapeutic Targets* 18 (12): 1377–93. doi:10.1517/14728222.2014.956085.

Manfredi, Mark G, Jeffrey A Ecsedy, Arijit Chakravarty, Lee Silverman, Mengkun Zhang, Kara M Hoar, Stephen G Stroud, et al. 2011. “Characterization of Alisertib (MLN8237), an Investigational Small-Molecule Inhibitor of Aurora A Kinase Using Novel in Vivo Pharmacodynamic Assays.” *Clinical Cancer Research : An Official Journal of the American Association for Cancer Research* 17 (24): 7614–24. doi:10.1158/1078-0432.CCR-11-1536.

Marcu, Loredana, and Ian Olver. 2006. “Tirapazamine: From Bench to Clinical Trials.” *Current Clinical Pharmacology* 1 (1): 71–79.

Masai, Hisao, Seiji Matsumoto, Zhiying You, Naoko Yoshizawa-Sugata, and Masako Oda. 2010. “Eukaryotic Chromosome DNA Replication: Where, When, and How?” *Annual Review of Biochemistry* 79 (January). Annual Reviews: 89–130. doi:10.1146/annurev.biochem.052308.103205.

Matsuyama, Tomokazu, Kuniaki Nakanishi, Takuya Hayashi, Yutaka Yoshizumi, Satoshi Aiko, Yoshiaki Sugiura, Takao Tanimoto, Maki Uenoyama, Yuichi Ozeki, and Tadaaki Maehara. 2005. "Expression of Hypoxia-Inducible Factor-1alpha in Esophageal Squamous Cell Carcinoma." *Cancer Science* 96 (3): 176–82. doi:10.1111/j.1349-7006.2005.00025.x.

Matteucci, Mark, Jian-Xin Duan, Hailong Jiao, Jacob Kaizerman, and Steve Ammons. 2007. "Phosphoramidate Alkylator Prodrugs." US, WO 2007/002931.

Matthews, Thomas P, Alan M Jones, and Ian Collins. 2013. "Structure-Based Design, Discovery and Development of Checkpoint Kinase Inhibitors as Potential Anticancer Therapies." *Expert Opinion on Drug Discovery* 8 (6): 621–40. doi:10.1517/17460441.2013.788496.

Matthews, Thomas P, Suki Klair, Samantha Burns, Kathy Boxall, Michael Cherry, Martin Fisher, Isaac M Westwood, et al. 2009. "Identification of Inhibitors of Checkpoint Kinase 1 through Template Screening." *Journal of Medicinal Chemistry* 52 (15). American Chemical Society: 4810–19. doi:10.1021/jm900314j.

Matthews, Thomas P, Tatiana McHardy, Suki Klair, Kathy Boxall, Martin Fisher, Michael Cherry, Charlotte E Allen, et al. 2010. "Design and Evaluation of 3,6-Di(hetero)aryl imidazo[1,2-A]pyrazines as Inhibitors of Checkpoint and Other Kinases." *Bioorganic & Medicinal Chemistry Letters* 20 (14): 4045–49. doi:10.1016/j.bmcl.2010.05.096.

Maya-Mendoza, Apolinar, Eva Petermann, David A F Gillespie, Keith W Caldecott, and Dean A Jackson. 2007. "Chk1 Regulates the Density of Active Replication Origins during the Vertebrate S Phase." *The EMBO Journal* 26 (11): 2719–31. doi:10.1038/sj.emboj.7601714.

McKeown, S R. 2014. "Defining Normoxia, Physoxia and Hypoxia in Tumours-Implications for Treatment Response." *The British Journal of Radiology* 87 (1035): 20130676. doi:10.1259/bjr.20130676.

McNeely, S, R Beckmann, and A K Bence Lin. 2014. "CHEK Again: Revisiting the Development of CHK1 Inhibitors for Cancer Therapy." *Pharmacology & Therapeutics* 142 (1): 1–10. doi:10.1016/j.pharmthera.2013.10.005.

McNeely, Samuel, Chiara Conti, Tahir Sheikh, Himali Patel, Sonya Zabludoff, Yves Pommier, Gary Schwartz, and Archie Tse. 2010. "Chk1 Inhibition after Replicative Stress Activates a Double Strand Break Response Mediated by ATM and DNA-Dependent Protein Kinase." *Cell Cycle (Georgetown, Tex.)* 9 (5): 995–1004.

Meijer, Tineke W H, Johannes H A M Kaanders, Paul N Span, and Johan Bussink. 2012. "Targeting Hypoxia, HIF-1, and Tumor Glucose Metabolism to Improve Radiotherapy Efficacy." *Clinical Cancer Research : An Official*

Journal of the American Association for Cancer Research 18 (20): 5585–94. doi:10.1158/1078-0432.CCR-12-0858.

Melillo, Giovanni. 2007. “Targeting Hypoxia Cell Signaling for Cancer Therapy.” *Cancer Metastasis Reviews* 26 (2): 341–52. doi:10.1007/s10555-007-9059-x.

Meng, Fanying, James W Evans, Deepthi Bhupathi, Monica Banica, Leslie Lan, Gustavo Lorente, Jian-Xin Duan, et al. 2012. “Molecular and Cellular Pharmacology of the Hypoxia-Activated Prodrug TH-302.” *Molecular Cancer Therapeutics* 11 (3): 740–51. doi:10.1158/1535-7163.MCT-11-0634.

Menoyo, A, H Alazzouzi, E Espín, M Armengol, H Yamamoto, and S Schwartz. 2001. “Somatic Mutations in the DNA Damage-Response Genes ATR and CHK1 in Sporadic Stomach Tumors with Microsatellite Instability.” *Cancer Research* 61 (21): 7727–30.

Miranda, Elena, Ida K Nordgren, Abigail L Male, Charlotte E Lawrence, Franciane Hoakwie, Francesco Cuda, William Court, et al. 2013. “A Cyclic Peptide Inhibitor of HIF-1 Heterodimerization That Inhibits Hypoxia Signaling in Cancer Cells.” *Journal of the American Chemical Society* 135 (28): 10418–25. doi:10.1021/ja402993u.

Misra, Raj N., David B. Rawlins, Hai-yun Xiao, Weifang Shan, Isia Bursuker, Kristin A. Kellar, Janet G. Mulheron, et al. 2003. “1H-Pyrazolo[3,4-B]pyridine Inhibitors of Cyclin-Dependent Kinases.” *Bioorganic & Medicinal Chemistry Letters* 13 (6): 1133–36. doi:10.1016/S0960-894X(03)00034-9.

Misra, Raj N., Hai-yun Xiao, David B. Rawlins, Weifang Shan, Kristen A. Kellar, Janet G. Mulheron, John S. Sack, John S. Tokarski, S.David Kimball, and Kevin R. Webster. 2003. “1H-Pyrazolo[3,4-B]pyridine Inhibitors of Cyclin-Dependent Kinases: Highly Potent 2,6-Difluorophenacyl Analogues.” *Bioorganic & Medicinal Chemistry Letters* 13 (14): 2405–8. doi:10.1016/S0960-894X(03)00381-0.

Mitchell, James B, Rajani Choudhuri, Kristin Fabre, Anastasia L Sowers, Deborah Citrin, Sonya D Zabludoff, and John A Cook. 2010. “In Vitro and in Vivo Radiation Sensitization of Human Tumor Cells by a Novel Checkpoint Kinase Inhibitor, AZD7762.” *Clinical Cancer Research : An Official Journal of the American Association for Cancer Research* 16 (7): 2076–84. doi:10.1158/1078-0432.CCR-09-3277.

Miyata, Yoshinari, Xiaokai Li, Hsiu-Fang Lee, Umesh K Jinwal, Sharan R Srinivasan, Sandlin P Seguin, Zapporah T Young, et al. 2013. “Synthesis and Initial Evaluation of YM-08, a Blood-Brain Barrier Permeable Derivative of the Heat Shock Protein 70 (Hsp70) Inhibitor MKT-077, Which Reduces Tau Levels.” *ACS Chemical Neuroscience* 4 (6). American Chemical Society: 930–39. doi:10.1021/cn300210g.

Moeller, Benjamin J, Rachel A Richardson, and Mark W Dewhirst. 2007. "Hypoxia and Radiotherapy: Opportunities for Improved Outcomes in Cancer Treatment." *Cancer Metastasis Reviews* 26 (2): 241–48. doi:10.1007/s10555-007-9056-0.

Montano, Ryan, Injae Chung, Kristen M Garner, David Parry, and Alan Eastman. 2012. "Preclinical Development of the Novel Chk1 Inhibitor SCH900776 in Combination with DNA-Damaging Agents and Antimetabolites." *Molecular Cancer Therapeutics* 11 (2): 427–38. doi:10.1158/1535-7163.MCT-11-0406.

Montano, Ryan, Ruth Thompson, Injae Chung, Huagang Hou, Nadeem Khan, and Alan Eastman. 2013. "Sensitization of Human Cancer Cells to Gemcitabine by the Chk1 Inhibitor MK-8776: Cell Cycle Perturbation and Impact of Administration Schedule in Vitro and in Vivo." *BMC Cancer* 13 (January): 604. doi:10.1186/1471-2407-13-604.

Mordes, Daniel A, Gloria G Glick, Runxiang Zhao, and David Cortez. 2008. "TopBP1 Activates ATR through ATRIP and a PIKK Regulatory Domain." *Genes & Development* 22 (11): 1478–89. doi:10.1101/gad.1666208.

Morgan, Meredith A, Leslie A Parsels, Lili Zhao, Joshua D Parsels, Mary A Davis, Maria C Hassan, Sankari Arumugarajah, et al. 2010. "Mechanism of Radiosensitization by the Chk1/2 Inhibitor AZD7762 Involves Abrogation of the G2 Checkpoint and Inhibition of Homologous Recombinational DNA Repair." *Cancer Research* 70 (12): 4972–81. doi:10.1158/0008-5472.CAN-09-3573.

Murga, Matilde, Stefano Campaner, Andres J Lopez-Contreras, Luis I Toledo, Rebeca Soria, Maria F Montaña, Luana D'Artista, et al. 2011. "Exploiting Oncogene-Induced Replicative Stress for the Selective Killing of Myc-Driven Tumors." *Nature Structural & Molecular Biology* 18 (12): 1331–35. doi:10.1038/nsmb.2189.

Muro, Fumihito, Shin Iimura, Yuuichi Sugimoto, Yoshiyuki Yoneda, Jun Chiba, Toshiyuki Watanabe, Masaki Setoguchi, et al. 2009. "Discovery of Trans-4-[1-[[2,5-Dichloro-4-(1-Methyl-3-Indolylcarboxamido)phenyl]acetyl]-(4S)-Methoxy-(2S)-Pyrrolidinylmethoxy]cyclohexanecarboxylic Acid: An Orally Active, Selective Very Late Antigen-4 Antagonist." *Journal of Medicinal Chemistry* 52 (24). American Chemical Society: 7974–92. doi:10.1021/jm901154c.

Niida, Hiroyuki, Yuko Katsuno, Birendranath Banerjee, M Prakash Hande, and Makoto Nakanishi. 2007. "Specific Role of Chk1 Phosphorylations in Cell Survival and Checkpoint Activation." *Molecular and Cellular Biology* 27 (7): 2572–81. doi:10.1128/MCB.01611-06.

Nikonova, Anna S, Igor Astsaturov, Ilya G Serebriiskii, Roland L Dunbrack, and Erica A Golemis. 2013. "Aurora A Kinase (AURKA) in Normal and Pathological Cell Division." *Cellular and Molecular Life Sciences : CMLS* 70 (4): 661–87. doi:10.1007/s00018-012-1073-7.

Niwa, T, N Koide, T Tsuji, S Imaoka, F Ishibashi, Y Funae, and M Katagiri. 1996. "Cytochrome P450s of Isolated Rat Hepatocytes in Spheroid and Monolayer Cultures." *Research Communications in Molecular Pathology and Pharmacology* 91 (3): 372–78.

Nordlund, Pär, and Peter Reichard. 2006. "Ribonucleotide Reductases." *Annual Review of Biochemistry* 75 (January). Annual Reviews: 681–706. doi:10.1146/annurev.biochem.75.103004.142443.

O'Connor, Liam J., Cindy Cazares-Körner, Jaideep Saha, Charles N. G. Evans, Michael R. L. Stratford, Ester M. Hammond, and Stuart J. Conway. 2015. "Efficient Synthesis of 2-Nitroimidazole Derivatives and the Bioreductive Clinical Candidate Evofosfamide (TH-302)." *Org. Chem. Front.* 2 (9). The Royal Society of Chemistry: 1026–29. doi:10.1039/C5QO00211G.

Olcina, Monica, Philip S Lecane, and Ester M Hammond. 2010. "Targeting Hypoxic Cells through the DNA Damage Response." *Clinical Cancer Research : An Official Journal of the American Association for Cancer Research* 16 (23): 5624–29. doi:10.1158/1078-0432.CCR-10-0286.

Olcina, Monica M, Iosifina P Foskolou, Selvakumar Anbalagan, Joana M Senra, Isabel M Pires, Yanyan Jiang, Anderson J Ryan, and Ester M Hammond. 2013. "Replication Stress and Chromatin Context Link ATM Activation to a Role in DNA Replication." *Molecular Cell* 52 (5): 758–66. doi:10.1016/j.molcel.2013.10.019.

Overgaard, J. 1994. "Clinical Evaluation of Nitroimidazoles as Modifiers of Hypoxia in Solid Tumors." *Oncology Research* 6 (10-11): 509–18.

Overgaard, Jens. 2011. "Hypoxic Modification of Radiotherapy in Squamous Cell Carcinoma of the Head and Neck--a Systematic Review and Meta-Analysis." *Radiotherapy and Oncology : Journal of the European Society for Therapeutic Radiology and Oncology* 100 (1): 22–32. doi:10.1016/j.radonc.2011.03.004.

Oza, Vibha, Susan Ashwell, Lynsie Almeida, Patrick Brassil, Jason Breed, Chun Deng, Thomas Gero, et al. 2012. "Discovery of Checkpoint Kinase Inhibitor (S)-5-(3-Fluorophenyl)-N-(piperidin-3-Yl)-3-Ureidothiophene-2-Carboxamide (AZD7762) by Structure-Based Design and Optimization of Thiophenecarboxamide Ureas." *Journal of Medicinal Chemistry* 55 (11): 5130–42. doi:10.1021/jm300025r.

Pacek, Marcin, and Johannes C Walter. 2004. "A Requirement for MCM7 and Cdc45 in Chromosome Unwinding during Eukaryotic DNA Replication." *The EMBO Journal* 23 (18): 3667–76. doi:10.1038/sj.emboj.7600369.

Pangborn, Amy B., Michael A. Giardello, Robert H. Grubbs, Robert K. Rosen, and Francis J. Timmers. 1996. "Safe and Convenient Procedure for Solvent Purification." *Organometallics* 15 (5). American Chemical Society: 1518–20. doi:10.1021/om9503712.

Parker, L L, and H Piwnica-Worms. 1992. “Inactivation of the p34cdc2-Cyclin B Complex by the Human WEE1 Tyrosine Kinase.” *Science (New York, N.Y.)* 257 (5078): 1955–57.

Parveen, Ifat, Declan P Naughton, William J.D Whish, and Michael D Threadgill. 1999. “2-Nitroimidazol-5-Ylmethyl as a Potential Bioreductively Activated Prodrug System: Reductively Triggered Release of the Parp Inhibitor 5-Bromoisoquinolinone.” *Bioorganic & Medicinal Chemistry Letters* 9 (14): 2031–36. doi:10.1016/S0960-894X(99)00306-6.

Peixoto, Sabrina, Tuan Minh Nguyen, David Crich, Bernard Delpech, and Christian Marazano. 2010. “One-Pot Formation of Piperidine- and Pyrrolidine-Substituted Pyridinium Salts via Addition of 5-Alkylaminopenta-2,4-Dienals to N-Acyliminium Ions: Application to the Synthesis of (±)-Nicotine and Analogs.” *Organic Letters* 12 (21). American Chemical Society: 4760–63. doi:10.1021/ol101783c.

Petermann, Eva, Manuel Luís Orta, Natalia Issaeva, Niklas Schultz, and Thomas Helleday. 2010. “Hydroxyurea-Stalled Replication Forks Become Progressively Inactivated and Require Two Different RAD51-Mediated Pathways for Restart and Repair.” *Molecular Cell* 37 (4): 492–502. doi:10.1016/j.molcel.2010.01.021.

Petermann, Eva, Mick Woodcock, and Thomas Helleday. 2010. “Chk1 Promotes Replication Fork Progression by Controlling Replication Initiation.” *Proceedings of the National Academy of Sciences of the United States of America* 107 (37). National Academy of Sciences: 16090–95. doi:10.1073/pnas.1005031107.

Petitjean, Audrey, Ewy Mathe, Shunsuke Kato, Chikashi Ishioka, Sean V Tavtigian, Pierre Hainaut, and Magali Olivier. 2007. “Impact of Mutant p53 Functional Properties on TP53 Mutation Patterns and Tumor Phenotype: Lessons from Recent Developments in the IARC TP53 Database.” *Human Mutation* 28 (6): 622–29. doi:10.1002/humu.20495.

Pfister, Rolf, Janne Ihalainen, Peter Hamm, and Christoph Kolano. 2008. “Synthesis, Characterization and Applicability of Three Isotope Labeled Azobenzene Photoswitches.” *Organic & Biomolecular Chemistry* 6 (19). The Royal Society of Chemistry: 3508–17. doi:10.1039/b804568b.

Phillips, Roger M, Hans R Hendriks, and Godefridus J Peters. 2013. “EO9 (Apaziquone): From the Clinic to the Laboratory and Back Again.” *British Journal of Pharmacology* 168 (1): 11–18. doi:10.1111/j.1476-5381.2012.01996.x.

Pires, I M, M M Olcina, S Anbalagan, J R Pollard, P M Reaper, P A Charlton, W G McKenna, and E M Hammond. 2012. “Targeting Radiation-Resistant Hypoxic Tumour Cells through ATR Inhibition.” *British Journal of Cancer* 107 (2). Cancer Research UK: 291–99. doi:10.1038/bjc.2012.265.

Pires, Isabel M, Zuzana Bencokova, Chris McGurk, and Ester M Hammond. 2010. “Exposure to Acute Hypoxia Induces a Transient DNA Damage Response Which Includes Chk1 and TLK1.” *Cell Cycle (Georgetown, Tex.)* 9 (13): 2502–7. doi:10.4161/cc.9.13.12059.

Pires, Isabel M, Zuzana Bencokova, Manuela Milani, Lisa K Folkes, Ji-Liang Li, Mike R Stratford, Adrian L Harris, and Ester M Hammond. 2010. “Effects of Acute versus Chronic Hypoxia on DNA Damage Responses and Genomic Instability.” *Cancer Research* 70 (3): 925–35. doi:10.1158/0008-5472.CAN-09-2715.

Platel, Marie, Arach Goldar, Jennifer M. Wiggins, Pedro Barbosa, Pierre Libeau, Pierre Priam, Hemalatha Narassimprakash, Xenia Grodzenski, and Kathrin Marheineke. 2015. “Tight Chk1 Levels Control Replication Cluster Activation in Xenopus.” Edited by Ester Hammond. *PLOS ONE* 10 (6): e0129090. doi:10.1371/journal.pone.0129090.

Plumb, J A, and P Workman. 1994. “Unusually Marked Hypoxic Sensitization to Indoloquinone EO9 and Mitomycin C in a Human Colon-Tumour Cell Line That Lacks DT-Diaphorase Activity.” *International Journal of Cancer. Journal International Du Cancer* 56 (1): 134–39.

Poli, Jérôme, Olga Tsaponina, Laure Crabbé, Andrea Keszthelyi, Véronique Pantesco, Andrei Chabes, Armelle Lengronne, and Philippe Pasero. 2012. “dNTP Pools Determine Fork Progression and Origin Usage under Replication Stress.” *The EMBO Journal* 31 (4): 883–94. doi:10.1038/emboj.2011.470.

Quiroga, Jairo, Jaime Portilla, Rodrigo Abonía, Braulio Insuasty, Manuel Nogueras, and Justo Cobo. 2008. “Synthesis of Novel 5-Amino-1-Aroylpyrazoles.” *Tetrahedron Letters* 49 (41): 5943–45. doi:10.1016/j.tetlet.2008.07.166.

Rapisarda, Annamaria, Badarch Uranchimeg, Olivier Sordet, Yves Pommier, Robert H Shoemaker, and Giovanni Melillo. 2004. “Topoisomerase I-Mediated Inhibition of Hypoxia-Inducible Factor 1: Mechanism and Therapeutic Implications.” *Cancer Research* 64 (4): 1475–82.

Reader, John C, Thomas P Matthews, Suki Klair, Kwai-Ming J Cheung, Jane Scanlon, Nicolas Proisy, Glynn Addison, et al. 2011. “Structure-Guided Evolution of Potent and Selective CHK1 Inhibitors through Scaffold Morphing.” *Journal of Medicinal Chemistry* 54 (24). American Chemical Society: 8328–42. doi:10.1021/jm2007326.

Rischin, Danny, Lester J Peters, Brian O’Sullivan, Jordi Giralt, Richard Fisher, Kally Yuen, Andy Trotti, et al. 2010. “Tirapazamine, Cisplatin, and Radiation versus Cisplatin and Radiation for Advanced Squamous Cell Carcinoma of the Head and Neck (TROG 02.02, HeadSTART): A Phase III Trial of the Trans-Tasman Radiation Oncology Group.” *Journal of Clinical Oncology :*

Official Journal of the American Society of Clinical Oncology 28 (18): 2989–95. doi:10.1200/JCO.2009.27.4449.

Rodenko, Boris, Mohammed I Al-Salabi, Ibrahim A Teka, William Ho, Nasser El-Sabbagh, Juma A M Ali, Hasan M S Ibrahim, Martin J Wanner, Gerrit-Jan Koomen, and Harry P de Koning. 2011. “Synthesis of Marine-Derived 3-Alkylpyridinium Alkaloids with Potent Antiprotozoal Activity.” *ACS Medicinal Chemistry Letters* 2 (12). American Chemical Society: 901–6. doi:10.1021/ml200160k.

Sakya, Subas M, and Bryson Rast. 2003. “Efficient Synthesis of 5-Alkyl Amino and Thioether Substituted Pyrazoles.” *Tetrahedron Letters* 44 (41): 7629–32. doi:10.1016/j.tetlet.2003.08.054.

Sambrook, Joseph, and David W. Russell. 2001. *Molecular Cloning - a Laboratory Manual*. New York: Cold Spring Harbour Laboratory Press.

Sancar, Aziz, Laura A Lindsey-Boltz, Keziban Unsal-Kaçmaz, and Stuart Linn. 2004. “Molecular Mechanisms of Mammalian DNA Repair and the DNA Damage Checkpoints.” *Annual Review of Biochemistry* 73 (January). Annual Reviews 4139 El Camino Way, P.O. Box 10139, Palo Alto, CA 94303-0139, USA: 39–85. doi:10.1146/annurev.biochem.73.011303.073723.

Sanchez, Y, C Wong, R S Thoma, R Richman, Z Wu, H Piwnica-Worms, and S J Elledge. 1997. “Conservation of the Chk1 Checkpoint Pathway in Mammals: Linkage of DNA Damage to Cdk Regulation through Cdc25.” *Science (New York, N.Y.)* 277 (5331): 1497–1501.

Saunders, M P, M Jaffar, A V Patterson, J Nolan, M A Naylor, R M Phillips, A L Harris, and I J Stratford. 2000. “The Relative Importance of NADPH: Cytochrome c (P450) Reductase for Determining the Sensitivity of Human Tumour Cells to the Indolequinone EO9 and Related Analogues Lacking Functionality at the C-2 and C-3 Positions.” *Biochemical Pharmacology* 59 (8): 993–96.

Sausville, Edward, Patricia Lorusso, Michael Carducci, Judith Carter, Mary F Quinn, Lisa Malburg, Nilofer Azad, et al. 2014. “Phase I Dose-Escalation Study of AZD7762, a Checkpoint Kinase Inhibitor, in Combination with Gemcitabine in US Patients with Advanced Solid Tumors.” *Cancer Chemotherapy and Pharmacology* 73 (3): 539–49. doi:10.1007/s00280-014-2380-5.

Savitsky, K, A Bar-Shira, S Gilad, G Rotman, Y Ziv, L Vanagaite, D. Tagle, et al. 1995. “A Single Ataxia Telangiectasia Gene with a Product Similar to PI-3 Kinase.” *Science* 268 (5218): 1749–53. doi:10.1126/science.7792600.

Scanlon, S. E., and P. M. Glazer. 2014. “Hypoxic Stress Facilitates Acute Activation and Chronic Downregulation of Fanconi Anemia Proteins.” *Molecular Cancer Research* 12 (7): 1016–28. doi:10.1158/1541-7786.MCR-13-0628.

Scanlon, Susan E, and Peter M Glazer. 2015. “Multifaceted Control of DNA Repair Pathways by the Hypoxic Tumor Microenvironment.” *DNA Repair* 32 (August): 180–89. doi:10.1016/j.dnarep.2015.04.030.

Schenk, Erin L, Brian D Koh, Karen S Flatten, Kevin L Peterson, David Parry, Allan D Hess, B Douglas Smith, Judith E Karp, Larry M Karnitz, and Scott H Kaufmann. 2012. “Effects of Selective Checkpoint Kinase 1 Inhibition on Cytarabine Cytotoxicity in Acute Myelogenous Leukemia Cells in Vitro.” *Clinical Cancer Research : An Official Journal of the American Association for Cancer Research* 18 (19): 5364–73. doi:10.1158/1078-0432.CCR-12-0961.

Schmidt, Ulrich, and Friedhelm Geiger. 1963. “Totalsynthese Der Antibiotika Thiolutin Und Holomycin.” *Justus Liebigs Annalen Der Chemie* 664 (1): 168–88. doi:10.1002/jlac.19636640114.

Schmitt, Estelle, Rose Boutros, Carine Froment, Bernard Monsarrat, Bernard Ducommun, and Christine Dozier. 2006. “CHK1 Phosphorylates CDC25B during the Cell Cycle in the Absence of DNA Damage.” *Journal of Cell Science* 119 (Pt 20): 4269–75. doi:10.1242/jcs.03200.

Schofield, Christopher J., and Peter J. Ratcliffe. 2004. “Oxygen Sensing by HIF Hydroxylases.” *Nature Reviews Molecular Cell Biology* 5 (5). Nature Publishing Group: 343–54. doi:10.1038/nrm1366.

Seiler, Jennifer A, Chiara Conti, Ali Syed, Mirit I Aladjem, and Yves Pommier. 2007. “The Intra-S-Phase Checkpoint Affects Both DNA Replication Initiation and Elongation: Single-Cell and -DNA Fiber Analyses.” *Molecular and Cellular Biology* 27 (16): 5806–18. doi:10.1128/MCB.02278-06.

Sells, Todd B., Ryan Chau, Jeffrey A. Ecsedy, Rachel E. Gershman, Kara Hoar, Jessica Huck, David A. Janowick, et al. 2015. “MLN8054 and Alisertib (MLN8237): Discovery of Selective Oral Aurora A Inhibitors.” *ACS Medicinal Chemistry Letters* 6 (6). American Chemical Society: 630–34. doi:10.1021/ml500409n.

Semenza, Gregg L. 2013. “HIF-1 Mediates Metabolic Responses to Intratumoral Hypoxia and Oncogenic Mutations.” *The Journal of Clinical Investigation* 123 (9): 3664–71. doi:10.1172/JCI67230.

Semenza, Gregg L. 2003. “Targeting HIF-1 for Cancer Therapy.” *Nature Reviews Cancer* 3 (10): 721–32. doi:10.1038/nrc1187.

Seto, Takashi, Taito Esaki, Fumihiko Hirai, Shuji Arita, Kaname Nosaki, Akitaka Makiyama, Takuro Kometani, et al. 2013. “Phase I, Dose-Escalation Study of AZD7762 Alone and in Combination with Gemcitabine in Japanese Patients with Advanced Solid Tumours.” *Cancer Chemotherapy and Pharmacology* 72 (3): 619–27. doi:10.1007/s00280-013-2234-6.

Shaheen, Montaser, Christopher Allen, Jac A Nickoloff, and Robert Hromas. 2011. “Synthetic Lethality: Exploiting the Addiction of Cancer to DNA Repair.” *Blood* 117 (23): 6074–82. doi:10.1182/blood-2011-01-313734.

Shannon, Aoife M, David J Bouchier-Hayes, Claire M Condron, and Deirdre Toomey. 2003. “Tumour Hypoxia, Chemotherapeutic Resistance and Hypoxia-Related Therapies.” *Cancer Treatment Reviews* 29 (4): 297–307.

Shigenaga, Akira, Keiji Ogura, Hiroko Hirakawa, Jun Yamamoto, Koji Ebisuno, Licht Miyamoto, Keisuke Ishizawa, Koichiro Tsuchiya, and Akira Otaka. 2012. “Development of a Reduction-Responsive Amino Acid That Induces Peptide Bond Cleavage in Hypoxic Cells.” *Chembiochem : A European Journal of Chemical Biology* 13 (7): 968–71. doi:10.1002/cbic.201200141.

Shiloh, Yosef, and Michael B. Kastan. 2001. “ATM: Genome Stability, Neuronal Development, and Cancer Cross Paths.” *Advances in Cancer Research* 83: 209–54. doi:10.1016/S0065-230X(01)83007-4.

Shimada, Midori, Hiroyuki Niida, Doaa H Zineldeen, Hideaki Tagami, Masafumi Tanaka, Hiroyuki Saito, and Makoto Nakanishi. 2008. “Chk1 Is a Histone H3 Threonine 11 Kinase That Regulates DNA Damage-Induced Transcriptional Repression.” *Cell* 132 (2): 221–32. doi:10.1016/j.cell.2007.12.013.

Siemann, Dietmar W, and Michael R Horsman. 2015. “Modulation of the Tumor Vasculature and Oxygenation to Improve Therapy.” *Pharmacology & Therapeutics* 153 (June): 107–24. doi:10.1016/j.pharmthera.2015.06.006.

Siim, B G, D R Menke, M J Dorie, and J M Brown. 1997. “Tirapazamine-Induced Cytotoxicity and DNA Damage in Transplanted Tumors: Relationship to Tumor Hypoxia.” *Cancer Research* 57 (14): 2922–28.

Silljé, H H, K Takahashi, K Tanaka, G Van Houwe, and E A Nigg. 1999. “Mammalian Homologues of the Plant Tousled Gene Code for Cell-Cycle-Regulated Kinases with Maximal Activities Linked to Ongoing DNA Replication.” *The EMBO Journal* 18 (20): 5691–5702. doi:10.1093/emboj/18.20.5691.

Singleton, Rachelle S, Christopher P Guise, Dianne M Ferry, Susan M Pullen, Mary J Dorie, J Martin Brown, Adam V Patterson, and William R Wilson. 2009. “DNA Cross-Links in Human Tumor Cells Exposed to the Prodrug PR-104A: Relationships to Hypoxia, Bioreductive Metabolism, and Cytotoxicity.” *Cancer Research* 69 (9): 3884–91. doi:10.1158/0008-5472.CAN-08-4023.

Skovsgaard, Torben. 1977. “Transport and Binding of Daunorubicin, Adriamycin, and Rubidazone in Ehrlich Ascites Tumour Cells.” *Biochemical Pharmacology* 26 (3): 215–22. doi:10.1016/0006-2952(77)90306-9.

Smith, M L, I T Chen, Q Zhan, P M O’Connor, and A J Fornace. 1995. “Involvement of the p53 Tumor Suppressor in Repair of U.v.-Type DNA Damage.” *Oncogene* 10 (6): 1053–59.

Smits, Veronique A J, Philip M Reaper, and Stephen P Jackson. 2006. “Rapid PIKK-Dependent Release of Chk1 from Chromatin Promotes the DNA-Damage Checkpoint Response.” *Current Biology : CB* 16 (2). Elsevier: 150–59. doi:10.1016/j.cub.2005.11.066.

Soede-Huijbregts, C., M. van Laren, F. B. Hulsbergen, J. Raap, and J. Lugtenburg. 2001. “Improved Specific Synthesis of [1?-15N]- and [3?-15N]L-Histidine.” *Journal of Labelled Compounds and Radiopharmaceuticals* 44 (12): 831–41. doi:10.1002/jlcr.507.

Sørensen, Claus Storgaard, Lasse Tengbjerg Hansen, Jaroslaw Dziegielewski, Randi G Syljuåsen, Cecilia Lundin, Jiri Bartek, and Thomas Helleday. 2005. “The Cell-Cycle Checkpoint Kinase Chk1 Is Required for Mammalian Homologous Recombination Repair.” *Nature Cell Biology* 7 (2): 195–201. doi:10.1038/ncb1212.

Sørensen, Claus Storgaard, and Randi G Syljuåsen. 2012. “Safeguarding Genome Integrity: The Checkpoint Kinases ATR, CHK1 and WEE1 Restrain CDK Activity during Normal DNA Replication.” *Nucleic Acids Research* 40 (2): 477–86. doi:10.1093/nar/gkr697.

Sørensen, Claus Storgaard, Randi G Syljuåsen, Jacob Falck, Tine Schroeder, Lars Rönnstrand, Kum Kum Khanna, Bin-Bing Zhou, Jiri Bartek, and Jiri Lukas. 2003. “Chk1 Regulates the S Phase Checkpoint by Coupling the Physiological Turnover and Ionizing Radiation-Induced Accelerated Proteolysis of Cdc25A.” *Cancer Cell* 3 (3): 247–58.

Sørensen, Claus Storgaard, Randi G Syljuåsen, Jiri Lukas, and Jiri Bartek. 2004. “ATR, Claspin and the Rad9-Rad1-Hus1 Complex Regulate Chk1 and Cdc25A in the Absence of DNA Damage.” *Cell Cycle (Georgetown, Tex.)* 3 (7): 941–45.

Speroni, Juliana, María Belén Federico, Sabrina F Mansilla, Gastón Soria, and Vanesa Gottifredi. 2012. “Kinase-Independent Function of Checkpoint Kinase 1 (Chk1) in the Replication of Damaged DNA.” *Proceedings of the National Academy of Sciences of the United States of America* 109 (19): 7344–49. doi:10.1073/pnas.1116345109.

Srinivasan, Seetha V, David Dominguez-Sola, Lily C Wang, Olivier Hyrien, and Jean Gautier. 2013. “Cdc45 Is a Critical Effector of Myc-Dependent DNA Replication Stress.” *Cell Reports* 3 (5): 1629–39. doi:10.1016/j.celrep.2013.04.002.

Stukenberg, P T, P S Studwell-Vaughan, and M O’Donnell. 1991. “Mechanism of the Sliding Beta-Clamp of DNA Polymerase III Holoenzyme.” *The Journal of Biological Chemistry* 266 (17): 11328–34.

Su, Jiechuang, Yongchuan Gu, Frederik B Pruijn, Jeff B Smaill, Adam V Patterson, Christopher P Guise, and William R Wilson. 2013. “Zinc Finger Nuclease Knock-out of NADPH:cytochrome P450 Oxidoreductase (POR) in

Human Tumor Cell Lines Demonstrates That Hypoxia-Activated Prodrugs Differ in POR Dependence." *The Journal of Biological Chemistry* 288 (52): 37138–53. doi:10.1074/jbc.M113.505222.

Sulli, Gabriele, Raffaella Di Micco, and Fabrizio d'Adda di Fagagna. 2012. "Crosstalk between Chromatin State and DNA Damage Response in Cellular Senescence and Cancer." *Nature Reviews. Cancer* 12 (10). Nature Publishing Group, a division of Macmillan Publishers Limited. All Rights Reserved.: 709–20. doi:10.1038/nrc3344.

Sun, Jessica D, Qian Liu, Jingli Wang, Dharmendra Ahluwalia, Damien Ferraro, Yan Wang, Jian-Xin Duan, et al. 2012. "Selective Tumor Hypoxia Targeting by Hypoxia-Activated Prodrug TH-302 Inhibits Tumor Growth in Preclinical Models of Cancer." *Clinical Cancer Research : An Official Journal of the American Association for Cancer Research* 18 (3): 758–70. doi:10.1158/1078-0432.CCR-11-1980.

Syljuåsen, Randi G, Grete Hasvold, Sissel Hauge, and Åslaug Helland. 2015. "Targeting Lung Cancer through Inhibition of Checkpoint Kinases." *Frontiers in Genetics* 6 (January): 70. doi:10.3389/fgene.2015.00070.

Syljuåsen, Randi G, Claus Storgaard Sørensen, Lasse Tengbjerg Hansen, Kasper Fugger, Cecilia Lundin, Fredrik Johansson, Thomas Helleday, Maxwell Sehested, Jiri Lukas, and Jiri Bartek. 2005. "Inhibition of Human Chk1 Causes Increased Initiation of DNA Replication, Phosphorylation of ATR Targets, and DNA Breakage." *Molecular and Cellular Biology* 25 (9): 3553–62. doi:10.1128/MCB.25.9.3553-3562.2005.

Takahashi, I, E Kobayashi, K Asano, M Yoshida, and H Nakano. 1987. "UCN-01, a Selective Inhibitor of Protein Kinase C from Streptomyces." *The Journal of Antibiotics* 40 (12): 1782–84.

Takai, H, K Tominaga, N Motoyama, Y A Minamishima, H Nagahama, T Tsukiyama, K Ikeda, K Nakayama, and M Nakanishi. 2000. "Aberrant Cell Cycle Checkpoint Function and Early Embryonic Death in Chk1(-/-) Mice." *Genes & Development* 14 (12): 1439–47.

Takayama, Yuko, Yoichiro Kamimura, Mariko Okawa, Sachiko Muramatsu, Akio Sugino, and Hiroyuki Araki. 2003. "GINS, a Novel Multiprotein Complex Required for Chromosomal DNA Replication in Budding Yeast." *Genes & Development* 17 (9): 1153–65. doi:10.1101/gad.1065903.

Takeda, Kotaro, Hector L Aguila, Nehal S Parikh, Xiping Li, Katie Lamothe, Li-Juan Duan, Hiromi Takeda, Frank S Lee, and Guo-Hua Fong. 2008. "Regulation of Adult Erythropoiesis by Prolyl Hydroxylase Domain Proteins." *Blood* 111 (6). American Society of Hematology: 3229–35. doi:10.1182/blood-2007-09-114561.

Tanabe, Kazuhito, Yuji Makimura, Yukihiro Tachi, Akemi Imagawa-Sato, and Sei-ichi Nishimoto. 2005. "Hypoxia-Selective Activation of 5-Fluorodeoxyuridine

Prodrug Possessing Indolequinone Structure: Radiolytic Reduction and Cytotoxicity Characteristics." *Bioorganic & Medicinal Chemistry Letters* 15 (9): 2321–24. doi:10.1016/j.bmcl.2005.03.013.

THOMLINSON, R H, and L H GRAY. 1955. "The Histological Structure of Some Human Lung Cancers and the Possible Implications for Radiotherapy." *British Journal of Cancer* 9 (4): 539–49.

Thomson, Peter, Matthew A Naylor, Steven A Everett, Michael R L Stratford, Gemma Lewis, Sally Hill, Kantilal B Patel, Peter Wardman, and Peter D Davis. 2006. "Synthesis and Biological Properties of Bioreductively Targeted Nitrothienyl Prodrugs of Combretastatin A-4." *Molecular Cancer Therapeutics* 5 (11): 2886–94. doi:10.1158/1535-7163.MCT-06-0429.

Thomson, Peter, Matthew A Naylor, Michael R L Stratford, Gemma Lewis, Sally Hill, Kantilal B Patel, Peter Wardman, and Peter D Davis. 2007. "Hypoxia-Driven Elimination of Thiopurines from Their Nitrobenzyl Prodrugs." *Bioorganic & Medicinal Chemistry Letters* 17 (15): 4320–22. doi:10.1016/j.bmcl.2007.05.018.

Tocher, Joanne H. 1997. "Reductive Activation of Nitroheterocyclic Compounds." *General Pharmacology: The Vascular System* 28 (4): 485–87. doi:10.1016/S0306-3623(96)00283-2.

Toledo, Luis I, Matilde Murga, Rafal Zur, Rebeca Soria, Antonio Rodriguez, Sonia Martinez, Julen Oyarzabal, Joaquin Pastor, James R Bischoff, and Oscar Fernandez-Capetillo. 2011. "A Cell-Based Screen Identifies ATR Inhibitors with Synthetic Lethal Properties for Cancer-Associated Mutations." *Nature Structural & Molecular Biology* 18 (6). Nature Publishing Group, a division of Macmillan Publishers Limited. All Rights Reserved.: 721–27. doi:10.1038/nsmb.2076.

Touchefeu, Yann, Aadil A Khan, Gerben Borst, Shane H Zaidi, Martin McLaughlin, Victoria Roulstone, David Mansfield, et al. 2013. "Optimising Measles Virus-Guided Radiovirotherapy with External Beam Radiotherapy and Specific Checkpoint Kinase 1 Inhibition." *Radiotherapy and Oncology : Journal of the European Society for Therapeutic Radiology and Oncology* 108 (1): 24–31. doi:10.1016/j.radonc.2013.05.036.

Treat, J, E Johnson, C Langer, C Belani, B Haynes, R Greenberg, R Rodriquez, et al. 1998. "Tirapazamine with Cisplatin in Patients with Advanced Non-Small-Cell Lung Cancer: A Phase II Study." *Journal of Clinical Oncology : Official Journal of the American Society of Clinical Oncology* 16 (11): 3524–27.

Tsai, Ming-Ying, Christiane Wiese, Kan Cao, Ona Martin, Peter Donovan, Joan Ruderman, Claude Prigent, and Yixian Zheng. 2003. "A Ran Signalling Pathway Mediated by the Mitotic Kinase Aurora A in Spindle Assembly." *Nature Cell Biology* 5 (3): 242–48. doi:10.1038/ncb936.

Tselepis, C, C D Morris, D Wakelin, R Hardy, I Perry, Q T Luong, E Harper, R Harrison, S E A Attwood, and J A Z Jankowski. 2003. “Upregulation of the Oncogene c-Myc in Barrett’s Adenocarcinoma: Induction of c-Myc by Acidified Bile Acid in Vitro.” *Gut* 52 (2): 174–80.

Ulhaq, Mazhar, Gunnar Carlsson, Stefan Örn, and Leif Norrgren. 2013. “Comparison of Developmental Toxicity of Seven Perfluoroalkyl Acids to Zebrafish Embryos.” *Environmental Toxicology and Pharmacology* 36 (2): 423–26. doi:10.1016/j.etap.2013.05.004.

Van Hooser, A, D W Goodrich, C D Allis, B R Brinkley, and M A Mancini. 1998. “Histone H3 Phosphorylation Is Required for the Initiation, but Not Maintenance, of Mammalian Chromosome Condensation.” *Journal of Cell Science* 111 (Pt 2 (December): 3497–3506.

Vanderpool, Darin, Ted O Johnson, Chen Ping, Simon Bergqvist, Gordon Alton, Soneprasith Phonephaly, Eugene Rui, et al. 2009. “Characterization of the CHK1 Allosteric Inhibitor Binding Site.” *Biochemistry* 48 (41): 9823–30. doi:10.1021/bi900258v.

Vaupel, P, F Kallinowski, and P Okunieff. 1989. “Blood Flow, Oxygen and Nutrient Supply, and Metabolic Microenvironment of Human Tumors: A Review.” *Cancer Research* 49 (23): 6449–65.

Vaupel, Peter, and Louis Harrison. 2004. “Tumor Hypoxia: Causative Factors, Compensatory Mechanisms, and Cellular Response.” *The Oncologist* 9 Suppl 5 (Supplement 5). AlphaMed Press: 4–9. doi:10.1634/theoncologist.9-90005-4.

Vaupel, Peter, and Arnulf Mayer. 2007. “Hypoxia in Cancer: Significance and Impact on Clinical Outcome.” *Cancer Metastasis Reviews* 26 (2): 225–39. doi:10.1007/s10555-007-9055-1.

Von Rahden, Burkhard H A, Hubert J Stein, Franziska Pühringer-Oppermann, and Mario Sarbia. 2006. “C-Myc Amplification Is Frequent in Esophageal Adenocarcinoma and Correlated with the Upregulation of VEGF-A Expression.” *Neoplasia (New York, N.Y.)* 8 (9): 702–7. doi:10.1593/neo.06277.

Vousden, Karen H, and Xin Lu. 2002. “Live or Let Die: The Cell’s Response to p53.” *Nature Reviews. Cancer* 2 (8): 594–604. doi:10.1038/nrc864.

Walton, Michael I, Paul D Eve, Angela Hayes, Melanie Valenti, Alexis De Haven Brandon, Gary Box, Kathy J Boxall, et al. 2010. “The Preclinical Pharmacology and Therapeutic Activity of the Novel CHK1 Inhibitor SAR-020106.” *Molecular Cancer Therapeutics* 9 (1): 89–100. doi:10.1158/1535-7163.MCT-09-0938.

Walton, Mike I, Paul D Eve, Angela Hayes, Melanie R Valenti, Alexis K De Haven Brandon, Gary Box, Albert Hallsworth, et al. 2012. “CCT244747 Is a Novel

Potent and Selective CHK1 Inhibitor with Oral Efficacy Alone and in Combination with Genotoxic Anticancer Drugs." *Clinical Cancer Research : An Official Journal of the American Association for Cancer Research* 18 (20): 5650–61. doi:10.1158/1078-0432.CCR-12-1322.

Walworth, N, S Davey, and D Beach. 1993. "Fission Yeast chk1 Protein Kinase Links the Rad Checkpoint Pathway to cdc2." *Nature* 363 (6427): 368–71. doi:10.1038/363368a0.

Wang, G L, and G L Semenza. 1995. "Purification and Characterization of Hypoxia-Inducible Factor 1." *The Journal of Biological Chemistry* 270 (3): 1230–37.

Wang, Gary T, Gaoquan Li, Robert A Mantei, Zehan Chen, Peter Kovar, Wendy Gu, Zhan Xiao, et al. 2005. "1-(5-Chloro-2-Alkoxyphenyl)-3-(5-Cyanopyrazin-2-Yl)ureas [correction of Cyanopyrazi] as Potent and Selective Inhibitors of Chk1 Kinase: Synthesis, Preliminary SAR, and Biological Activities." *Journal of Medicinal Chemistry* 48 (9). American Chemical Society: 3118–21. doi:10.1021/jm048989d.

Wang, Weidong. 2007. "Emergence of a DNA-Damage Response Network Consisting of Fanconi Anaemia and BRCA Proteins." *Nature Reviews. Genetics* 8 (10): 735–48. doi:10.1038/nrg2159.

Wang, Wen-Jun, Si-Pei Wu, Jia-Bin Liu, Yong-Sheng Shi, Xue Huang, Qian-Bing Zhang, and Kai-Tai Yao. 2013. "MYC Regulation of CHK1 and CHK2 Promotes Radioresistance in a Stem Cell-like Population of Nasopharyngeal Carcinoma Cells." *Cancer Research* 73 (3): 1219–31. doi:10.1158/0008-5472.CAN-12-1408.

Wang, Yujuan, Junfeng Niu, Lilan Zhang, and Jianghong Shi. 2014. "Toxicity Assessment of Perfluorinated Carboxylic Acids (PFCAs) towards the Rotifer Brachionus Calyciflorus." *The Science of the Total Environment* 491-492 (September): 266–70. doi:10.1016/j.scitotenv.2014.02.028.

Wardman, P. 2007. "Chemical Radiosensitizers for Use in Radiotherapy." *Clinical Oncology (Royal College of Radiologists (Great Britain))* 19 (6): 397–417. doi:10.1016/j.clon.2007.03.010.

Wei, Y, C A Mizzen, R G Cook, M A Gorovsky, and C D Allis. 1998. "Phosphorylation of Histone H3 at Serine 10 Is Correlated with Chromosome Condensation during Mitosis and Meiosis in Tetrahymena." *Proceedings of the National Academy of Sciences of the United States of America* 95 (13): 7480–84.

Wei, Y, L Yu, J Bowen, M A Gorovsky, and C D Allis. 1999. "Phosphorylation of Histone H3 Is Required for Proper Chromosome Condensation and Segregation." *Cell* 97 (1): 99–109.

Weiss, Glen J, Ross C Donehower, Tara Iyengar, Ramesh K Ramanathan, Karen Lewandowski, Eric Westin, Karla Hurt, Scott M Hynes, Stephen P Anthony, and Scott McKane. 2013. “Phase I Dose-Escalation Study to Examine the Safety and Tolerability of LY2603618, a Checkpoint 1 Kinase Inhibitor, Administered 1 Day after Pemetrexed 500 mg/m(2) Every 21 Days in Patients with Cancer.” *Investigational New Drugs* 31 (1): 136–44. doi:10.1007/s10637-012-9815-9.

Williamson, S. K. 2005. “Phase III Trial of Paclitaxel Plus Carboplatin With or Without Tirapazamine in Advanced Non-Small-Cell Lung Cancer: Southwest Oncology Group Trial S0003.” *Journal of Clinical Oncology* 23 (36): 9097–9104. doi:10.1200/JCO.2005.01.3771.

Wilsker, Deborah, Eva Petermann, Thomas Helleday, and Fred Bunz. 2008. “Essential Function of Chk1 Can Be Uncoupled from DNA Damage Checkpoint and Replication Control.” *Proceedings of the National Academy of Sciences of the United States of America* 105 (52): 20752–57. doi:10.1073/pnas.0806917106.

Wilson, William R, and Michael P Hay. 2011. “Targeting Hypoxia in Cancer Therapy.” *Nature Reviews. Cancer* 11 (6). Nature Publishing Group, a division of Macmillan Publishers Limited. All Rights Reserved.: 393–410. doi:10.1038/nrc3064.

Woodward, Anna M, Thomas Göhler, M Gloria Luciani, Maren Oehlmann, Xinquan Ge, Anton Gartner, Dean A Jackson, and J Julian Blow. 2006. “Excess Mcm2-7 License Dormant Origins of Replication That Can Be Used under Conditions of Replicative Stress.” *The Journal of Cell Biology* 173 (5): 673–83. doi:10.1083/jcb.200602108.

Yang, Heekyoung, Su Jin Yoon, Juyoun Jin, Seung Ho Choi, Ho Jun Seol, Jung-Il Lee, Do-Hyun Nam, and Hae Yong Yoo. 2011. “Inhibition of Checkpoint Kinase 1 Sensitizes Lung Cancer Brain Metastases to Radiotherapy.” *Biochemical and Biophysical Research Communications* 406 (1): 53–58. doi:10.1016/j.bbrc.2011.01.106.

Yu, Qiang, JiHyun La Rose, Hongliang Zhang, Haruyuki Takemura, Kurt W. Kohn, and Yves Pommier. 2002. “UCN-01 Inhibits p53 up-Regulation and Abrogates Γ-Radiation-Induced G2-M Checkpoint Independently of p53 by Targeting Both of the Checkpoint Kinases, Chk2 and Chk1.” *Cancer Research* 62 (20): 5743–48.

Yun, Zhong, and Peter M Glazer. 2015. “Tumor Suppressor p53 Stole the AKT in Hypoxia.” *The Journal of Clinical Investigation* 125 (6): 2264–66. doi:10.1172/JCI82058.

Zabludoff, Sonya D, Chun Deng, Michael R Grondine, Adam M Sheehy, Susan Ashwell, Benjamin L Caleb, Stephen Green, et al. 2008. “AZD7762, a Novel Checkpoint Kinase Inhibitor, Drives Checkpoint Abrogation and Potentiates

DNA-Targeted Therapies." *Molecular Cancer Therapeutics* 7 (9): 2955–66. doi:10.1158/1535-7163.MCT-08-0492.

Zeman, E M, J M Brown, M J Lemmon, V K Hirst, and W W Lee. 1986. "SR-4233: A New Bioreductive Agent with High Selective Toxicity for Hypoxic Mammalian Cells." *International Journal of Radiation Oncology, Biology, Physics* 12 (7): 1239–42.

Zeman, Michelle K, and Karlene A Cimprich. 2014. "Causes and Consequences of Replication Stress." *Nature Cell Biology* 16 (1): 2–9. doi:10.1038/ncb2897.

Zhang, Cathy, Zhengming Yan, Cory L Painter, Qin Zhang, Enhong Chen, Maria E Arango, Kyle Kuszpit, et al. 2009. "PF-00477736 Mediates Checkpoint Kinase 1 Signaling Pathway and Potentiates Docetaxel-Induced Efficacy in Xenografts." *Clinical Cancer Research : An Official Journal of the American Association for Cancer Research* 15 (14): 4630–40. doi:10.1158/1078-0432.CCR-08-3272.

Zhao, Baoguang, Michael J Bower, Patrick J McDevitt, Huizhen Zhao, Stephen T Davis, Kyung O Johanson, Susan M Green, Nestor O Concha, and Bin-Bing S Zhou. 2002. "Structural Basis for Chk1 Inhibition by UCN-01." *The Journal of Biological Chemistry* 277 (48): 46609–15. doi:10.1074/jbc.M201233200.

Zhu, Rui, Mao-Chin Liu, Mei-Zhen Luo, Philip G Penketh, Raymond P Baumann, Krishnamurthy Shyam, and Alan C Sartorelli. 2011. "4-Nitrobenzyloxycarbonyl Derivatives of O(6)-Benzylguanine as Hypoxia-Activated Prodrug Inhibitors of O(6)-Alkylguanine-DNA Alkyltransferase (AGT), Which Produces Resistance to Agents Targeting the O-6 Position of DNA Guanine." *Journal of Medicinal Chemistry* 54 (21): 7720–28. doi:10.1021/jm201115f.

Zou, Lee, David Cortez, and Stephen J Elledge. 2002. "Regulation of ATR Substrate Selection by Rad17-Dependent Loading of Rad9 Complexes onto Chromatin." *Genes & Development* 16 (2): 198–208. doi:10.1101/gad.950302.

Zou, Lee, and Stephen J Elledge. 2003. "Sensing DNA Damage through ATRIP Recognition of RPA-ssDNA Complexes." *Science (New York, N.Y.)* 300 (5625): 1542–48. doi:10.1126/science.1083430.